Science and Technology of Nuclear Installations

Innovative Gas–Cooled Reactors

Guest Editors: Jan Leen Kloosterman, Jim Kuijper, Colin Mitchell, and Guglielmo Lomonaco

Innovative Gas-Cooled Reactors

Science and Technology of Nuclear Installations

Innovative Gas-Cooled Reactors

Guest Editors: Jan Leen Kloosterman, Jim Kuijper, Colin Mitchell, and Guglielmo Lomonaco

Contents

Hindawi Publishing Corporation
Science and Technology of Nuclear Installations
Volume 2009, Article ID 573263, 1 page
doi:10.1155/2009/573263

Editorial

Innovative Gas-Cooled Reactors

Jan Leen Kloosterman,[1] Jim Kuijper,[2] Colin Mitchell,[3] and Guglielmo Lomonaco[4]

[1] *Delft University of Technology (TUD), 2628 Delft, The Netherlands*
[2] *Nuclear Research & Consultancy Group (NRG), 1755 ZG Petten, The Netherlands*
[3] *AMEC-NNC, Knutsford WA16 8QZ, UK*
[4] *Department of Mechanics, Nuclear and Production Engineering (DIMNP), University of Pisa (UNIPI), 56126 Pisa, Italy*

Correspondence should be addressed to Guglielmo Lomonaco, g.lomonaco@ing.unipi.it

Received 31 December 2009; Accepted 31 December 2009

Innovative gas-cooled reactors, either with a thermal (HTGR) or fast (GCFR) neutron spectrum, are widely considered by academia, research centres, and industry to be among the most promising reactor concepts for the next generation. These reactors are characterized by a fully ceramic core and a noncorrosive coolant (helium or carbon dioxide), which is transparent for neutrons. Due to these characteristics, it is possible to have high operating temperatures.

R&D projects are currently under way in many countries from China, European Union, Japan, Russia, South Africa, South Korea, to the United States, of which many are cooperating through large international projects, such as the framework programmes of the EU, the Generation IV International Forum (GIF), and the International Project on Innovative Nuclear Reactors, and the Fuel Cycles (INPRO) programme of the IAEA.

In terms of safety and competitiveness, the high temperature gas-cooled reactor (HTGR) has very attractive characteristics. It is generally considered to be the most promising candidate at short term and seems to offer at least a partial solution to the growing world energy demand. The operational experience obtained from the HTTR and the HTR-10, in conjunction with the experience already available from other reactors and research projects, constitutes a strong technological basis for the commercial development of HTGRs. Additionally, the fuel cycle flexibility of the HTGR offers the possibility to use this reactor type for the reduction of plutonium and minor actinides stockpiles, as recent studies indicate.

Recently, the gas cooled fast reactor (GCFR) has also gained the interest of industry and the international scientific community. Due to the positive characteristics common to all fast reactors (the improved sustainability by generation of fuel from fertile nuclides and the possibility for efficient burning of nuclear waste) combined with the advantages of gas coolants (no phase change, and no nuclear or chemical reactions in the core), the GCFRs represent a very interesting prospect for future nuclear technology. Their development takes advantage of the high temperature gas coolant technology arising from the HTGRs.

In view of the above, it has been decided to bring out the special issue "Innovative gas-cooled reactors". Looking to the manuscripts, they could be subdivided into three groups.

(1) Three papers are related to HTR/VHTR systems (mainly safety and fuel cycles related aspects).

(2) Two papers are related to symbiotic fuel cycles and scenarios involving LWR, HTR and GCFR.

(3) Six papers are related to GCFR systems (covering many aspects, from the historical background to the present international research activities).

As a result, this widespread interest in innovative gas-cooled reactors from industry to research centres and universities is a stimulus for the rejuvenation of the industry, attracting young talents to the universities to become the scientists and engineers of the future.

Jan Leen Kloosterman
Jim Kuijper
Colin Mitchell
Guglielmo Lomonaco

Hindawi Publishing Corporation
Science and Technology of Nuclear Installations
Volume 2009, Article ID 687634, 11 pages
doi:10.1155/2009/687634

Research Article

Modelling of HTR Confinement Behaviour during Accidents Involving Breach of the Helium Pressure Boundary

Joan Fontanet,[1] Luis E. Herranz,[1] Alastair Ramlakan,[2] and Lolan Naicker[2]

[1] *Unit of Nuclear Safety Research, CIEMAT, Avenida Complutense, 22 28040 Madrid, Spain*
[2] *Pebble Bed Modular Reactor (Pty) Limited, 1279 Mike Crawford Avenue, 0046 Centurion, South Africa*

Correspondence should be addressed to Joan Fontanet, joan.fontanet@ciemat.es

Received 30 January 2009; Revised 18 May 2009; Accepted 4 June 2009

Recommended by Jim Kuijper

Development of HTRs requires the performance of a thorough safety study, which includes accident analyses. Confinement building performance is a key element of the system since the behaviour of aerosol and attached fission products within the building is of an utmost relevance in terms of the potential source term to the environment. This paper explores the available simulation capabilities (ASTEC and CONTAIN codes) and illustrates the performance of a postulated HTR vented confinement under prototypical accident conditions by a scoping study based on two accident sequences characterized by Helium Pressure Boundary breaches, a small and a large break. The results obtained indicate that both codes predict very similar thermal-hydraulic responses of the confinement both in magnitude and timing. As for the aerosol behaviour, both codes predict that most of the inventory coming into the confinement is eventually depleted on the walls and only about 1% of the aerosol dust is released to the environment. The crosscomparison of codes states that largest differences are in the intercompartmental flows and the in-compartment gas composition.

1. Introduction

Modern High Temperature Reactors (HTRs) are designed in such a way that their inherent features provide adequate protection against hypothetical accidents. The main characteristics directly related to safety are the coated fuel particles (CFPs), the use of helium as a coolant, the passive decay heat removal, the negative temperature-reactivity coefficient, and a large margin between fuel operation and fuel damage temperature. As a result, HTRs do not require active safety systems or prompt operator actions to prevent any significant fuel failure or fission product release.

Helium has important plant safety implications from the point of view of plant confinement. Its noncondensable nature has two major implications: firstly, no large local temperature increases should be expected during anticipated operational occurrences (phenomena like departure from nucleate boiling cannot happen); secondly, the effectiveness of an LWR conventional containment gets substantially reduced since pressure suppression by condensation is ruled out. In the case of a primary circuit depressurization event, the helium would behave as a radionuclide carrier from the reactor cooling system, passing through the confinement building, to the environment.

Furthermore, the combination of high heat capacity, low power density, and high effective thermal conductivity in HTR cores results in slow thermal transients: fuel temperatures peak days after the initiating event. This means that in case of any delayed fission product release driven by high fuel temperatures, it would occur long after the depressurization was over. In the case of a confinement approach, at that time no helium would be available within the circuit to carry any fission product and aerosol from the primary system to the building. Therefore, a much lower offsite dose than in the case of an LWR would be expected. In the HTR context, filtration of the early release (i.e., dust and circulating activity in the HPB) becomes critical in reducing the source term to the environment.

Dust exiting the HPB will include fission and activation products so that the aerosol behaviour within the building is of utmost relevance in terms of the potential source term to the environment. Several phenomena, such as intercell flow, particle agglomeration, and settling, would be responsible for the radioactivity evolution within the

confinement building. Hence, all those processes should be properly encapsulated in any analytical tool.

This paper illustrates, through a scoping study based on two postulated HPB break accidents, two key aspects of HTR safety analysis: predictability of current analytical tools and the performance of an alternate PBMR-type plant confinement. The predictability is discussed based on the range of validity of the models inside two accredited codes in the field of LWR safety analysis: ASTEC v1.3 [1] and CONTAIN 2.0 [2]. Both thermal-hydraulic and aerosol performance are reported according to estimates obtained by both codes. Furthermore, the code-to-code comparison highlights the strengths and weaknesses of these two codes.

2. Models Applicability

2.1. Particle Characterization. The applicability of the thermal-hydraulics and aerosol models encapsulated in ASTEC v1.3 and CONTAIN 2.0 for HTR safety analysis needs to be assessed.

The aerosol behaviour is closely linked to the dimensionless Knudsen number ($\mathrm{Kn} = 2 \cdot \lambda/d_p$), which conditions the medium resistance force to particle motion. According to its value, four different regimes are considered: continuum ($\mathrm{Kn} \ll 1$), slip flow ($\mathrm{Kn} < 0.25$), transition ($0.1 < \mathrm{Kn} < 1.0$), and free molecule ($\mathrm{Kn} > 10$) [3]. According to pressure and temperature ranges anticipated in HTR confinement accident scenarios (1–1.5 bar, 300–400 K, resp.) the mean free path would range between 10^{-7}–$2.5 \cdot 10^{-7}$ m (pure helium) and $3 \cdot 10^{-8}$ to $9 \cdot 10^{-8}$ m (pure air). On the other side, AVR data [4] indicates that the expected particle size should be in the range of 10^{-6} to 10^{-5} m. As a result, Kn may be readily estimated to be around 0.1. In other words, particles would lay inside the limits of the slip flow regime even for pure helium. Only in the case of the smallest particles, Kn would increase up to 0.2 (helium-air mixture) or even 0.5 (pure helium), that is, right at the border slip flow and transition regimes.

Therefore, aerosol behaviour within the HTR confinement building during a postulated accident scenario should be described with models valid within the slip flow regime. Even in quite specific and extreme conditions, like those in the discharge compartment during a fast primary circuit depressurization, models capable of dealing with "slip-flow" conditions would still be suitable.

2.2. Aerosol Models. Most of the aerosol models included in ASTEC and CONTAIN are very similar since the models in both codes originate from the MAEROS code [5]. The key depletion and agglomeration models are presented next.

2.2.1. Depletion Models. Four deposition mechanisms are modelled into ASTEC and CONTAIN: gravitational settling, diffusion, thermophoresis, and diffusiophoresis.

(i) *Gravitational deposition* on the compartment floor is characterized by the settling velocity, v_{set}, which is given by the following expression [6]:

$$v_{\mathrm{set}} = C_C \cdot \frac{\rho_p \cdot g \cdot d_p^2}{18 \cdot \mu_g \cdot \chi}. \tag{1}$$

This equation was derived based on the Stokes theory for small Reynolds numbers ($\mathrm{Re} = \rho_g v_{\mathrm{set}} d_p/\mu < 1$) and particles larger than 10^{-9} m. According to AVR data [4], the largest particle expected in Pebble Bed Reactors will be around $8 \cdot 10^{-6}$ m of diameter. For these particles, the estimated value of Re is about $5 \cdot 10^{-6}$, which is well within the applicable range of the model.

(ii) *Diffusive deposition* onto surfaces is customarily modelled assuming that the turbulent flow in the gas bulk provides a uniform concentration everywhere beyond a thin boundary layer next to the surface. In the boundary layer, of thickness δ_{dif}, flow is laminar and the concentration is assumed to decrease linearly to zero at the surface. Under these conditions the deposition velocity is given by $v_{\mathrm{dif}} = D/\delta_{\mathrm{dif}}$. Using the Stokes-Einstein equation for the diffusion coefficient the velocity is expressed as [6]

$$v_{\mathrm{dif}} = \frac{k \cdot T_g \cdot C_C}{3\pi \cdot \chi \cdot \mu_g \cdot d_p \delta_{\mathrm{dif}}}. \tag{2}$$

The hypotheses used in the derivation of this expression are independent from the gas nature. Thus, there is no inconsistency in applying it to the HTR scenario.

(iii) The depletion due to *thermophoresis* (i.e., driven by temperature gradient between gas and wall surfaces) is obtained from theory using a perturbation approach with appropriated boundary conditions [7]. Talbot et al. [8] proposed a fitting formula useful for the entire range of Knudsen numbers within a 20% error margin for the available data

$$v_{\mathrm{tph}} = \frac{2 \cdot C_s \cdot \mu_g \cdot C_C \cdot \left(C_t \cdot \mathrm{Kn} + \lambda_g/\lambda_p\right) \cdot \nabla T}{\chi \cdot \rho_g \cdot T_g \cdot (1+3 \cdot \mathrm{Kn} \cdot C_m) \cdot \left(1+2 \cdot C_t \cdot \mathrm{Kn} + 2\lambda_g/\lambda_p\right)}. \tag{3}$$

Parameters C_t and C_m depend on the gas and particle nature whereas C_s is practically independent of the gas [9]. Based on the kinetic gas theory, Talbot et al. [8] recommended values of $C_t = 2.18$, $C_m = 1.14$, and $C_s = 1.17$.

Since the expected temperature gradients in the confinement will be approximately 50 K, thermophoretic deposition will not play a significant role.

2.2.2. Agglomeration Models. Both codes used in this work have the same model for the different contributions to the collision and coagulation of two particles: Brownian, Turbulent, and Gravitational.

(i) The *Brownian agglomeration* coefficient is given by

$$\beta_{\mathrm{Brow}} = \frac{2\pi \cdot \left(D_i + D_j\right) \cdot \left(\gamma_i \cdot d_i + \gamma_j \cdot d_j\right)}{F}. \tag{4}$$

This expression is derived semiempirically [3, 10] for the continuum regime up to the transition regime (i.e., $\mathrm{Kn} < 10$).

(ii) The *Turbulent agglomeration* coefficient was derived by Saffman and Turner [11] in terms of the energy dissipation rate, Q_T, and it consists of two contributions: the shearing and inertial part, respectively,

$$\beta_{T1} = \sqrt{\frac{\pi^2 \cdot Q_T}{120 \cdot \nu_g}} \left(\gamma_i \cdot d_i + \gamma_j \cdot d_j\right)^3, \tag{5}$$

$$\beta_{T2} = \frac{0.04029 \cdot \rho_g^{1/4} \cdot Q_T^{3/4}}{\mu_g^{5/4}} \left(\gamma_i \cdot d_i + \gamma_j \cdot d_j\right)^3 \cdot C_{\text{grav}} \cdot \left| \frac{\rho_i \cdot C_{C,i} \cdot d_i^2}{\chi_i} - \frac{\rho_j \cdot C_{C,j} \cdot d_j^2}{\chi_j} \right|, \tag{6}$$

where the total coefficient is calculated as $\beta = \sqrt{\beta_{T1}^2 + \beta_{T2}^2}$. Expressions (5) and (6) were derived on theoretical grounds and do not seem to be subject to any restriction for their application, except that particles should be smaller than the eddies responsible for their relative motion.

(iii) The *Gravitational coefficient* depends on the relative settling velocity of the two colliding particles by [12]

$$\beta_{\text{grav}} = C_{\text{grav}} \cdot \frac{\pi}{4} \cdot \left(\gamma_i \cdot d_i + \gamma_j \cdot d_j\right)^2 \cdot \left| v_{\text{set},i} - v_{\text{set},j} \right|, \tag{7}$$

and its range of applicability is the same as for the aerosol deposition (i.e., Re < 1).

2.3. Intercompartmental Gas Flow Model. Generally, ASTEC and CONTAIN simulate the thermal-hydraulic behaviour of the confinement in a similar way. Nonetheless, a closer analysis of these codes reveals small but relevant differences in the model for the gas flow rate between adjacent compartments. The ASTEC code includes two mechanisms for gas mass flow [13]. The first mechanism, based on the equation of momentum, is driven by pressure gradients accordingly to

$$\dot{G}_{\text{conv}} = \frac{A_{s-t}}{L_{s-t}} \left(\Delta P_{s-t} - \zeta \frac{G|G|}{2\ \bar{\rho} A_{s-t}^2} \right), \tag{8}$$

and the second, the diffusion term, is generated by differences in concentration of each gas component and given as

$$\dot{G}_{\text{dif},c} = \frac{D_c A_{s-t}}{L_{s-t}} \frac{M_c}{10^3 R} \frac{d}{dt} \left(\frac{\Delta p_{c,s-t}}{\bar{T}} \right). \tag{9}$$

However, in CONTAIN [2] the flow is estimated only by (8). Thus, each code estimates different fractions of incoming hot helium to be mixed with the existing gas in a compartment as well as different gas transfers to surrounding chambers. In this way, the gas flow patterns between confinement compartments are different in both codes and, consequently, the in-compartment molar fraction of gases and the net aerosol amount carried by gases. ASTEC predicts a balanced mix of gases in the confinement whereas in CONTAIN the gas mixing is not as uniform. The difference in code results will be discussed in this paper.

2.4. Gas Properties. The atmosphere in the confinement will contain a fraction of helium that, in the large break scenario, can reach significant levels for a short period of time in the discharge and adjacent compartments. Thus, not considering helium in the calculation of gas properties will lead to a deviation in the agglomeration and depletion predictions. This influence on deposition velocity can be estimated with gas properties: basically the viscosity, μ, and the Cunningham factor, C_C (1) and (2). For pure helium the viscosity is about 10% higher than for air in the range of pressures and temperatures representative of HTR accidents and C_C will be about 20% higher for the smallest particle (with Kn ~ 0.2). Thus, the dependency of gravitational and diffusive deposition on C_C/μ would lead to a maximum difference of about 10% depending on the particle size. Dependency of thermophoretic deposition (3) on gas density would lead to a more significant effect (5 times higher for a pure helium atmosphere) in the case that this mechanism had been important.

For agglomeration models, the same approach has been taken and results for pure helium and pure air atmospheres differ to the order of 10% for Brownian and gravitational agglomeration (4) and (7). For turbulent agglomeration models, the shearing part (5) is similar for both atmospheres and the inertial part (6) is about 30% lower in helium.

Considering that gas composition will actually be a mixture of air and helium with the fraction depending on the released helium mass flow rate (i.e., breach size), it can be concluded that the error introduced in the calculation, by not considering helium in gas atmosphere, is acceptable for these kinds of simulations.

3. Analysis Approach: Helium Pressure Boundary Breaks

3.1. Scenario Description. A break in the Helium Pressure Boundary (HPB) will lead to a primary circuit depressurization and the injection of helium into the Power Conversion Unit (PCU) building area. This helium injection will result in the pressurization of the specific compartment, where the break is located. The flow connection between PCU compartments will distribute the excess helium to other rooms. If the break is large enough, the Pressure Relief System (PRS) directs the helium flow towards the Depressurization Vent Shaft (DVS) system, through which the gas is released to the environment. Filter chambers at the top of the building, before the vent stack, can retain aerosols carried by the gas to limit the release of radioactive material to the environment. The DVS is connected to the PCU building through rupture panels that break if the pressure differential reaches 5 kPa.

Two different accident sequences belonging to the Licensing Basis Events (LBEs) have been simulated. Both of them consist of a breach in the HPB. The first LBE modelled is a large break (LB), 230 mm double ended guillotine break in the PCU piping directly coupled to the core at the bottom of the reactor. The second accident event modelled is a small break (SB), 10 mm diameter, located at the precooler inlet.

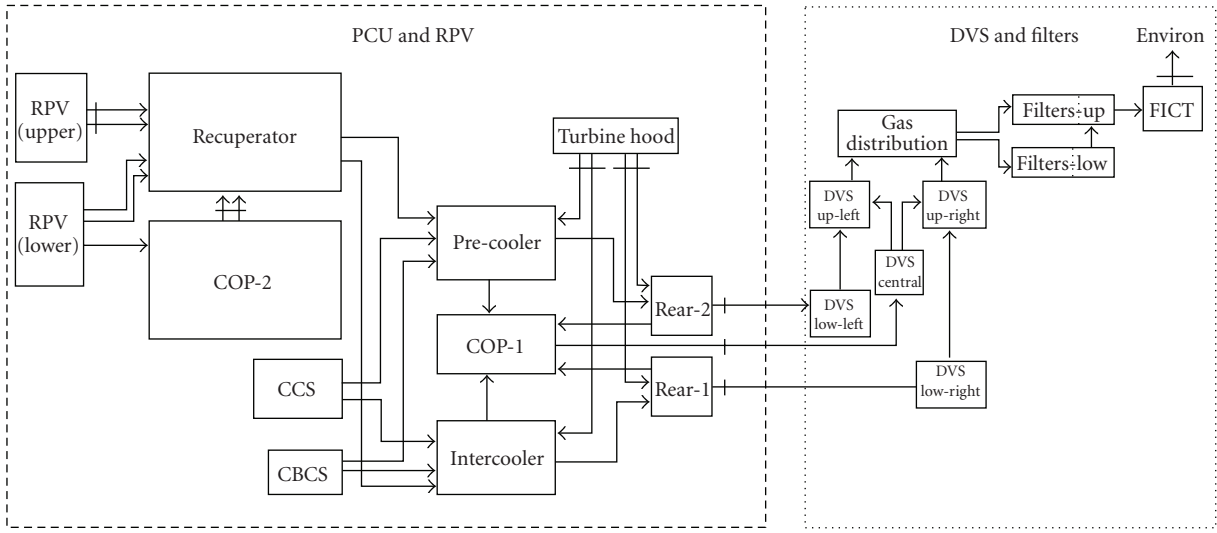

Figure 1: Diagram of the confinement building layout, including the PCU, RPV, and DVS, and the flow path connection between compartments.

The confinement building modelled in this study has a total volume of about 35 000 m^3 with the PCU, DVS, and filtration chambers included. The PCU is divided into 12 volumes including the Reactor Pressure Vessel compartments. The DVS comprises 8 volumes, which collectively lead to two filter compartments and these filter compartments are further split into a total of 24 chambers. This gives a total number of 42 volumes to be modelled in the ASTEC v1.3 and CONTAIN 2.0 codes. Figure 1 shows the nodalization diagram of the confinement model and the flow path between compartments.

3.2. Analytical Tools. ASTEC is an integral code devoted to the simulation of LWR severe accidents phenomena from the initiating event to the possible release of radioactive isotopes to the environment. It is being developed by IRSN (France) and GRS (Germany) helped in part by projects of the European Union research work programme. Several modules are integrated in ASTEC, of which CPA simulates the containment behaviour in accident scenarios. CONTAIN is a system code developed by the US National Regulatory Commission and has been extensively used in containment accident analysis in LWRs. Both codes use lumped parameter models to simulate the thermal-hydraulics and aerosol phenomena in multicompartment containments.

3.3. Hypotheses and Approximations. As far as is feasible, the same hypotheses and approximations adopted in the confinement modelling (i.e., compartment geometry, intercell junctions, and structure thermal properties) have been adopted in ASTEC v1.3 and CONTAIN 2.0.

Helium mass escaping the HPB through the breach is estimated with FLOWNEX [14]. Aerosols present in the primary circuit at the time of the break are carried by helium into the confinement. The helium flow rate, together with entrained aerosol mass rate, is given as a boundary condition in input decks. The dust mass entering the confinement is estimated as a fraction of the total aerosol mass accumulated within the HPB during operation. An approximation of the resuspended fraction from the circuit surfaces is calculated with the Shear Ratio Model [15] using flow conditions determined for each break size.

For the large break (LB) scenario the primary circuit depressurization is predicted to last 10 seconds. Figure 2 shows the evolution of the helium flow calculated with FLOWNEX [14]. The mass flow is very high at the beginning of the break and then decreases quickly as the pressure differential driving force between the circuit and the confinement dissipates. The helium temperature drops in a few seconds. This behaviour is due to the break location, assumed to be in the hot part of the circuit. As a consequence, the hot helium closest to the break escapes first followed by helium from further and cooler parts of the circuit (the steep decline in the temperature curve). The temperature rise after 2 seconds is due to the heat transfer from the core to the reduced helium mass available in the circuit.

During the small break (SB) accident sequence the helium, as well as the aerosol dust, is injected into the precooler compartment over a long period of time (more than 7 hours) at a constant rate (three orders of magnitudes lower than in the LB case).

With regards to aerosols, the particles are assumed to be spherical and nonhygroscopic. Additionally, it is worth mentioning that the particle-particle collision efficiency has been estimated according to Fuch's equation [12].

The aerosol size distribution is defined in the ASTEC input deck based on data from the AVR [4]. However, CONTAIN only accepts lognormal distributions; thus the data is approximated as the lognormal function that better fits the experimental distribution. The resulting distribution has a Mass Median Diameter (MMD) of $5.4 \cdot 10^{-6}$ m and a Geometric Standard Deviation (GSD) of 1.35. Figure 3 shows both aerosol size distributions used for ASTEC and CONTAIN calculations. As will be shown later, in spite of

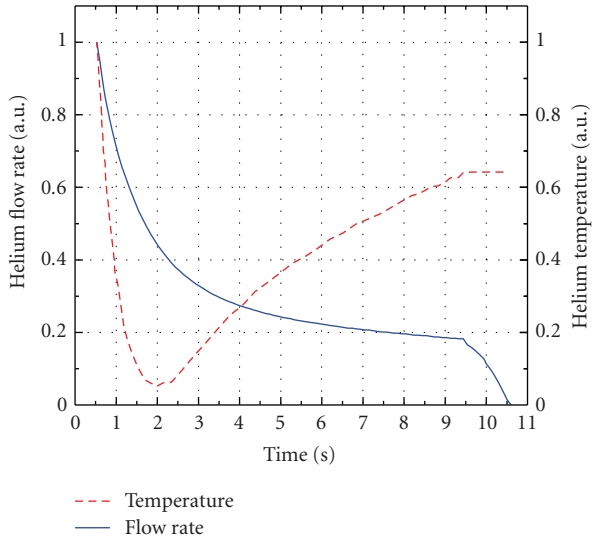

Figure 2: Evolution of helium flow rate and temperature escaping from primary circuit breach in the LB accident.

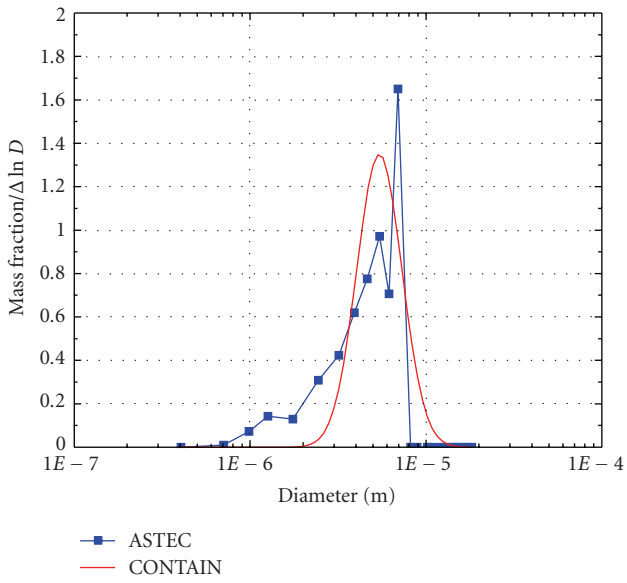

Figure 3: Aerosol size distribution defined in both code simulations.

this approximation, CONTAIN simulation results are very similar to those of ASTEC.

The total dust mass estimated to exit the HPB during the large and the small break is assumed to enter into the confinement at the same rate as the helium flow (i.e., the carrier gas). This assumption implies that the total amount of escaping dust is actually circulating in the primary circuit at the moment the accident begins.

4. Results and Discussion

The results below should be considered as exploratory. The approximation made above and the nonreactor specific characteristics put the emphasis of this study on its qualitative nature (i.e., trends and orders of magnitude) more than in the precise number presented below. A quantitative assessment would require a set of parametric and sensitivity calculations on all those uncertain variables discussed above.

The main thermal-hydraulic figures of merit from the point of view of the confinement safety are the gas pressure and temperature of the different compartments. Furthermore, the evolution of the accident (i.e., the confinement pressurization and helium release to the environment) is governed by the gas flow rate between adjoining compartments. Differences in the code models can drive differences in gas flow rates but also in flow patterns inside the confinement building.

Regarding the aerosol behaviour, the main safety relevant figures of merit are the aerosol mass released to the environment and the concentration remaining suspended in the confinement at the end of the accident. The rest of the aerosol mass coming into the confinement (the confinement inventory defined as "c.i.") will be depleted there, either on the filters or on compartment walls.

4.1. Large Break Scenario. In the large break sequence the primary depressurization is very fast and the injection of helium into the turbine hood compartment is quite vigorous, so two periods can be distinguished in the confinement pressurization: the first period extends from the initiation of the helium blow down to the break of the panels between turbine hood and the rest of the PCU building; the second is the subsequent homogeneous pressurization of the entire confinement. Once the HPB is depressurized, the helium blow down stops and the confinement pressure decreases as the gas is released to the environment.

4.1.1. Thermal-Hydraulics. The high helium injection during the first 0.5 seconds after the break yields a sudden pressurization of the turbine hood compartment. As a consequence of pressure differences between the turbine hood and adjacent compartments, the rupture panel connections break and helium is distributed to the other PCU compartments. As the injection flow into the turbine hood is higher than the distribution flow from the turbine hood, the pressure in the turbine hood cell increases faster than in the other volumes. This results in a sharp local peak in the turbine hood pressure. Afterwards, the inter-compartment flow is higher than the helium injection mass rate and the pressure in the PCU compartment homogenizes that is; the turbine hood depressurizes and the pressure rises in the other PCU and DVS compartments. Figure 4 plots the ratio of the actual pressure to the initial pressure for different compartments. As observed, even though the PCU-DVS and filters-environment rupture panels break soon after the onset of the accident, the pressure peaks in the confinement at about 7 seconds. After the end of the helium injection (10.5 seconds) the PCU depressurization is so fast that at about 20 seconds the confinement pressure is approximately equal to the initial pressure (Figure 4).

Both codes predict very similar evolutions of the pressure through the different periods described above. This means that both codes predict very similar flow rates during this

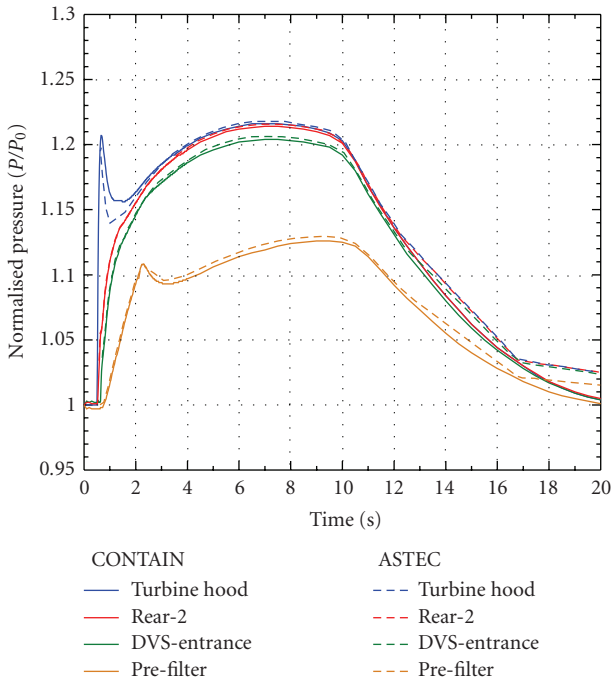

Figure 4: Pressure evolution in the main confinement compartments for the LB sequence.

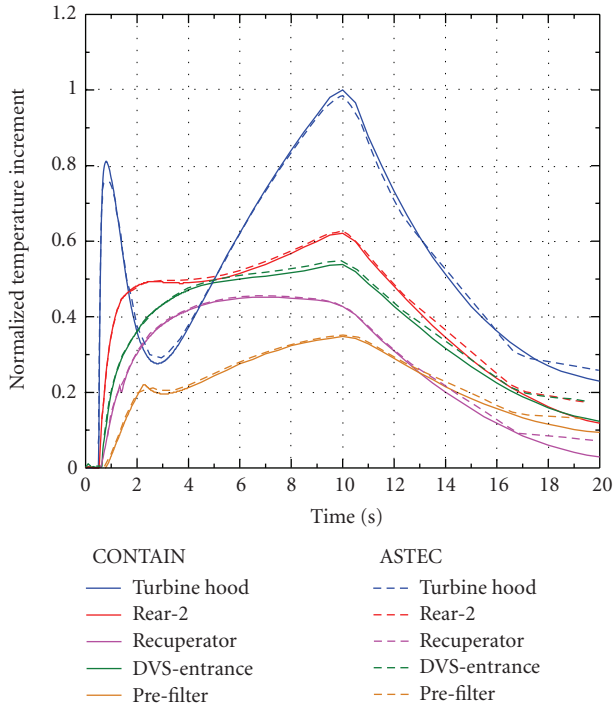

Figure 5: Temperature evolution in the main confinement compartments for the LB sequence.

sequence despite their model differences. That is, the diffusion flow is negligible compared with the convection flow.

Generally speaking, temperature follows pressure evolution since hot helium is the main heating mechanism, although the thermal inertia and heat transfer to the walls and structures result in the temperature evolution being slightly slower than the pressure evolution. Figure 5 shows the temperature evolution normalized to its maximum increment. In the turbine hood the temperature quickly increases, reaching a peak at 0.8 seconds. The temperature in other compartments behaves similarly to the trend in the turbine hood but with a smoothed evolution, which is more significant at volumes far from the discharge compartment (e.g., the filters) and for the largest ones (as in the recuperator).

As shown in Figure 5, both codes predict the same temperature evolution for the entire compartment. This fact reinforces the interpretation that the effect of ignoring the diffusive term in the evaluation of the gas flow rate is negligible in this sequence.

4.1.2. Aerosols. The aerosol concentration in a given compartment is governed by the inflow mass rate (carried by the inlet helium) and by losses due to deposition on walls and to the outlet mass rate to adjoining compartments. The highest concentration is expected in the discharge compartment, the turbine hood, whose maximum concentration (0.016% of c.i) is reached at 3.04 seconds. The compartments surrounding this chamber receive aerosols from it at a higher rate than those further away, for example, the DVS entrance or filter chambers. Thus, aerosol concentrations in the latter compartments are lower (see Figure 6). It is

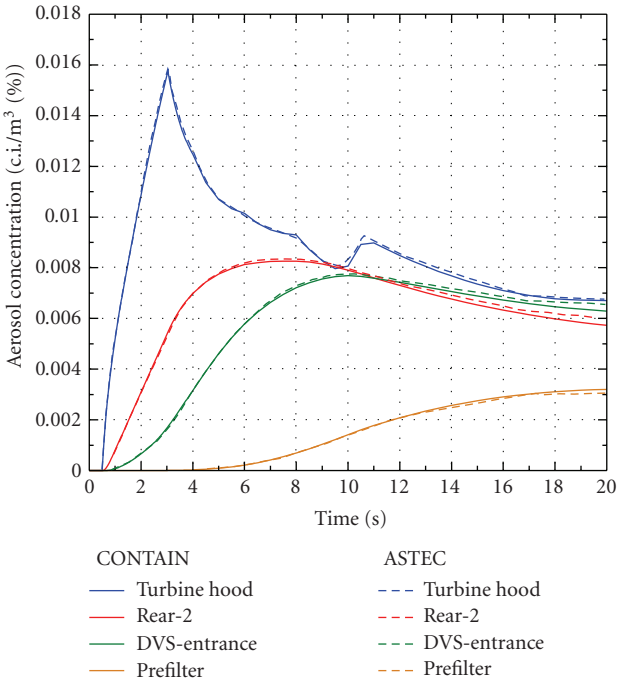

Figure 6: Airborne aerosol concentration evolution in the main confinement compartments for the LB sequence.

important to note that in the short term, that is, during the injection period and shortly after it, ASTEC and CONTAIN predict a very similar concentration evolution for all the compartments.

At a later time (between 50 seconds and 400 seconds), CONTAIN predicts higher concentrations in the turbine

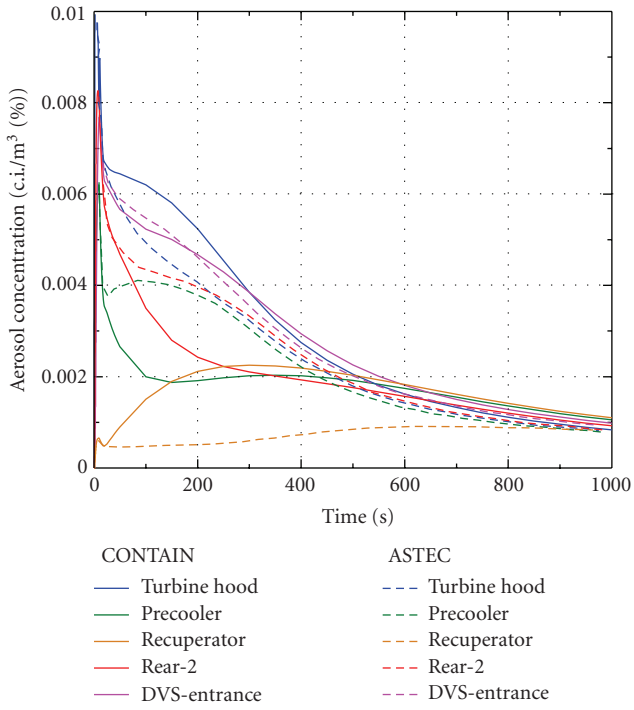

Figure 7: Airborne aerosol concentration evolution in the main confinement compartments for the LB sequence (long term simulation).

hood (around 30%) and lower concentrations in the rear compartments and precooler/intercooler volumes (30% and 50% lower, resp.), compared with ASTEC estimates. Nevertheless, at about 500 seconds the two simulations converge as is shown in Figure 7. This behaviour can be explained by the differences in the inter-compartment flow model rather than by differences in aerosol modelling. During the first phase of the accident the gas flow is mainly driven by pressure gradients but at about 20 seconds the pressure in the confinement reaches a steady value and the flow between compartments is mainly due to diffusion. Given the absence of the diffusive term in the CONTAIN momentum equations, the intercell flow predicted from then on by ASTEC is different to that of CONTAIN and, as a consequence, the net aerosol mass entering compartments is also different. Furthermore, the particle size distribution is influenced too since agglomeration is proportional to the particle concentration squared and the dominant depletion mechanisms, such as sedimentation, affect large particles preferentially.

In spite of these code-to-code differences in the in-confinement aerosol evolution, they hardly affect the aerosol mass balance at the end of the simulation (Table 1). Both codes predict that most of the injected mass (more than 60%) is deposited on the confinement walls and that most of this mass (above 95%) is depleted on the floors by gravitational settling. The second contribution to the aerosol mass balance is the aerosol remaining suspended in the confinement building at the end of the simulation (between 20–30%). The total mass released to the environment represents only about

Table 1: Aerosol mass balance for the LB sequence.

	ASTEC (% of c.i.)	CONTAIN (% of c.i.)
Airborne mass in the confinement	20.1	27.3
Released mass to the environment	0.6	1.6
Deposited mass on walls	61.4	64.8
Deposited mass in filters	17.9	14.4

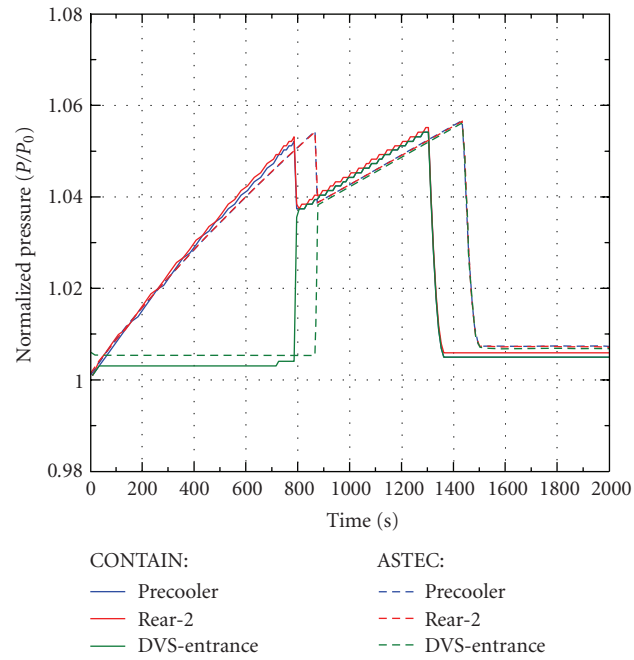

Figure 8: Pressure evolution in the main confinement compartments for the SB sequence.

1% of the confinement inventory (0.6% for ASTEC and 1.6 for CONTAIN results).

Although the aerosol models in both codes originate from the MAEROS code [5], there are some differences in the capabilities of each code. The most significant is that CONTAIN does not have a model for filter retention. This will cause the main difficulty in estimating the filtered and released mass in an HTR confinement analysis; however, an ad hoc calculation can be done after code simulation. Using CONTAIN output data of the prefilter aerosol concentration, flow through the filters and based on the filter efficiency, the filtered mass is calculated via the following expression:

$$M_{\text{fil}} = \varepsilon_{\text{fil}} \cdot \sum_{\text{chamber}} \sum_{t_i=t_0}^{t_{\text{end}}} C_{\text{aer},k}(t_i) \cdot G_{\text{fil},k}(t_i) \Delta t_i. \tag{10}$$

This method for calculating the filter retention introduces an error in the mass balance of about 8.1%.

Given the high gas flow rates attained in this scenario and the direction and cross-section changes in gas flows, particle impaction could become a significant depletion mechanism. As ASTEC and CONTAIN do not include models for this process, it should be expected that the above estimates are conservative.

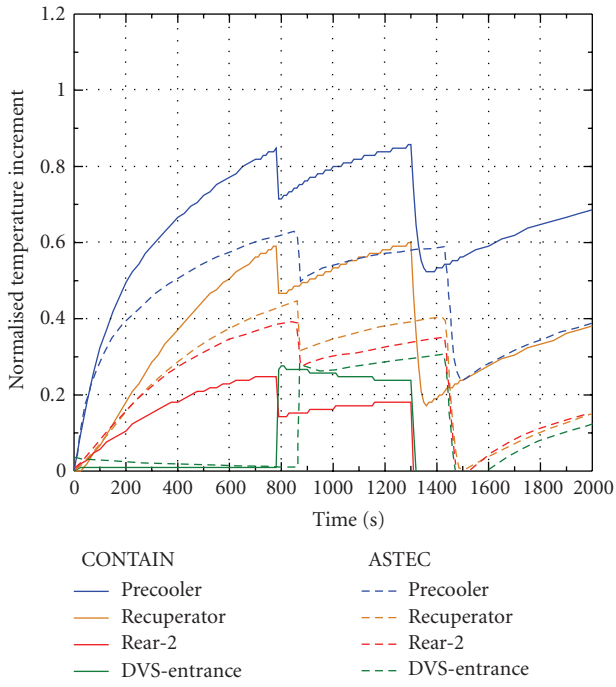

Figure 9: Temperature evolution in the main confinement compartments for the SB sequence (short term simulation).

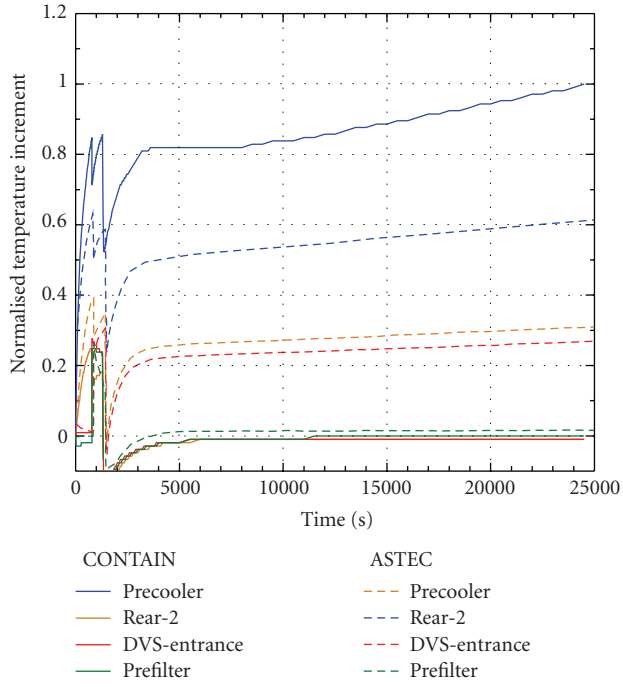

Figure 10: Temperature evolution in the main confinement compartments for the SB sequence (long term simulation).

4.2. Small Break Scenario. The general behaviour of the confinement is very different than that in the LB accident. Slow helium blowdown into the precooler compartment yields a smooth pressure increase so that effects of helium diffusion are nonnegligible compared with the convection driven force for gas flow.

4.2.1. Thermal-Hydraulics. The helium flow entering the precooler compartment is distributed to other PCU compartments and the pressure in the PCU building increases homogenously (Figure 8). Later on, at about 800 seconds, the rupture panels between the PCU compartment and the DVS break, the gas passes through the DVS to the filters chambers, breaks the rupture panels after the filters, and passes to the environment at 1400 seconds.

Slight differences are observed in the simulation of the ASTEC and CONTAIN codes. ASTEC predicts a slightly delayed rupture of panels between the PCU and DVS and between the DVS stack and the environment (800 and 1430 seconds); whereas CONTAIN predictions are 780 and 1300 seconds, respectively (Figure 8).

As in the previous case, the intercell flow model is responsible for most of the discrepancies in the codes estimates. As a consequence of the exchange enhancement driven by the diffusive term, ASTEC predicts a more uniform gas temperature in different chambers since hot helium is capable of reaching farther from the break point. This difference together with that in mole number in each cell is the basis of the pressure discrepancies between both codes.

Figure 9 shows that in the short term the temperature evolution follows the trend of the pressure (i.e., net helium injection into the compartment). In the long term, after the environment rupture panels break, the temperature increases slowly due to the long helium injection and maximum temperature is reached in the precooler compartment at the end of the simulation (Figure 10).

4.2.2. Aerosols. The effect of differences in the flow models is more evident in the simulation of the aerosol mass concentration in specific compartments. As mentioned previously, one of the main variables influencing the aerosol concentration is the balance of the inlet/outlet mass flow rate carried by the gas. Figure 11 plots the aerosol concentration predictions of some of the main compartments given by ASTEC and CONTAIN. Since ASTEC predicts higher gas flows and more homogeneous helium distribution in the confinement, the aerosol mass is also distributed more homogeneously in ASTEC calculation than in CONTAIN.

In spite of these large differences in the aerosol concentration the general behaviour of aerosols is similarly predicted by both codes. The total airborne and deposited mass in the entire PCU and DVS buildings is fairly similar in both code simulations as is shown in Figure 12, with the highest difference in the airborne mass occurring in the PCU compartments.

Concerning the aerosol mass balance, both codes predict that most of the injected dust mass (about 60%) is deposited on the confinement floor (Table 2). For ASTEC, the second contribution to the mass balance is the filter retention and thereafter the airborne mass. However, in CONTAIN more mass remains suspended in the confinement than retained in filters. The aerosol release to the environment is about 1% (0.7% for ASTEC simulation whereas CONTAIN estimates 1.2% of c.i.). The total aerosol mass differs in both codes, as

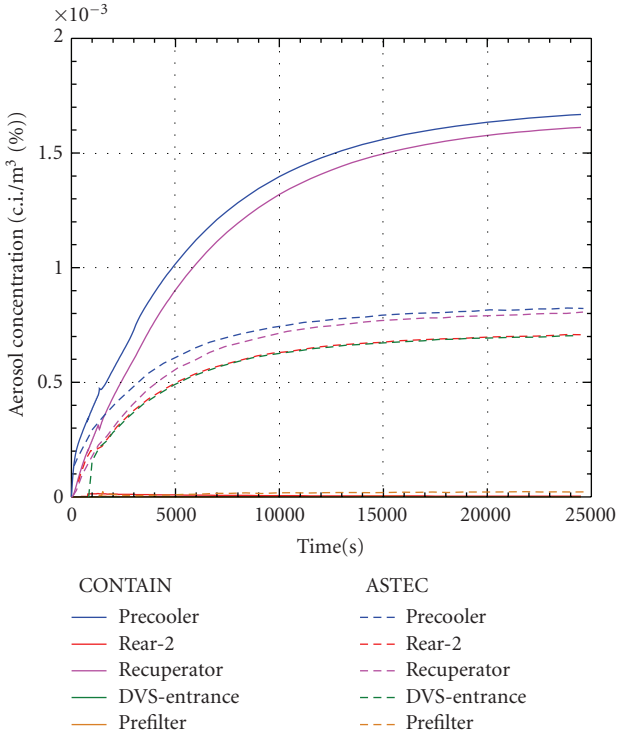

Figure 11: Aerosol concentration evolution in the main confinement compartments for the SB sequence.

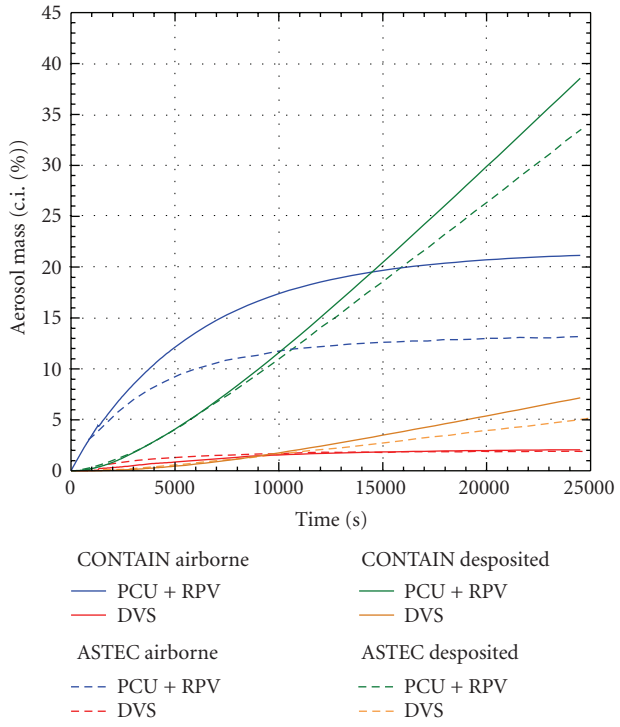

Figure 12: Airborne and deposited mass evolution in the confinement for the SB sequence.

Table 2: Aerosol mass balance for the SB sequence.

	ASTEC (% of c.i.)	CONTAIN (% of c.i.)
Airborne mass in the confinement	16.3	24.7
Released mass to the environment	0.7	1.2
Deposited mass on walls	61.0	56.8
Deposited mass in filters	22.0	10.6

in the case of the LB, because of the ad doc calculation of filter retention. In this calculation the difference is about 6.7% of the confinement inventory (Table 2).

For the SB accident, the aerosol mass entering the confinement is 2000 times lower than in the LB scenario and the injection time extends over more than 7 hours. However, comparison of Tables 1 and 2 shows that the aerosol mass balance, in terms of relative mass, is qualitatively similar in both scenarios.

5. Conclusions

Safety is a key aspect of nuclear systems development. Any innovative system, particularly HTR ones, requires a thorough safety study to be carried out, which includes accident analyses to demonstrate compliance with regulatory dose and risk limits for both the public and the worker during accident conditions. Confinement building performance is, therefore, a key element of the system. This paper has jointly explored two important issues: available simulation capabilities at hand and performance of postulated HTR confinement under prototypical accident conditions.

ASTEC and CONTAIN, although mainly developed in LWR field, have been shown to be largely applicable to HTR confinement scenarios. An estimate of the Knudsen number in expected conditions under HPB breaks accidents indicates that these scenarios lie in the continuum or slip flow regimes, well inside the range of validity of the models encapsulated within both codes.

Additionally, their simulation capabilities have been illustrated by comparing their response under two accident scenarios with breaks in the HPB: a large and a small break. In both sequences, the same hypotheses and approximations have been used for both code simulations. The main conclusions for this comparison from a thermal-hydraulic point of view are the following.

(i) ASTEC v1.3 and CONTAIN 2.0 predict very similar confinement performance in both magnitude and time.

(ii) Differences have been found in the inter-compartment gas flow modelling. These differences affect the gas composition in specific compartments but they do not result in any substantial discrepancy in the overall variables characterizing the scenario. The effect of these flow differences is more significant in the small break accident, where the injected helium and intercell flows are smaller and the flow is driven mainly by diffusion.

The main observations regarding aerosol behaviour are as follows.

(i) Most of the aerosol inventory coming into the confinement is depleted on the walls and only about 1% of the aerosol mass is released to the environment.

(ii) ASTEC v1.3 and CONTAIN 2.0 predict similar evolution of aerosols in the confinement, especially in the large break accident, even though the injected size distributions used in both codes are not entirely the same.

(iii) Minor differences in the aerosol concentration evolution in specific compartments have been found due to the differences in inter-compartment gas flow code estimates.

With regard to the availability of models, ASTEC has a specific model for aerosol retention in filters whereas CONTAIN does not have this feature available. This requires the user to set up an independent way of estimating the filtration effect in the case of CONTAIN. On the other hand, in the scenarios analysed, CONTAIN has demonstrated to be more robust under a large step injection of gas and aerosol.

Finally, even though the absence of a model for depletion by impaction in both codes leads to conservative results, in further studies it is recommended that the quantitative effect of this mechanism to be assessed.

Nomenclature

A: Flow path section
D: Diffusivity
C: Concentration of aerosols
C_C: Cunningham correction factor
C_{grav}: Gravitational collision efficiency
C_m: Constant
C_s: Constant
C_t: Constant
d: Particle diameter
F: Correction factor
G: Flow rate
g: Gravitation constant
k: Boltzmann constant
Kn: Knudsen number
L: Flow path length
M: Aerosol mass
P: Pressure
Q_T: Dissipation rate of the turbulent energy
R: Universal gass constant
T: Temperature
t: Time step
v: Velocity

Greek

β: Agglomeration coefficient
γ: Agglomeration shape factor
δ: Boundary layer thickness
ε: Retention efficiency
λ: Average free path length
λ: Heat conductivity
μ: Dynamic viscosity
ν: Kinematics viscosity
ρ: Density
χ: Dynamic shape factor
ζ: Flow resistance

Subscripts and Superscripts

aer: Aerosol
Brow: Brownian
c: Gas componenet
con: Convective
dif: Diffusion
dph: Diffusiophoresis
fil: Filter
g: Gas atmosphere
grav: Gravitational
i: Particle i
j: Particle j
k: Filter chamber index
p: Particle
s: Source compartment
set: Settling
t: Target compartment
tph: Thermophoresis

List of Acronyms

CFP: Coated fuel particle
DVS: Depressurization vent shaft
HPB: Helium pressure boundary
HTR: High temperature reactor
LB: Large break
LWR: Light water reactor
MMD: Mass median diameter
PCU: Power conversion unit
PRS: Pressure relief system
RPV: Reactor pressure vessel
SB: Small break

Acknowledgment

This work has been developed under the PBMR-CIEMAT agreement for confinement analysis.

References

[1] J. P. Van Dorsselaere and B. Schwinges, "Overview of the integral code ASTEC V1.3," IRSN Technical Note DPAM/ASTEC 2006-362, 2006, GRS Technical Note GRS ASTEC 06/02.

[2] K. K. Murata, "Code manual for CONTAIN 2.0: a computer code for nuclear reactor containment analysis," NUREG/CR-6533, SAND97/1735, 1997.

[3] M. Sitarski and J. H. Seinfeld, "Brownian coagulation in the transition regime," *Journal of Colloid And Interface Science*, vol. 61, no. 2, pp. 261–271, 1977.

[4] U. Wawrzik, P. Biedermann, and H. F. Oetjen, "Staub im Avr-Reaktor; Verhalten Bei Transienten Strömungsbedingungen," in *Proceedings of the Jahrestagung Kerntechnik*, Karlsruhe, Germany, 1987.

[5] F. Gelbard, "MAEROS users manual," NUREG/CR-1931, SAND80-0822, 1982.
[6] W. C. Hinds, *Aerosol Technology*, John Wiley & Sons, New York, NY, USA, 2nd edition, 1999.
[7] J. R. Brock, "On the theory of thermal forces acting on aerosol particles," *Journal of Colloid Science*, vol. 17, no. 8, pp. 768–780, 1962.
[8] L. Talbot, R. K. Cheng, R. W. Schefer, and D. R. Willis, "Thermophoresis of particles in a heated boundary layer," *Journal of Fluid Mechanics*, vol. 101, part 4, pp. 737–758, 1980.
[9] B. K. Annis, "Thermal creep in gases," *The Journal of Chemical Physics*, vol. 57, no. 7, pp. 2898–2905, 1972.
[10] N. A. Fuchs, *The Mechanics of Aerosols*, Pergamon Press Book, New York, NY, USA, 1964.
[11] P. G. Saffman and J. S. Turner, "On the collision of drops in turbulent clouds," *Journal of Fluid Mechanics*, vol. 1, pp. 16–30, 1956.
[12] G. Weber, "ASTEC V0 Description of aerosol models in the containment part of ASTEC (CPA)," ASTEC-V0/DOC/99-20, 1999.
[13] W. Klein-Hessling and B. Schwinges, "ASTEC V0. CPA module program reference manual," ASTEC-V0/DOC/01-34, 1998.
[14] A. Pitso, "MPS pipe break analysis calculation report," private communication, 2007.
[15] K. Sawa, T. Nishimoto, and Y. Miyamoto, "Experimental study of dust behaviour during depressurization," *Journal of Nuclear Science and Technology*, vol. 29, no. 10, pp. 1018–1025, 1992.

Hindawi Publishing Corporation
Science and Technology of Nuclear Installations
Volume 2009, Article ID 214285, 7 pages
doi:10.1155/2009/214285

Research Article

Physics Features of TRU-Fueled VHTRs

Tom G. Lewis III and Pavel V. Tsvetkov

Department of Nuclear Engineering, Texas A&M University, 129 Zachry Engineering Center, 3133 TAMU, College Station, TX 77843-3133, USA

Correspondence should be addressed to Pavel V. Tsvetkov, tsvetkov@tamu.edu

Received 9 April 2009; Accepted 14 April 2009

Recommended by Jan Leen Kloosterman

The current waste management strategy for spent nuclear fuel (SNF) mandated by the US Congress is the disposal of high-level waste (HLW) in a geological repository at Yucca Mountain. Ongoing efforts on closed-fuel cycle options and difficulties in opening and safeguarding such a repository have led to investigations of alternative waste management strategies. One potential strategy for the US fuel cycle would be to make use of fuel loadings containing high concentrations of transuranic (TRU) nuclides in the next-generation reactors. The use of such fuels would not only increase fuel supply but could also potentially facilitate prolonged operation modes (via fertile additives) on a single fuel loading. The idea is to approach autonomous operation on a single fuel loading that would allow marketing power units as nuclear batteries for worldwide deployment. Studies have already shown that high-temperature gas-cooled reactors (HTGRs) and their Generation IV (GEN IV) extensions, very-high-temperature reactors (VHTRs), have encouraging performance characteristics. This paper is focused on possible physics features of TRU-fueled VHTRs. One of the objectives of a 3-year U.S. DOE NERI project was to show that TRU-fueled VHTRs have the possibility of prolonged operation on a single fuel loading. A 3D temperature distribution was developed based on conceivable operation conditions of the 600 MWth VHTR design. Results of extensive criticality and depletion calculations with varying fuel loadings showed that VHTRs are capable for autonomous operation and HLW waste reduction when loaded with TRU fuel.

1. Introduction

The current waste management strategy for spent nuclear fuel (SNF) mandated by the US Congress is the disposal of high-level waste (HLW) in a geological repository at Yucca Mountain [1]. Ongoing efforts on closed-fuel cycle options and difficulties in opening and safeguarding such a repository have led to investigations of alternative waste management strategies [2]. One potential strategy for the US fuel cycle would be to make use of fuel loadings containing high concentrations of transuranic (TRU) nuclides in the next generation reactors [1, 3]. The use of such fuels would not only increase fuel supply but could also potentially facilitate prolonged operation modes (via fertile additives) on a single fuel loading [4, 5].

To meet the demand for clean and reliable energy sources, the GEN-IV International Forum (GIF) was founded in early 2000 to investigate and develop technologies that could be incorporated into the next generation of power reactors [6, 7]. Through this international partnership around 100 different systems were evaluated to meet goals set forth by the forum. Of the nearly 100 systems studied by GIF, six were chosen in late 2002 to best meet goals set by the forum. Of these six concept systems, the VHTR is the most likely GEN IV system to be available in the near term.

The VHTR technology is based on the concepts originally developed for the US Fort St. Vrain and Peach Bottom reactors, as well as on the extensive international experience involving such facilities as the German AVR and THTR, Swiss PROTEUS, Chinese HTR-10, Japanese HTTR, and Russian GROG and ASTRA. The VHTR concept should be designed as a high-efficiency system capable of supplying electricity and process heat to a broad spectrum of high-temperature and energy-intensive processes. The reference reactor is a 600 MWth, helium-cooled core connected to an intermediate heat exchanger to deliver process heat, although direct cycles without the need of a heat exchanger have been proposed [7].

Table 1: Parameters of the Reference VHTR Design.

Parameter	Value	Parameter	Value
Fuel	UO_2	Power (MW_{th})	600
Enrichment (%)	15	Power Density (W/cm^3)	6.9
Coolant	He	Pressure (MPa)	7.0
		Inlet/Outlet Temperature (°C)	490/950
# of Columns	102	# of fuel columns	66
		# of control columns	36
		# of blocks/column	13
Block Pitch (cm)	36	# of fuel pins/fuel block	32
Block Height (cm)	58	# of B_4C rods/fuel block	2
		Control rods/control block	2
		Emergency rods/control block	1
		Compact pitch (cm)	5.15
		Fuel hole radius (cm)	4.1
		Compact inner radius (cm)	0.5
		Compact outer radius (cm)	1.3
Packing (%)	30	10.41 g/cm^3 kernel radius (cm)	0.02985
		1.14 g/cm^3 buffer radius (cm)	0.03588
		1.89 g/cm^3 PyC1 radius (cm)	0.03895
		3.20 g/cm^3 SiC radius (cm)	0.04184
		1.87 g/cm^3 PyC2 radius (cm)	0.04645
		Matrix (g/cm^3)	1.77
		Block (g/cm^3)	1.69

The remarkable capability of TRISO-coated fuel particles to withstand radiation damage without failing allows for their use as a high burnup fuel form, as demonstrated in the "Deep Burn Concept" proposed by General Atomics (GAs) [5]. To account for radiation damage effects, fuel performance limits are expressed in terms of fast neutron fluence. For TRISO particles, the fast neutron fluence limits, depending on TRISO configuration, are around 5×10^{25} n/m^2 [8]. Utilization of TRUs/MAs in VHTRs facilitates development of advanced fuel cycles and supports fuel supply sustainability. Under certain spectral conditions, TRUs/MAs would be able to contribute to a core neutron balance compensating for depletion. The resulting self-stabilization of advanced actinide fuels is expected to prolong operation on a single fuel loading up to lifetimes limited by structural/integrity characteristics [4]. With spectrum shifting, there is a possibility to use VHTRs in waste management. The spectrum shifting takes advantage of the more favorable fission cross-sections for nuclides in TRUs at higher energies.

A TRUs/MAs-bearing fuel is the major challenge in the development of the partitioning and transmutation engineering technologies. To support analysis of the VHTR configurations with advanced actinide fuels, the present studies were focused on actinide compounds that are currently being considered and/or are under development for use as TRUs/MAs-bearing transmutation fuels [5]. This information is used to facilitate realistic studies of the VHTRs with MAs. The utilization of TRU/MAs, from light-water reactor (LWR) fuel, for the prolonged-life VHTRs would reduce the need for the creation of more geological repository volume per decade of reactor operation [9].

2. Reference VHTR Configuration

In the present analysis, the TRU-fueled VHTR blocks have been designed using the HTTR geometry data [10]. Table 1 summarizes parameters of the reference VHTR design. To assure comprehensive and realistic assessment, extensive benchmark evaluations were performed based on the HTTR experimental program results [4, 10]. Obtained benchmark results are in agreement with the available HTTR data and confirm applicability of the chosen modeling approach as it described in what follows [4].

The overall layout of the basis reference case is developed according to the VHTR/NGNP specifications. The reactor is assumed to be operated at 600 MWth. [11] The major difference with the VHTR/NGNP point design is that the reference case uses HTTR block specifications.

3. Prototypic PWR Spent Fuel Composition

To assure realistic quantification of the advanced actinide fuels, the characteristics of the materials, which DOE has considered for disposal in the proposed Yucca Mountain repository, are used to derive the reference nuclide distributions in the present analysis. The published final environmental impact statement data are the basis for the

Table 2: PWR TRU vector (41,200 MWd/MTHM, 3.75% BOL enrichment, 23 years decay).

Element	Nuclide	Decay Heat (W/g)	TRU Composition (atom %)
Np	^{237}Np	0.00002	6.121
Pu	^{238}Pu	0.56000	1.986
	^{239}Pu	0.00200	51.718
	^{240}Pu	0.00700	21.899
	^{241}Pu	0.00400	4.104
	^{242}Pu	0.00010	4.451
Am	^{241}Am	0.11000	8.250
	^{242m}Am	—	0.020
	^{243}Am	0.00700	1.230
Cm	^{243}Cm	1.70000	0.003
	^{244}Cm	2.80000	0.194
	^{245}Cm	—	0.021
	^{246}Cm	—	0.003
			100.00

derived TRU composition used in the present analysis [9]. Table 2 provides the TRU composition that can be obtained for typical PWRs assuming burnup levels of 41.200 MWd/MTHM followed by cooling for 23 years.

4. Methodology

The analysis is performed using the ORNL SCALE 5.1 code system, and MatLab tool boxes. The code systems and tools for evaluations of uncertainty effects (nuclear and design/performance uncertainties) were developed on the basis of MatLab tool boxes and environments to support uncertainty analysis methodologies. The chosen approach links the applied neutronics code system and the generalized codes for universal sensitivity analysis, calibration, and uncertainty evaluations in a framework.

The applied overall computational approach takes advantage of the whole-core exact geometry Monte Carlo-deterministic analysis methodology that has been implemented for coupled design studies of VHTRs with TRUs. Figure 1 shows the major modules and the code system framework formed and implemented for studies presented in this research. The neutronics analysis using a 3D whole-core VHTR model was performed using the ORNL SCALE code system [12]. The standard SCALE 5.1 TRITON sequence has been upgraded to allow fuel cycle modeling accounting for double heterogeneity effects. A combination of Matlab, Excel, and Perl was used to build SCALE input files and analyze SCALE output data as shown in Figure 1.

CSAS25 is one of several control sequences within CSAS that uses KENO V.a to evaluate criticality of 3D systems. CSAS25 is used exclusively in this research for the determination of VHTR performance characteristics at the beginning of life (BOL). CSAS25 allows for near-explicit accounting for lattice effects due to double heterogeneity

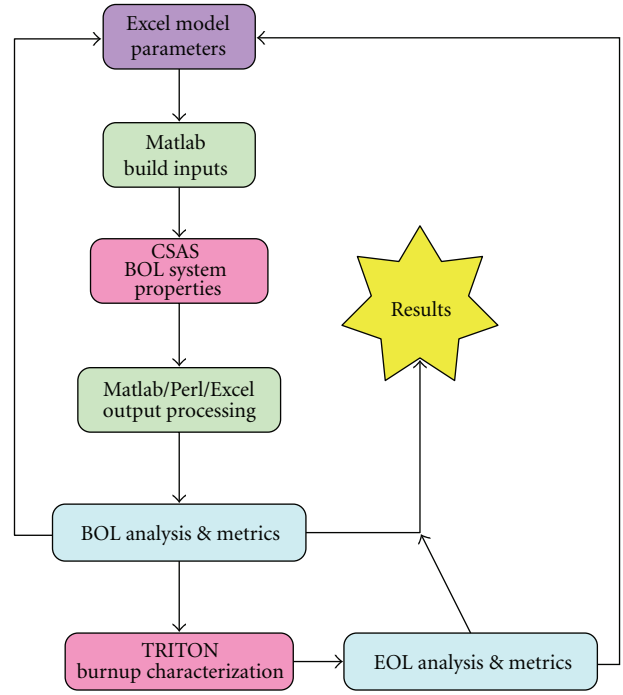

Figure 1: Applied computer code system.

features that are characteristic for all HTGRs including VHTRs.

Double heterogeneity can be thought of as a double-level geometry. In VHTRs, the first geometry level is formed by randomly-distributed TRISO-coated particles within a graphite matrix of the fuel compact. The second level is formed by a regular hexagonal lattice of fuel compacts within fuel blocks. A special treatment must be used for such systems because of substantial differences in neutron distributions at each heterogeneity level. Each compact has a fuel region containing thousands of microparticles that form a universe, which clearly exhibits features of an infinite lattice by itself. Only peripheral particles feel the presence of neighboring compacts. As a result, the core neutron distribution is formed by neutron media within each compact and then at the block and the whole core level.

To illustrate physics features of VHTRs and how they are accounted for in the applied multi-heterogeneity modeling approach, the fluxes calculated with SCALE 5.1/CSAS25 at various multiheterogeneity treatment levels are shown in Figure 2:

Infinite TRISO lattice (CENTRM calculations)—the calculations are performed at the infinite TRISO lattice level accounting explicitly for TRISO micro-particles and graphite matrix. The observed hard spectrum is the result of a closed packed lattice with the limited amount of moderating materials (TRISO coatings and matrix graphite only). These calculations are performed to prepare shielded cross-sections for compact lattice calculations.

Infinite compact lattice (CENTRM calculations)—the calculations are performed at the infinite compact lattice level with properly homogenized fuel regions in compacts

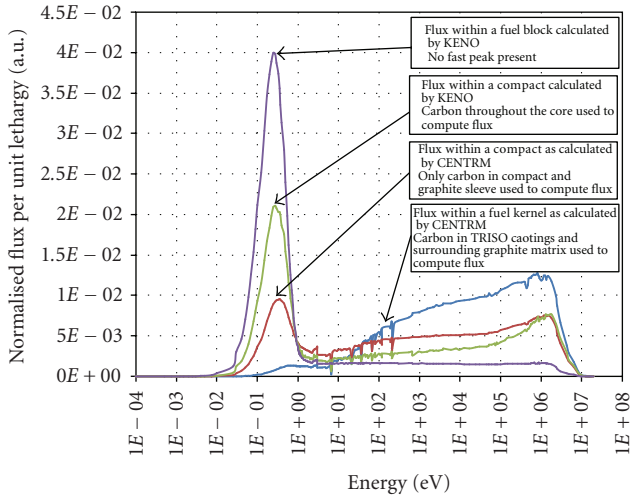

Figure 2: Fluxes in VHTRs at different levels of the double heterogeneity treatment.

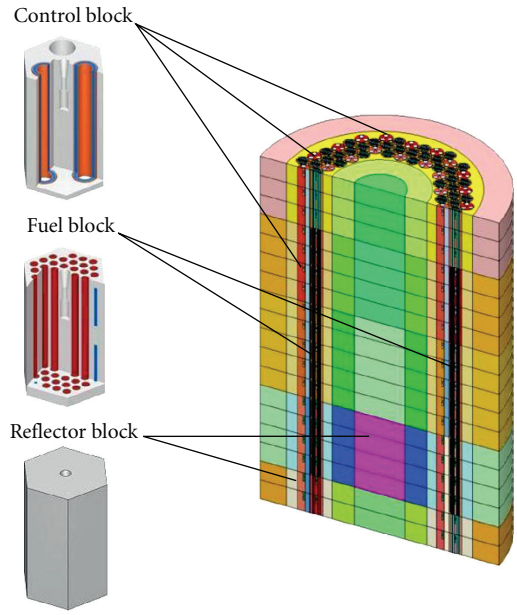

Figure 3: 3D whole-core model of the reference VHTR configuration.

using cross-sections from the earlier step. At this level, the model includes both the homogenized mix of TRISO microparticles and compact matrix graphite and the graphite block graphite. Fuel compact external dimensions and their arrangement are preserved. Because of the significantly larger amount of moderating materials, the compact lattice flux exhibits the well-defined thermal peak. These calculations are performed to prepare cross-sections for use in whole-core Monte Carlo calculations with KENO V.a.

Finite compact lattice (KENO V.a calculations)—the calculations are performed at the whole-core exact geometry level using the homogenized cross-sections for compact fuel regions. The difference between infinite and finite lattice calculations are clearly visible and are due to the increased amount of moderating materials as well as fast neutron streaming through various passages in the VHTR core hexagonal block assembly.

Figure 2 is also showing the overall VHTR block-averaged neutron distribution that was produced with multi-group cross-sections prepared following the lattice/configuration structures as described earlier.

The SCALE/TRITON was developed to handle 2D and 3D depletion scenarios such as axial enrichment of boiling water reactors (BWRs) and the effects associated with strong absorbers. There are 5 TRITON sequences, each one having unique abilities while sharing common subroutines. In this research, the TRITON T5-DEPL sequence was used with a modification to allow for depletion of double heterogeneous materials. This sequence uses the KENO V.a functional module at the 3D whole-core modeling level.

The model was developed taking advantage of the robust capabilities of SCALE 5.1, including the complexity of adding a temperature distribution to the model. This temperature distribution was implemented in the VHTR model through additional materials and regions. This is exemplified in the most complex model, where a total of 511 different materials were used to encompass major features of a VHTR. These features range from graphite blocks to the individual coatings of TRISO particles. The sequential creation of SCALE inputs and their corresponding output required an automated process. This process was managed via the Matlab script that was capable of producing and managing the creation of inputs and postprocessing evaluations of the corresponding outputs. Figure 3 shows the applied 3D whole-core VHTR model [11].

The geometry of the VHTR was created for use with SCALE 5.1 sequences focusing on KENO V.a. at the whole-core modeling level. As described earlier, the model created is a near exact depiction of the expected physical description of a power-size VHTR. The fundamental building blocks of the reactor (e.g., fuel blocks and its constituents) and the ratio of these blocks (control rod guide blocks to fuel block ratio) to one another are based on HTTR design parameters, while the overall configuration of the reactor has been developed following the DOE VHTR design requirements. The modeling adequacy is confirmed by performing series of experiment-to-code benchmark evaluations [4].

5. Parametric Analysis at the Beginning of Life Conditions

The series of BOL VHTR configurations were analyzed using the CSAS25 sequence of the SCALE 5.1 code system. Analysis of BOL cores is important to determine systems with acceptable safety characteristics, as well as a desirable BOL reactivity margins. Further analysis was done to determine system's performance characteristics during operation.

Figure 4 shows the 3D BOL neutron distribution in the reference LEU-fueled VHTR configuration. The specification of this design is given in Table 1. The neutron leakage effects at the core top and bottom resulted in decreasing thermal

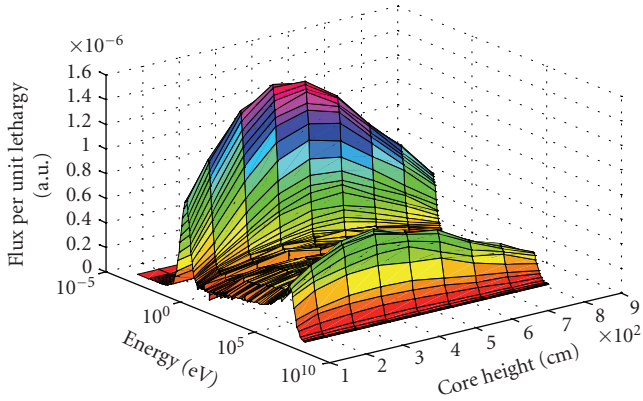

Figure 4: 3D space-energy neutron distribution in the reference LEU-fueled VHTR (neutron fluxes in compacts of the innermost fuel ring as a function of their axial locations in the VHTR core).

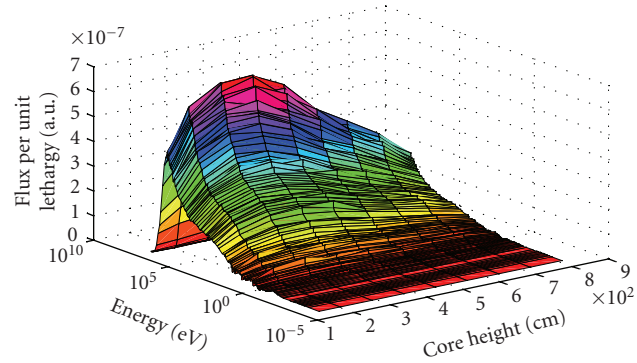

Figure 5: 3D space-energy neutron distribution in the TRU-fueled VHTR (neutron fluxes in compacts of the innermost fuel ring as a function of their axial locations in the TRU-fueled core (55.86% fissile atom fraction, C/HM = 25)).

Table 3: Reactor physics parameters for three and four ring LEU-VHTR configurations.

Number of rings	Enrichment	Effective multiplication factor	Average neutron lethargy causing fission (eV)
3	3	0.863	n/a
3	8	1.181	0.2188
3	9	1.214	0.2316
3	10	1.239	0.2463
3	15	1.328	0.3168
3	20	1.409	0.3994
3	40	1.481	0.8380
4	3	0.903	n/a
4	8	1.218	0.2229
4	9	1.252	0.2106
4	10	1.278	0.2524
4	15	1.365	0.3295
4	20	1.414	0.4158
4	40	1.510	0.8926

and fast flux peak magnitudes. The distribution is typical for LEU VHTRs and will be used as the reference basis for evaluations of TRU-fueled VHTRs.

In the present analysis, recognizing configuration flexibility of VHTRs, the annular cores with three and four fuel block rings are taken into consideration. The effect of enrichment on the basic reactor physics characteristics of VHTRs is illustrated in Table 3. Table 3 illustrates "number of rings" effects in LEU-fueled systems by providing the multiplication factors and the corresponding neutron lethargies causing fissions as a function of enrichment. The lethargies are given to illustrate anticipated spectral changes due to enrichment and core configuration variations.

Table 4 illustrates the corresponding effects of design modifications in the TRU-fueled systems. The analysis was performed assuming 100% TRU-filled kernels. Because the fissile content of TRUs is determined by the composition, the carbon-to-heavy metal (C/HM) atom ratio is varied inside a fuel compact for VHTRs with TRUs. In the VHTR systems, these variations can be accomplished by changing numbers of TRISO particles per compact. As for the LEU-cases, lethargies are provided to characterize spectral fluctuations in response to the considered design modifications. The packing fractions and the corresponding C/HM ratios are provided. It has to be noted that this analysis is performed for the TRU-fueled VHTR configurations with packing fractions under 8%. These packing fractions are consistent with currently feasible TRU loadings per compact and the refueling intervals of approximately 2 years [5, 8].

As shown later (see Table 6), the packing fractions under 8% lead to relatively short refueling intervals. Only the TRU-fueled systems with packing fractions over 8% are capable for prolonged operation on a single fuel loading assuming the same power density as in the reference configuration. These high-TRU-content systems are very different from the conventional LEU-fueled VHTRs because the effect of C/HM on the flux in the TRU-fueled VHTRs is far more complex when compared to the effects on LEU systems. For comparison, the flux shown in Figure 5 is for a TRU-fueled VHTR with a C/HM atom ratio of 25. The flux shape in this reactor has no thermal peak present in the compact. This suggests that low C/HM TRU-fueled systems are capable of utilizing fast neutrons much better than higher ratio systems. The ability of these systems to manage utilization of neutrons is beneficial for optimization efforts to attain prolonged refueling intervals.

Reactivity coefficients were calculated to evaluate safety characteristics of TRU-fueled VHTRs. Four isothermal VHTR configurations were modeled with CSAS25. The results are shown in Table 5. In these studies, the C/HM atom ratios are varies from 70 to 25 for the TRU-fueled systems and from 80 to 30 for the LEU-fueled systems. The variations are chosen to achieve the same neutron multiplication levels in TRU- and LEU-fueled systems.

In TRU systems, the low C/HM atom ratio leads to the temperature reactivity coefficient that is approximately two times larger in its absolute value than the temperature

Table 4: Reactor physics parameters for three and four ring TRU-VHTR configurations.

Number of rings	Packing fraction (%)	C/HM	Effective multiplication factor	Average neutron lethargy causing fission (eV)
3	2.0	733	1.0759	0.25
3	3.0	520	1.0840	0.27
3	4.0	414	1.0808	0.29
3	6.0	308	1.0645	0.39
3	8.0	255	1.0521	0.53
4	2.0	632.44	1.1134	0.25
4	3.0	504.66	1.1155	0.27
4	4.0	419.47	1.1105	0.30
4	6.0	249.10	1.0945	0.41
4	8.0	176.08	1.0818	0.55

Table 5: BOL isothermal temperature reactivity coefficients of VHTRs with LEU and TRU.

Case summary	Temperature reactivity coefficient ($\Delta k/k/K$)
LEU, C/HM = 80, Enrichment = 15%	−1.95E-05
LEU, C/HM = 30, Enrichment = 15%	−3.43E-05
TRU, C/HM = 70	−5.07E-05
TRU, C/HM = 25	−7.16E-05

Table 6: Lifetime of VHTRs with TRUs*.

C/HM atom ratio	Core life [years]
9	9
11	8
23	7
33	6
53	6
112	5
229	2

* Packing fraction of 30% corresponds to the C/HM ratio of 138 (12467 particles per compact).

reactivity coefficient in the corresponding low C/HM LEU-system.

6. Single-Batch Operation of the TRU-Fueled VHTRs

Several TRU-fueled VHTR configurations have been analyzed to determine the effect of the C/HM atom ratio on the single-batch core lifetime. All of the considered TRU-fueled VHTR configurations were developed on the basis of the developed reference VHTR design (see Table 1). As illustrated in Table 6, the longest core lifetimes are shown to be approximately nine years for TRU-VHTRs.

The refueling interval was constrained by excess reactivity requirements although fast fluence levels were evaluated. It was assumed that the effective multiplication factor should not drop below 1.01 during operation. This value was chosen as the EOL criterion.

The computed fast fluences are within published performance limits for all considered LEU- and TRU-fueled VHTRs [8]. For example, the TRU-fueled VHTR system is capable of operation for approximately 4 years assuming the volume fraction of 30% (C/HM = 138). The corresponding fast fluence is 2.14×10^{22} n/cm^2. The extended batch mode operation without refueling can be prolonged further by decreasing power densities in the TRU-fueled VHTR cores.

7. Conclusions

The effects of C/HM atom ratio variations on BOL excess reactivity levels and neutron distributions in the VHTR configurations have been analyzed by varying the packing fraction of TRISO particles inside the compact. Larger values of the C/HM atom ratios result in smaller BOL excess reactivity levels for the VHTR configurations with the same refueling interval. Consequently, these design adjustments can be used as a tool to minimize reactivity swings in the feasible VHTR design. The C/HM atom ratio adjustments allow controlling neutron distributions in the VHTR cores and potentially may lead to prolonged refueling intervals. Although indicating some technical limitations and challenges, studies of VHTRs with TRUs/MAs definitely suggest promising performance and possibility to utilize the core configurations with TRUs/MAs gaining prolonged operation and self-sustainability.

Fluence-related limitations (radiation damage) are the most significant constraints on achievable operation times. This constraint can be relaxed or even eliminated by reducing power density levels and using advanced radiation-tolerant materials for extended-life VHTR configurations. However, the use of advanced materials will adversely impact economics characteristics. It is instructive to note that acceptable safety characteristics have been observed for all configurations.

The extended-lifetime approach could reduce the technical need for additional repositories and should also improve

marketability of the Generation IV VHTR designs as small-to-medium internationally deployable energy sources for electricity generation and industrial heat applications. The TRU-fueled VHTRs offer performance characteristics that would be difficult to achieve in analogous LEU-fueled systems: almost a decade-long batch mode operation without intermediate refueling; significant reductions of initial excess reactivity levels (smaller lifetime reactivity swings); and inherently higher achievable burnup levels.

Disclaimer

This paper was prepared as an account of work sponsored by an agency of the United States Government. Neither the United States Government nor any agency thereof, nor any of their employees, makes any warranty, express, or implied, or assumes any legal liability or responsibility for the accuracy, completeness, or usefulness of any information, apparatus, product, or process disclosed, or represents that its use would not infringe privately owned rights. Reference herein to any specific commercial product, process, or service by trade name, trademark, manufacturer, or otherwise does not necessarily constitute or imply its endorsement, recommendation, or favoring by the United States Government or any agency thereof. The views and opinions of authors expressed herein do not necessarily state or reflect those of the United States Government or any agency thereof.

Nomenclature

AFCI: Advanced fuel cycle initiative
BOL: Beginning-of-life
C/HM: Carbon-to-heavy metal atom ratio
DB: Deep-burn concept
EOL: End-of-life
HLW: High level waste
HM: Heavy metal
HTGR: High temperature gas-cooled reactor
LANL: Los Alamos National Laboratory
LEU: Low-enriched uranium
LLW: Low level waste
LWR: Light water reactor
MA: Minor actinides (Np, Am, Cm)
NERI: Nuclear energy research initiative
ORNL: Oak Ridge National Laboratory
P&T: Partitioning and transmutation
SNF: Spent nuclear fuel
TRU: Transuranic nuclides
VHTR: Very high temperature reactor
a.u.: Arbitrary units

Acknowledgment

This paper is based upon work supported by the US Department of Energy under Award Number DE-FC07-05ID14655 (05-094).

References

[1] E. ElBaradei, "Nuclear power and sustainable development," IAEA, 2006.
[2] "Report to Congress on advanced fuel cycle initiative: the future path for advanced spent fuel treatment and transmutation research," Tech. Rep. 03-GA50439-06, U.S. DOE, 2003.
[3] "Report to Congress on Spent Nuclear Fuel Recycling Program Plan," U.S. DOE, 2006.
[4] P. V. Tsvetkov, D. E. Ames II, A. B. Alajo, and T. G. Lewis III, "Spectrum shifting as a mechanism to improve performance of VHTRs with advanced actinide fuels," *Nuclear Engineering and Design*, vol. 238, no. 8, pp. 1958–1964, 2008.
[5] T. Kim, T. Taiwo, R. Hill, W. Yang, and F. Venneri, "A feasibility study of reactor-based deep-burn concepts," Tech. Rep. ANL-AFCI-155, Argonne National Laboratory, 2005.
[6] Office of Nuclear Energy, Science, and Technology, "The US generation IV implementation strategy," 03-GA50439-06, United States of America, 2003.
[7] "Generation IV Nuclear Energy Systems Ten Year Program Plan Volume I," Office of Nuclear Energy, Science, and Technology, U.S. DOE, March 2005.
[8] D. Hanson, "Screening Tests for Selection of VHTR Advanced Fuel," General Atomics, San Diego, Calif, USA, 2003.
[9] "Final Environmental Impact Statement for a Geologic Repository for the Disposal of Spent Nuclear Fuel and High-Level Radioactive Waste at Yucca Mountain, Nye County, Nevada," Vol. 2, Appendix A, "Inventory and Characteristics of Spent Nuclear Fuel, High-Level Radioactive Waste, and Other Materials", DOE/EIS-0250, U.S. DOE, 2002.
[10] "Evaluation of high temperature gas-cooled reactor performance: benchmark analysis related to initial testing of the HTTR and HTR-10," Tech. Rep. IAEA-TECDOC-1382, International Atomic Energy Agency, Vienna, Austria, 2003.
[11] P. M. Mills, R. Soto, and G. Gibbs, "Next generation nuclear plant pre-conceptual design report," INL Report INL/EXT-07-12967 Rev. 1, NGNP Project, 2007.
[12] "SCALE: a modular code system for performing standardized computer analyses for licensing evaluation," Tech. Rep. ORNL/TM-2005/39, Ver. 5.1, Oak Ridge National Laboratory, Oak Ridge, Tenn, USA, November 2006.

Hindawi Publishing Corporation
Science and Technology of Nuclear Installations
Volume 2009, Article ID 749736, 13 pages
doi:10.1155/2009/749736

Research Article

The Use of Th in HTR: State of the Art and Implementation in Th/Pu Fuel Cycles

Guido Mazzini,[1] Eleonora Bomboni,[1] Nicola Cerullo,[1,2] Emil Fridman,[3] Guglielmo Lomonaco,[1,2] and Eugene Shwageraus[4]

[1] *Department of Mechanical, Nuclear and Production Engineering (DIMNP), University of Pisa, CIRTEN, Largo L. Lazzarino No. 2, 56126 Pisa, Italy*
[2] *Energy and Environmental Conditioning Department (DIPTEM), University of Genova, Via all'Opera Pia No. 15/a, 16145 Genova, Italy*
[3] *Accident Analysis Division (FWSS), Forschungszentrum Dresden-Rossendorf (FZD), P.O. Box 51 01 19, 01314 Dresden, Germany*
[4] *Department of Nuclear Engineering, Ben Gurion University of the Negev, P.O. Box 653, 84105 Beer Sheva, Israel*

Correspondence should be addressed to Nicola Cerullo, cerullo@docenti.ing.unipi.it

Received 28 March 2009; Accepted 1 September 2009

Recommended by Jim Kuijper

Nowadays nuclear is the only greenhouse-free source that can appreciably respond to the increasing worldwide energy demand. The use of Thorium in the nuclear energy production may offer some advantages to accomplish this task. Extensive R&D on the thorium fuel cycle has been conducted in many countries around the world. Starting from the current nuclear waste policy, the EU-PUMA project focuses on the potential benefits of using the HTR core as a Pu/MA transmuter. In this paper the following aspects have been analysed: (1) the state-of-the-art of the studies on the use of Th in different reactors, (2) the use of Th in HTRs, with a particular emphasis on Th-Pu fuel cycles, (3) an original assessment of Th-Pu fuel cycles in HTR. Some aspects related to Thorium exploitation were outlined, particularly its suitability for working in pebble-bed HTR in a Th-Pu fuel cycle. The influence of the Th/Pu weight fraction at BOC in a typical HTR pebble was analysed as far as the reactivity trend versus burn-up, the energy produced per Pu mass, and the Pu isotopic composition at EOC are concerned. Although deeper investigations need to be performed in order to draw final conclusions, it is possible to state that some optimized Th percentage in the initial Pu/Th fuel could be suggested on the basis of the aim we are trying to reach.

1. Introduction

Since the beginning of the nuclear age, the possibility of using Thorium as a nuclear fuel in thermal reactors appeared a very promising alternative to uranium exploitation. First of all, Thorium natural resources are three times more abundant than Uranium ones. What's more, the lower mass number of the fertile element (Th^{232}) entails a by far smaller build-up of high mass number TRU, which are as known responsible for the most of the long-term radiotoxicity of the nuclear waste. On the other hand, natural Thorium is composed of a single isotope (Th^{232}) that is not fissile, but only fertile. By a neutron capture, Th^{232} transmutes into U^{233}, which is a fissile nuclide characterized by an excellent neutronic behaviour in the thermal range [1, 2]. Hence, Th-based fuels need some amounts of U^{235} or Pu acting as a driver. Conversely, this kind of fertilization process produces, by $(n, 2n)$ reaction, some U^{232}, which is a very pernicious nuclide because of its strong γ-emitting decay daughter. Clearly, it results particularly problematic if SNF reprocessing is envisaged.

The High-Temperature gas-cooled Reactor (HTR or HTGR) is a graphite moderated, He cooled nuclear reactor that was studied and realised in the past, and that it has been recovered today in the framework of the Generation IV Initiative. HTR shows unique features due to its peculiar fuel form (TRISO-coated particles embedded in cylindrical or spherical fuel elements made of graphite) as well as to its inert coolant (He). The gaseous coolant allows us the possibility to make the neutronics and the thermalfluiddynamics of the core substantially independent of each other.

What's more, He is an inert coolant from the chemical point of view as well, and it does not absorb neutrons parasitically. The TRISO-coated particles permit us the possibility to reach burn-ups that are by far longer than those of LWRs (i.e., in principle up to 800 GWd/tHM without leakages of Fission Products).

Starting from these consideration and taking into account the unique characteristics of the HTR concept, it is possible to appreciate the potentialities of loading the HTR core with a Th-based fuel. First of all, reaching very long burn-ups without needing to reprocess the fuel in-between in principle enables us to exploit Th without the drawbacks previously mentioned (strong γ-rays of its daughter). Moreover, the excellent neutron economy of Th-fuels is coupled with the excellent neutron economy of HTR itself (indeed, He and graphite are the main components of this core). Nevertheless, a driver fuel is necessary to sustain the chain reaction at BOC.

As far as the driver fuel is concerned, two main options are available, that is, enriched U or Pu. Although enriched U undoubtedly would be the best choice from the neutronic point of view, Gen. IV aims suggest Pu exploitation.

In the present paper, on the basis of some work performed by our group in the past, Pu (RG) is adopted as a driver fuel instead of HEU. Particularly, a pebble-bed HTR using Thorium along with 1st generation Plutonium has been considered, analogously to the fuel considered in the framework of the EU PUMA project [3]. This work aims at analysing the influence of the initial Pu/Th mass ratio in the fresh fuel as far as the main neutronic and burn-up parameters are concerned: reactivity at BOC, possibility to reach very long irradiation cycles, Pu isotopic composition versus burn-up, energy released. Hence, the following aspects will be analysed:

(i) the state of art about the studies focusing on the use of Th in different core concepts,

(ii) the use of Th in HTRs, with a particular emphasis on Th-Pu fuel cycles,

(iii) an original assessment of Th-Pu fuel cycles in HTR, assuming, as evaluating parameters,

  (a) the total energy produced,

  (b) the energy produced per initial loaded Pu,

  (c) the ratio between final (discharged) and initial (loaded) Pu mass.

2. Thorium Resources, Drawbacks of the Current Fuel Cycle, and Proliferation Concerns: A Brief Overview

With more than 300 NPPs running worldwide, LWR is currently the most widespread nuclear reactor technology. Developed and applied successfully since the 1950s, this technology is safe, reliable, and well proven [4]. Its main drawback consists of the extremely small U resource exploitation (less than 1%), which implies what follows:

(i) concerns about the limitation of U resource availability,

(ii) proliferation risk due to Pu content of SNF (please remember that the end of Cold War raised concerns about the proliferation risk, due to the large stockpiles of Pu produced by civil and military applications),

(iii) long-term toxicity of the final waste, mainly due to TRUs built up in SNF.

Indeed, an integral U exploitation would entail not only a huge availability of nuclear fuel resources but also a nuclear waste mainly composed of FPs instead of HMs.

The commonly mentioned design objectives of Th-based fuel cycles include the following:

(i) increasing nuclear fuel resources by breeding U^{233} from thorium,

(ii) improving fuel utilization in thermal reactors,

(iii) reducing significantly the U^{235} enrichment requirements,

(iv) reducing the build-up of Pu and of other TRU in comparison with uranium-based fuel cycles,

(v) burning Pu (RG or WP) without reprocessing, then reducing existing Pu stockpiles,

(vi) increasing the possibility to breed U^{233} and to incinerate long lived radiotoxic isotopes by combining the thorium-based fuel cycle with accelerator driven systems (ADS) and/or hybrid fusion driven systems.

A Th-based fuel cycle for HTR is not a new idea: the THTR experience represents and summarizes the effort made in that direction. What is more, as shown by some past work, adopting the Th fuel cycle in HTR using Pu as a driver would allow us what follows:

(i) increase of the efficiency in TRU reduction, as illustrated in Figure 1,

(ii) achieving higher fuel burn-ups.

As previously mentioned, Th is by far more abundant than U in the earth's crust. The primary natural Th resource [5] is monazite, which is a thorium phosphate mineral. Thorium deposits have been found in several countries [5] as shown in Figure 2. According to the US Geological Survey [5], the world thorium reserves and reserve base (resources) are shown in Figure 3.

Moreover, Th extraction technology as well as processes to recover valuable material from Th-based SNF (e.g., THOREX process) had been studied since a long time [2].

Basic researches and developments on the Th fuel cycle [1] have been conducted in many countries, and a considerable experience about Th-based fuels has been gained in power reactors worldwide (i.e., determination of material data, fabrication tests on the laboratory scale, irradiation experiments in material test reactors, use of Th-based fuel in HTRs, LWRs (including WWERs), LMFBRs, and (potentially) in MSRs, postirradiation examinations of

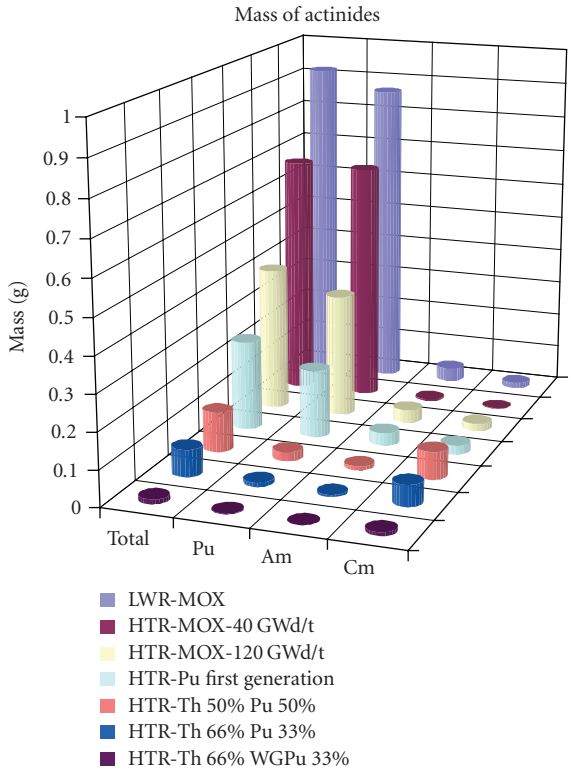

Figure 1: Mass of actinides at EOC starting from 1 g of Pu [4].

spent Th-based fuels, fabrication of Th-based fuel, both on pilot and semi-industrial scale (AVR)). Further activities are on-going worldwide, aiming at using Th to burn MA in both Gen-IV reactors and/or ADS.

Due to the lack of data, it seems impractical to develop meaningful cost projections [5] for any nuclear energy systems using thorium. Historical examples give some ideas of the funds that may be required. As an example, in the 1970s, Germany spent the equivalent of 500 million Euros in current money to develop a thorium fuel cycle and 2.5 billion Euros for the development of HTR. More recently, the GIF in its technology roadmap estimated that the only assessment of viability and performance of a nuclear system requires around one billion dollars (before any decision to develop and build a demonstrator, which of course would require large additional funding). The market of Th raw material [5], that is, ores or concentrates of oxide of thorium, is extremely small and limited to not-energy employments (such as high-temperature ceramics, crucibles, catalysts, welding electrodes, and some specific alloys). Additionally, the use of thorium in most of these products has been continuously decreasing, due to the burden associated with its natural radioactivity. Then, a nearly constant commercial price in the range 30–35 US $/kg [5] was published in the 1960s and 1970s, but this publication was suspended due to the progressively decreasing demand. Thus, nowadays a commercial Th price is not available. What is more, fluctuations of Th price have been minimized by a supply that by far exceeds the demand due to Th by-product build-up. That means that many countries have fairly large stockpiles of thorium that they consider as a waste.

If Th were exploited to produce electricity in the future, a Th market would develop. On the basis of what previously explained, it is reasonable to suppose that the raw material contribution to the cost of the electricity generated will remain low, comparable with or lower than that of the uranium cycle. So, from the economical point of view, the idea of using Th as a fertile material will virtually have no significant cost.

3. A Brief Review of Thorium-Based Fuel Cycles for Different Core Concepts

3.1. Thorium-Plutonium Fuel in LWR. The possibility of using Th-based fuels for LWR has been extensively analysed since a long time. Performances of Th-U and Th-Pu mixtures have been studied and compared with other more common concepts. Just to set an example, among some interesting comparisons between MOX and Pu-Th fuels shown in [6], the case of Korean 900 MW_e PWR can be taken into account. Its infinite multiplication factors when fuelled by Th-based and MOX fuel assembly, respectively, were calculated by means of the HELIOS code [7]. The boron concentration was kept constant (500 ppm). Figure 4 shows the results obtained. This example is useful to appreciate the very good neutronic behaviour of Th-based fuels, but we have to underline that there are not any advantages concerning the long-term radiotoxicity of the final waste.

Indeed, Cm^{244} contribution at the beginning and Pu^{239} and Th^{229} contribution successively make the radiotoxicity of the considered Th-based fuels higher than that of conventional UO_2 PWR SNF.

3.2. Thorium-Uranium Fuel in CANDU Reactors. The possibility of using Th as fertile material in CANDU has been largely considered [8]. Particularly, three main types of fuel mixtures have been analysed: mixed SEU and ThO_2 bundles, gadolinium-doped mixed bundles, and high burn-up ThO_2 bundles. The variation of lattice k_{inf} as well as the change in fissile content as a function of the bundle average burn-up is shown in Figure 5, for each of these considered compositions. Physical properties of natural UO_2 and natural ThO_2 fuels, respectively, have been shown for comparison purposes.

Please note that the initial fissile content of the high burn-up thorium bundles has been carefully chosen so that the depletion rate of the fissile material is almost the same as the conversion rate of the fertile Th^{232} into fissile U^{233}. Consequently, the reactivity and the fissile content of the high burn-up Th bundles are almost constant throughout the entire lifetime of the bundles.

3.3. Thorium-Uranium Fuel in Molten-Salt Reactors. Although the MSR core appears very different from all the other nuclear reactor concepts, the graphite-moderate MSR actually owns some features that are substantially similar to those belonging to High-Temperature Gas-Cooled Reactor (HTGR). Indeed, in both concepts the graphite moderator

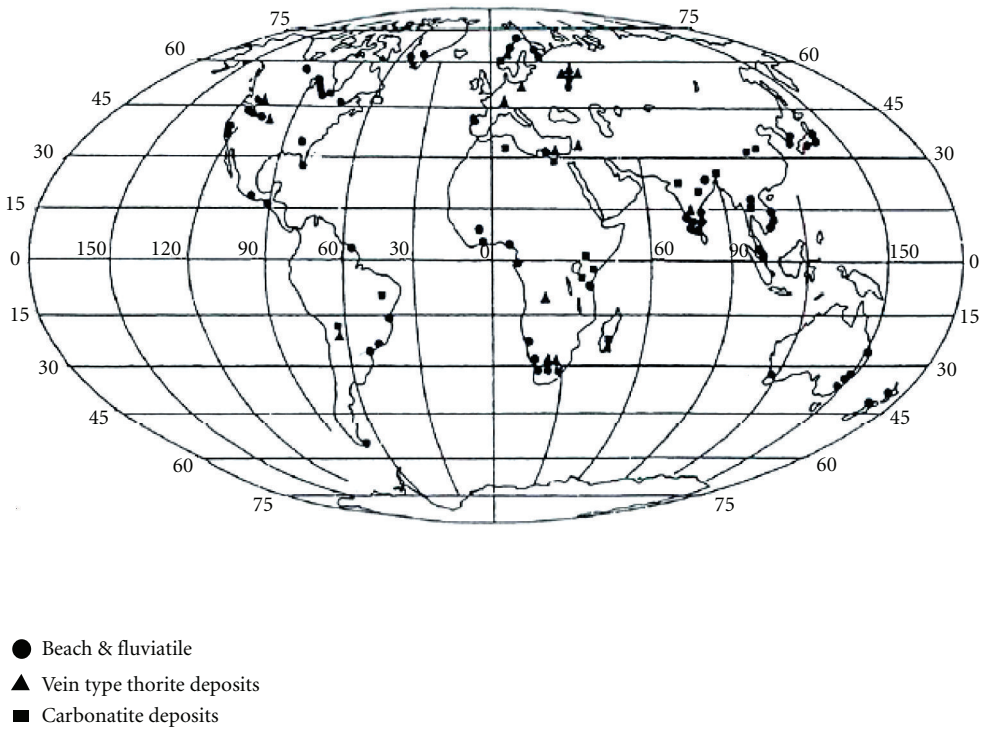

Figure 2: Thorium Deposits in the World [5].

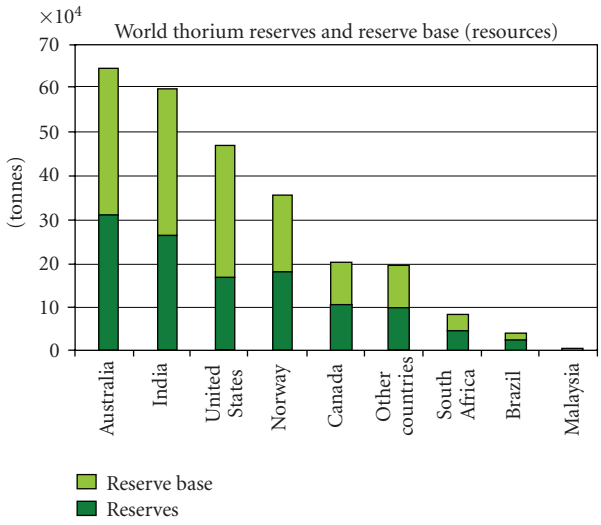

Figure 3: The World Thorium Reserves and Reserve Base [5].

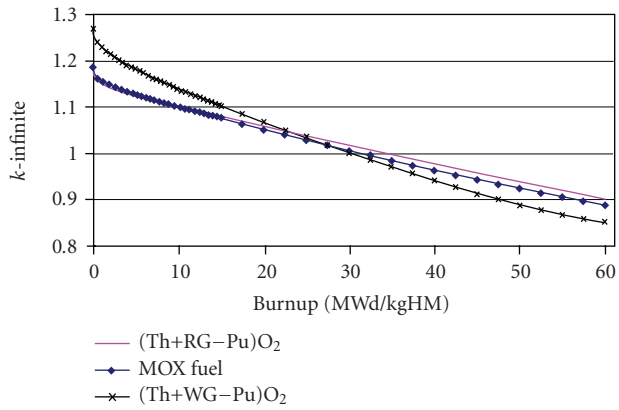

Figure 4: k-infinite as a function of burn-up [6].

is at an average temperature between 600–700°C, a Th-U mixture can be adopted as a fuel, and the moderation ratios are very close to each other. Therefore, a large part of the thermal reactor technology (and, particularly, of HTGRs) is directly applicable to this kind of MSR design. Therefore, nuclear data and methods for calculating neutron fluxes, reactivity temperature coefficients, and so on developed for HTGR can be applied for the MSR design, even though not-negligible differences remain. Some examples of applications of Th-based fuel in MSR could be found in [9, 10].

4. The Use of Thorium in HTR

4.1. Preliminary Considerations on TH-PU Cycle in HTR. The reduction of Pu stockpiles as well as the discharge of a nuclear waste that is very poor from the Pu content point of view is among the main goals of the current nuclear research. Then, Th-Pu-based fuels have to be considered as promising candidates to reach these objectives. What is more, the possibility of very long irradiation cycles allowed by HGTR cores has on the other hand to be taken into account as well. These considerations justify the efforts to develop Th-U and Th-Pu fuel cycles in HTGR core concepts [11–15]. Among the others, a few researches on Th-Pu fuel cycle in HTR were performed by our group in the past [4, 16].

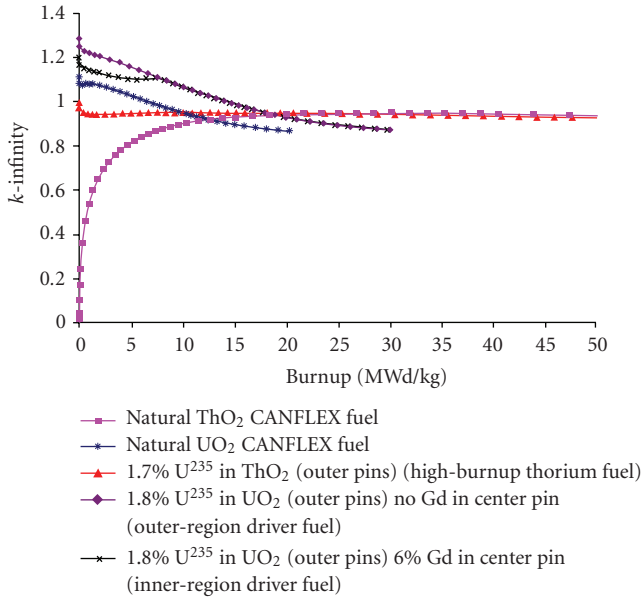

Figure 5: k_{inf} as a function of burn-up in CANDU [8].

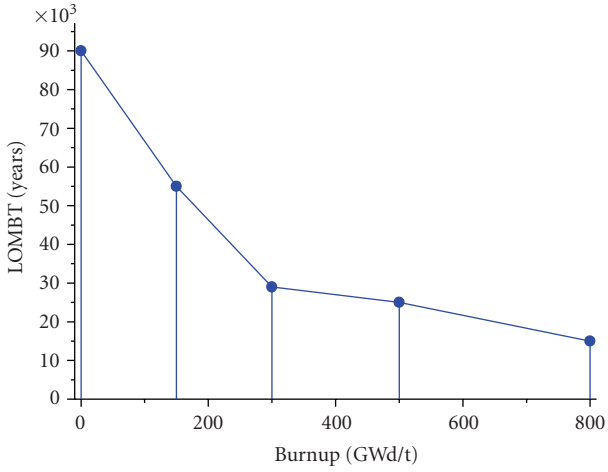

Figure 6: LOMBT versus Burn-up (2/3 Th – 1/3 Pu) [4].

The results shown in [4] lead us to draw some considerations concerning the behaviour of *highly-burned* (i.e., up to 800 GWd/tHM) Thorium-Plutonium fuel. Figure 6 reports the Level Of Mine Balancing Time (LOMBT) trend as a function of burn-up: it is clear that the best choice in terms of radiotoxicity reduction is to reach a burn-up that is as high as possible. This results is mainly due to a progressively larger Pu consumption.

Considering the rather long LOMBT of a typical LWR SNF, the reduction of the final radiotoxicity and of the total amount of waste is of course a key issue. Looking at this latter, the actinide mass reduction in the final waste to be stored in a permanent repository is another very attractive characteristic of HTRs (Figure 7).

Despite a larger production of curium isotopes (especially Cm^{244}), it is clearly shown by Figure 8 that reaching

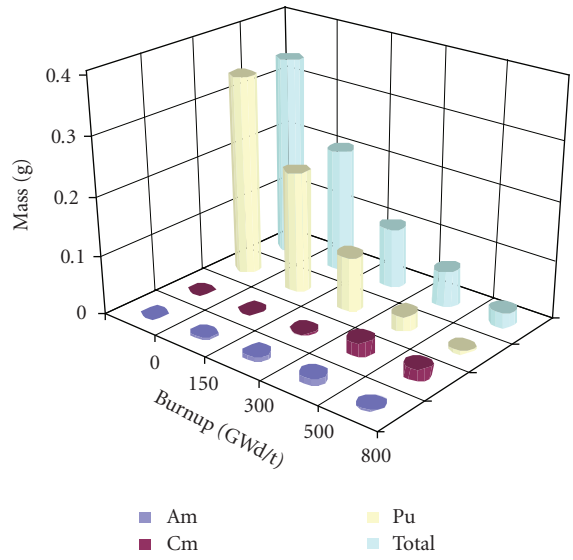

Figure 7: Masses of actinides versus fuel discharge burn-up (2/3 Th – 1/3 Pu) [4].

high burn-ups allows us to strongly reduce the masses of dangerous actinides.

The main results of [4] are summarized in Table 1.

4.2. The PUMA Project. Recently, Th as fuel for HTR has been considered, among the others, in the framework of the EU PUMA project [5]. Starting from the current legacy of nuclear waste as well as from the (V)HTR good capabilities of Pu burning, the PUMA activities focus on core physics investigations, in order to further demonstrate the potential benefits of using the HTR core as a Pu/MA transmuter (as known, annually a 1000 MW_e PWR produces about 30 tons of SNF (burn-up around 30 GWD/tHM) with the following average composition [7]: 94% U^{238}, 1% U^{235}, 1% Pu, 0.1% MA (Np, Am and Cm), 3–4% FP). Moreover, as (V)HTR Pu/MA transmuters are foreseen to operate in a global system of reactor designs and fuel cycle facilities, fuel cycle studies and socioeconomic/environmental assessments have been carried out. The PUMA consortium gathers 16 organisations from 9 countries (BE, DE, FR, IT, NL, PL, SE, UK, USA), including research organisations, leading nuclear engineering and fuel cycle firms, a fuel manufacturer, a utility, universities and institutes, and consultancy SMEs. The work carried out in the framework of PUMA represents part of the EURATOM contribution to the GIF [9].

Among the other activities of PUMA project, a deep burn-up fuel cycle strategy using the Th-Pu fuel in PBMR reactor [8] has been investigated.

Many of the data used in the following sections are based on PUMA project findings.

5. Calculations and Results

5.1. Calculation Parameters and Models. In this research, on the basis of the advantages outlined in previous paragraphs,

Table 1: Summary of obtained results ($k_\infty \sim 1.05$) [4].

Fuel/Pebble	EFPD	LOMBT	Energy/Pebble	Pu_{out}/Pu_{in}	TRN^*/Pu_{in}
1 g Pu 1st gen.	600	43000	51.8 GJ	32.9%	37.6%
1.5 g Pu 2nd gen.	645	35000	55.7 GJ	46.4%	54.9%
1 g Pu 1st + 2 g Th	705	34000	60.9 GJ	26.6%	32.8%

NOTE: $^*TRN = Pu_{out} + Am + Cm$.

Table 2: $(Pu\text{-}Th)O_2$ fuel general characteristics in accordance with PUMA Project [10, 11].

Description	Value
Fuel pebble	
Fuel pebble outer radius	3.0 cm
Thickness of fuel free zone	0.5 cm
Total heavy metal loading per fuel pebble	2.0 g
Matrix density	1.74 g/cm^3
Packing fraction in pebble bed	61%
Coated particle	
Kernel Coating Material	C/C/SiC/C
Layer thickness	90/40/35/40 μm
Layer densities	1.05/1.90/3.18/1.90 g/cm^3
Fuel kernel	
Fuel kernel diameter	200 micron
Kernel material type	$(Pu\text{-}Th)O_{2.0}$
Th-oxide density	9.55 g/cm^3 (95% TD) [13]
Pu-oxide density	10.89 g/cm^3 (95% TD) [12]

Table 3: Composition of 1st generation Pu [10, 11].

Pu isotopes	First Generation (weight %)
238	2.59
239	53.85
240	23.66
241	13.13
242	6.78

we investigated the main neutronic characteristics related to the utilization of Th as fertile material in PBMR loaded with a Pu/Th fuel, by means of MCNP5 [17] code.

The model used to perform these analyses is described in the following lines.

In our simulations Pu-RG (i.e., Plutonium produced during irradiation of UO_2 fuel in a typical LWR) has been chosen as driver fuel. In principle, Pu-RG is not suitable for proliferation purposes, due to its high content of even isotopes (Pu^{238}, Pu^{240}, Pu^{242}), which are characterized by a high spontaneous fission rate and, at least in the case of Pu^{238}, by a high decay heat as well. Th content in the considered pebble has been varied from 0% to 100% of the HM constituting the fuel. Table 2 shows the main parameters of the analyzed PBMR fuel elements, while Table 3 shows the Pu-RG (1st gen. Pu) isotopic vector.

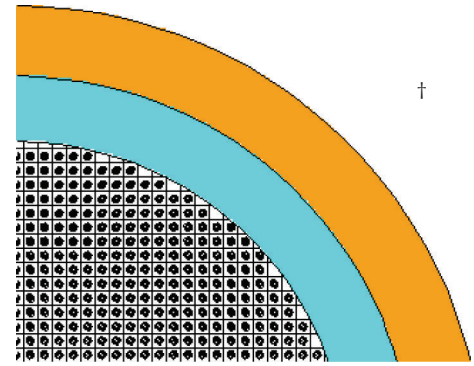

Figure 8: MCNP model without cut CPs [16].

Additionally, we fixed the following calculation parameters.

(i) An infinite lattice of stochastically arranged pebble has been considered for each fuel composition, by modelling a single sphere (with the He gap associated) with white boundary conditions.

(ii) Each of the considered pebbles contains 2 g HM (Pu/Th) [5].

(iii) Due to the lack of data and for the sake of simplicity, the density of $(Pu,Th)O_2$ fuel (with Th content varying from 0% to 100% of HM) has been assumed as varying linearly from the density of PuO_2 kernels (10.89 g/cm^3 [12]) to the density of ThO_2 kernels (9.55 g/cm^3 [13]), as a function of the Th fraction.

(iv) Geometric error reduction: the pebbles have been modelled as actual as possible (Figure 15), also on the basis of the results obtained in [16].

(v) No temperature profile inside the pebble: the temperature is uniform everywhere and equal to 1200 K.

(vi) The cross section libraries used in this work are JEFF3.1 [18].

(vii) Helium Gap: according to the average packing fraction of the PBMR core (61% [8]) the helium gap has been explicitly modelled.

Figure 8 shows an x-y view of the pebble model adopted to perform these calculations. Please note that clipped CPs along the boundary of the fuelled zone have been eliminated.

5.2. Preliminary Results. The variation of the k-infinite at BOC as a function of Th percentage is shown in Figure 9.

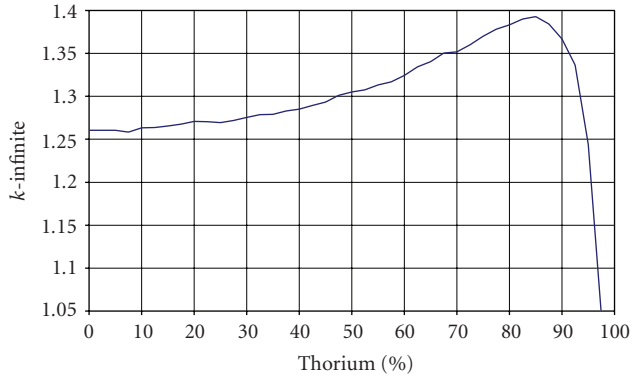

FIGURE 9: Variation of k-infinite at BOC as a function of Th content.

Analysing the trend of this curve, we can note that some trends can be recognised on the basis of Th content:

(i) 0% ≤ Th% < 10%: the k-infinite value remains near 1.26 (flat trend);

(ii) 10% ≤ Th% < 30%: a slightly positive gradient is shown (the k-infinite increases from 1.26 to 1.27);

(iii) 30% ≤ Th% < 84.5%: the value of k-infinite increases linearly from ∼1.27 and to ∼1.39;

(iv) 84.5% ≤ Th% < 100%: the k-infinite decreases from the peak at 84.5% ($k_\infty = 1.39274$, $\sigma = 0.00154$) to 1.

In order to complete this analysis, the fuel behaviour as a function of burn-up has to be considered. All the following burn-up calculations has been performed by means of the BGCore code [19].

5.3. BGCore Code. The burn-up calculations were performed with BGCore. BGCore is a software package for comprehensive computer simulation of nuclear reactor systems and their fuel cycles. It consists of a number of modules:

(i) 3-dimensional coupled neutronic and thermal hydraulic module, which calculates the reactor core criticality, as well as the core power and temperature distributions; only steady state core analysis is considered at this stage of the BG-Core package development; no thermal feedback features were used in this analysis;

(ii) fuel depletion and decay module, which calculates the fuel isotopic composition;

(iii) auxiliary modules for basic data processing and management.

5.4. k-Effective versus k-Infinite Burn-Up Calculations Comparison. The "real" k-effective in PBMR depends not only from the material and the core geometry, as in LWR reactors, but also from a random contribution due to pebbles recirculation [20]. Then, a not-negligible approximation is introduced by calculating the k-effective fixing the pebble arrangement in the core. In addition, even adopting this approximation, k-effective calculations are quite expensive form the computational point of view.

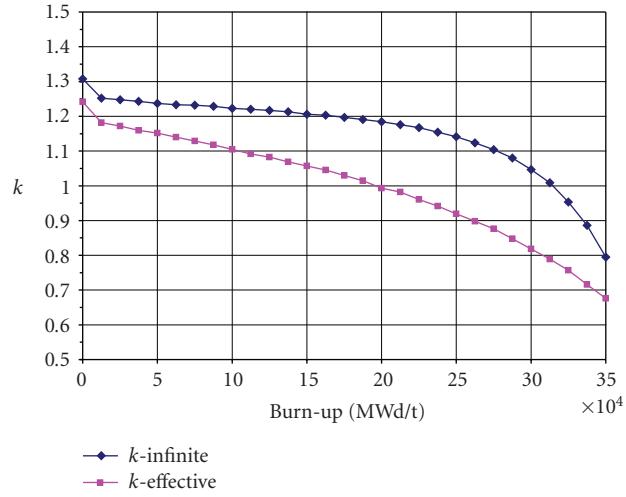

FIGURE 10: k-infinite and k-effective trends as a function of burn-up (expressed in MWd/tHM).

Hence, in order to roughly estimate the differences between k-effective model (i.e., fixed geometry) and k-infinite one, we made a preliminary evaluation, performing two burn-up calculations with a representative fuel composition. Particularly, a fuel composed of 50% Th and 50% Pu was adopted. This choice was also due to the fact that the results obtained can be directly compared with an independent calculation performed by FZJ [15].

Figure 10 and Table 4 show our main results.

Thus, we can outline some considerations.

(i) If we adopt k-inf = 1 as exit conditions for the burn-up calculations, we obtain a reasonable discharge burnup (comparable to that one we can obtain in a real pebble-bed HTR for a discharged pebble with the same initial composition).

(ii) The shape of k trends versus burn-up are quite similar.

(iii) The ratios (OUT/IN) among Pu isotopes have (in the two cases) the same order of magnitude.

(iv) The total ratio Pu_{out}/Pu_{in} in the two cases considered is comparable.

(v) Finally the discharge burn-up obtained in the FZJ calculation is quite similar ($\Delta \sim 5\%$) to that we obtained assuming $k = 1$ as exit condition for the k-infinite calculation (see Table 5).

For the reasons described above and because of the kind of study (preliminary parametric evaluation), we performed the calculations shown in the following paragraphs using a simplified k-infinite model instead of a k-effective one.

5.5. Burn-Up Results. As anticipated above, we analysed some Th/Pu compositions by means of BGCore, in order to assess the fuel behaviour as a function of burn-up. The basic assumptions for these calculations are the following:

Table 4: Pu_{out}/Pu_{in} for k-infinite and k-effective models.

	$Pu^{238}{}_{out}/Pu^{238}{}_{in}$	$Pu^{239}{}_{out}/Pu^{239}{}_{in}$	$Pu^{240}{}_{out}/Pu^{240}{}_{in}$	$Pu^{241}{}_{out}/Pu^{241}{}_{in}$	$Pu^{242}{}_{out}/Pu^{242}{}_{in}$	$Pu^{tot}{}_{out}/Pu^{tot}{}_{in}$
k-infinite	43,76%	5,46%	23,25%	48,63%	189,23%	28,64%
k-effective	42,57%	9,05%	53,65%	55,51%	185,46%	38,38%

Table 5: Comparison between k-infinite model and FZJ [15] results.

Heavy metal load and composition per pebble	FZJ calculation—discharge burn-up [MWd/kgHM]	k-infinite calculation—discharge burn-up [MWd/kgHM)]
1 g Pu, 1.0 g Th-232	332.38	314.42

(i) times steps of 25 days at full power,

(ii) power per pebble fixed at 1 kW,

(iii) uniform fuel temperature (1200 K) inside the pebble,

(iv) discharge burn-up is set at the time when k-infinite becomes equal to 1, to give a preliminary estimation of the theoretical nuclear burn-up.

(As already underlined, please note that the real PBMR will not be fuelled with pebbles at the same burn-up level, but with a mixture of pebbles at different burn-ups [21]: the real discharge burn-up in principle could be extremely high [21], i.e., up to twice the assumed discharge burnup. On the other hand, we calculated the k-infinite instead of k-effective (so we have not took into account leakages and effects related to the structures surrounding the core)).

The results concerning k-inf are summarized in Figure 11. Please note that all the standard deviations are around 100 pcm, which is the value commonly accepted in this kind of calculation by means of MC codes.

As anticipated in the introduction, we evaluated the fuel behaviour on the basis of the following parameters:

(i) the total energy produced,

(ii) the energy produced per initial Pu mass,

(iii) the ratio between final (discharged) and initial (loaded) masses for the Pu isotopes.

The obtained results are shown in Figures 12–19.

Starting from the previous figures, it is possible to highlight some interesting features.

(i) k-infinite at BOC increases with initial Th content (Figure 11).

(ii) Regardless of the initial fuel composition, k-infinite versus burn-up curves show the same qualitative trend (Figure 11).

(iii) Regardless of the initial fuel composition, the only Pu isotope increasing from BOC to EOC is Pu^{242} (Figure 18).

(iv) In order to achieve a reasonably high burn-up (i.e., 100 GWd/tHM at least), initial Th concentration should not be larger than 80% (Figure 11).

(v) The presence of 30% Pu in fresh fuel is the threshold to obtain a discharge burn-up higher than 190 GWd/tHM (Figure 11).

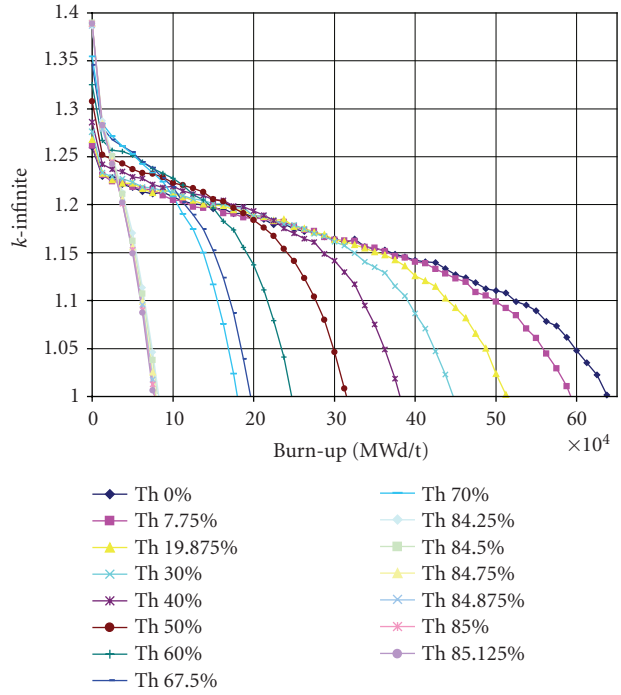

Figure 11: k-infinite variation as a function of burn-up (expressed in MWd/tHM).

(vi) Increasing Th fraction entails an even smaller Pu consumption per unit energy, although this trend is not monotonous (Figure 19). Up to a Th concentration not higher than 70%, the smallest fissile Pu consumption per unit energy corresponds to an initial Th percentage that is equal to 67.5% (Figures 15 and 17).

(vii) Up to a Pu concentration equal to 70%, we have the largest Pu mass at EOC, if the initial Th content is 67.5. Then, this composition corresponds to the best exploitation of Th itself. What is more, a smaller Pu consumption means a smaller production of Am and Cm, which generally build up in HTR cores. This behaviour can be considered positive or negative depending on what we are aiming at.

(viii) All the SNF compositions here obtained are strongly proliferation resistant, because of their high content in even Pu nuclides (Figures 14, 16, and 18).

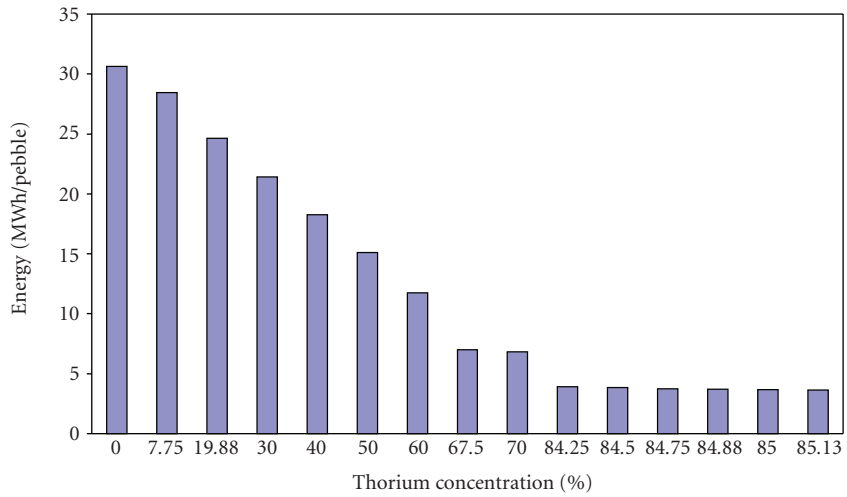

Figure 12: Produced energy (from BOC up to the time at which k-infinite becomes equal to unity) versus Th concentration.

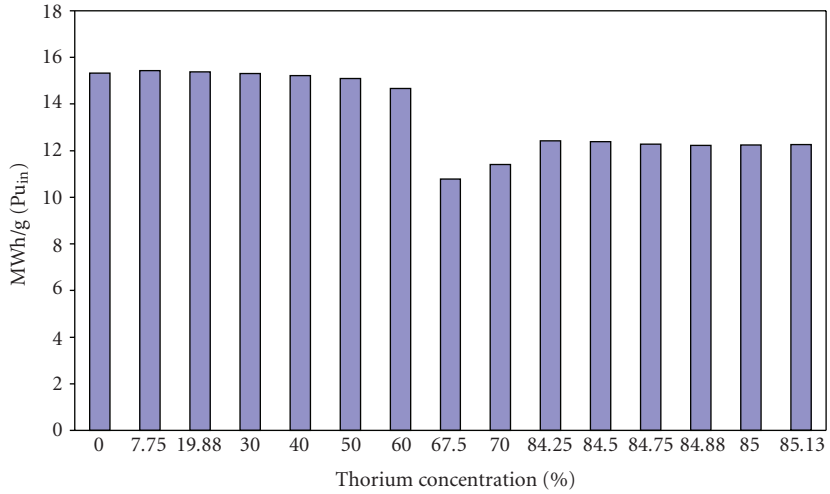

Figure 13: Energy produced per g_{Pu}^{in} versus Th concentration.

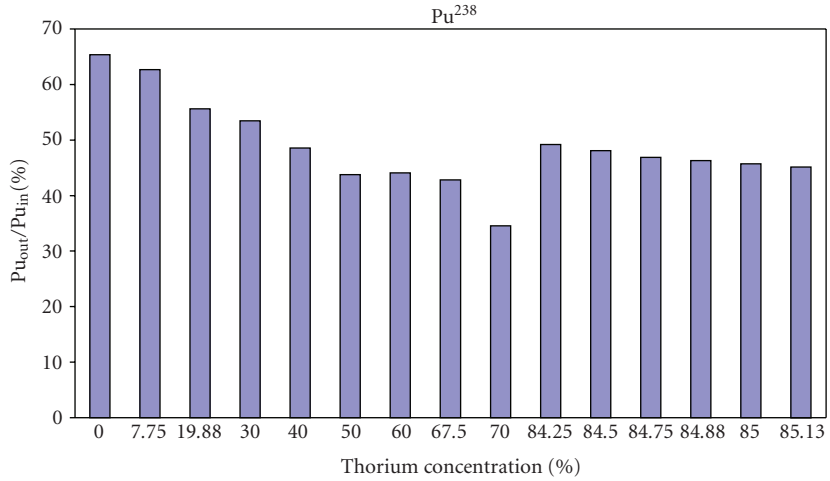

Figure 14: $Pu^{238}{}_{out}/Pu^{238}{}_{in}$ versus Th concentration.

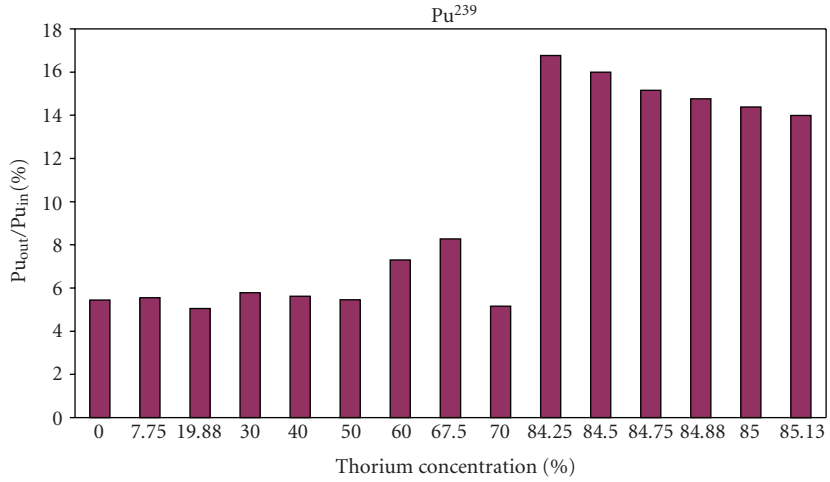

Figure 15: $Pu^{239}{}_{out}/Pu^{239}{}_{in}$ versus Th concentration.

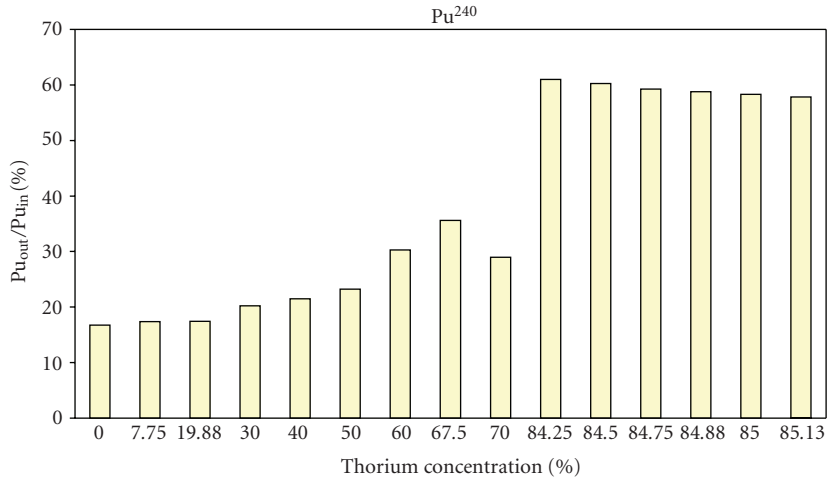

Figure 16: $Pu^{240}{}_{out}/Pu^{240}{}_{in}$ versus Th concentration.

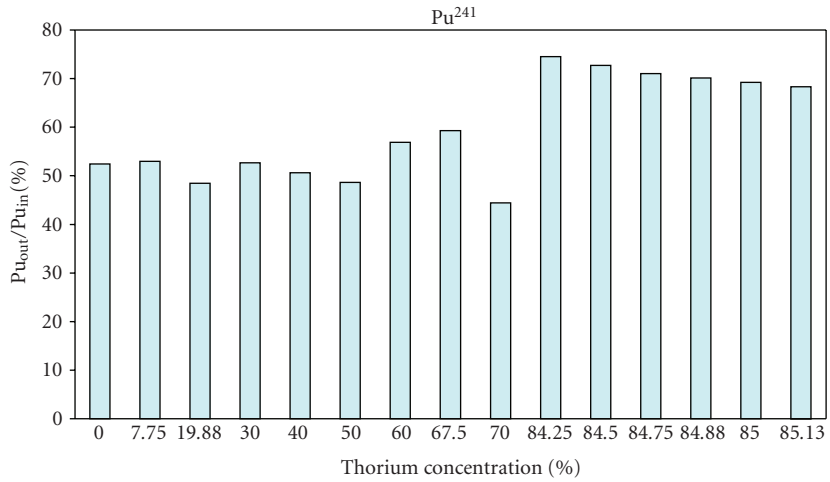

Figure 17: $Pu^{241}{}_{out}/Pu^{241}{}_{in}$ versus Th concentration.

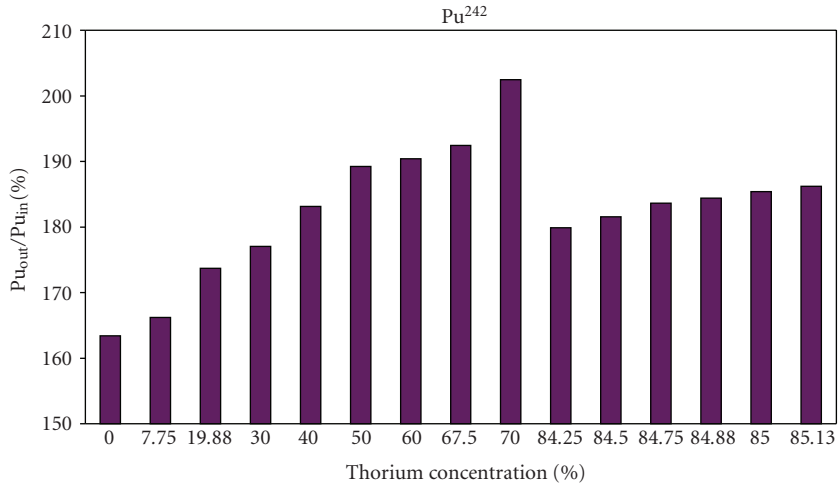

Figure 18: $Pu^{242}{}_{out}/Pu^{242}{}_{in}$ versus Th concentration.

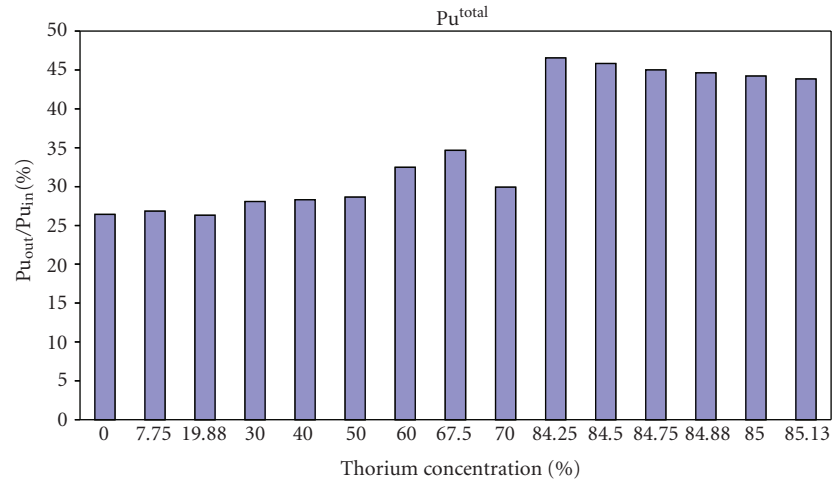

Figure 19: $Pu^{tot}{}_{out}/Pu^{tot}{}_{in}$ versus Th concentration.

(ix) Except for Pu^{238} and Pu^{242}, there are not significant differences changing the Th initial concentration from 0% to 50%. That means, up to 50% in Pu content, that Th contribution to energy production is substantially low (Figure 13). Conversely, Th content influences in a negative way the possibility of reaching higher burn-ups (Figure 11). Above the point corresponding to 50% initial Th percentage, the behaviour is much more determined by Th content. The highest Th exploitation per single cycle is reached with 67.5% initial Th content. That entails also a lower transmutation rate of Pu in Am and Cm (positive from the long-term radiotoxicity point of view).

6. Conclusions

Some aspects related to Thorium exploitation were outlined, with a particular emphasis on its suitability for working in pebble-bed HTRs as a fertile element in a Th-Pu fuel cycle. That is a promising kind of fuel, which was also considered in the framework of the EU PUMA project. Particularly, the influence of the Th/Pu weight fraction at BOC in a typical HTR pebble was analysed as far as the reactivity trend versus burn-up, the energy produced per Pu unit mass, and the Pu isotopic composition at EOC are concerned. On the basis of a preliminary comparative analysis (between a k-infinite and a k-effective model) and because of the kind of assessment presented here (i.e., a preliminary parametric evaluation), we chose a (simplified) k-infinite model instead of a k-effective one to perform our calculations.

Some general trends depending on the initial Th content can be recognized, and particularly the following.

(i) k-infinite versus burn-up shows the same qualitative trend regardless of the initial Th content (Figure 11).

(ii) k-infinite at BOC increases with initial Th content in a proportional way, and its decrease is as sharp as the Th content itself is high (Figure 11). That may make the reactivity control somewhat difficult.

(iii) The final burn-up increases with initial Th percentage decrease (Figure 11). If the content of Th is larger than 80%, the system becomes subcritical after less than 100 GWd/tHM burn-up (Figure 11).

(iv) Up to a Th concentration not higher than 70%, the smallest fissile Pu consumption per unit energy corresponds to an initial Th percentage that is equal to 67.5% (Figures 15 and 17).

(v) All Pu nuclides except to Pu^{242} decrease from BOC to EOC regardless of the initial Th content (Figure 15).

(vi) The point corresponding of a minimum in Pu consumption per unit energy produced (i.e., 67.5% Th, Figure 13) corresponds to the highest Th exploitation and to the lowest transmutation of Pu into heavier nuclides (Pu^{242}, Am, and Cm).

These results suggest us that there is not a "best" composition for the PBMR Pu/Th fuel, although deeper investigations need to be performed in order to draw final conclusions. Particularly, at least from the neutronic point of view, the influence of Th percentage on the reactivity coefficients as well as on the delayed neutron fraction should be determined. Thus, at the moment it is possible to state that some optimized Th percentage in the initial Pu/Th fuel could be suggested on the basis of the aim we are trying to reach.

(i) If we aim at Pu reducing, a Pu fertile-free fuel or a Th concentration ~20% has to be adopted (Figure 19), because these fuels allow us to reach the highest burn-up and the highest Pu consumption with a single irradiation cycle.

(ii) If we aim at maximising the natural resource exploitation (i.e., of both Th and U), Th content has to be around 67.5%.

(iii) In any case, there does not seem to be any advantages in inserting more than 70% of Th in the fresh fuel (higher initial reactivity to be controlled, higher content of heavier elements, shorter cycle length, smaller consumption of the driver fuel).

This work, although quite deep, has to be considered not completed; so it needs of some further work. Looking at the future developments of these research, in order to have a complete knowledge of the analyzed problem, it would be necessary to evaluate the following:

(i) reactivity coefficients,

(ii) short- and long-term radiotoxicity evolution,

(iii) materials behaviour and compatibility in the analyzed cases (e.g., under high fluence, at high temperature, etc.),

(iv) fuel cycles in the frame of the energetic scenarios (taking into account also environmental and economical aspects),

(v) nonproliferation issues.

Abbreviations

AVR:	Arbeitsgemeinschaft Versuch Reaktor
BG:	Breeding Gain
BOC:	Begin Of Cycle
BWR:	Boiling Water Reactor
CEA:	Commissariat à l'Énergie Atomique
CP:	Coated Particle
DIMNP:	Dipartimento di Ingegneria Meccanica, Nucleare e della Produzione
DRAGON:	European Prototype HTGR at Winfrith in England built and operated by UKAEA
DU:	Depleted Uranium
EFPD:	Effective Full Power Days
EOC:	End Of Cycle
EURATOM:	European Atomic Energy Community
FIMA:	Fission per Initial Metal Atom
FP6:	6th Framework Program
FP:	Fission Products
FZJ:	ForschungsZentrum Jülich
GCFR:	Gas Cooled Fast Reactor
GIF:	Generation IV International Forum
HEU:	Highly Enriched Uranium
HLW:	High Level Waste
HM:	Heavy Metal (Actinides)
HTGR:	High Temperature Gas cooled Reactor
HTR:	High gas Temperature Reactor
LEU:	Low Enriched Uranium
LMFBR:	Liquid Metal Fast Breeder Reactor
LOMBT:	Level Of Mine Balancing Time
LWR:	Light Water Reactor
MA:	Minor Actinides
MC:	Monte Carlo
MCNP:	A general Monte Carlo N-Particle transport code, Version 5
MOX:	Mixed OXide
MSR:	Molten Salt Reactor
NEC:	Nuclear Energy Centre
PBMR:	Pebble Bed Modular Reactor
PCU:	power conversion system
PUMA:	European project on Plutonium and Minor Actinides management in THTR
PWR:	Pressurized Water Reactor
RG:	Reactor Grade
SEU:	Slightly Enriched Uranium
SME:	Small and Medium Enterprises
SNF:	Spent Nuclear Fuel
THTR:	Thorium High Temperature Reactor
TRISO:	TRiple ISOtropic Coated Particles
TRU:	TRans-Uranics
VHTR:	Very High Temperature Reactor
WG:	Weapon Grade
WWER:	Russian pressurized light water reactor.

Acknowledgments

The work presented in this paper was partly funded by the European Union Sixth Framework Program, under contracts PuMA and RAPHAEL. First of all the authors want to thank

Dr. J. C. Kuijper, Dr. B. Petrov, and Dr. K. Bakker of NRG, for useful information about HTRs' fuel composition and the chemical behaviour of the elements analysed in the fuel proposed in this article. They want also to thank Professor G. Forassassi for his support and Professor J. L. Kloosterman for many interesting suggestions.

References

[1] International Atomic Energy Agency, "Thorium based fuel options for the generation of electricity," IAEA-TECDOC-1155, May 2000.

[2] M. Benedict, T. H. Pigford, and H. W. Levi, *Nuclear Chemical Engineering*, McGraw-Hill, New York, NY, USA, 2nd edition, 1981.

[3] http://www.puma-project.eu.

[4] N. Cerullo, D. Bufalino, G. Forasassi, G. Lomonaco, P. Rocchi, and V. Romanello, "An additional performance of HTRS: the waste radiotoxicity minimisation," *Radiation Protection Dosimetry*, vol. 115, no. 1–4, pp. 122–125, 2005.

[5] N. Cerullo, D. Bufalino, G. Forasassi, G. Lomonaco, P. Rocchi, and V. Romanello, "The capabilities of htrs to burn actinides and to optimize plutonium exploitation," in *Proceedings of the 12th International Conference on Nuclear Engineering (ICONE '04)*, vol. 1, pp. 495–501, Arlington, Va, USA, April 2004.

[6] Thorium Report Committee, "Thorium as an energy source—Opportunities for Norway," January 2008, http://www.ect2008.com/publish_files/Kara.pdf.

[7] International Atomic Energy Agency, "Potential of thorium based fuel cycles to constraint plutonium and reduce long lived waste toxicity," IAEA-TECDOC-1349, April 2003.

[8] W. Chernock and K. E. Horton, "Status of liquid metal cooled fast reactor development in the USA," IAEA-TECDOC-791, Vienna, 1995.

[9] International Atomic Energy Agency, "Thorium fuel utilization: options and trends," IAEA-TECDOC-1319, November 2002.

[10] M. W. Rosenthal, P. W. Haubenreich, and R. B. Brigge, "The development status of Molten-Salt Breeder Reactor," OAK Ridge National Laboratory, August 1972.

[11] L. Mathieu, D. Heuer, E. Merle-Lucotte, et al., "Possible configurations for the thorium molten salt reactor and advantages of the fast nonmoderated version," *Nuclear Science & Engineering*, vol. 161, no. 1, pp. 78–89, 2009.

[12] H. J. Rütten and K. A. Haas, "Research on the incineration of plutonium in a modular HTR using thorium-based fuel," *Nuclear Engineering and Design*, vol. 195, no. 3, pp. 353–360, 2000.

[13] H. Chang, Y. Yang, X. Jing, and Y. Xu, "Thorium-based fuel cycles in the modular high temperature reactor," *Tsinghua Science and Technology*, vol. 11, no. 6, pp. 731–738, 2006.

[14] E. Mulder and E. Teuchert, "Characteristics of a different fuel cycle in a PBMR-400 for burning reactor grade plutonium," *Nuclear Engineering and Design*, vol. 238, no. 11, pp. 2893–2897, 2008.

[15] J. C. Kuijper, E. Bomboni, N. Cerullo, et al., "Pu and MA management in thermal HTGRs—impact at fuel, reactor and fuel cycle levels," in *Proceedings of the 4th International Topical Meeting on High Temperature Reactor (HTR '08)*, Washington, DC, USA, September 2008.

[16] H. J. Rütten and K. A. Haas, "Incineration of LWR-Plutonium (1. Generation and 2. Generation) in a Modular HTR using Thorium-based Fuel," HTR-N-02/05-D-3.2.2, 2004.

[17] E. Bomboni, N. Cerullo, and G. Lomonaco, "EPEME, Error in PEbble Modelling Evaluation code," NT-009(2008), Department of Mechanics, Nuclear and Production Engineering (DIMNP), Pisa, Italy, 2008.

[18] X-5 Monte Carlo Team, "MCNP—a general Monte Carlo N-particle transport code," Version 5, October 2005.

[19] O. Cabellos, "Processing of the JEFF-3.1 cross section library into a continuous energy Monte Carlo radiation transport and criticality data library," OECD NEA Data Bank, May 2006, NEA/NSC/DOC(2006)18, http://www.nea.fr/abs/html/nea-1768.html.

[20] C. Pohl, "Additional calculations for fuel compositions of PuO2 and ThO2 in the PBMR-PUMA pebble bed high temperature reactor," PUMA, Work Package 1, Deliverable D123, August 2009.

[21] E. Fridman, E. Shwageraus, and A. Galperin, "Implementation of multi-group cross-section methodology in BGCore MC-depletion code," in *Proceedings of the International Conference on the Physics of Reactors (PHYSOR '08)*, Interlaken, Switzerland, September 2008.

Hindawi Publishing Corporation
Science and Technology of Nuclear Installations
Volume 2009, Article ID 193594, 14 pages
doi:10.1155/2009/193594

Research Article

Assessment of LWR-HTR-GCFR Integrated Cycle

Eleonora Bomboni,[1] Nicola Cerullo,[1,2] and Guglielmo Lomonaco[1]

[1] *DIMNP, University of Pisa, CIRTEN, Largo Lucio Lazzarino n. 2, 56126 Pisa, Italy*
[2] *DIPTEM, University of Genova, Via all'Opera Pia 15/a, 16145 Genova, Italy*

Correspondence should be addressed to Nicola Cerullo, cerullo@docenti.ing.unipi.it

Received 1 March 2009; Accepted 1 July 2009

Recommended by Jim Kuijper

Preliminary analyses already performed showed that innovative GCRs, both thermal and fast, are very promising candidate to reach the Gen-IV sustainability goal. The integrated LWR-HTR-GCFR basically aims at closing the current nuclear fuel cycle: in principle, thanks to the unique characteristics of Helium coolant reactors, LWR SNF along with DU become valuable material to produce energy. Additionally, burning HMs of LWR SNF means not only a drastic reduction in the U^{nat} demand but also a remarkable decrease in the long-term radiotoxic component of nuclear waste to be geologically stored. This paper focuses on the analyses of the LWR-HTR-GCFR cycle performed by the University of Pisa in the frame of the EU PUMA project (6th FP). Starting from a brief outline of the main characteristics of HTR and GCFR concepts and of the advantages of linking LWR, HTR and GCFR in a symbiotic way, this paper shows the integrated cycle involving a typical LWR (1000 MW_e), a PBMR (400 MW_{th}) and a GCFR-"E" (2400 MW_{th}). Additionally, a brief overview of the main technological constraints concerning (Pu+MA)-based advanced fuels is given, in order to explain and justify the choices made in the framework of the considered cycle. Thereafter, calculations performed and results obtained are described.

1. Introduction

Currently there are more than 440 power reactors running worldwide, supplying 16% of the total electricity produced. Nuclear power is, as known, the only CO_2-free source that is capable to satisfy today's increasing energy demand. Nuclear power, thanks to the well-proven LWR technology, is very reliable and safe. Although among power plants Nuclear Power Plants (NPPs) have by far the highest ratio between energy supplied and waste produced, actually waste is their major drawback. Indeed, nuclear waste contains elements that are dangerous for more than 100 000 years; additionally, the natural resources of nuclear fuel are badly exploited by the LWR technology, because of both neutronic and technological reasons. It has been being clear since the beginning of nuclear age that the nuclear fuel availability could be substantially increased by the FR technology, which is capable of utilizing almost 100% of U from mine against less than 1% of LWRs. Additionally, fissioning the whole U amount extracted from mine means to reduce the long-term radiotoxicity of the final waste as well. Thus, in order to reach these two goals contemporarily and to realize a "sustainable" nuclear power, more than one kind of reactors has to be used, linked each other in a "symbiotic" way. Although long and deep analyses are still requested, it is possible to draw a first assessment highlighting the potentialities of symbiotic cycles involving two of the most promising *Generation IV* reactor concepts: (V)HTR and GCFRs [1–7].

2. The LWR Spent Nuclear Fuel

As known, the discharge burnup of fuel elements depends on both nuclear and technological reasons, consequently it can be quite different for different kinds of reactor. Regarding LWR, the most widespread concept worldwide, it lies in the range between 30 000 and 60 000 MWd/tHM. That entails that the mass loaded into a typical LWR (electric output equal to 1 GW_e and efficiency around 33%) amounts to about 25/30 tons of HM per Full Power Year (FPY) and

Table 1: Spent LWR HM composition (burnup 33 GWD/tHM; initial enrichment 3.2%U^{235}; 5 years cooling).

	Isotope	Quantity [g/t HM]	Mass fraction [%]
Pu	Pu^{238}	140	1.5
	Pu^{239}	5470	59.0
	Pu^{240}	2230	24.0
	Pu^{241}	956	10.3
	Pu^{242}	486	5.2
MA	Np^{237}	437	51.6
	Am^{241}	296	35.0
	Am^{243}	83.8	9.9
	Cm^{242}	6.2	0.7
	Cm^{244}	24	2.8

is followed by the same discharge rate of spent fuel, of which an important fraction is composed of TRansUranics (TRU).

After about 3 years of permanence inside the reactor core, the spent fuel is transferred to cooling pools. Approximately 350 different nuclides (200 of which radioactive) were created during irradiation, with the following average composition:

(i) 94%U^{238},

(ii) 1% U^{235} (hence, Spent Nuclear Fuel (SNF) is still enriched if compared to U^{nat}),

(iii) 1% Pu,

(iv) 0.1% MA,

(v) 3 ÷ 4% Fission Products (FP).

As far as the isotopic composition of Pu and MAs is concerned, it is shown in Table 1.

FP dangerousness decays in few centuries but Pu and MAs are very long-living, even more than 100 000 years. Therefore, the management, the minimization of its quantity, and the safe disposal of the SNF are key issues for the present and the future of nuclear energy.

However, it is important to recognize that what is called "nuclear waste" is actually composed largely of recyclable material. In principle, all actinides are able to produce energy by fission, either directly or indirectly by transmutation into fissile nuclei by one or more neutronic captures. That means, ~96% of SNF is potentially recyclable, whereas only FPs are "waste," at least from the energy production point of view (indeed, some of them could be extracted and used, as an example, for technological or medical applications) (as an exemple, some of them could be extracted and used for technological or medical applications).

At the moment, only Pu is partially recycled in Mixed Oxide (MOX) fuels for LWRs in some countries. MOX technology allows the possibility to double the current natural resource exploitation, which corresponds to less than 1% with the Once Through Then Out (OTTO) cycle. However, an integral use of U resources can be achieved

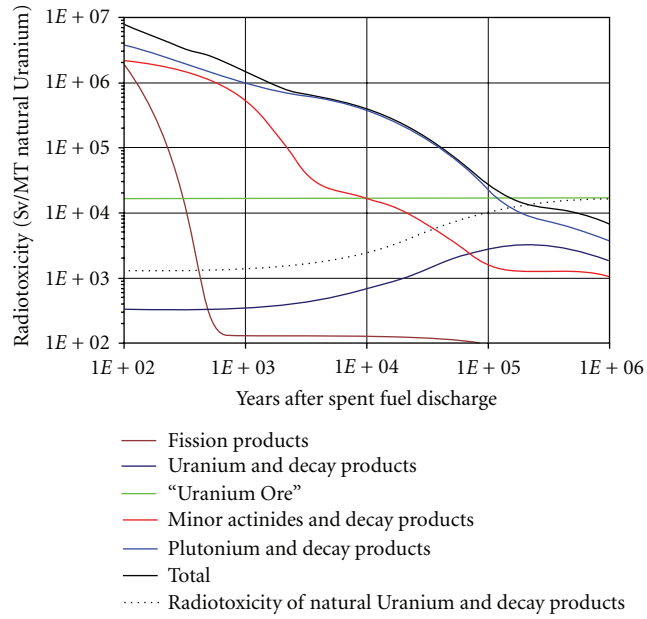

Figure 1: Radiotoxicity of SNF versus time.

only with the FR technology. Indeed, the *Generation IV Initiative*, aiming at a *sustainable* nuclear power, proposes 6 reactor concepts, among which 3 are fast: Sodium Fast Reactor (SFR), Lead Fast Reactor (LFR), along with the already mentioned GCFR. Additionally, recycling all HMs from SNF reduces the mass of the material to be stored in geological repositories and may also reduce its long-term radiotoxicity. This reduction will be very strong if the final waste is constituted of only FPs (see Figure 1): indeed, their radiotoxicity balances the reference level (the so-called *Level Of Mine*, LOM: the LOM corresponds to the radiotoxicity of that natural Uranium (U_{nat}) mass from which the considered waste descends) in less than 500 years.

Moreover, recycling HMs entails high neutronic fluencies on them and, consequently, the buildup of MAs and Pu nuclides with higher mass number (240 or more). That means, HMs are made useless for military purposes (it is useful to remember that at least 93% of Pu-Weapons Grade (Pu-WG) is composed of Pu^{239}, because Pu-WG cannot contain more than 7% of Pu^{240} due to the relatively high self-fission probability of this latter isotope), because many of these heavier isotopes are characterized by both a high decay power and a high probability of self-fission (Table 2).

3. Partitioning and Transmutation (P&T) of Pu- and MA-based Advanced Fuels

As partially anticipated in previous paragraphs, *closing* the nuclear fuel cycle (i.e., all HM from mine is exploited to produce energy by fission, directly or indirectly by transmutation, it is then reprocessed and recycled; the final nuclear waste consists of only FPs) would permit the possibility to solve almost all the open issues regarding nuclear power, while assuring the energy supply worldwide for the future

Table 2: Decay power and other properties of some actinide nuclides [1].

Nuclide	Half-life (years)	Specific activity			Dose coefficients (10^{-7}Sv/Bq)
		(Ci/g)	(W/g)	(Neutron $\min^{-1}\text{mg}^{-1}$)	
^{237}NP	2.14×10^{6}	7.07×10^{-4}	2.07×10^{-5}	$<7\times10^{-6}$	1.1
^{238}PU	87.404	17.2	0.570	155	2.3
^{239}PU	2.4413×10^{4}	6.13×10^{-2}	1.913×10^{-3}	1.35×10^{-3}	2.5
^{240}PU	6580	0.227	7.097×10^{-3}	53.7	2.5
^{241}PU	14.98	99.1	4.06×10^{-3}		4.7
^{242}PU	3.869×10^{5}	3.82×10^{-3}	1.13×10^{-4}	95.3	2.4
^{241}AM	432.7	3.43	0.1145	3.55×10^{-2}	2.0
^{242m}AM	144	10.3	3.08×10^{-2}		1.9
^{243}AM	7370	0.200	6.42×10^{-3}		2.0
^{242}CM	0.445	3.32×10^{3}	122	1.21×10^{6}	0.13
^{244}CM	18.099	80.94	2.832	6.87×10^{5}	1.6
^{243}CM	8265	0.177	5.89×10^{-3}		3.0
^{252}CF	2.64	537	38.3	2.3×10^{12}	0.98

centuries. Of course, there are some challenging aspects at the moment as far as Partitioning and Transmutation (P&T) are concerned. Probably, the best way to close the nuclear fuel cycle would be an *integral fuel cycle* (as proposed for GCFR reactors). In such an approach, the reprocessed spent fuel from LWRs is part of the feed for FRs. Then, the spent fuel of FRs is reprocessed in situ, and all HMs are recovered together (i.e., without chemical separation of the different elements) and reused to produce new fuel for the same FR fleet (multiple *homogeneous* recycle), while FPs constitutes the final waste. Such a strategy is at the moment quite challenging, because an economically feasible process is needed, allowing the possibility to treat highly radioactive materials and to extract HMs with a very high efficiency (more than 99%). What is more, treating not-negligible quantities of MAs (particularly Cm, due to its strong γ and neutron emissions) seems to be quite difficult due to radioprotection problems, particularly in large facilities along with large amounts of all the other HMs. Additionally, all the processes involved should be very effective as far as the separation of HMs from FPs and the recoverability of reactants are concerned. Hence, at the moment it seems to be simpler recycling U, Pu, Np, and, if appropriate, Am. Indeed, Np can be partitioned during the PUREX process, although this procedure has not yet been developed on an industrial scale. Regarding Cm, it seems to be advisable to store it temporarily, while waiting for its decay into Pu (half-life of Cm^{244} is around 18 years), it is also quite challenging to separate it from Am due to their similar chemical behavior. Then, storing Cm could entail to store Am together as well. On the other hand, Am and Cm could be recovered in some smaller dedicated facilities and reused in dedicated assemblies (*heterogeneous* recycle) for critical reactors or for Accelerator Driven Systems (ADs). In this connection it is important to take into account that the following hold.

(i) Recycling Cm entails the production of not-negligible quantities of Cf^{252}, which is a very strong neutrons emitter (much stronger than Cm itself, Table 2) and, consequently, it is very difficult to be managed.

(ii) The opportunity of recycling Am without Cm has to be deeply assessed: indeed, it does not reduce the long-term radiotoxicity very much (not more than a factor 10 o less, due to the production of Cm by neutron capture). That means a challenging procedure of partitioning could eventually not be very effective from the long-term radiotoxicity reduction point of view.

(iii) In principle, building dedicated facilities for Am and Cm recycling could not be economical.

As far as transmutation is concerned, a single reactor concept is probably not enough to burn HMs effectively, but this purpose can be reached by chains of different reactors, each doing what the others are not able to do. LWRs can be considered the starting point of all the possible chains, due to their current large diffusion worldwide, their proven technology and reliability, as well as, last but not least, the large amounts of LWR SNF worldwide. Additionally, as shown above, LWR SNF is rich in fissionable elements. Nevertheless, it is not possible to burn HMs completely in LWRs because of neutronic and technological reasons. Instead, FRs can exploit Pu by breeding U^{238}, thus increasing largely the availability of nuclear fuel. Additionally, the good neutron economy of the fast spectrum enables us to transmute even Pu isotopes and MAs as well. Of course, thorough analyses are requested in order to use these new fuels, particularly concerning the dynamic behavior of the core. Indeed, the introduction of large fractions of Pu and MAs tends to make worse safety parameters like the Fuel Temperature Coefficient (FTC) and the effective delayed

neutrons fraction (β_{eff}). In this connection it is clear that cores with a high neutron economy are advisable, since they are able to reach and maintain the criticality with small fractions of Pu.

On the basis of the considerations outlined until now, a fuel cycle is proposed in the following paragraphs that involves current LWRs, (V)HTRs, and GCFRs in a "symbiotic" way in order to exploit nuclear waste (Pu, Np, and Depleted Uranium from reprocessing plants if necessary) as fresh fuel.

4. Computer Codes and Libraries

MCNP [8] is a general purpose 3D MC code that can be used for neutron, photon, electron, and coupled neutron/photon/electron transport, including the capability to calculate the eigenvalues for critical systems. The current version has new interesting features, among which the capability to treat stochastic geometries like that characterizing HTR cores. As a general neutronic code, MCNP is able to calculate fluxes, one- or multigroup cross sections and other parameters typical of nuclear systems.

ORIGEN [9] is a deterministic depletion code based on the matrix exponential method. ORIGEN needs initial quantities of each material in the system, one-group cross-sections, total power, and irradiation time of the system being analysed to calculate its burnup. If necessary, the user can supply feed and/or removal rate of each material to be burnt.

Monteburns [10] is a code coupling MCNP with a depletion code in order to perform burnup calculations. It consists of a Perl [11] script interacting with FORTRN77 program (*monteb.f*). Particularly, Monteburns2.0 requires Active PERL 5.6.1 build 635 for Windows. The current version 2.0 is able to use MCNP-4C, MCNP5, or MCNPX2.5 [12] with ORIGEN2.2 or CINDER90 [13]. The flowchart in Figure 2 shows how Monteburns works.

The primary way in which MCNP and ORIGEN interact through *MONTEBURNS* is that MCNP provides one-group microscopic cross-sections and fluxes to ORIGEN for burnup calculations. After ORIGEN and MCNP have been run, results for each burn step are written into output files, and the isotopic compositions obtained from ORIGEN are used to generate a new MCNP input file for the next burn step. This MCNP input file contains the adjusted composition and density of each material being analysed. To increase the accuracy of the burnup calculation, a "predictor" step is used in which ORIGEN is run halfway through the designated burn step. One-group cross-sections are then calculated at the midpoint of the burn step by MCNP. This assumes that the nuclides of the system at the midpoint are a reasonable approximation of the nuclides over the entire burn step (actually it is important only that the neutron flux energy spectrum be representative of the entire burn step). The user must be aware of this assumption and consequently ensure that burn intervals are not too long. After the predictor step is executed, then ORIGEN is re-executed with the new one-group cross-sections.

Monteburns supplies, as output data, the following:

(i) K_{eff} versus time,

(ii) recoverable energy per fission versus. time,

(iii) neutron flux versus time,

(iv) macroscopic fission cross section per material versus time,

(v) power generation versus time,

(vi) burnup versus time (GWd/ton of heavy metal),

(vii) (n,γ), (n,f) (n,2n) microscopic XS per material versus time,

(viii) flux spectrum versus time,

(ix) grams of material versus time,

(x) activity of material versus time,

(xi) inhalation and ingestion radiotoxicity versus time.

As mentioned previously, we used MCNP5 and ORIGEN2.2 for the burnup calculation performed here.

In order to obtain the best reliability, we used the most recent cross-section libraries we have at the moment. Consequently, we chose the JEFF3.1 libraries for MCNP code. Anyway, for cross-sections not provided by MCNP, ORIGEN uses values from its own library. ORIGEN libraries are supplied as one-group tables of data, each of which is somewhat representative of a given type of reactor. They are substantially based on ENDF/B-IV nuclear data. Unfortunately, there is no library relevant to HTR of GCFR systems and consequently we used the generic THERMAL.LIB file for calculations on PBMR-400, and the FFTC.LIB file (library developed to simulate fast reactor spectra) for the GCFR core.

Regarding the FP yield model, we adopted the ORIGEN one [9].

5. The PBMR-400 and the GCFR "E" Cores: Main Characteristics and Computational Models

This work has been performed focusing on the PBMR-400 as a reference HTR pebble-bed core concept [1], and on the GCFR "E" 2400 as a GCFR core (plate type) concept [1].

PBMR is a pebble-bed, 400 MWth HTR core. It is an 11 m high annular core, with a central column of graphite as a reflector. Its refuelling scheme is a continuous one. The fuel elements are 6 cm diameter pebbles filled by TRISO-coated particles. In the frame of the PUMA EU project [2], kernels are composed of Pu-oxide without any fertile elements (U or Th). In the current analysis, PBMR kernels are composed of 1st generation Pu+Np-oxide. That means Pu and Np coming from an LWR are recovered as fresh fuel for the PBMR, whereas Am, Cm, and FPs are stored as waste.

GCFR "E" is a 2400 MWth He-cooled fast reactor. Its fuel assemblies are hexagonal, containing plates made of a (U,Pu)C and SiC matrix. Thanks to its core composition with an extremely low content of parasitic absorbers, GCFR is able to reach criticality with a fuel composed of 82% (as an atomic

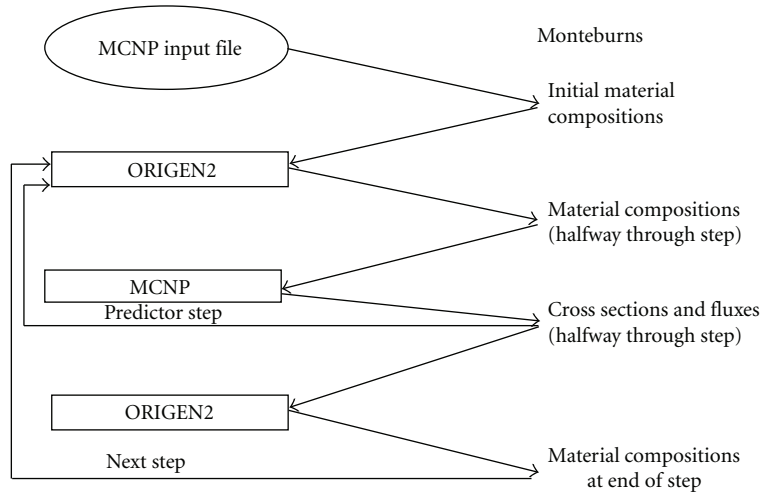

Figure 2: Monteburns workflow.

fraction) Depleted Uranium (DU), as well as to sustain very long irradiation period without becoming subcritical. Since for this core concept 10% FIMA burnup is envisaged, we analysed GCFR multiple cycles that are more than 3100 days long. What is more, multiple recycles of the GCFR SNF have been analysed: the SNF of a cycle is recovered and reused as a fresh fuel for the following cycle. Am, Cm, and FPs are substituted by DU in order to keep constant the core fuel inventory.

Describing in detail PBMR and GCFR is a very challenging matter, not only for the huge computational time requested, but also for the lack of some data. Then, the main approximations we introduced to perform calculations are the following.

PBMR model.

(i) Pebbles are regularly arranged inside the core (BCC or CHPOP lattices have been both analysed and compared); as a comparison, calculations have been performed on a infinite lattice of pebbles as well.

(ii) Pebbles are fixed inside the core, that is, each pebble occupies the same position from BOC to EOC. Of course, such an approximation is a very rough one, but it may be considered a first step to refine the model with which a pebble-bed core is usually described in MC simulations (a single pebble with white boundary conditions).

(iii) Control rods have been considered fully extracted during the whole life.

(iv) The core has been supposed as symmetric and only one twelfth of the core has been modelled.

(v) Radial and axial core temperature profiles have not been taken into account, due to the code limitations; in order to roughly assess the effect of such an approximation, a comparison has been performed with a model divided into two axial zones as described in [1].

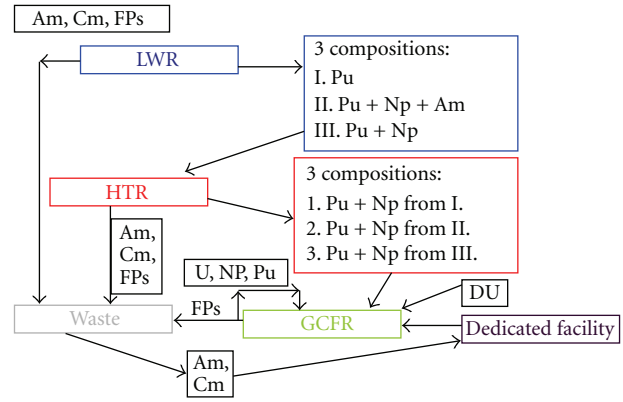

Figure 3: Sketch of the proposed cycle.

(vi) The ratio of the HM to the graphite mass is around 0.01.

GCFR model.

(i) As for the PBMR model, radial and axial core temperature profiles have not been taken into account, due to the code limitations; in order to roughly assess the effect of such an approximation, a comparison has been performed with a model with two axial zones.

(ii) Control rods have not been modelled.

(iii) No refuelling scheme has been considered (single batch).

6. Calculations and Results

A sketch of the proposed cycle is shown in Figure 3.

The initial Heavy Metal composition of the PBMR fuel is shown in Table 3.

The PBMR core has been irradiated as a single-batch: that is, of course, not realistic, but it is due to the current code limitations. All the core models considered resulted to

Table 3: PBMR initial HM composition (coming from typical LWR SNF; please see Table 1).

	Np^{237}	Pu^{238}	Pu^{239}	Pu^{240}	Pu^{241}	Pu^{242}
Mass fraction [%]	7.09	3.02	51.58	23.98	9.19	5.11

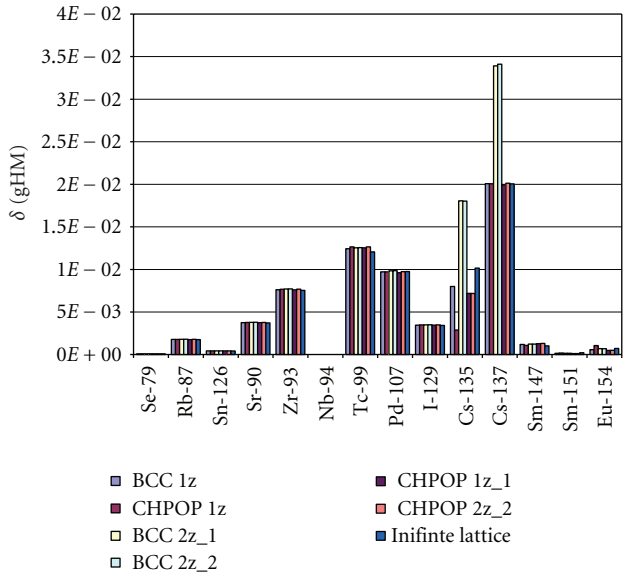

Figure 4: Production (grams) of some FPs per initial HM mass in the different PBMR core models (after 1063 EFPD).

maintain criticality up to about 800 Effective Full Power Days (EFPD).

Figures 4, 5, and 6 show the results we obtained as far as the fuel isotopic composition is concerned (BCC 1z is the Body Cubic Centered (BCC), 1-zone model; BCC 2z_1 is the BCC, 2-zone (axially) model, of which the composition of the upper (1) zone is considered; CHPOP 1z is the Column Hexagonal Point On Point (CHPOP), 1-zone model; etc.). We evaluated these compositions after 1062.50 EFPD, corresponding to about 530 GWd/tHM, in order to assess the difference arising with the different models in case of very high burnup.

Conversely, as an isotopic vector of Pu and Np to be inserted into the GCFR fuel, the PBMR fuel after 712.50 EFPD (about 356 GWd/tHM) has been considered. That is the burnup at which all the considered models are still critical. Of course, in this way we consider the worst case as far as the waste to energy ratio is concerned, obtaining a sort of upper limit for this parameter.

It is interesting to note that the considered core model does not strongly affect the fuel isotopic evolution, excepted for its Cs, Am^{243}, and Cm^{244} content. For these nuclides, the influence of the pebble arrangement (infinite lattice or BCC versus CHPOP) is more strong than the influence of the temperature profile (infinite lattice or 1-zone versus 2-zones). That is an interesting result, since it demonstrates that rough models like the infinite lattice work reasonably well at least for survey calculations, as far as the prediction of the fuel isotopic evolution is concerned.

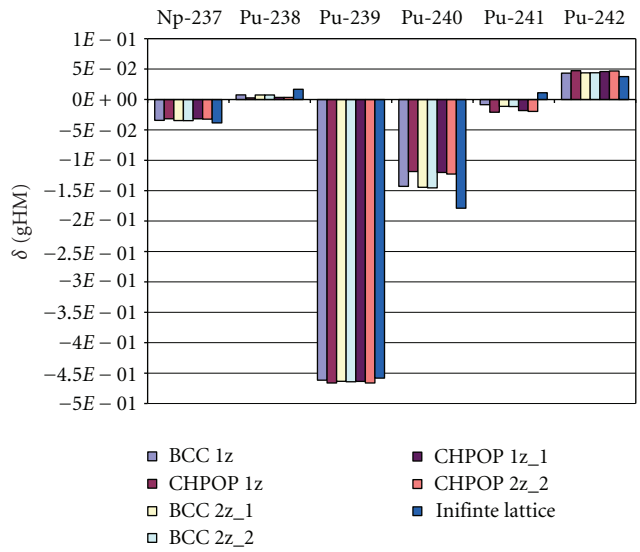

Figure 5: Production (grams) of Pu nuclides per initial HM mass in the different PBMR core models (after 1063 EFPD).

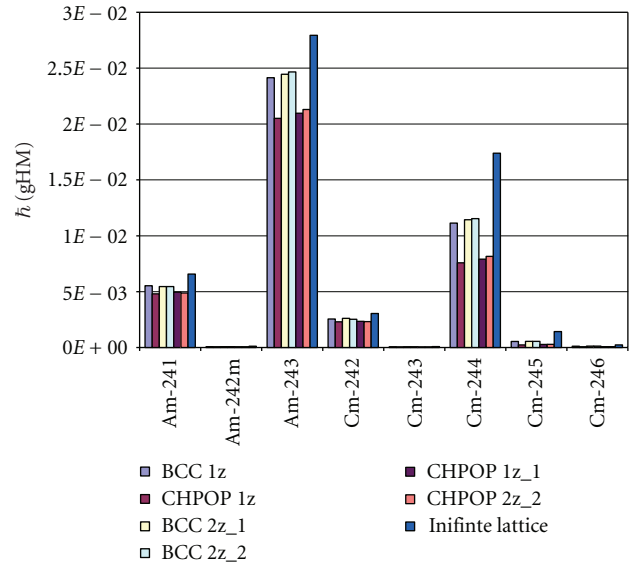

Figure 6: Production (grams) of Am and Cm nuclides per initial HM mass in the different PBMR core models (after 1063 EFPD).

Many of the results found in past work[1–7] are again confirmed: PBMR is a strong Pu and Np burner, but Am and Cm inventories increase substantially.

The isotopic Np and Pu vector in Table 4 constitutes the Pu+Np vector for the GCFR fuel, which is shown in Table 5.

The length of each irradiation cycle has been set in order to reach a 10% FIMA burnup. The cooling time between a cycle and the following has not been taken into account for the sake of simplicity. At the end of each considered cycle, the core is still critical. Then, if the fuel were still able to sustain irradiation from the damage point of view, its length could be further increased. The results obtained are illustrated in the Figures 7, 8, and 9. Please note that masses

Table 4: PBMR HM composition after 713 EFPD.

	Np^{237}	Pu^{238}	Pu^{239}	Pu^{240}	Pu^{241}	Pu^{242}	Am^{241}	Am^{243}	Cm^{242}	Cm^{244}	Others
Mass fraction (%)	7.97	5.48	25.97	29.31	16.54	11.18	0.91	1.85	0.19	0.41	0.19

Table 5: GCFR initial HM composition (82% at DU + 18% Pu+Np from PBMR; please see Table 4).

	U^{235}	U^{238}	Np^{237}	Pu^{238}	Pu^{239}	Pu^{240}	Pu^{241}	Pu^{242}
Mass fraction (%)	0.20	81.71	1.50	1.03	4.88	5.50	3.11	2.11

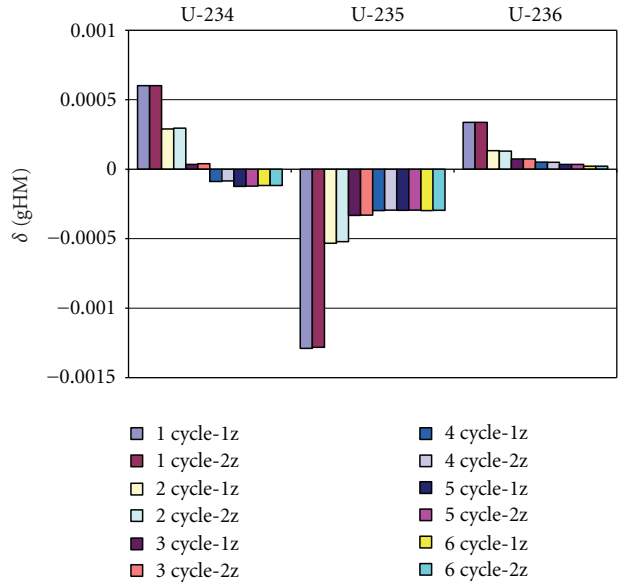

Figure 7: Production/destruction of some U nuclides per initial HM mass in the different GCFR core models, for each recycle.

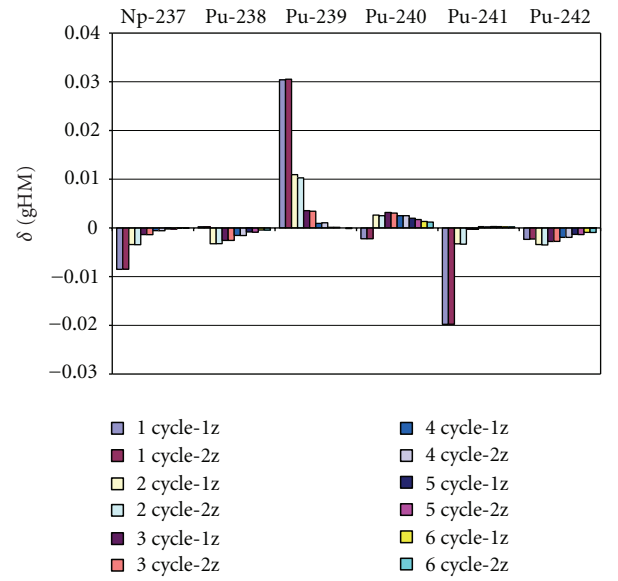

Figure 8: Production/destruction of some Np and Pu nuclides per initial HM mass in the different GCFR core models, for each recycle.

here reported are referred to the average content of the whole core, regardless of the number of the axial zone number (1 or 2). It is interesting to note that, similarly to the PBMR models, having 1 or 2 axial zones does not influence strongly the prediction of the isotopic composition.

As an additional result, it has been found that k_{eff} at BOC increases with multiple recycling [1].

As observed for the PBMR core model, using 1-zone instead of 2-zone model does not cause significant changes in the final composition of SNF (Figures 7, 8, and 9). Conversely, the model is very important when dynamic parameters are under investigation. However, much more detailed investigations are needed to evaluate dynamic parameters of the core and their trends.

We can also observe that the condition of "zero breeding gain," envisaged for GCFR, is progressively obtained by multiple recycling (see Pu^{239} and Pu^{241} in Figure 8).

The strategy of the GCFR "E" fuel cycle shows the following advantages.

(i) First of all, removing Am and Cm from the spent fuel allows in principle the possibility to recycle U, Pu, and Np a large number of times, since the neutronic dose and the heatload of the SNF are kept constant. Then, a virtually full exploitation of U resources is obtained.

(ii) Pernicious Pu isotopes are monotonously decreasing from cycle to cycle.

(iii) Am and Cm increase from BOC to EOC even slower from cycle to cycle.

(iv) The isotopic evolution of the fuel from cycle to cycle is good from the safety point of view (after the relatively small drop between first and second cycle, U content increases.)

(v) Waste produced per unit energy is extremely small (please see next paragraph).

Nevertheless, there are some drawbacks as well, include the follwing.

(i) Times to reach equilibrium composition are very long (after about 60 years equilibrium has still to be reached.)

(ii) The reactivity at BOC tends to increases from cycle to cycle. That may be a problem from the point of view of the control reactivity device design.

(iii) The reduction of the long term radiotoxicity of the final waste (i.e., FPs, Am, and Cm) might be obtained by designing dedicated assemblies.

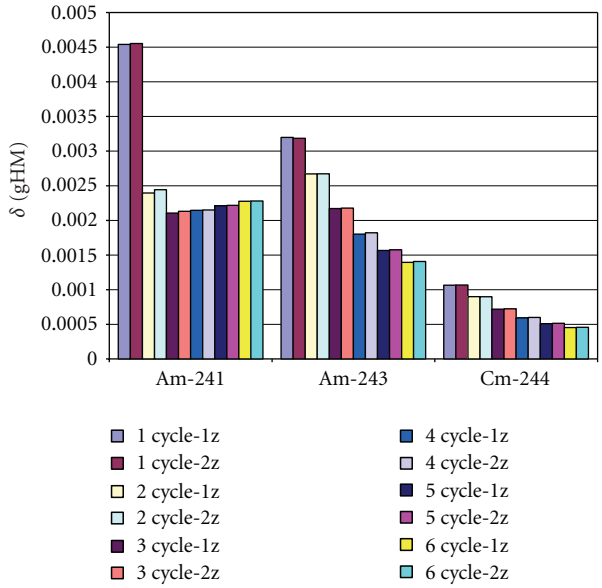

Figure 9: Production/destruction of some Am and Cm nuclides per initial HM mass in the different GCFR core models, for each recycle.

7. Radiotoxicity and Heatload of the Final Waste

First of all, calculating of the Level Of Mine (LOM) is useful to assess the impact of the integrated cycle strategy regarding the radiotoxicity of the final waste.

LOM calculation procedure has been extensively explained in [4].

In the considered case, we have to take into account that the following hold.

(i) Every year about 250 kg of Pu+Np are discharged by the LWR considered as a reference.

(ii) Considering 712.5 EFPD the discharge burnup for PBMR pebbles, this core requires about 155 kg/year of Pu+Np from LWR. That means each PBMR needs 0.62 LWR supplying its annual fuel charge.

(iii) In order to feed the first GCFR core, containing 13.7 t of Pu+Np from PBMR SNF (712.50 EFPD, i.e., 356 GWd/tHM), SNF from about 56 PBMRs is required.

(iv) The radiotoxicity of the natural U is 20 mSv/g.

(v) To obtain 1 g of U enriched to 3/4%, 10 g of natural U are required.

(vi) We will assume equal to zero the radiotoxicity of DU (in order to obtain the worst conditions).

The numerical ratio between LWR, HTR, and GCFR is not particularly favorable from the economical point of view. Indeed, yearly 1 PBMR is able to burn the Pu+Np inventory coming from 0.62 LWR. However, 1.3 PBMR, which can burn the whole Np+Pu mass coming from 1 LWR, correspond to 800 MWth while 1 LWR corresponds to 3030 MWth. What is more, 56 PBMR cores are capable for supplying the fuel mass to start a new GCFR core. Hence, it is clear that this is a very difficult matter and, in order to evaluate this aspect rigorously, we should perform a complete analysis of the scenario in which our cycle could be inserted [1].

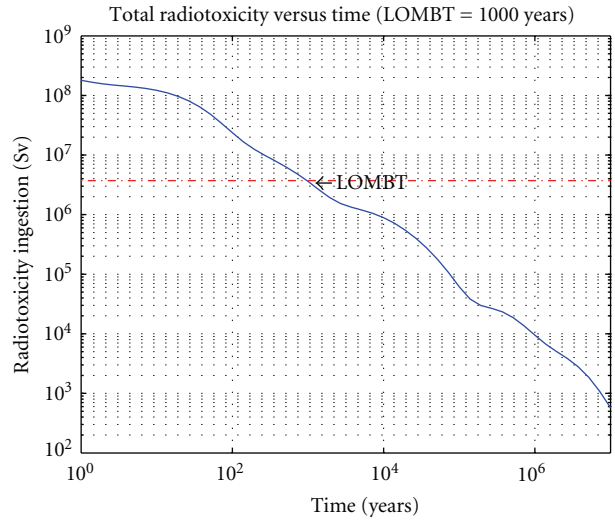

Figure 10: LOMBT of PBMR SNF (FPs, Am, and Cm).

Then, we are capable for calculating the LOM of the SNF of each reactor of our chain.

Since there are not any significant differences between 1-zone and 2-zore core models as far as the isotopic composition is concerned, we will show the results related to the 1-zone model for the sake of simplicity.

The results are summarized in the following Table 6.

As know, the Level Of Mine Balancing Time (LOMBT) of LWR SNF, in the case of OTTO fuel cycle, is around 150 000 years, since waste is composed of U, Pu, MA, and FPs.

The integrated LWR-HTR-GCFR cycle causes a change of point of view, because U, Pu, and Np are fuel, and not waste anymore. Then, a strong reduction of the waste produced per unit energy ratio will occur (Table 7).

Results related to Radiotoxicity versus time as well as Heatload versus time are shown in the following Figures 10, 11, 12, 13, 14, 15, 16, 17, 18, 19, 20, 21, 22, 23, 24, 25, 26, 27, 28, 29, 30, and 31.

It is interesting to highlight the following.

(i) First of all, the LOMBT is always lower than 20 000 years. GCFR SNF reaches LOM after about 10 000 except for the first cycle. PBMR SNF reaches LOM after 1000 years. Nevertheless, we have to remember that this low values are obtained thanks to recycling both Pu and Np. If that was not true, the LOMBT would increase by an order of magnitude (e.g., cf. Figure 10, and 11).

(ii) The LOMBT of GCFR SNF decreases monotonously with multiple recycling. That is due to the progressive decrease of MA content of SNF.

(iii) It is interesting to note that the long-term radiotoxicity of GCFR SNF is substantially due to Am instead of Cm's daughters (this is different from what found in some past studies focusing on homogeneous multiple recycling in GCFR; please see [1–6]). This is in

Table 6: LOM for SNF of the considered reactors.

	LWR	PBMR	GCFR*	Whole cycle
LOM [Sv]	6×10^6	3.72×10^6	2.10×10^8	2.10×10^8

*Actually this value should be increased by the radiotoxicity of DU added to replace Am, Cm, and FPs of the GCFR SNF. However, no significant changes of results will happen, since the radiotoxicity of DU is lower than that of U_{nat}.

Table 7: Waste per unit energy: comparison (chain composed of 1 GCFR "E", 1.3 PBMR-400, 0.806 LWR).

	LWR 1000	PBMR-400	GCFR "E"	Integrated cycle
FP [g/year]	9.67×10^5	2.34×10^4	1.33×10^5	1.12×10^6
Am [g/year]	1.19×10^4	9.93×10^3	4.48×10^4	6.66×10^4
Cm [g/year]	9.23×10^2	2.34×10^3	8.37×10^3	1.16×10^4
Thermal Energy [TWh/year]	21×39	4.56	21.02	46.97
Electric Energy [TWh/year]	7.06	2.19	10.09	19.34
Ratio waste/energy* [g/TWh_{th}]	1.13×10^6	7.83×10^3	8.87×10^3	2.56×10^4
Ratio waste/energy* [g/TWh_e]	3.43×10^6	1.63×10^4	1.85×10^4	6.23×10^4

*This results is obtained considering 30 t/years of SNF for LWR (OTTO cicle).

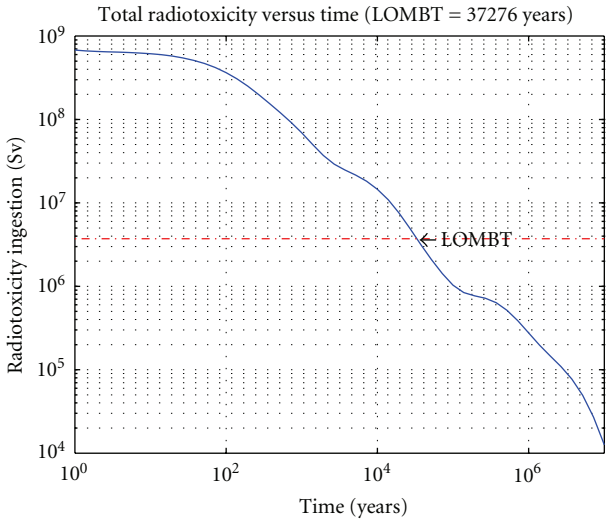

Figure 11: LOMBT of PBMR SNF (FPs, Pu, Am, and Cm).

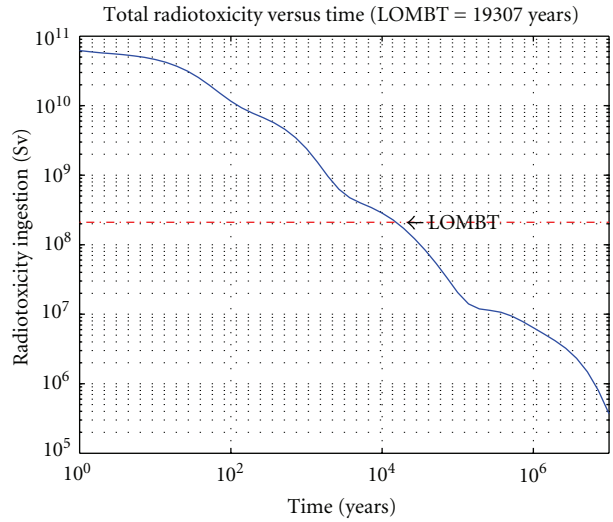

Figure 12: LOMBT of GCFR SNF end first cycle (FPs, Am, and Cm).

principle an advantage of the strategy here chosen, because Cm decays in relatively small times while Am can be burnt in dedicated assemblies. Then, the results here achieved give us an important hint about a possible and feasible way to close the nuclear fuel cycle.

(iv) Heatload versus time does not show any remarkable behaviour.

8. Conclusions

The analysis performed in the framework of the EU project PUMA substantially confirms previous findings, but adding some remarkable developments.

Once again, as found out in previous researches, the integrated LWR-HTR-GCFR shows very good capabilities to achieve a sustainable nuclear fuel cycle.

As stated before, LWR-HTR-GCFR allows us the possibility to meet the following criteria.

(i) Excellent exploitation of U resources intrinsically coupled with the strong reduction of the mass of the final waste (ratio waste/energy decreases by two orders of magnitude compared to OTTO).

(ii) Reduction of the radiotoxicity of the final waste to that of FPs and MAs (i.e., reduction of LOMBT by an order of magnitude compared to OTTO).

(iii) Strong reduction of Pu (and, if necessary, Np) stockpiles thanks to HTR loaded with fertile-free fuel, in parallel with an important change of its isotopic composition, which becomes extremely proliferation resistant (fuel that contains high masses of strong heat- and neutron-emitters).

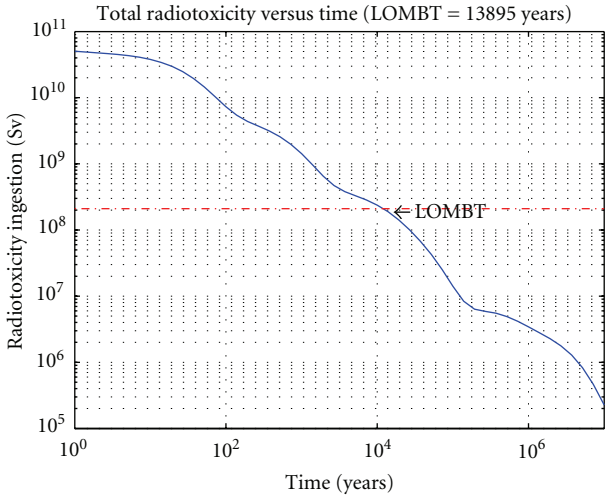

Figure 13: LOMBT of GCFR SNF end second cycle (FPs, Am, and Cm).

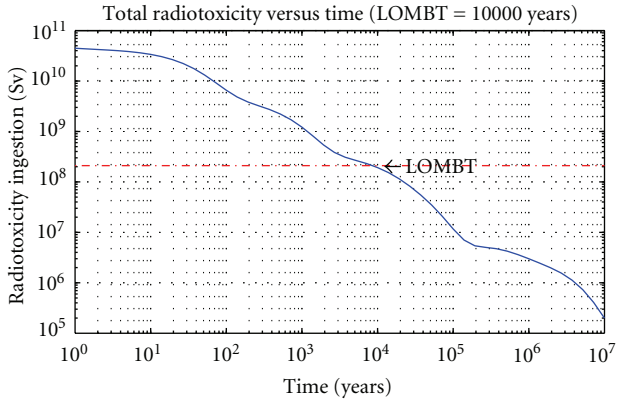

Figure 14: LOMBT of GCFR SNF end third cycle (FPs, Am, and Cm).

(iv) Very long fuel cycles thanks to the very favourable neutron economy that is typical of He-cooled reactors

Additionally, the strategy here developed permits us some others improvements.

(i) Heterogeneous recycling of SNF (separating FPs, Am, and Cm from U, Np, and Pu) in principle removes any technological limit to the possibility of recycling HMs many times. Indeed pernicious nuclides (these are, in any case, relatively small amounts.) like Cm isotopes are stored as a final waste or recycled in dedicated facilities.

(ii) Multiple recycling of GCFR SNF coupled to removing Am, Cm, and FPs shows the following important trends.

(a) Am and Cm amounts increase even slower from cycle to cycle.

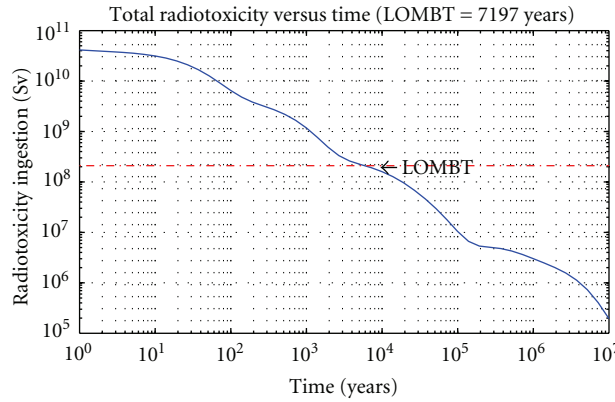

Figure 15: LOMBT of GCFR SNF end fourth cycle (FPs, Am, and Cm).

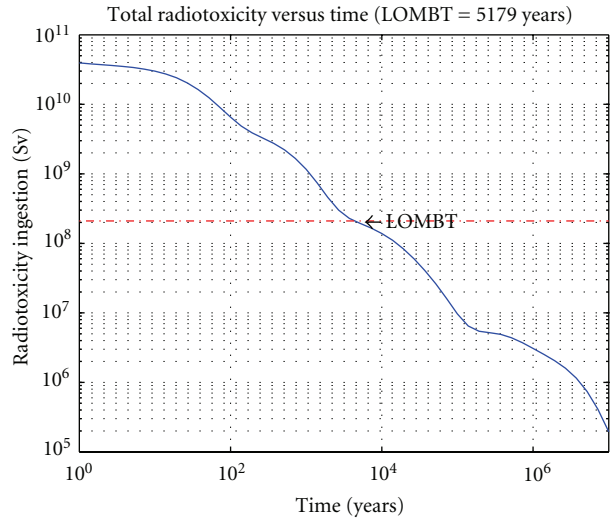

Figure 16: LOMBT of GCFR SNF end fifth cycle (FPs, Am, and Cm).

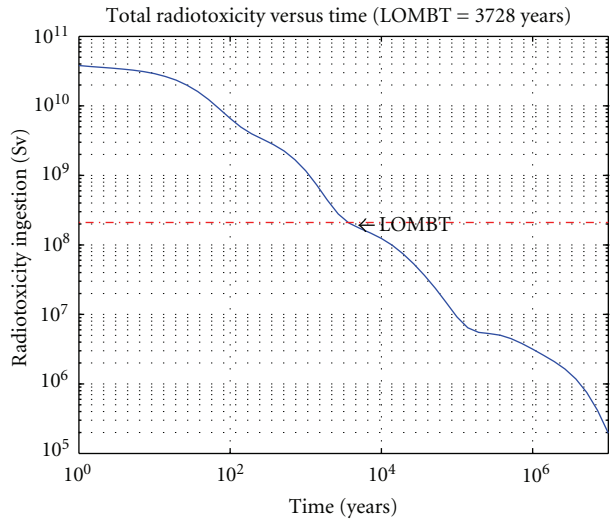

Figure 17: LOMBT of GCFR SNF end sixth cycle (FPs, Am, and Cm).

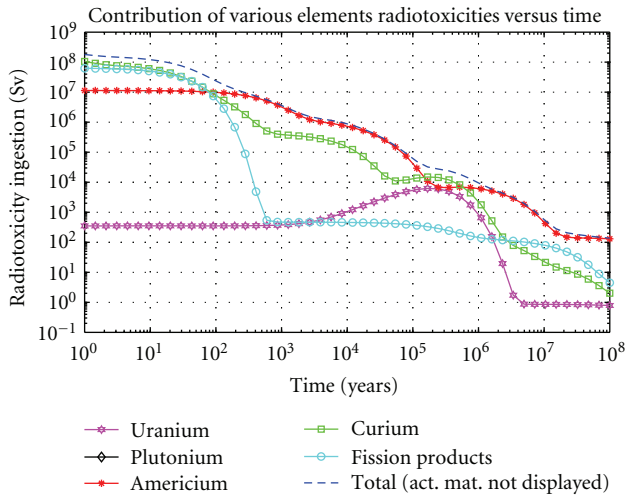

Figure 18: Contributions to radiotoxicity versus time—PBMR SNF.

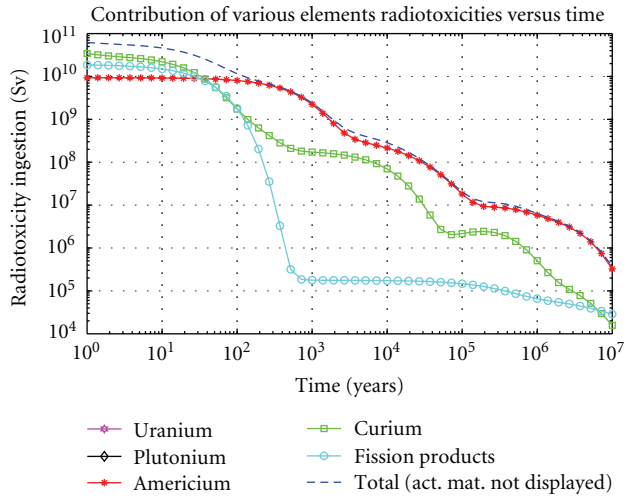

Figure 19: Contributions to radiotoxicity versus time—GCFR SNF end first cycle.

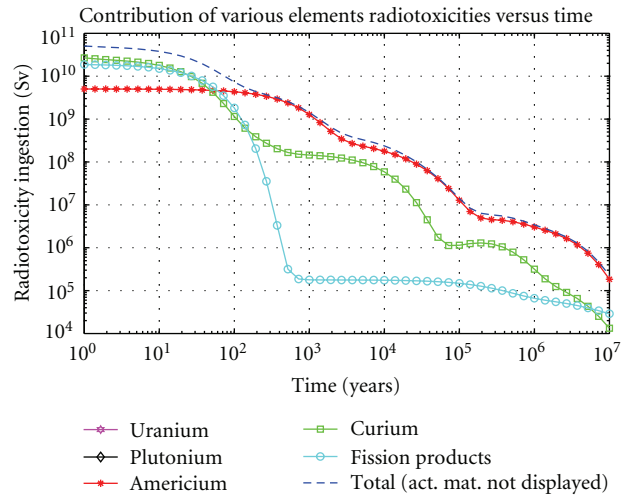

Figure 20: Contributions to radiotoxicity versus time—GCFR SNF end second cycle.

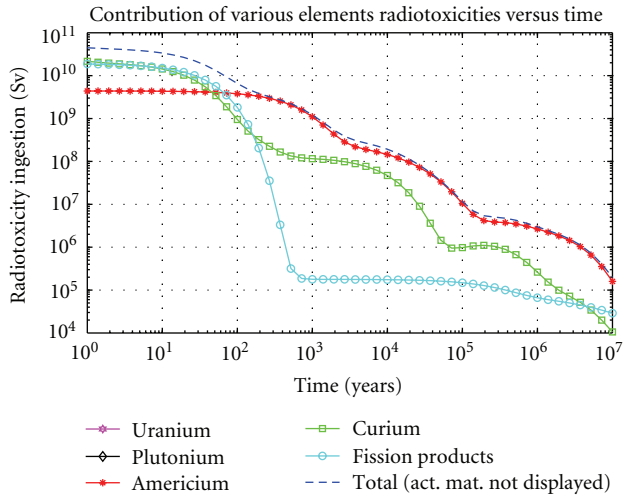

Figure 21: Contributions to radiotoxicity versus time—GCFR SNF end third cycle.

(b) As a consequence, the LOMBT of GCFR SNF (Am, Cm, and FPs) decreases from cycle to cycle.

(c) Pu isotopic composition is good enough to sustain very long irradiation cycles (more than 9 years in principle), but it is not suitable for military uses (high content of Pu^{240}).

(d) Np is always burnt by both HTR and GCFR.

(e) Pu^{238}, which is a strong alpha- and neutron-emitter and then which could be pernicious for reprocessing, decreases during multiple recycling.

(iii) Radiotoxicity of GCFR SNF, after less than 100 years, is essentially due to Am nuclides instead of Cm ones: that indicates designing of a dedicated assembly to burn Am, along with an opportune cooling time of SNF, as a straightforward way to close the cycle effectively.

(iv) The excellent GCFR neutron economy and its huge DU inventory permits us the possibility to insert some dedicated assemblies to burn Am and Cm without significant consequences concerning core safety.

What is more, the analysis here performed gives us some clues regarding He-cooled reactor core modelling as well. Particularly, we found that the following hold.

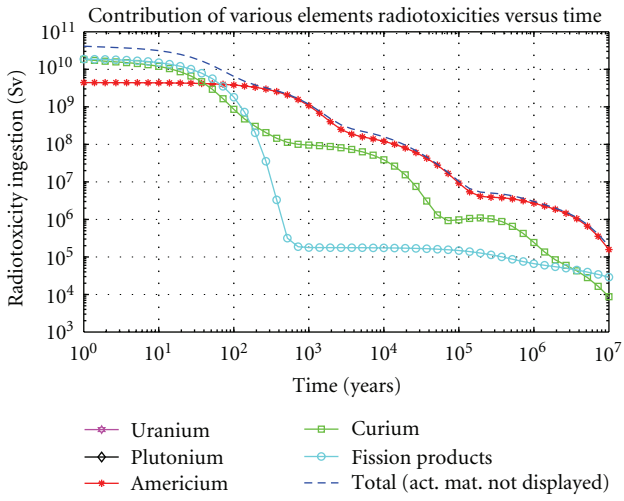

Figure 22: Contributions to radiotoxicity versus time—GCFR SNF end fourth cycle.

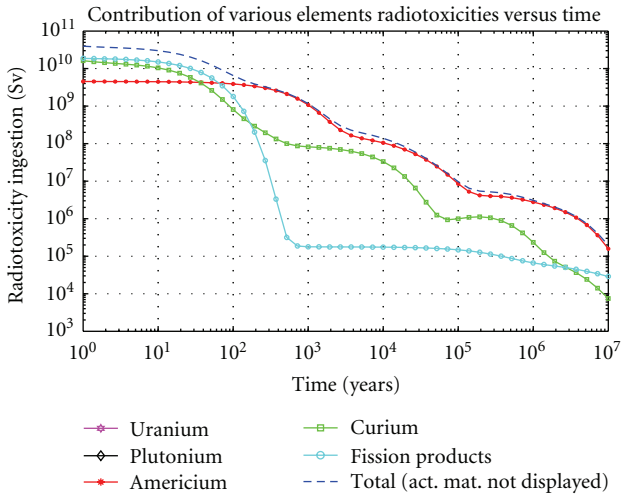

Figure 23: Contributions to radiotoxicity versus time—GCFR SNF end fifth cycle.

(i) As far as PBMR modelling is concerned, burnup calculations give results in good agreement with each other regardless the kind of (simplified) model chosen to describe the core itself [14]. Then, also due to the characteristics of the simulated reactor and taken into account the commonly used modelization approach (infinite lattice of pebbles with white conditions on the boundary), the use of quite rough models can be a good approximation, at least if we are only interested in the final isotopic composition. What is more, current MCNP based burnup codes still do not allow us by far to simulate such a complex core like the pebble-bed HTRs one, then the use of approximated models is necessary, at least at the moment. Conversely, dynamic parameters are very badly estimated by approximated models, thus we cannot rely on results supplied by this kind of calculation (some further explanations on this matter can be found in [1, 14]).

(ii) Both PBMR and GCFR isotopic inventory versus burnup seems to be only slightly influenced by the axial temperature profile that can be described with Monteburns2.0 (i.e., varying only the temperature of not-burnable materials), so that it is not worth

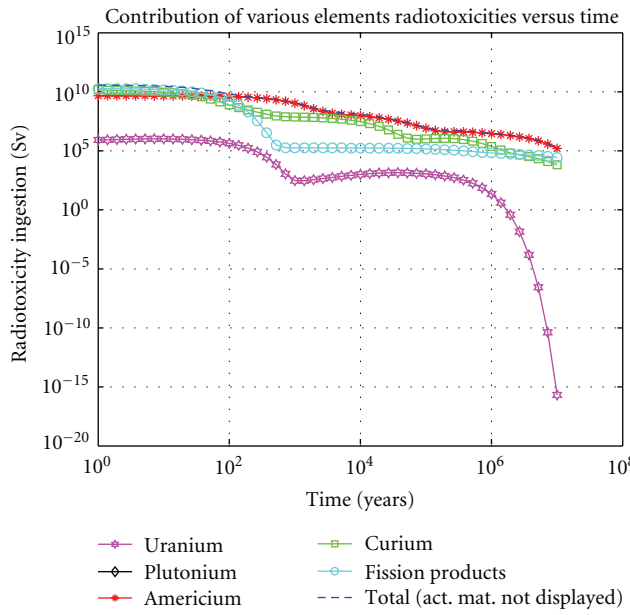

Figure 24: Contributions to radiotoxicity versus time—GCFR SNF end sixth cycle.

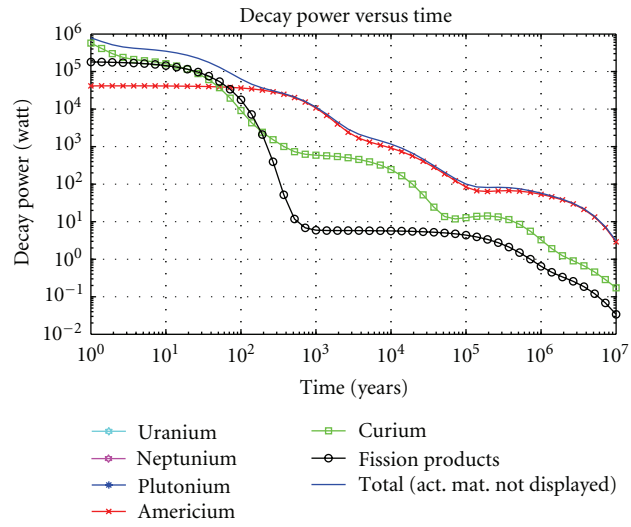

Figure 25: Contributions to heatload versus time—PBMR SNF.

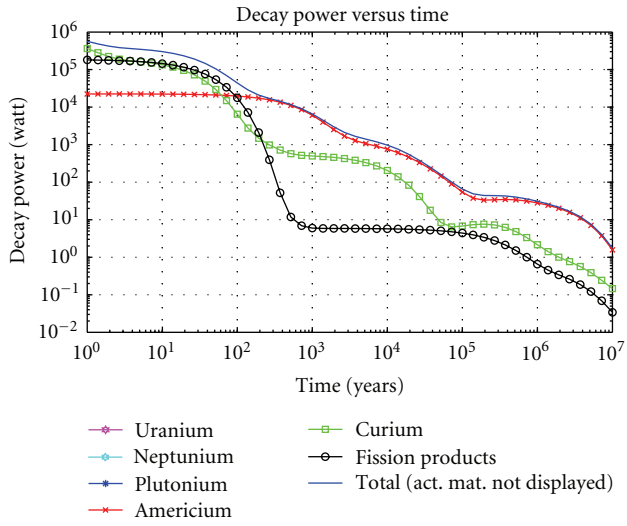

Figure 26: Contributions to heatload versus time—GCFR SNF end first cycle.

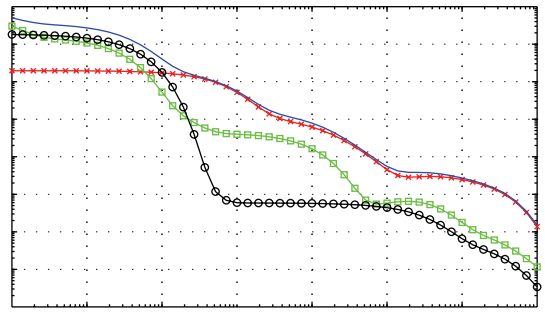

Figure 27: Contributions to heatload versus time—GCFR SNF end second cycle.

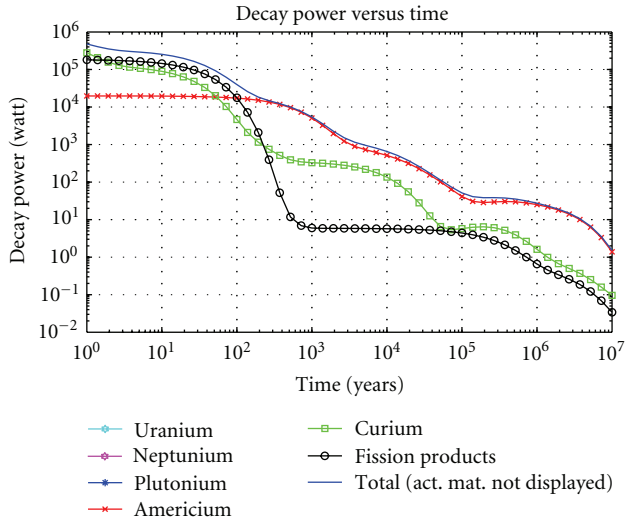

Figure 28: Contributions to heatload versus time—GCFR SNF end third cycle.

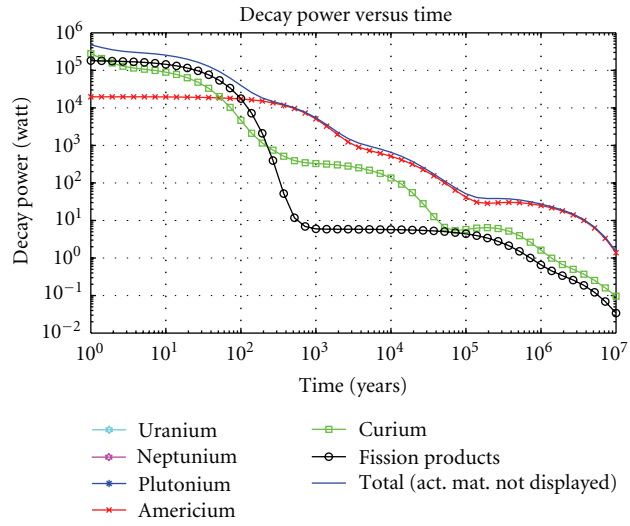

Figure 29: Contributions to heatload versus time—GCFR SNF end fourth cycle.

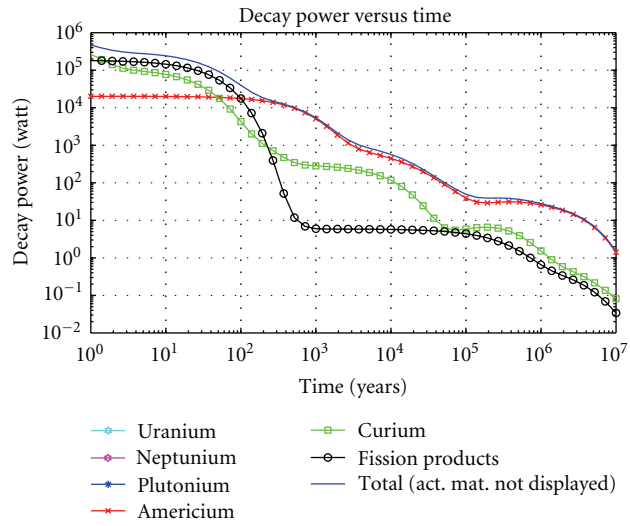

Figure 30: Contributions to heatload versus time—GCFR SNF end fifth cycle.

increasing calculation time because of a 2-zone model. Thus, we can adopt 1-zone models to simulate irradiation histories of these cores, having an higher calculation speed as a benefit.

(iii) On the other hand, GCFR reactivity parameters are also strongly influenced by axial temperature profile, so that we cannot rely on the results found with our approximated models.

As a future work, to close this cycle effectively, designing a dedicated assembly for Am and Cm burning is requested. Of course, a fuelling scheme for the GCFR core is necessary as well.

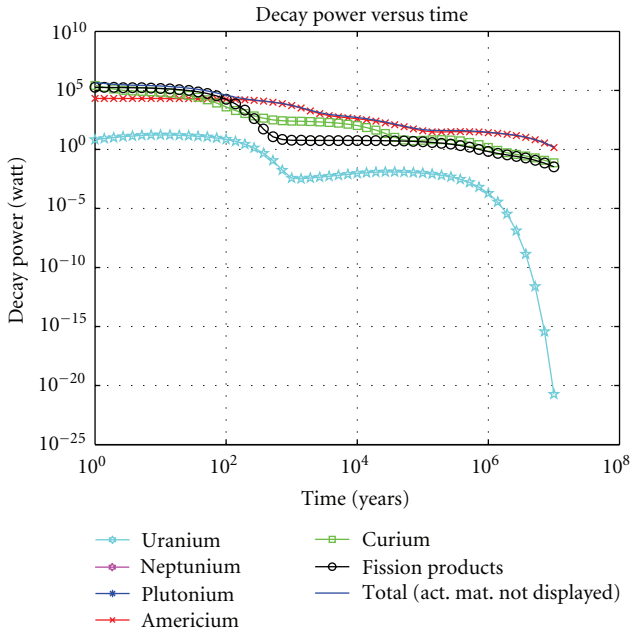

FIGURE 31: Contributions to heatload versus time—GCFR SNF end sixth cycle.

Finally the obtained results should be very useful if inserted in a more complete scenario analysis (see also [15]).

However, the obtained results seems to be very promising as far as finding this final solution is concerned.

Acknowledgments

The work presented in this paper was partly funded by the European Union Sixth Framework Program, under contracts PuMA, GCFR, and RAPHAEL. First of all we would like to thank Dr. Somers of ITU, Dr. Mitchell of AMEC-NNC, Dr. Kuijper and Dr. van Heek both of NRG, and Prof. Kloosterman of TUD, Dr. von Lensa of FZJ for the collaboration. Finally, we want to thank Prof. Forasassi of DIMNP for his strong support and Dr. Bufalino of SORIT for his precious suggestions and help.

References

[1] E. Bomboni, N. Cerullo, and G. Lomonaco, "Assessment of LWR-HTR-GCFR integrated fuel cycle," EU PUMA Project, Work Package 1.2, Deliverable D127, February 2009.

[2] http://www.puma-project.eu/.

[3] E. Bomboni, N. Cerullo, G. Lomonaco, and V. Romanello, "Nuclear waste impact reduction using multiple fuel recycling strategies," in *Proceedings of the 1st International Conference on Physics and Technology of Reactors Applications (PHYTRA '07)*, Marrakech, Morocco, March 2007.

[4] E. Bomboni, N. Cerullo, G. Lomonaco, and V. Romanello, "A critical review of the recent improvements in minimizing nuclear waste by innovative gas cooled reactors," *Science and Technology of Nuclear Installations*, vol. 2008, Article ID 265430, 18 pages, 2008.

[5] E. Bomboni, "New developments in actinides burning with symbiotic LWR-HTR-GCFR fuel cycles," in *Proceedings of the International Youth Nuclear Congress*, Interlaken, Switzerland, September 2008.

[6] E. Bomboni, N. Cerullo, and G. Lomonaco, "New developments in actinides burning with symbiotic LWR-HTR-GCFR fuel cycles: perspectives and challenges," in *Proceedings of the 10th International Exchange Meeting on Partitioning and Transmutation (IEMPT '08)*, Mito, Japan, October 2008.

[7] http://www.gcfr.org/.

[8] J. F. Briefmeister, "MCNP^{TM}—a general Monte Carlo n-particle transport code," Tech. Rep. LA-CP-03-0245, version 5, Los Alamos National Laboratory.

[9] A. G. Croff, "A User's Manual for the ORIGEN2 Computer Code," ORNL/TM-7175, July 1980.

[10] D. L. Poston and H. R. Trellue, "User's Manual Version 2.0 for Monteburns 1.0," LA-UR-99-4999, September 1999.

[11] http://www.perl.com/.

[12] W. Haeck and B. Verboomen, "A validated MCNP(X) cross section library based on JEFF3.1," Open Report SCK-CEN-BLG-1034 Rev. 0, October 2006.

[13] T. R. England, W. B. Wilson, and M. G. Stamatelatos, "Users manual for EPRI-CINDER code and data," EPRI-NP-356, LANL, December 1976.

[14] E. Bomboni, N. Cerullo, and G. Lomonaco, "Simplified models for pebble-bed HTR core burn-up calculations with MONTEBURNS2.0," *Annals of Nuclear Energy*.

[15] B. Vezzoni, N. Cerullo, G. Forasassi, et al., "Preliminary evaluation of a nuclear scenario involving innovative gas cooled reactors," *Science and Technology of Nuclear Installations*.

Hindawi Publishing Corporation
Science and Technology of Nuclear Installations
Volume 2009, Article ID 815394, 2 pages
doi:10.1155/2009/815394

Erratum

Erratum for "Assessment of LWR-HTR-GCFR Integrated Cycle"

Eleonora Bomboni,[1] Nicola Cerullo,[1] and Guglielmo Lomonaco[2]

[1] *DIMNP, University of Pisa, Italy*
[2] *University of Pisa, Italy*

Correspondence should be addressed to Guglielmo Lomonaco, g.lomonaco@ing.unipi.it

Received 15 December 2009; Accepted 15 December 2009

Assessment of LWR-HTR-GCFR Integrated Cycle

Erratum. Please substitute the old Figure 10 with the following new Figure 1, the old Figure 11 with the following new Figure 2, Please substitute the old Figure 18 with the following new Figure 3, the old Figure 25 with the following new Figure 4, and the paragraph (i) at page 8, column 2, with the following:

"First of all, the LOMBT is always lower than 50000 years. GCFR SNF reaches LOM after about 10000 except for the 1st and the 2nd cycle (Figures 12 and 17). As far as PBMR is concerned, its waste composed of Am, Cm and FPs is characterized by a LOMBT three time higher than that of the average GCFR waste (Figure 10). Furthermore, considering all the HM coming from PBMR as a waste (i.e., including Np and Pu; that corresponds to a OTTO cycle for PBMR), the LOMBT increases by two orders of magnitude (please compare Figures 10 and 11) and becomes even worse than that of LWR waste. Hence, the advantages of recycling Pu and Np coming from PBMR are confirmed."

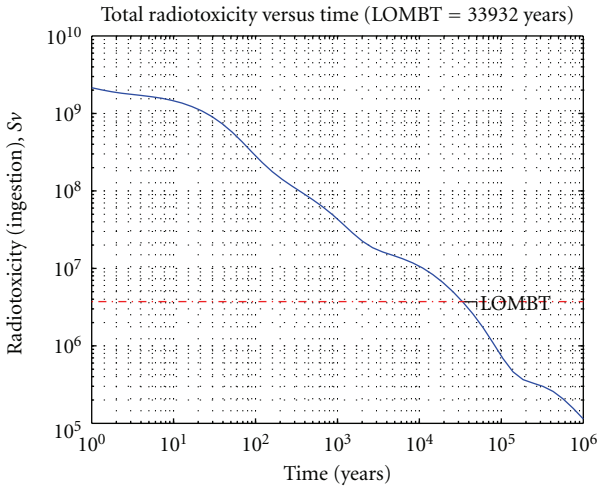

Figure 1

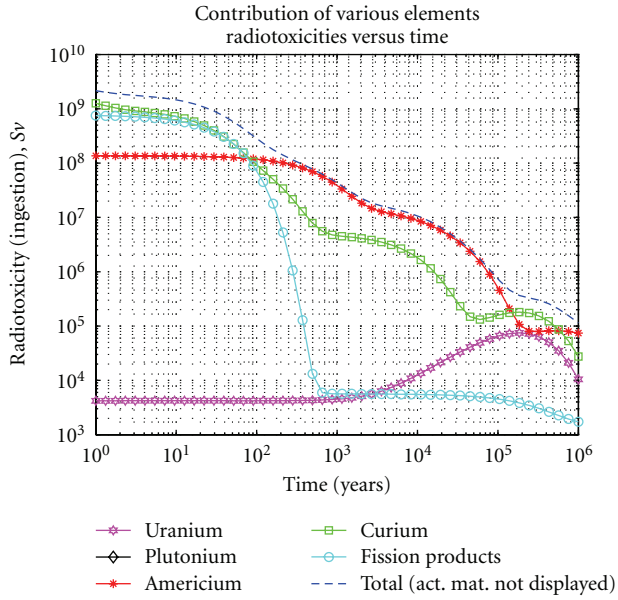

Figure 3

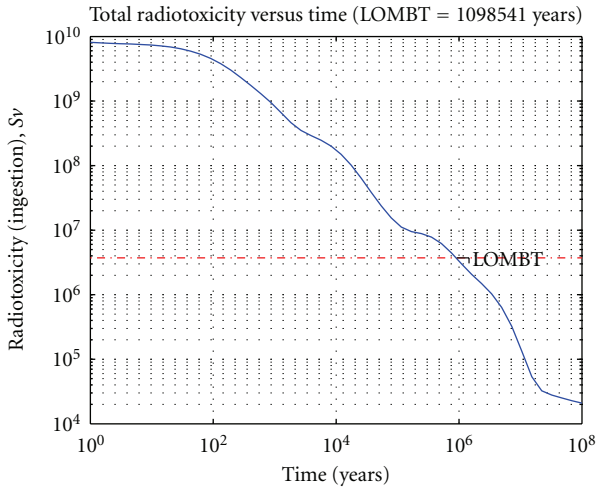

Figure 2

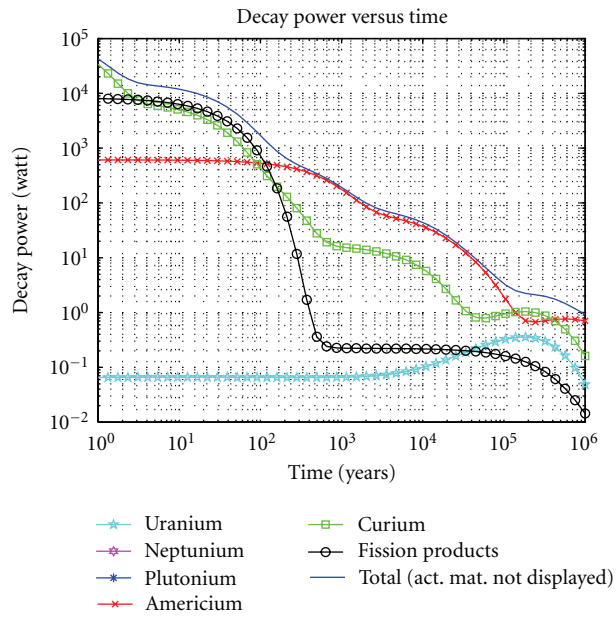

Figure 4

Hindawi Publishing Corporation
Science and Technology of Nuclear Installations
Volume 2009, Article ID 940286, 16 pages
doi:10.1155/2009/940286

Research Article

Preliminary Evaluation of a Nuclear Scenario Involving Innovative Gas Cooled Reactors

Barbara Vezzoni,[1] Nicola Cerullo,[1,2] Giuseppe Forasassi,[1] Emil Fridman,[3] Guglielmo Lomonaco,[1,2] Vincenzo Romanello,[4] and Eugene Shwageraus[5]

[1] *Department of Mechanical, Nuclear and Production Engineering (DIMNP), University of Pisa, CIRTEN, Largo L. Lazzarino No. 2, 56126 Pisa, Italy*
[2] *Energy and Environmental Conditioning Department (DIPTEM), University of Genova, Via all'Opera Pia n. 15/a, 16145 Genova, Italy*
[3] *Accident Analysis Division (FWSS), Forschungszentrum Dresden-Rossendorf (FZD), P.O. Box 51 01 19, 01314 Dresden, Germany*
[4] *Institute for Nuclear and Energy Technologies (IKET), Karlsruhe Institute for Tecnology (KIT), Hermann-von-Helmholtz-Platz 1, 76344 Eggenstein, Leopoldshafen, Germany*
[5] *Department of Nuclear Engineering, Ben Gurion University of the Negev, P.O. Box 653, Beer Sheva 84105, Israel*

Correspondence should be addressed to Nicola Cerullo, cerullo@docenti.ing.unipi.it

Received 31 March 2009; Accepted 1 September 2009

Recommended by Jim Kuijper

In order to guarantee a sustainable supply of future energy demand without compromising the environment, some actions for a substantial reduction of CO_2 emissions are nowadays deeply analysed. One of them is the improvement of the nuclear energy use. In this framework, innovative gas-cooled reactors (both thermal and fast) seem to be very attractive from the electricity production point of view and for the potential industrial use along the high temperature processes (e.g., H_2 production by steam reforming or I-S process). This work focuses on a preliminary (and conservative) evaluation of possible advantages that a symbiotic cycle (EPR-PBMR-GCFR) could entail, with special regard to the reduction of the HLW inventory and the optimization of the exploitation of the fuel resources. The comparison between the symbiotic cycle chosen and the reference one (once-through scenario, i.e., EPR-SNF directly disposed) shows a reduction of the time needed to reach a fixed reference level from ∼170000 years to ∼1550 years (comparable with typical human times and for this reason more acceptable by the public opinion). In addition, this cycle enables to have a more efficient use of resources involved: the total electric energy produced becomes equal to ∼630 TWh/year (instead of only ∼530 TWh/year using only EPR) without consuming additional raw materials.

1. Introduction

The fossil fuels extensive use for the energy production is, nowadays, no longer sustainable. Therefore new innovative strategies for the energy sector have to be found.

Focusing on the electricity production sector, central role could be entrusted to the nuclear energy production, because it is the only source of energy able to provide a large quantity of energy without greenhouse gas releases (or with very small quantity if the whole nuclear energy chain is taken into account) [1].

The present work focuses on the analysis of a possible symbiotic cycle linking European Pressurized Reactors (EPRs) with Pebble Bed Modular Reactors (PBMRs) and Gen-IV Gas Cooled Fast Reactors (GCFRs).

In particular, the advantages concerning the final wastes minimization and the exploitation of the fuel resources involved have been compared with a chosen reference scenario (the Once-through scenario). The investigation of these two aspects is in agreement also with the Gen-IV sustainability goals [2].

One of the major questions that public opinion asks to nuclear community is: how the nuclear fuel cycle could be closed?

Worldwide, some strategies have been indicated and the most agreed is the adoption of a geological disposal

in synergy with the development of new facilities able to minimize during their life the produced wastes (e.g., using fast fission processes).

The present work is inserted in this framework. Gas cooled reactors adoption (thermal and fast solutions) has been analyzed, because these facilities seem to be very attractive for the future primary energy supply (not only for electricity chain), as consequence of the potential flexibility for a coupling with industrial high temperature processes.

In addition the innovative gas cooled reactors (HTRs and GCFRs) have some features (e.g., neutron economy) that seem to be particularly useful in order to minimize the long-term waste radiotoxicity and to improve the fuel exploitation.

2. General Aspects

The strong reliance on fossil fuels (83% of total energy supply and 66% of total electricity production [3]) has originated some social and environmental problems.

In fact, the geological distribution of fossil fuels involves only few countries that, in the most of the cases, do not have a stable political situation. This implies that the future supply could not be guaranteed a priori on the basis of the fossil fuels availability only. In addition, the extensive use of fossil fuels has involved an increase of greenhouse gas (GHG) emissions with effects on the world average energy temperature respect the preindustrial level [4].

Concerning nuclear energy resources, the situation is quite different, because Uranium is more homogeneously spread than oil, and in general in politically stable countries (e.g., Canada or Australia), so it is possible to be more confident for the future supply, considering also that nuclear energy has very low greenhouse gas emission rates (even if we look at the whole life cycle).

Even if the whole scientific community is not unanimous in this approach, the problem of climate change has motivated research activities at different level in several organizations. The Intergovernmental Panel on Climate Change (IPCC) has affirmed that the only way to arrest this warming process is to tangibly reduce the CO_2 emissions before 2050 (where the desirable level is between 85% and 50% of actual releases) [4].

Taking into account this technical information, the G8 Heiligendamm Summit (2007) has fixed the value at 50% of reduction in 2050 to achieve by the change of energy-electricity production chains [5], sector responsible for a very large fraction of CO_2 emissions.

In order to reach, as soon as possible, this goal EU has fixed some intermediate objectives (the so-called 3×20 objectives) up to 2020: 20% of GHG emissions reduction achievable by the improvement of 20% of energy saving and the extension up to 20% of the renewable sources in the total energy mix [6].

In this framework, the worldwide agreement is essential, in fact some actions, nowadays deeply analysed, have been identified [7]:

(i) the improvement of energy efficiency in every sectors,

(ii) the extensive use of renewable sources (hydro, biomass, wind, and solar),

(iii) the improvement on nuclear energy production and on new carbon capture and sequestration (CCS) technologies.

This work focus on the analysis of the nuclear energy role considering the advantages coming from the introduction of new facilities (e.g., Gas cooled reactors proposed within Gen-IV frame) [1, 8].

In addition, the social acceptability of nuclear energy has been considered as a base criterion to develop a new energy strategy; therefore solutions, as symbiotic cycle, with the aim to minimize final radioactive wastes (in particular Minor Actinides-MAs and High Level Waste) by the recycling of Plutonium and the transmutation of MAs (Am and Np) became more and more attractive.

3. Uranium Resources

From the sustainability point of view, particular attention has to be directed to the optimization of the resources involved in a specific scenario.

As a matter of fact, Gen-IV reactors will not be ready before 2040 and till this date nuclear reactors will be Uranium consuming type (considering Gen-II reactors, and Gen-III and Gen-III$^+$ facilities). As a consequence, the analysis of resources is a basilar aspect to treat.

Therefore, the main question concerning resources could be [9]: will the Uranium resources be sufficient to cover the growth of reactor capacity, required to follow the energy-electricity demand?

The answer to this question is not easy because it depends on several different factors. Anyhow, scenario analysis could be a useful "tool" for this investigation. As presented in [10], the Identified Resources (available at cost <130 USD/kgU) are estimated at $5.469 \cdot 10^6$ tonU, where $3.338 \cdot 10^6$ tonU are Reasonably Assured Resources (RARs) and $2.13 \cdot 10^6$ tonU are Inferred Resources (IRs). At which could be added 2.8 million of tonU as prognosticate undiscovered resources, 22 million of tonU in phosphates and $6.078 \cdot 10^6$ tonTh (fertile fuel that could be used in nuclear reactors, e.g., HTR).

These values are only the boundaries for the scenario analysis, in fact a more interesting comparison is between the U annual production versus the U annual demand.

The total U annual demand in 2007 (407 reactors in operation worldwide) has been 69110 tonU; whereas the U annual production in 2007 has been 43328 tonU; this means that each year, to cover the demand, the stock pile of Uranium (collected during the previous years of nuclear energy use) is driven down [10]. In fact, as presented in Figure 1, starting from 1990 the uranium requirements are larger than the uranium production; therefore a correct and integrated strategy, starting from the U mines, has to be pursued.

A more complex situation seems to happen if the projections up to 2030 proposed by the IEA [11] will be realized. In fact, considering both the HIGH and LOW energy demand cases proposed, the nuclear capacity installed

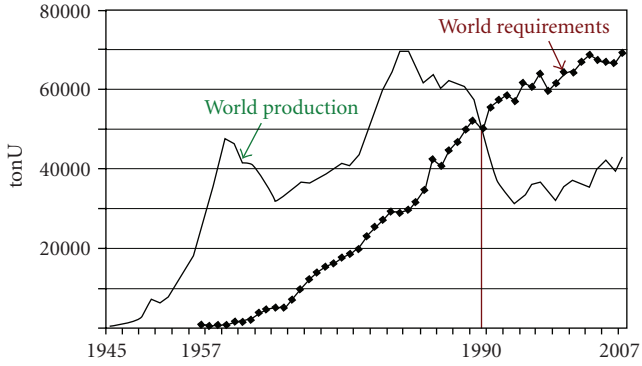

Figure 1: Historical data on Uranium World requirements and production [10].

worldwide will pass from 370 GWe net to 509 GWe and 663 GWe, respectively, that means in 2030 the Uranium requirements will be 93775 tonU/year in the LOW case and 121955 tonU/year in the HIGH case (of course the projections change considerably from region to region [10]). Starting from these considerations the Uranium resources (<130 $/kgU considering also the IR) could be sufficient to cover the demand only up to 2050 [9] and for the future needs only the introduction of fast reactors (perhaps in addition with new U resources discovered) will be the only solution to adopt.

4. Future Energy Demand

In this work, the European situation has been analyzed considering a LOW and a HIGH energy envelopes, where the nuclear energy share in the period 2008–2050 has been evaluated.

The International Organizations (such as IPCC, IEA, IAEA), working in the energy scenario sector, have analysed the problem in a multidisciplinary way using complex models, where economical, political, and environmental considerations are taken into account simultaneously [4, 5, 11]. Data used in this paper is coming from the IAEA publications [3, 5, 12].

Starting from the actual situation (130 reactors in the Western Europe for 884 TWh [13], 19180 tonU/year [10]), in order to evaluate the energy demand in 2050, some rates for the HIGH and the LOW estimates have been furnished and shown in Table 1.

With regard to electricity and nuclear production, the annual rates for the LOW scenario are, respectively, +1% and −2.2%, while for the HIGH scenario these are +2.8% and +0.9%, as presented in Table 1.

Under these conditions Europe will pass from 884 TWh/year in 2007 to 1356 TWh/year (LOW case) or 2898.4 TWh/year (HIGH case) that means a substantial increase in few years. This implies that without nuclear energy it will be impossible to cover the energy needs. On the other hand, the only use of nuclear energy will not be sufficient and the adoption of an integrated energy mix is a central point to analyse, too.

Table 1: Annual growth rates for Western Europe [3, 13].

Parameter	Annual rates	
	LOW	HIGH
Period	2008–2050	
Population	~0.2%	
Primary energy	+0.2%	+0.9%
Electric energy	+1.0%	+2.8%
Nuclear capacity	−2.2%	+0.9%

The World situation is even more significant (because it takes into account developing countries such as China and India). In this case the production in 2007 has been 2608 TWh/year and the projections up to 2050 are [12] 5858.6 TWh/year for the case LOW (annual rate of 1.9%) and 10534 TWh/year for HIGH case (annual rate 3.3%).

Therefore, in this context, the search of the best solutions for the nuclear fleet (fuel cycles and different facilities) is a central point for the future nuclear development process, taking into account that also the U resources are not unlimited.

The analysis of fuel cycle, where evolutionary reactors (such as EPR) are inserted for the medium term and innovative reactors, HTR and GCFR, are used to reach the equilibrium condition will be very useful also for the decision making process.

In particular, HTR has several fundamental characteristics features, which distinguish them from other types of reactors and provide significant operational advantages.

First of all, the fuel is in the form of small ceramic coated particles, able to reach very high temperature operation and material burnup. In addition, the moderator is solid graphite and the coolant is neutronically and chemically inert helium.

Furthermore, HTRs are able to accommodate a wide variety of mixtures of fissile and fertile materials without any significant modifications of the core design, that enables to reach an ultra-high discharge burn-up (>750 GWd/tHM).

This is useful from the resource utilization point of view (complete plutonium fission in a single step minimizes the proliferation risk in the use of this fuel form) and the high temperature reached by the cooling gas, Helium, (>900°C) could be used not only for the electricity production but also for various industrial process, such as Hydrogen production by steam reforming or I-S process [14, 15].

5. Symbiotic Cycle Investigated: EPR-PBMR-GCFR

A preliminary investigation of the advantage that a symbiotic cycle could give, in order to minimize the radioactive wastes and to save U resources, has been performed.

A symbiotic fuel cycle is a strategically planned chain, where the output of a reactor is the input of the following. Each link of such a chain is a different kind of reactors, because each one is able to perform a different task. Of course, between two different steps, the fuel has to be cooled and reprocessed.

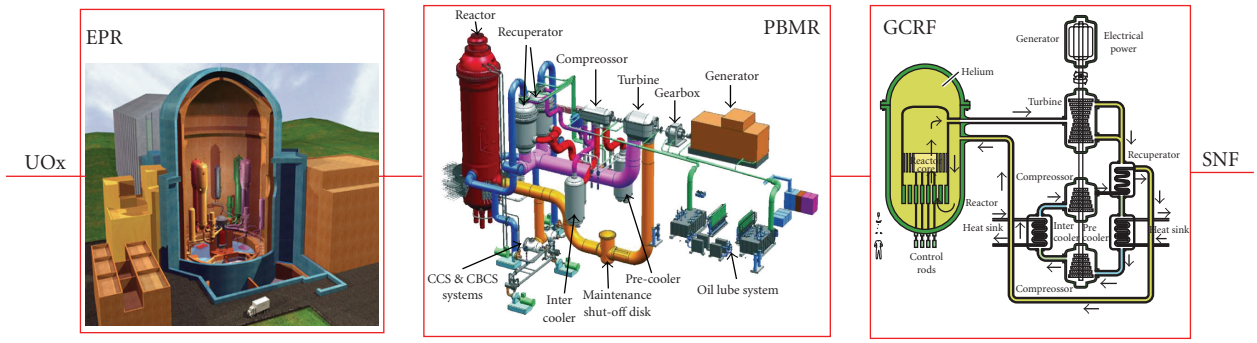

Figure 2: The symbiotic cycle investigated: EPR-PBMR-GCFR.

The symbiotic cycle investigated is presented in Figure 2, where the discharged fuel from EPR is inserted in an HTR (a PBMR has been adopted in this analysis) and after the irradiation it is inserted into the GCFR. The analyzed cycle was already considered in the previous papers [16–18].

Of course for a correct approach respecting reprocessing strategy, the time between the spent fuel extraction from the first facility and the introduction of new fuel in the second one has to be taken into account in synergy with the isotopic composition changes during this period. Because the performed analysis has to be considered as a first preliminary investigation, this issue has been, as a first approximation, neglected.

The simplified models adopted for each reactor are described briefly in the following parts.

In the past, several fuel cycles involving HTR have been studied [14, 18], where the comparison of merits and drawbacks of all solutions has been analyzed. In particular, different HTR compositions (high U enrichment −83%— and Th, low U enrichment −5% to 12%—, medium U enrichment −20%— and Th, only Pu content) could be analysed. In this case, the HTRs have been considered loaded only with reactor grade Pu, further activities will be directed to investigate other fuel compositions.

For this preliminary activity, as presented later on, the symbiotic cycle chosen has been compared with the once-through strategy, such as the direct disposal of the SNF coming from EPR (without adopting reprocessing and separation of Pu and MAs).

Finally, as a first preliminary approximation, k-eff = 1 has been chosen as exit condition for all the calculations; of course an important and necessary improvement for the future calculations will be to estimate a realistic discharge burn-up for every reactor type taking into account the EPR multiple batch loading scheme, the PBMR continuous reloading, and so forth.

5.1. EPR Simulation. The European Pressurized Reactor (EPR) is an evolutionary PWR designed by AREVA-NP company. It is a four loop reactor with a thermal power of 4500 MW_{th} (1600 MW_e) with significant safety improvements; in fact, redundancy and diversification of the Emergency Safety Features-ESF (4 loops) enable to reduce the core damage frequency (CDF) at $6.1 \cdot 10^{-7}$ reactor/year instead of the $5.1 \cdot 10^{-5}$ reactor/year of the present in operation LWRs.

This type of reactor is under construction in Europe (Flamanville-France and Olkiluoto-Finland) and also in UK where the possibility to built this kind of facility is under evaluation [19].

Table 2: Isotopic composition of EPR fuel (weight fraction).

Isotopic composition			
Isotope	g/cm^3	Isotope	g/cm^3
O^{16}	1.18551E-01	U^{235}	3.79023E-02
U^{234}	2.73249E-04	U^{238}	8.43045E-01

For the simulation of the symbiotic cycle some approximations were assumed in order to minimize calculation time without compromising the acceptability of the work.

A single fuel assembly has been simulated, and modeled taking into account the real length (420 cm) and adding reflective boundary conditions in the radial direction (Figures 3 and 4). To take into account the distribution of neutron flux in Z-direction, the fuel assembly modeled has been inserted in a coaxial cylinder (*cz*) with a total height of 8400 mm, filled by borated water, also in order to simulate the contribution of neutron reflection in z direction of the borated water above and below the assembly. As a preliminary approximation, the real axial burnup distribution in the core has not been taken into account.

The fuel assembly is a 17×17 square lattice (made up of 265 fuel rods and 24 guide thimbles) and the core is composed of 241 assemblies organized into three regions at different enrichments (external dimensions of assembly are 21.4×21.4 cm).

In this preliminary and simplified model, the U enrichment adopted is 4.3% in U^{235} (values in literature are between 4% and 5%), the composition simulated is presented in Table 2. Main data, extrapolated from the preliminary safety report of the UK-EPR [19], are summarized in Table 3.

The irradiation period was simulated by BGCore burnup code [20], considering three subsequent irradiation cycles of 600 effective full power days (EFPDs) spaced out by a decay period of 30 days, necessary to take into account the reactor internal fuel cycle (three zones radial shuffling).

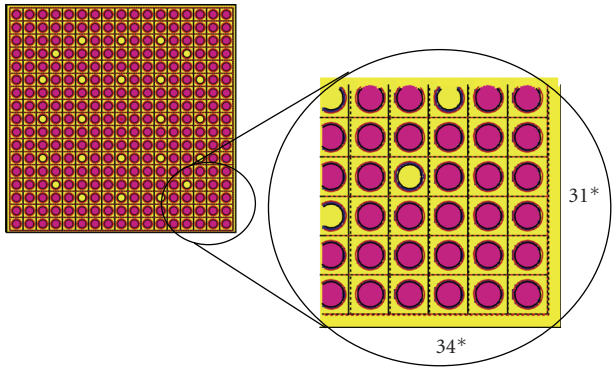

Figure 3: MCNP model of EPR fuel assembly: *xy*-section [19].

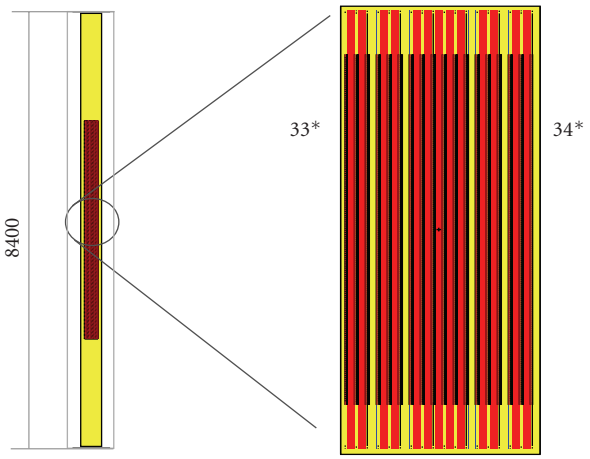

Figure 4: MCNP model of EPR fuel assembly: *xz*-section [19].

The behaviour of k-eff during the irradiation is shown in Figure 5, and additional details (burnup and std error) are summarized in Table 4. Of course, in our simplified model, the effect of radial leakage has been not directly taken into account.

Please note that the Xe effect has been "spread" (due to the chosen time steps) over the first 25 days (i.e., on the whole first time step).

In fact, on the basis of the composition evaluated after the burning in the EPR, the fuel composition for PBMR has been defined, as described in the following paragraph.

5.2. PBMR Simulation. In this preliminary version of symbiotic cycle, a PBMR loaded by Pu reactor grade has been simulated (the Pu and Np considered derived from the EPR modeled and described above). As known, the PBMR is a pebble-bed HTR.

HTRs are thermal reactors which are moderated by graphite and cooled by helium, where the chemical inertness of helium allows high coolant outlet temperatures (around 900°C). That leads to very high thermal efficiencies (up to 50%) to be attained in electrical generation. This high temperature makes the HTR attractive also for other industrial applications different from the electricity production (e.g., the H_2 production by steam-reforming or I-S).

Table 3: EPR parameters adopted for the model [19].

Reactor design parameters	
Thermal power	4500 MW_{th}
N° of loops	4
Heat generated in fuel	97.4%
Nominal pressure	155 bar
Thermal design flow rate/loop	27195 m^3/h
Ave. velocity along fuel rods	4.8 m/s
Nominal inlet temperature	295.7 °C
Ave. in core temperature	313.7 °C
Ave. in vessel temperature	312.8 °C
Ave. core heat flux	54.7 W/cm^2
Ave. linear power density	163.4 W/cm
Fuel assembly (dimensions given at 20°C)	
Rod array	17 × 17
N° assembly	241
Fuel rods/assembly	265
Fuel assembly pitch	21.504 cm
Fuel assembly length	480 cm
Lattice rod pitch	1.26 cm
Overall transverse dimensions	21.4 × 21.4 cm
Guide thimbles/assembly	24
Fuel rods (dimensions given at 20°C)	
Number	63865
Outside diameter	9.50 mm
Diametrical gap	0.17 mm
Clad thickness	0.57 mm
Pellet diameter	8.19 mm

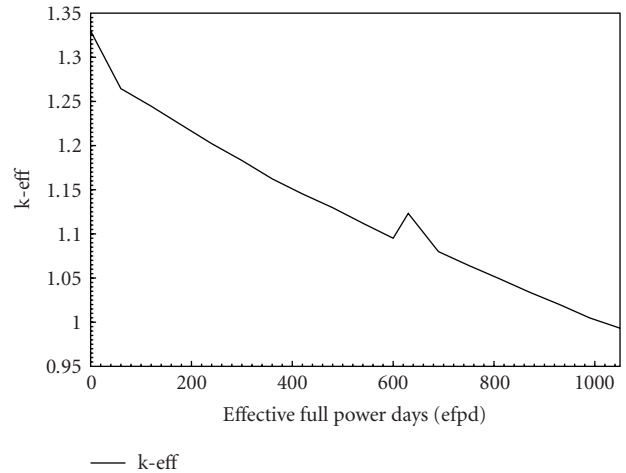

Figure 5: EPR simplified model: k-eff trend during irradiation period.

This kind of reactor has been and is under development within several European Projects (e.g., HTR-N1 [21], PUMA [22], RAPHAEL [23]) to achieve attractive goals in a future energy scenario, curbing the CO_2 emissions and reducing the energy cost.

In particular, as underlined by the Sustainable Nuclear Energy-Technical Platform (SNE-TP), HTR is in a privileged

Table 4: EPR irradiation parameters: k-eff and burnup behaviour during irradiation.

k-eff behaviour during irradiation			Burn-up
efpd	k-eff	pcm	GWd/tonHM
0	1.32984	±93	0.000
60	1.26447	±92	1.995
120	1.24461	±91	3.991
180	1.22331	±90	5.986
240	1.20226	±89	7.981
300	1.18313	±87	9.976
360	1.1624	±95	11.972
420	1.1453	±89	13.967
480	1.12973	±92	15.962
540	1.11207	±94	17.957
600	1.09508	±96	19.953
630	1.12319	±93	19.953
690	1.07986	±85	21.948
750	1.0642	±90	23.943
810	1.04939	±88	25.938
870	1.03414	±88	27.934
930	1.01997	±95	29.929
990	1.0048	±94	31.924
1050	0.99319	±91	33.920

position to address nonelectricity energy needs because it could provide an early nuclear process heat production without waiting for the Gen-IV development [24].

As just indicated, HTR is a flexible system able to accommodate a wide variety of mixtures of fuels without any significant modification of the core design and it could reach very high burn-ups, which are far beyond the possibilities offered by other than fast reactors (except the particular case of molten salt reactors).

In the past, considerable experience on HTR technology has been accumulated, and two technology demonstrator reactors are in operation nowadays: the HTTR and the HTR-10.

The HTTR is a prismatic core (150 fuel blocks) reactor in Japan of 30 MW_{th} containing UO_2 [25]. Instead the HTR-10 is a pebble bed core reactor of 10 MW_{th} currently operating in China that first attained criticality in 2000 [26].

Finally, the reactor proposed in this work, is a pebble bed core reactor (PBMR like) with a core diameter of about 3700 mm (without considering the radial reflector). The fuel element adopted is a pebble containing CP (TRISO), as shown in Figure 6.

In order to model this reactor, some specific parameters have been used and a summary of them is presented in Table 5. Please note the core has been simulated in a "realistic" way, so the moderator/fuel ratio in the MCNP model for PBMR approximates to that of the real core.

In particular only 1/12 of total core has been simulated as shown in Figure 7. In this figure only a simplified sketch is presented where it is possible to distinguish between the fuel zone (fuchsia zone) and the surrounded nonfuelled region

Table 5: PBMR parameters adopted for the model.

Reactor design parameters	
Thermal power	433 MW_{th}
Pebble radius	30 mm
Packing fraction	0.61
Core dimensions	
Internal radius	100 cm
External radius	185 cm
Height	1300 cm
Reflector dimension	
Rex central reflector	100 cm
Rin radial reflector	185 cm
Rex radial reflector	275 cm
Temperature	1200 K
Density	1.74 g/cm^3
Pebble parameters	
Kernel (Rex)	0.01 cm
Fuel density	10.89 g/cm^3
Fuel temperature	1200 K
Buffer (Rex)	0.019
Buffer density	1.05 g/cm^3
Buffer temperature	1200 K
Inner PyC (Rex)	0.023
PyC density	1.90 g/cm^3
PyC temperature	1200 K
SiC layer (Rex)	0.0265
SiC density	3.18 g/cm^3
SiC temperature	1200 K
Outer PyC (Rex)	0.0305
PyC density	1.90 g/cm^3
PyC temperature	1200 K

(blue part). Anyway in the complete model used in each pebble the heterogeneous matrix has been simulated, taking into account all the layers composing of the TRISO particles.

In the model adopted the composition of fuel chosen is calculated cording to the EPR discharged fuel and it is shown in Table 6. As shown in Table 6, the composition adopted in this preliminary calculation is analogous to the isotopic composition of Pu and Np obtained after the extraction from the EPR.

As anticipated this has to be considered a simplification. In any case, this assumption was made to reduce calculation time (in this first preliminary evaluation) and an additional improvement will be necessary for an accurate analysis, where the decay time and the relative composition changes will be correctly simulated.

The irradiation period was simulated by BGCore burnup code [20], considering a single irradiation cycle of 1500 EFPD. The fuel loading scheme is based on a continuous pebbles recirculation. So, the pebbles present for a fixed time in the core are at different levels of burn-up. Due to model limitations, in this preliminary configuration, where the core has been simulated as a steady core, the pebbles

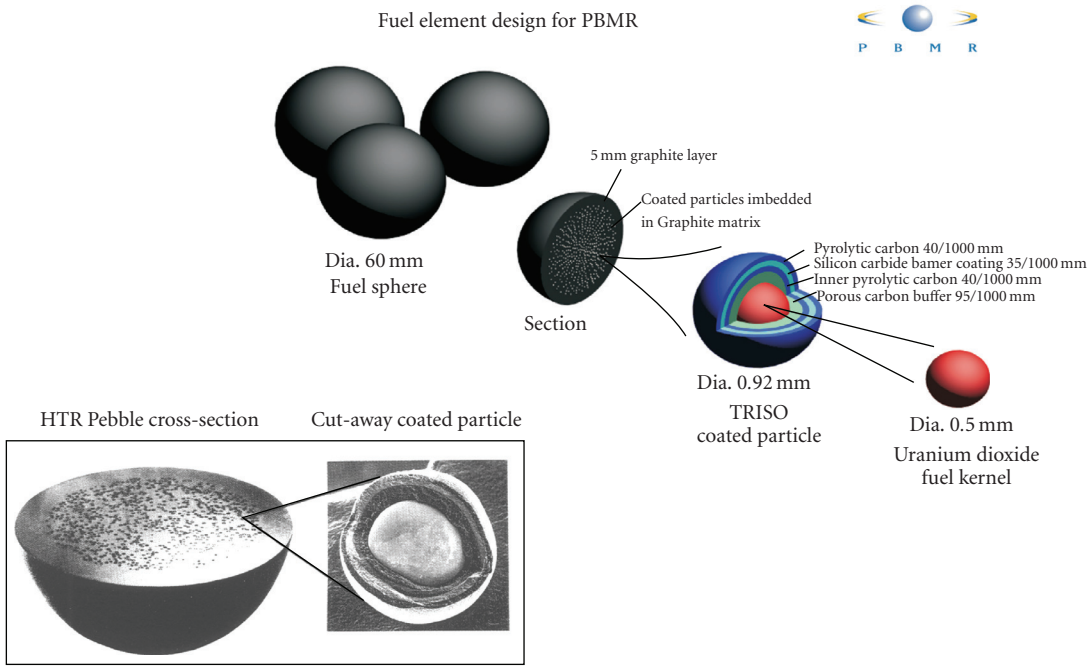

Figure 6: Fuel element design for HTR: pebble fuel containing TRISO CPs.

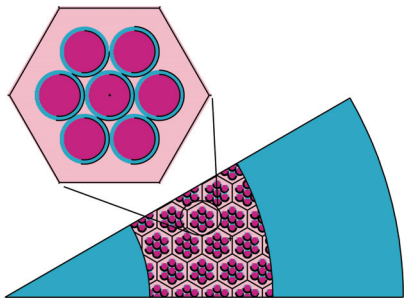

Figure 7: MCNP model of PBMR reactor.

were considered exhaust when the global k-eff becomes lower than unity. (Please note that the real PBMR will not be fuelled with pebbles at the same burn-up level, but with a mixture of pebbles at different burn-ups: the real discharge burn-up in principle could be extremely high, that is, up to twice the assumed discharge burnup. On the other hand, we have not took into account leakages and effects related to the structures surrounding the core, so this preliminary and conservative assumption could be acceptable.) In the calculations performed the residence time of the pebble inside the core has been estimated to be about 850 EFPD.

The global k-eff behavior during the irradiation is shown in Figure 8 and additional details (burn-up and standard error) are summarized in Table 7. As shown in the latter mentioned table, the burn-up reachable after 850 efpd, is ~500 GWd/tonHM, a conservative value that whatever enables to underline the good PBMR behavior with respect to the fuel exploitation.

Table 6: Isotopic composition of PBMR fuel (atomic fraction).

Isotope	Fuel Composition
Np235	1.46E-10
Np236	6.42E-08
Np237	1.55E-02
Np238	3.76E-05
Np239	2.78E-03
Pu236	1.39E-10
Pu237	6.66E-09
Pu238	4.02E-03
Pu239	2.21E-01
Pu240	7.24E-02
Pu241	4.33E-02
Pu242	1.13E-02
Pu243	2.60E-06
Pu244	3.60E-07
O16	6.30E-01

Please note that the Xe effect has been "spread" (due to the chosen time steps) over the first 25 days (i.e., on the whole first time step).

5.3. GCFR Simulation. After the fuel irradiation in a HTR, the last step simulated is the burning in a Gas-Cooled Fast Reactor (GCFR) loaded with Pu and MAs coming from the previous reactor. Even in this case the fuel extracted from the previous reactor is inserted directly in the final facility adopted in the cycle. Of course, as future development, the correct evaluation of cooling time after PBMR and

Table 7: HTR irradiation parameters: k-eff and burnup behaviour during irradiation.

K-eff behaviour during irradiation			Burn-up
efpd	k-eff	pcm	GWd/tonHM
0	1.28736	±130	0.000
25	1.24676	±129	12.568
50	1.2404	±125	25.136
75	1.2316	±121	37.704
100	1.22221	±121	50.272
125	1.21924	±123	62.840
150	1.213	±125	75.408
175	1.20535	±129	87.976
200	1.19871	±119	100.540
225	1.19139	±131	113.110
250	1.18784	±121	125.680
275	1.18232	±123	138.250
300	1.17541	±125	150.820
325	1.16742	±119	163.380
350	1.16256	±123	175.950
375	1.15622	±126	188.520
400	1.15019	±124	201.090
425	1.14296	±118	213.660
450	1.13729	±121	226.230
475	1.13081	±123	238.790
500	1.12329	±123	251.360
525	1.11716	±111	263.930
550	1.10962	±118	276.500
575	1.09993	±123	289.070
600	1.09524	±124	301.630
625	1.08551	±107	314.200
650	1.08023	±121	326.770
675	1.07045	±122	339.340
700	1.06385	±122	351.910
725	1.05637	±116	364.470
750	1.04411	±119	377.040
775	1.03984	±114	389.610
800	1.03049	±115	402.180
825	1.01761	±108	414.750
850	1.01017	±116	427.310
875	0.99903	±116	439.880

reprocessing and fabrication times (and feasibility) of GCFR fuel has to be analysed in order to have a more correct approach to the problem.

The choice to insert a GCFR as last facility for the symbiotic cycle is in agreement with sustainability and economic goals proposed in Generation IV [2]. In fact this facility, as it will be further clarified in the results discussion section, enables to reduce considerably the confinement time necessary for the final disposal.

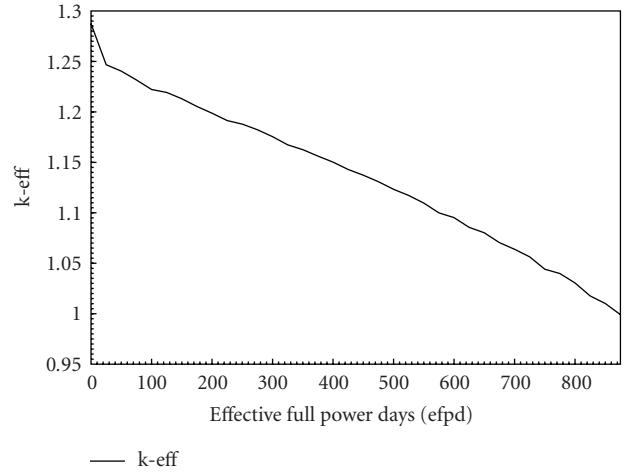

Figure 8: HTR simplified model: k-eff behaviour during irradiation period.

This reactor has specific characteristic for what concerns the fuel optimised use (high attainable burn-up and long reactivity limited irradiation time before becoming subcritical). In addition by using directly the high temperature reached by the Helium coolant (adopting the Brayton thermodynamic cycle), it could reach a high efficiency.

This kind of reactor is one of the six concepts proposed for development by the Generation IV international forum, and it could be considered interesting, as the HTR one, for the use in Hydrogen production and for other industrial processes.

Major design parameters of GCFR are summarized in Table 8, as presented by [2].

The model adopted in this work is a GCFR "E" (2400 MW_{th}) He-cooled fast reactor [27]. It is loaded by hexagonal fuel assemblies containing plates made of a (U,Pu)C and SiC matrix (Figure 9). The choice of carbide allows to improve the fuel performance.

One of the major advantages of this facility is the low content of parasitic absorbers, that enables GCFR to reach criticality with a fuel composed of 82% (as an atomic fraction) Depleted Uranium (DU) as well as to sustain very long irradiation period without becoming subcritical. Of course, the irradiation period has to be optimized taking into account the integrity of fuel structures, where the major cause of limitation probably will derive from the radiation damage (expressed in displacements from atoms, dpa) causes by fast neutrons and gamma spectra.

In the model adopted the composition of fuel chosen is based on the PBMR discharged fuel and it is shown in Table 9.

The irradiation period was simulated by BGCore burnup code [20], considering an irradiation cycles of 5500 EFPD before the reactor becomes subcritical (k-eff < 1).

The global k-eff behavior during the irradiation is shown in Figure 10 and additional details (burn-up and std. error) are summarized in Table 10.

Table 8: GCFR Major target parameter: reference values.

Reactor design parameters		
Reactor thermal power		2400 MW_{th}
Efficiency		48% (direct cycle helium)
Coolant inlet temperature		490°C
Coolant out temperature		850°C
Height/diameter ratio		0.65
Fissile height [mm]		2300
N° fuel assemblies		162 + 120
N° control rods		24
N° reflector assemblies (mixture of Zr_3Si_2, SiC, and He),		168
Nominal coolant pressure [MPa]		7.0
Power density		100 MW/m^3
Core		
Core external radius		300 cm
Core height		230 cm
(U, Pu)C fraction (%vol)		56
SiC (%vol)		16
Helium (%vol)		28
Density [g/cc]	(U,Pu)C	11.5855 (85% TD)
	SiC	3.16
	He	$3.53 \cdot 10^{-3}$ (T_{ref} = 660°C; P = 7 MPa)
Reflectors		
Axial top reflector height		50 cm
Axial bottom reflector height		50 cm

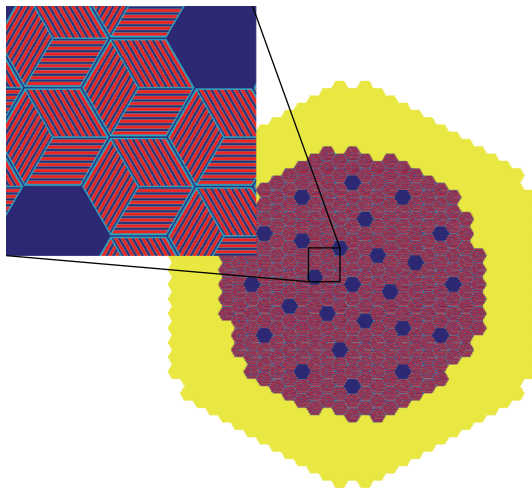

Figure 9: MCNP model of GCFR reactor.

Table 9: Isotopic composition of GCFR fuel (atomic fraction).

Isotope	Fuel composition
U235	1.79E-03
U238	7.21E-01
Np237	8.52E-03
Np238	1.48E-05
Pu238	5.36E-03
Pu239	4.76E-02
Pu240	4.85E-02
Pu241	3.12E-02
Pu242	1.88E-02
Pu243	2.30E-06
Pu244	8.46E-07
C	6.61E-02
Si28	4.65E-02
Si29	2.44E-03
Si30	1.68E-03
He	1.41E-04

6. Discussion of the Obtained Results

The analysis of the symbiotic cycle proposed is inserted in a wider context: the investigation of possible strategies for the nuclear fuel cycle closure.

For this reason the comparison between the symbiotic cycle and a reference scenario has been performed to underline the advantages and the drawbacks of this strategy.

The reference scenario chosen is the direct disposal of SNF coming from EPR, without reprocessing Pu (the so-called once-through strategy), that is the strategy at the moment worldwide (with some exceptions) adopted for the LWRs but that has to be changed if the long-term

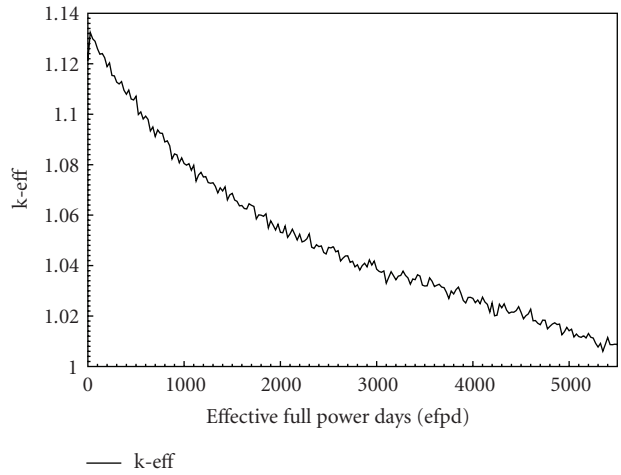

Figure 10: GCFR simplified model: k-eff behaviour during irradiation period.

Table 10: GCFR irradiation parameters: k-eff and burnup behaviours during irradiation.

k-eff behaviour during irradiation			Burn-up
efpd	k-eff	pcm	GWd/tonHM
0	1.1213	±129	0.000
50	1.12987	±130	1.578
100	1.12598	±123	3.156
200	1.11886	±121	6.312
300	1.11271	±130	9.469
400	1.10792	±128	12.625
500	1.10713	±130	15.781
600	1.09925	±137	18.937
700	1.09116	±128	22.093
800	1.08902	±112	25.250
900	1.08428	±109	28.406
1000	1.08047	±111	31.562
1500	1.06864	±115	47.343
2000	1.05319	±126	63.124
2500	1.04722	±110	78.905
3000	1.03857	±119	94.686
3500	1.03191	±114	111.632
4000	1.02702	±106	129.205
4500	1.02147	±105	147.288
5000	1.01417	±101	165.428
5500	1.0087	±105	183.801

sustainability for the nuclear electricity production has to be considered.

The analysis of various strategies to close the nuclear fuel cycle matches with one of the major questions that scientific community has to answer: how minimize the final wastes (and their potential risk) to be sent to geological disposal. Question still opened, a critical issue from the public opinion acceptability point of view.

A deep analysis of the minimization of volumes involved is important (even if the quantity produced up to now could be considered negligible with respect to the other conventional wastes related to the energy chain, e.g., coal energy chain). However, the evaluation of time needed to reach the Uranium reference level is an even more important parameter to be considered. This parameter could be evaluated by means of the radiotoxicity versus time evolution behaviour.

Finally the SNF decay heat evolutions (an important parameter for the integrity and the design of the geological disposal) have been evaluated.

Other parameters are not considered in this work but they will be very important for the choice of the reference cycle to adopt. For instance, a deeper analysis of the uranium-plutonium resources optimization is significant for the long-term sustainability.

The first step for a correct comparison between the two proposed scenarios is the characterization of the once-through by means of the already underlined parameters (radiotoxicity and power decay).

In order to perform this analysis, after the normalization to 1 ton of discharged HM, the evolution of spent fuel composition coming from EPR has been simulated by means of CARL2.3 depletion code [18]. It does not use fluxes and/or cross-sections for its calculations; it is simply a depletion code implementing a set of Bateman equations. CARL2.3's input is the output masses given by the neutron calculations. This code, developed at the University of Pisa, enables to solve the Bateman equations, starting from 55 father isotopes (mainly U, Pu, and MAs but also the long live fission products). These 55 fathers are the most significant isotopes for the radiotoxicity point of view (the CARL 2.3 code requires in input the masses (expressed in grams) of the following 55 elements: Th^{232}, U^{232},U^{233}, U^{234}, U^{235}, U^{238}, Np^{237}, Pu^{238}, Pu^{239}, Pu^{240}, Pu^{241}, Pu^{242}, Pu^{243}, Pu^{244}, Am^{241}, Am^{242m}, Am^{243}, Cm^{242}, Cm^{243}, Cm^{244}, Cm^{245}, Rb^{87}, Sr^{90}, Zr^{93}, Nb^{94}, Tc^{99}, Pd^{107}, Sn^{126}, I^{129}, Cs^{135}, Cs^{137}, Sm^{147}, Sm^{151}, Eu^{154}, Se^{7}, Cr^{51}, Mn^{56}, Fe^{59}, Co^{60}, Ni^{65}, Cu^{64}, Zn^{65}, Zn^{69}, Zr^{95}, Mo^{99}, Ta^{182}, W^{187}, Na^{24}, Ca^{45}, Br^{82}, Ba^{140}, Ir^{192}, Po^{218}, Ra^{226}, Ra^{228}); In fact as well known, the total radiotoxicity, as well as heat decay, is quantities driven by a few radionuclides. The radiotoxicity coefficients adopted are referred to ICRP72 values.

For the EPR once-through strategy, all the SNF is directed to geological disposal (MAs plus Pu). The total radiotoxicity versus Time evolution of SNF coming from EPR is shown in Figure 11. The time to reach the fixed radiotoxicity Reference level (i.e., the so-called LOMBT [18]) is equal to ~170 000 years. In this case all the discharged materials are considered as a waste.

If the contribution to the total radiotoxicity of each isotopes is taken into account (as shown in Figure 12), it is possible to underline that the major contribution for the long period depends on the Pu content evolution (black line in the Figure 12).

This consideration and the necessity to have a more optimised use of resources (that means to consider Pu as an optimal fuel for the development of nuclear reactors,

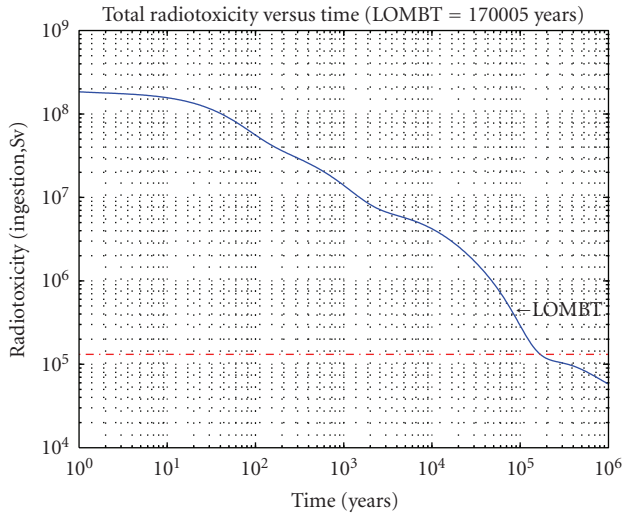

FIGURE 11: EPR Total radiotoxicity versus Time (values normalized to 1 ton HM) (the number of evaluated points in the considered period (1–1E+06 years) is equal to 500).

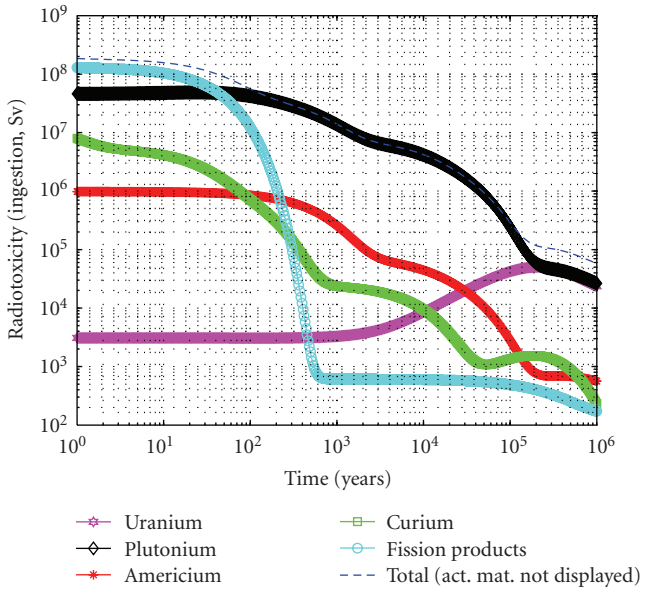

FIGURE 12: EPR contribution of each element to the total radiotoxicity versus time.

particularly fast spectrum ones) are at the basis of the analysis of different fuel strategies able to improve the use of the fuel.

Furthermore, as shown in Figure 13, Pu gives also the major contribution to the total Power Decay, that is the heat load source term for the long-term geological disposal (although for the first 300 years the major contributions to radiotoxicity and decay heat had arisen from fission products).

After the characterization of the reference scenario, some additional considerations have to be added to before comparing it with the simulated symbiotic cycle.

In the hypothesized scenario the SNF reprocessing has been assumed as important step but it has not modelled in

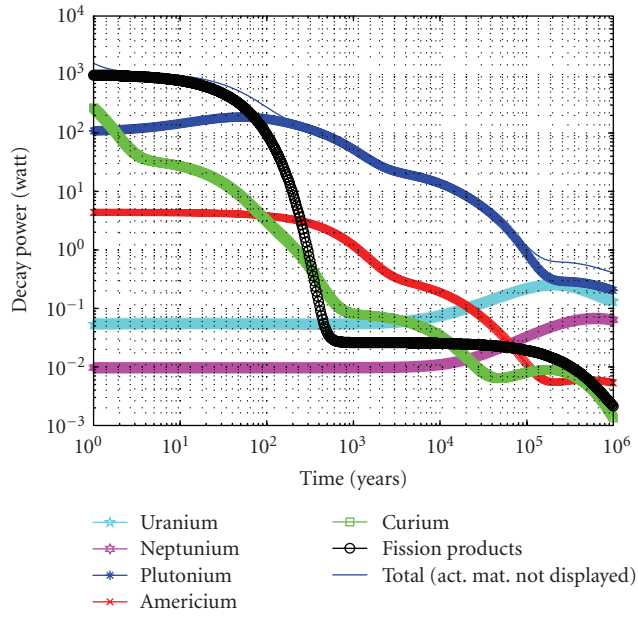

FIGURE 13: EPR contribution of each element to the total decay power versus time.

details. In particular the separation efficiency of the PUREX process (0.1% Pu left in wastes) is assumed as a reference value. We have assumed the feasibility of the separation of Pu+Np from the other TRUs with an efficiency similar to PUREX process (0.1% left in waste). The real technological implementation of this process has to be further analyzed as a future development of the present research. As a result of the previous hypotheses, the symbiotic cycle simulated assumes HTR and GCFR initial fuels composed by Pu+Np recycled from the previous reactor in the chain (resp., EPR and PBMR) plus additional materials (DU, SiC, etc.). One of the aim of these assumptions is to improve the Pu exploitation and, at least partially, to burn MA. It should be noted that the choice to exclude Am and Cm from the fresh "recycled" fuel is due to at least two different reasons [28].

(1) A fuel (re-)fabrication facility that have to manage Cm would have serious difficult, due to radiological and material issues.

(2) An efficient process to separate Am from Cm is far-off to be implemented (at least on an industrial scale).

As a first qualitative comparison among the Pu and MAs inventories after the irradiations in the three simulated reactors, Table 11 shows the inventory of the SNF (normalized to 1 ton of discharged HM, including U, too) at the end of the irradiation periods.

Before going on with the analyses, it is useful to underline two points (more deeply analyzed in [27]):

(i) 1 PBMR is able to burn the Pu+Np inventory coming from 0.62 LWR;

(ii) 56 PBMR cores are capable for supplying the fuel mass to start 1 new GCFR core.

Table 11: Inventory (values relative to 1 ton of HM) of Pu and MAs after the irradiation in EPR, PBMR, and GCFR.

Isotopes	EPR[(1)]	PBMR[(2)]	GCFR[(3)]
		g/ton	
Np237	4.28E+02	4.63E+04	3.21E+03
Pu238	1.11E+02	2.91E+04	7.92E+03
Pu239	6.14E+03	2.59E+05	9.85E+04
Pu240	2.02E+03	2.64E+05	6.34E+04
Pu241	1.21E+03	1.70E+05	1.00E+04
Pu242	3.18E+02	1.02E+05	1.99E+04
Pu243	7.35E-02	1.25E+01	4.38E-01
Pu244	1.02E-02	4.61E+00	4.68E-02
Am241	3.53E+01	1.20E+04	5.58E+03
Am242m	1.11E+00	3.06E+02	5.50E+02
Am243	5.08E+01	1.78E+04	4.78E+03
Cm242	9.15E+00	2.53E+03	2.26E+02
Cm243	1.58E-01	3.94E+01	2.86E+01
Cm244	1.17E+01	4.39E+03	2.38E+03
Cm245	5.62E-01	1.66E+02	3.86E+02

[(1)]990 efpd—UO_2 fuel (4.3% U^{235} enrichment). [(2)]850 efpd—Pu–Np content fuel. [(3)]5500 efpd—DU–Pu–Np content fuel (in inert matrix).

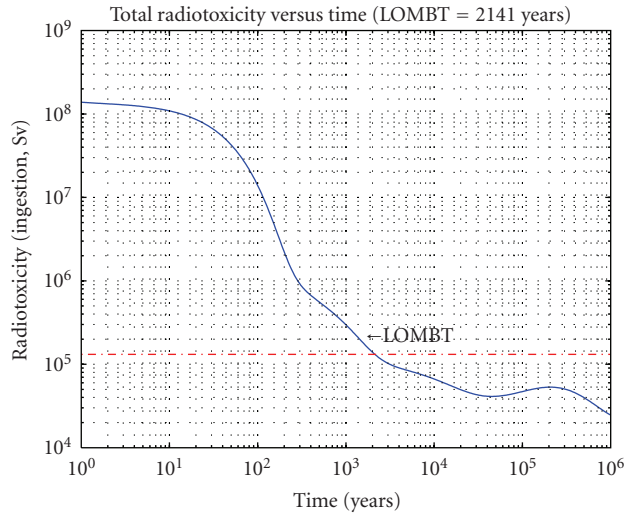

Figure 14: EPR total radiotoxicity versus time considering 0.1% of Pu and Np left in wastes (values normalized to 1 ton HM) (0.1% of Pu+Np left in waste (data assumed starting from what obtained for Pu in the PUREX process)).

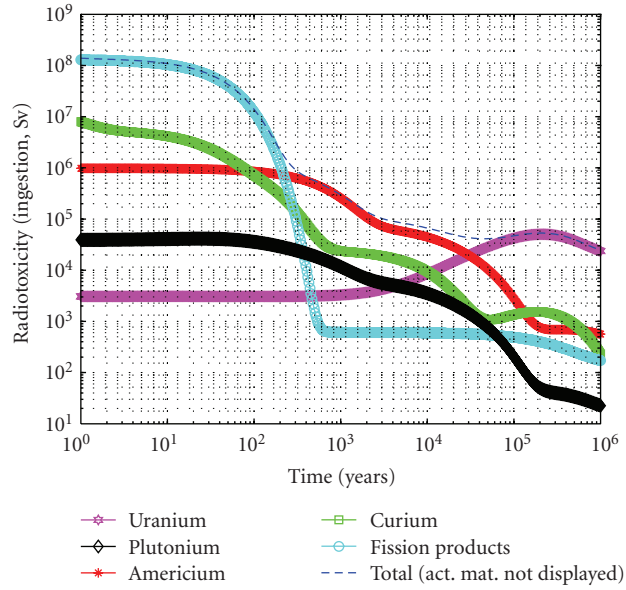

Figure 15: EPR contribution of each element to the total radiotoxicity versus time considering 99.9% Pu and Np separation.

So the choice of comparing 1 ton of discharged HM for all the reactors has to be considered just as a first approximation, useful to have a qualitative idea but to be corrected if implemented in a more complex and complete scenario analysis.

In order to underline the advantages that the symbiotic cycle could bring about, after the irradiation in an EPR, the separation of Pu and Np is performed (0.1% left in waste). Under these conditions, the new radiotoxicity and the decay power versus time trends are shown in Figures 14, 15, and 16.

The analysis of total radiotoxicity versus time (Figure 14) shows a new LOMBT equal to ~2150 years (assuming only Np and Pu separation).

At the same time, if the contribution of each isotope is analysed (Figure 15) the major contribution to total radiotoxicity (for the long period) arisen from Americium and Curium chains (red and green lines, Figure 15). As shown in Figure 16, these elements are the major contribution to the power decay, too.

As anticipated, PBMR is the second reactor considered in the chosen cycle. This reactor is characterized by the possibility to accommodate a wide variety of mixtures of fuels without any significant modification of the core design and it could reach very high burn-ups.

For this reactor, it is not clear, at least at the moment, if the reprocessing of pebble will be performed or not. This is the reason why the case of direct disposal of pebble is shown in Figure 17 and considered as term of comparison for the case with Pu and Np separation adopted (99.9% separation efficiency), shown in Figure 18. The LOMBT passes from ~70 100 (direct disposal) to ~3050 years.

As already discussed, the Pu and Np reprocessing has been assumed as an important step to perform in order to reach a really sustainable cycle. For this reason a deeper analysis for both the contributions to radiotoxicity and the decay power trends under this assumption has been performed. The obtained results are shown, respectively, in Figures 19 and 20.

As previously described, the last simulated facility is a GCFR. This kind of reactor is analysed in Gen-IV and it will became very attractive if the optimisation of resource involved will be taken into account.

The same approach adopted for the EPR and the HTR is applied to the GCFR evaluation. In fact the SNF radiotoxicity evolution without Pu and Np (only the 0.1% is left in waste)

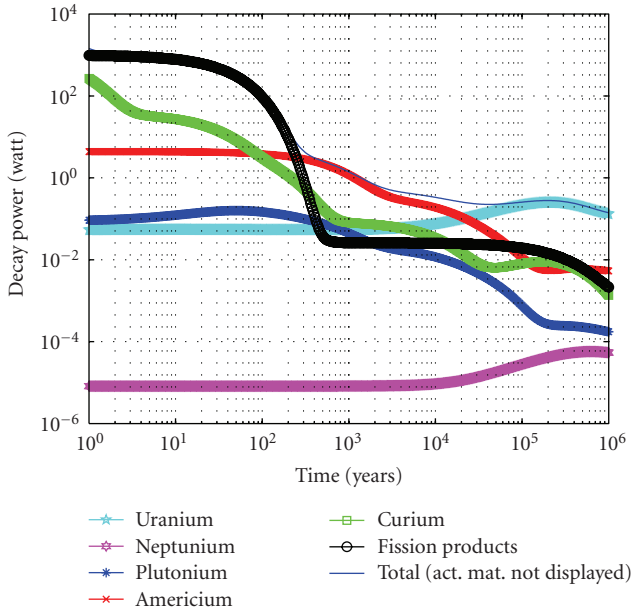

Figure 16: EPR contribution of each element to the total Decay Power versus time in the case of 99.9% of Pu and Np separation.

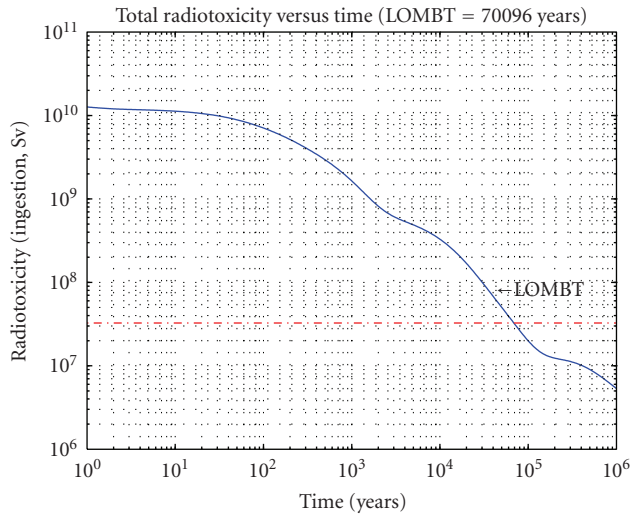

Figure 17: HTR (PBMR) total radiotoxicity versus time without pebble reprocessing.

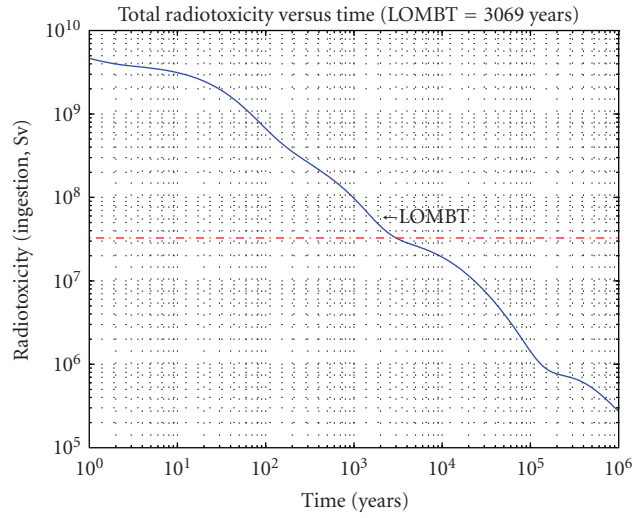

Figure 18: HTR (PBMR) total radiotoxicity versus time with pebble reprocessing (0.1% Pu and Np left in the final waste).

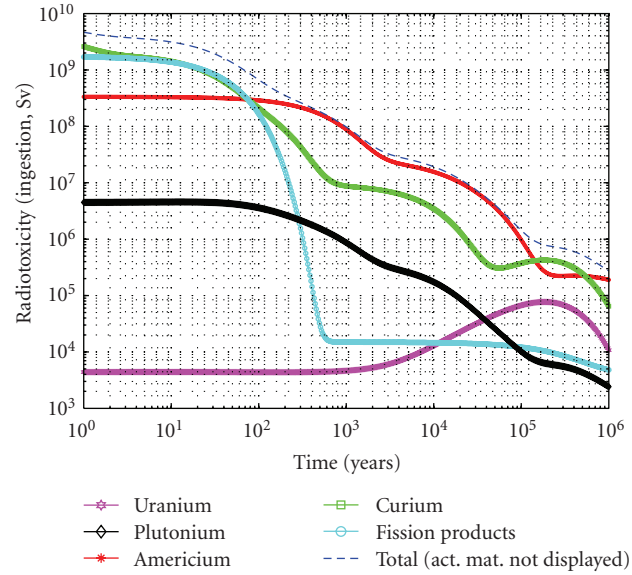

Figure 19: HTR (PBMR) contribution of each element to the total radiotoxicity versus time considering the Pu and Np separation.

has been simulated by means of CARL code, and shown in Figure 21. The LOMBT is equal to ~1550 years, that is, a time comparable with typical human "historical" time and so it could be acceptable for the geological disposal.

If a radiotoxicity contribution analysis is performed (Figure 22), again Cm and Am are the major contributors (at least for the medium and the long-term). These elements are also the major causes for the heat decay load (Figure 23).

Finally it is important to have a look at the energy produced by each of the reactors (it has been assumed to have an utilization factor (for all the considered reactors) equal to 90%). As already anticipated 1 PBMR is able to burn the Pu+Np inventory coming from 0.62 LWR and 56 PBMR cores are capable for supplying the fuel mass to start 1 new GCFR core. So, in order to perform a "realistic" analysis, it was assumed (as a first approximation) to have in the chain [27]:

(i) 1 GCFR,

(ii) 56 PBMR,

(iii) 42 EPR.

The results are shown in Table 12.

As a first consideration, it is important to highlight that, if we use an integrated EPR-PBMR-GCFR fuel cycle (instead of a single EPR), we can obtain a total electric energy equal to 630.54 TWh/year (instead of only 529.62 TWh/year). Of course, this result can be obtained without consuming additional raw materials.

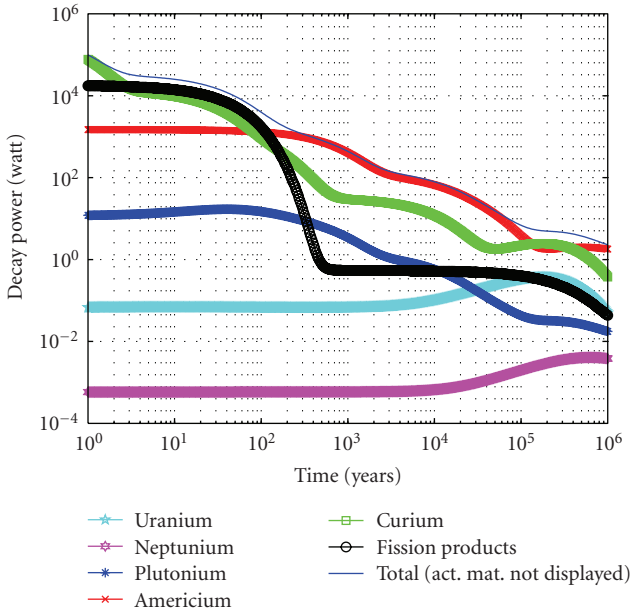

Figure 20: HTR (PBMR) contribution of each element to the total Decay Power versus time considering the Pu and Np separation.

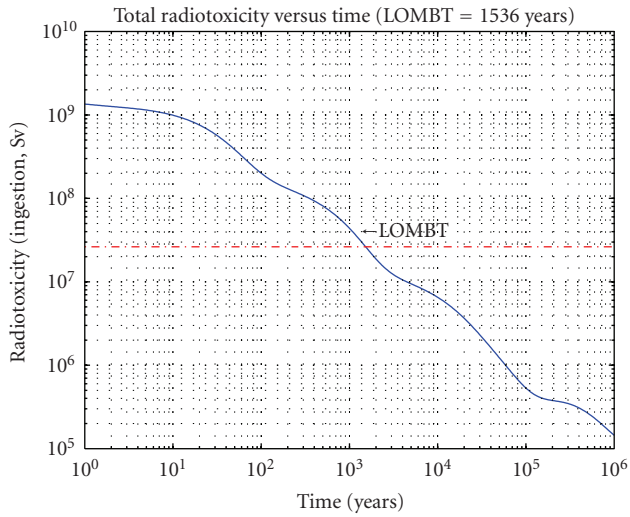

Figure 21: GCFR total radiotoxicity versus time (only 0.1% Pu and Np left in waste).

Before concluding this paragraph, it is useful (mainly for complete scenario evaluations) to underline some further points (deeply analyzed in [27]).

(i) To perform a deeper scenario analysis, also for the waste evaluations (in terms of LOMBT, decay power trends, volumes, etc.) a more refined ratio among EPR, PBMR, and GCFR would have to be taken into account.

(ii) A better utilization of GCFR implies the adoption of a multiple recycling strategy in this kind of reactor; following this approach the final LOMBT could be reduced to ~1/5 of the value calculated in this research [27].

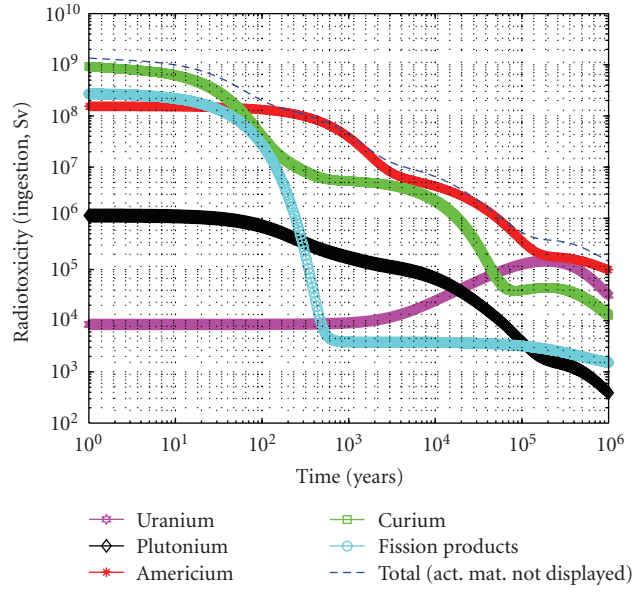

Figure 22: GCFR contribution of each element to the total radiotoxicity versus Time (only 0.1% Pu and Np left in waste).

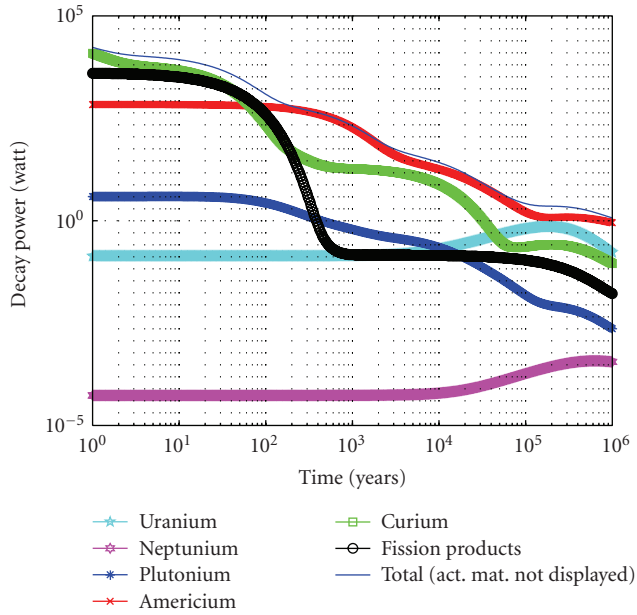

Figure 23: GCFR contribution of each element to the total Decay Power versus Time (only 0.1% Pu and Np left in waste).

7. Conclusions

The scientific community is called to find a sustainable solution to guarantee the supply of future energy demand without compromising the environment integrity, complementary but fundamental target to achieve. Central role in this process lies with the nuclear energy production because it is the only source of energy capable of providing a large quantity of energy without relevant greenhouse gas releases. But a special regard has to be paid to the reduction of the

Table 12: Energy produced by each reactor.

	EPR	PBMR	GCFR	Integrated cycle
Thermal energy [TWh/year]	1490.16	190.96	18.92	1700.04
Electric energy [TWh/year]	529.62	91.84	9.08	630.54

HLW inventory and to the optimization of the exploitation of the fuel resources.

Starting from these considerations, this work focused on the evaluation of possible advantages that a symbiotic cycle (EPR-PBMR-GCFR) could entail. The proposed cycle is considered in the frame of a general scenario analysis that takes into account also the resources availability. So the analyses have been carried out with the purposes of:

(i) maximizing the fuel exploitation by recycling part of the waste,

(ii) minimizing the long-term spent fuel radiotoxicity,

(iii) having a look at the waste decay heat evolution, in order to allow a safe storage for a long period of time.

Regarding the fuel exploitation, the use of a symbiotic fuel cycle allows to obtain a total electric energy equal to 630.54 TWh/year (instead of only 529.62 TWh/year) without consuming additional raw materials.

Regarding the waste radiotoxicity, from the obtained results it could be deduced that

(i) the use of PBMR reduces the LOMBT from ~170 000 (value for EPR waste) to ~70100 years, in the case of direct disposal of pebble, or to ~3100 years, if Pu and Np are separated (0.1% left in waste);

(ii) the use of GCFR further reduces the LOMBT from ~3100 (EPR+PBMR) to ~1500 years, than, of course, the Pu and the Np are separated in order to be reused as fuel in subsequent irradiation steps. In fact, the implementation of a multiple recycling strategy in GCFR could further reduce the LOMBT to values ~1/5 of the calculated one [27].

Another important topic is the decay heat evolution. In this frame it should be noted that, as expected, the major contribution arises from the Pu isotopes. In addition it should be noted that the worst trend can be found for the PBMR waste (mainly due to the total quantity of Pu in the spent fuel and to its isotopic vector).

The obtained results have to be considered just as a (very) preliminary evaluation of a symbiotic EPR-PBMR-GCFR fuel cycle, useful as a first step to be completed (performing more detailed calculations, too) and implemented also by means of dedicated scenario codes in a more general analysis.

In order to perform these deeper evaluations, other key points (e.g., environmental and economic aspects, waste volumes comparison, U consumption estimation, etc.) have to be taken into account. In addition, to perform a more realistic scenario analysis, also for the waste evaluations (in terms of LOMBT, decay power trends, volumes, etc.), a refined ratio among EPR, PBMR, and GCFR would have to be taken into account. In the frame of an analysis of a sustainable fuel cycle, it will be also important, in order to better characterize the fast reactor, to evaluate the Breeding Gain (BG) reached at the end of cycle.

Finally as further future works, it would be necessary to have a look to the real possibilities of technological implementations of the proposed fuel cycles (e.g., material technology, evaluation of the reprocessing processes on an industrial scale, etc.).

Abbreviations

BG: Breeding gain
BOC: Begin of cycle
CCS: Carbon capture and sequestration
CDF: Core damage frequency
DU: Depleted uranium
EFPD: Effective full power days
EOC: End of cycle
EPR: European pressurized reactor
ESF: Emergency safety features
EU: European union
GCFR: Gas cooled fast reactor
GHG: Greenhouse gas
HLW: High level waste
HM: Heavy metal
HTR: High temperature reactor
HTTR: High temperature engineering test reactor
IAEA: International Atomic Energy Agency
IEA: International Energy Agency
IPCC: Intergovernmental panel on climate change
IR: Inferred resources
MA: Minor actinides
NEA: Nuclear Energy Agency
P&T: Partitioning & transmutation
PUMA: Plutonium and minor actinides management in thermal high temperature reactors
RAPHAEL: ReActor for process heat, hydrogen, and eLectricity generation
RAR: Reasonable assured resources
SNE: TPSustainable nuclear energy—technical platform
TRISOT: ristructural-isotropic
USD: Unites States Dollar

Acknowledgments

The work presented in this paper was partly funded by the European Union Sixth Framework Program, under Contracts PuMA, GCFR, and RAPHAEL. First of all, The authors want to thank Dr. Bomboni of DIMNP for her strong support and Dr. Bufalino of SORIT for his precious suggestions and help. Finally they like to thank Dr. Mitchell of AMEC-NNC, Dr. Kuijper and Dr. van Heek both of NRG, Professor Kloosterman of TUD, and Dr. von Lensa of FZJ for the collaboration.

References

[1] NEA, "Nuclear energy outlook," Tech. Rep., Organisation for Economic Co-operation and Development, 2008.

[2] G. Nerac, "A technology roadmap for generation IV nuclear energy systems," Tech. Rep. GIF-002-00, Department of Energy, Washington, DC, USA, 2002.

[3] IAEA, "Energy, electricity and nuclear power: developments and projections," Tech. Rep. STI/PUB/1304, 2007.

[4] IPCC, "Emissions scenarios," Tech. Rep., Specification Representation Associates, 2000.

[5] IEA, "Energy technology perspectives," Tech. Rep., Organisation for Economic Co-operation and Development, 2008.

[6] EU Parliament, "Report on conventional energy sources and energy technology," Tech. Rep. A6-0348/2007, 2007.

[7] IEA, "World energy outlook," Tech. Rep., Organisation for Economic Co-operation and Development, 2008.

[8] NEA, "Risks and benefits of nuclear energy," Tech. Rep. 6242, Organisation for Economic Co-operation and Development, 2007.

[9] EWG, "Uranium resources and nuclear energy," Tech. Rep. 1/06, 2006.

[10] NEA, "Uranium 2007: resources, production and demand," Tech. Rep. 6345, Organisation for Economic Co-operation and Development, 2008.

[11] IEA, "World energy outlook," Tech. Rep., Organisation for Economic Co-operation and Development, 2006.

[12] IAEA, "Energy, electricity and nuclear power estimates for the period up to 2030," Tech. Rep. IAEA-RDS-1/28, 2008.

[13] EUROSTAT, "Electricity Statistics—provisional data for 2007," EU.

[14] EC, "Report on strategy study on LWR/HTR symbiosis," Tech. Rep. HTR-N1-04708-D3.3.1, 2004.

[15] G. Lomonaco, *Problematiche di sicurezza nella produzione di idrogeno mediante impianti HTR*, Bachelor Degree Thesis, University of Pisa, Pisa, Italy, December 2003, http://www.tesionline.it/default/tesi.asp?idt=10361.

[16] N. Cerullo, D. Bufalino, G. Forasassi, G. Lomonaco, P. Rocchi, and V. Romanello, "The capabilities of HTRs to burn actinides and to optimize plutonium exploitation," in *Proceedings of the 12th International Conference on Nuclear Engineering (ICONE12)*, vol. 1, pp. 495–501, Arlington, Va, USA, April 2004.

[17] N. Cerullo, D. Bufalino, G. Forasassi, G. Lomonaco, P. Rocchi, and V. Romanello, "An additional performance of HTRs: the waste raditoxicity minimization," *Radiation Protection Dosimetry*, vol. 115, no. 1–4, pp. 122–125, 2005.

[18] E. Bomboni, N. Cerullo, G. Lomonaco, and V. Romanello, "A critical review of the recent improvements in minimizing nuclear waste by innovative gas-cooled reactors," *Science and Technology of Nuclear Installations*, vol. 2008, Article ID 265430, 18 pages, 2008.

[19] AREVA-NP, "UK-EPR, fundamental safety overview," Tech. Rep., 2008.

[20] E. Fridman, E. Shwageraus, and A. Galperin, "Implementation of multi-group cross-section methodology in BGCore MC-depletion code," in *Proceedings of the International Conference on the Physics of Reactors (PHYSOR '08)*, Interlaken, Switzerland, September 2008.

[21] EC, "FP5-EAECTP C called also HTR-N1," Tech. Rep. FIKI-CT-2001-00169, European Commission, 2001–2005.

[22] EC, "PUMA—plutonium and minor actinides management in thermal high temperature reactors," EC, 2006–2009.

[23] EC, "ReActor for process heat, hydrogen and eLectricity generation," EC, 2006–2009.

[24] EC, "Sustainable nuclear energy technical platformml: strategic research agenda," Final Draft, 2009.

[25] N. Fujimoto, S. Fujikawa, H. Hayashi, et al., "Present status of HTTR project—achievement of 950°C reactor outlet coolant temperature," in *Proceedings of the IAEA 2nd International Topical Meeting on HTR Technology*, International Atomic Energy Agency, Beijing, China, September 2004.

[26] Y. Xu, "The HTR-10 project and its further development," in *Proceedings of the IAEA Conference on Humboldt-Table Rock-Steinauer (HTR '02)*, International Atomic Energy Agency, Petten, The Netherlands, April 2002.

[27] E. Bomboni, N. Cerullo, and G. Lomonaco, "Assessment of LWR-HTR-GCFR integrated cycle," *Science and Technology of Nuclear Installations*, vol. 2009, Article ID 193594, 14 pages, 2009.

[28] E. Bomboni, N. Cerullo, and G. Lomonaco, "New developments in actinides burning with symbiotic LWR-HTR-GCFR fuel cycles: perspectives and challenges," in *Proceedings of the 10th International Exchange Meeting on Partitioning and Transmutation (IEMPT '08)*, vol. 10, Mito, Japan, October 2008.

Hindawi Publishing Corporation
Science and Technology of Nuclear Installations
Volume 2009, Article ID 965757, 11 pages
doi:10.1155/2009/965757

Review Article

Gas-Cooled Fast Reactor: A Historical Overview and Future Outlook

W. F. G. van Rooijen

Nuclear and Radiological Engineering Program, Georgia Institute of Technology, 801 Ferst Dr. NW, Atlanta, GA 30332, USA

Correspondence should be addressed to W. F. G. van Rooijen, vanrooijen@mail.gatech.edu

Received 18 January 2009; Accepted 7 April 2009

Recommended by Guglielmo Lomonaco

A review is given of developments in the area of Gas-Cooled Fast Reactors (GCFR) in the period from roughly 1960 until 1980. During that period, the GCFR concept was expected to increase the breeding gain, the thermal efficiency of a nuclear power plant, and alleviate some of the problems associated with liquid metal coolants. During this period, the GCFR concept was found to be more challenging than liquid-metal-cooled reactors, and none were ever constructed. In the second part of the paper, we provide an overview of the investigations on GCFR since the year 2000, when the Generation IV Initiative rekindled interest in this reactor type. The new GCFR concepts focus primarily on sustainable nuclear power, with very efficient resource use, minimum waste, and a very strong focus on (passive) safety. An overview is presented of the main design characteristics of these Gen IV GCFRs, and a literature list is provided to guide the interested reader towards more detailed publications.

1. Fast Reactors: Background and History

Uranium as it occurs in nature contains 0.7% of the fissile isotope U-235, the rest being U-238. If bombarded with neutrons, U-238 can capture a neutron and transmute to the isotope of plutonium Pu-239, which is fissile. Thus there is a possibility to create fissile material in a nuclear chain reacting system, and maybe even the opportunity to create more fissile material than is being consumed in the reactor: one can breed fissile material (e.g., Pu-239) from fertile material (e.g., U-238). The number of new neutrons released by a fissile nucleus upon absorption of a neutron is given by the parameter η:

$$\eta = \frac{\nu\sigma_f}{\sigma_a}. \tag{1}$$

To maintain a critical reactor, one needs exactly one new neutron per fission, leaving $\eta - 1$ neutrons to bombard a fertile material. This number of available neutrons can be interpreted as the *breeding potential* of a given isotope. In practice, neutrons are lost from the system by leakage, and by parasitic capture (i.e., capture in nonfuel and nonfertile materials, such as coolant and structural components). Thus, one is left with the number of available neutrons equal to

$$\text{no.} = \eta - 1 - \text{leakage} - \text{parasitic capture} \tag{2}$$

for fertile to fissile transmutation reactions. The factor η is illustrated in Figure 1 as a function of the energy of the neutron causing fission. In general, η, and thus the breeding potential, is highest in fast spectrum systems, especially if the fissioning isotope is Pu-239 or Pu-241. At the same time, the capture cross-section of non-fuel isotopes generally decreases with energy. Thus, if one can construct a nuclear reactor in which the neutrons remain at high energy, one can minimize the parasitic losses and obtain a breeder reactor.

The potential of breeding fissile isotopes in fast reactors was recognized during the Manhattan Project, and in 1946 the first fast reactor, called Clementine, was constructed and operated at Los Alamos National Laboratory in the US. At that time, enrichment technology was still in its infancy, and the global reserves of uranium were thought to be small. It was generally accepted that there would not be enough natural uranium for a sizable fleet of civilian nuclear power plants. As a result, a feverish development program into Fast Breeder Reactors followed, leading to the start of

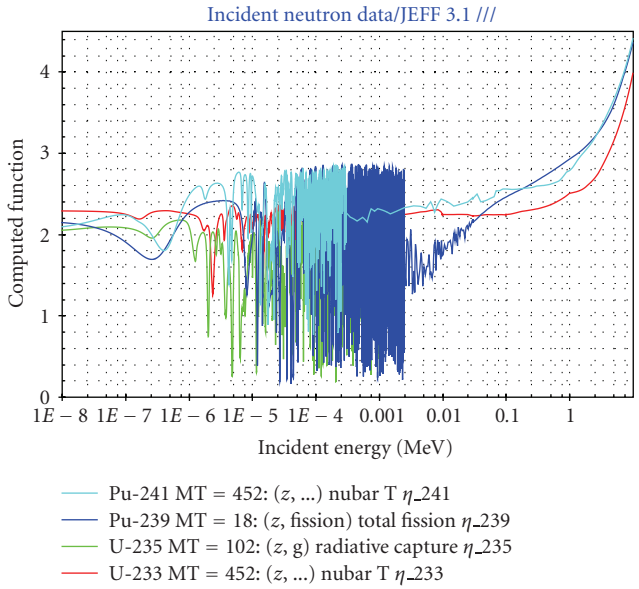

Figure 1: The η-factor for U-233, U-235, Pu-239, and Pu-241. Made with the JANIS data viewer (http://www.nea.fr/janis), based on JEFF-3.1 data. Note that U-235 has the lowest η of all isotopes in both the thermal and the fast range. For Pu-239, the breeding potential rapidly increases above 50 keV.

Experimental Breeder Reactor (EBR-I) in 1951 at the Idaho National Lab in the US. This reactor was the first reactor to produce electricity from nuclear power. The net breeding of fissile material was confirmed in EBR-I.

After the Atoms for Peace speech (1953), many industrialized nations embarked on a Fast Breeder Reactor research program for civilian applications, of which the most notable programs were in the Soviet Union, the UK, France, Germany, and Japan. In the following decades, several fast neutron test reactors and prototype power plants were constructed worldwide. But in the 1970s the situation for fast reactors changed; advances in enrichment technology made enrichment cheaper; fast reactors would always be more expensive than LWRs, and their engineering and safety aspects significantly are more challenging; uranium was more abundant than originally thought; and the nuclear power industry did not grow at the expected high rate. In the US, the decision in the late 1970s to disallow reprocessing in the civilian fuel cycle signified the end of any fast breeder reactor applications in the USA. In the 1990s, almost all major fast reactor programs in the world were either cancelled or significantly downsized. The interested reader is referred to the IAEA Fast Reactor Database for an overview of past fast reactor experiences worldwide (http://www.iaea.org/inisnkm/nkm/aws/frdb/index.html) .

Presently, fast reactors are gaining increasing attention for several reasons. If nuclear power is to grow significantly in the future, uranium will become scarce. Fast reactors can contribute to sustainable development by using a much larger fraction of the uranium resources. On the other hand, the high number of excess neutrons available in a fast reactor allows their application as actinide transmutation reactors, to reduce the long-term radiotoxicity of nuclear waste.

2. Engineering Choices for Gas-Cooled Fast Reactors

To obtain the highest breeding potential in any reactor, the amount of parasitic absorption should be minimized. This translates into the choice of a very tightly packed core in which the volume fractions of structural materials and coolant are kept to a minimum, commonly featuring a triangular lattice for the fuel pins. The number of capture reactions producing fissile material per unit time is proportional to the flux level in the reactor. For reasons of economics and fuel cycle characterestics, it is generally desirable to have the highest possible breeding rate, and thus generally the reactor core is designed to have a very high flux level. This high flux level generally translates into a very high fission rate, and as a result the power density in a fast reactor core is usually very high, typically of the order of 300 MW/m^3, which is 3 to 4 times higher than in LWRs. It should be noted that the high power density in a fast reactor is a result of design choices rather than an innate feature of this type of nuclear reactors.

The choice of coolant is dictated by the desire to introduce the smallest amount of absorption and moderation, while still being able to reliably remove the heat from this high power density configuration. Commonly a liquid metal is chosen, with sodium being the most common, but a gas coolant is also possible. The most common choices for gas-cooled fast reactors are helium, (supercritical) CO_2, and steam. (Special mention should be made of the supercritical water-cooled reactor concept, which is proposed with thermal, epithermal, and fast neutron spectra.) Even though all these coolants are composed of light isotopes, the amount of moderation is limited because of the low number density of gas coolants. In comparison with sodium, gas coolants have the following advantages for fast reactor applications.

(1) Chemical compatibility with water, obviating the need of an intermediate coolant loop, and generally good chemical compatibility with structural materials.

(2) Negligible activation of coolant.

(3) Optically transparent, simplifying fuel shuffling operations and inspection.

(4) Gas coolants cannot change phase in the core, reducing the potential of reactivity swings under accidental conditions.

(5) Reduction of the positive void effect typically associated with sodium.

(6) Gas coolants generally allow a harder neutron spectrum, which increases the breeding potential of the reactor.

Table 1: Design data for four early GCFR proposals. The small General Atomics GCFR was envisaged as a prototype, the GBRs were envisaged as large-scale commercial systems. From the three GBR concepts, the GBR-4 was adopted as the reference design. Note: pressure drop is over entire primary circuit for GA design; core only for GBR designs.

Reactor	GA GCFR	GBR-2	GBR-3	GBR-4
Coolant	He	He	CO_2	He
Thermal power [MW]	835	3000	3000	3450
Fuel type	pins	particle	particle	pins
Fuel material	$UPuO_2$	$UPuO_2$	$UPuO_2$	$UPuO_2$
$T_{core,in}$ [°C]	323	260	260	260
$T_{core,out}$ [°C]	550	700	650	560
Pressure [MPa]	8.5	12.0	6.0	12.0
Pressure drop [MPa]	0.37	0.34	—	0.24
Core height [m]	1.0	1.0	1.0	1.4
Core diameter [m]	2.0	—	—	—
Breeding Gain	0.4	0.43	0.36	0.42
Year of design data	1974	1972	1972	1974

(7) Since gas coolants have a low number density, one can allow a larger coolant fraction in the core without an unacceptable increase in parasitic capture. This more "open" core arrangement increases neutron leakage into the breeding blankets, improving the breeding gain.

Disadvantages of gas coolants include the following.

(1) Higher pumping power compared to liquid coolants.

(2) Need to maintain high pressure in the system, typically around 7 MPa for helium systems, to approximately 25 MPa for supercritical CO_2 (cf. PWR 15 MPa). For GCFRs, the operating pressure is chosen based on a tradeoff between pumping power (higher pressure is better), engineering reasons (lower pressure is easier and cheaper), and safety (higher operating pressure means larger depressurization effects).

(3) Gas coolant properties generally require artificial roughening of the cladding to maintain acceptable cladding temperature, resulting in an increased pressure drop over the core, and a higher requirement on pumping power. Besides, in a fast reactor the power densities of individual subassemblies vary considerably. To maintain adequate temperatures, either each assembly need to have an adjustable flow gag, or the amount of roughening of the cladding can be varied.

(4) High coolant flow velocity can lead to significant vibrations of the fuel pins.

(5) Decay heat extraction from the high power density core is difficult, becoming more so following a depressurisation event, requiring fast response and high reliability and, in the latter case, large pumping power.

In practice, the advantages of a simpler system layout in GCFRs, a higher breeding gain, and higher thermal efficiency are offset by the need of the engineered safety precautions for depressurization. In practice the temperature limits on conventional cladding material (stainless steel) do not allow operation at much higher temperature than in a typical sodium-cooled fast reactor. Overall, the economics of GCFRs were never shown to be better than Liquid Metal-cooled FBRs. No GCFRs were ever constructed, and the "classic" GCFR concept was abandoned in the late 1970s.

3. Overview of Past GCFR Programs

In what follows an overview is presented of the major GCFR programs which occurred in the past. This overview is not meant to be exhaustive, but rather it serves to illustrate that the GCFR concept has been well researched in the past. For more information, the reader is referred to [1].

3.1. Germany: The Gas Breeder Memorandum. In Germany the nuclear research establishments at Karlsruhe and Jülich, together with partners from industry, prepared a document on Gas Breeder Reactors known as the Gas Breeder Memorandum ("Gasbrüter-Memorandum", 1969 [2]). This memorandum defined 3 GCFR designs, all featuring helium cooling. Steam and CO_2 were reviewed as coolant candidates but deemed inadequate. In the Gas Breeder Memorandum the main focus was on a conventional core, with the fuel assembly design extrapolated from an LMFBR design, and a Prestressed Concrete Reactor Vessel (PCRV) extrapolated from thermal HTR, with pin-type fuel, stainless steel cladding, and a secondary steam cycle. All blowers and steam generators are integrated into the PCRV. Limited research was done into a direct-cycle reactor, and into coated particle fuel, although the two were not necessarily combined into one concept. Some design data can be found in [2]. The German GCFR design reached a considerable level of detail, with material irradiations planned in the BR-2 reactor in Mol (Belgium) in the mid to late 1970s. The German design is interesting because it already emphasized the need of keeping an elevated backup pressure (2 to 3 bar overpressure) around

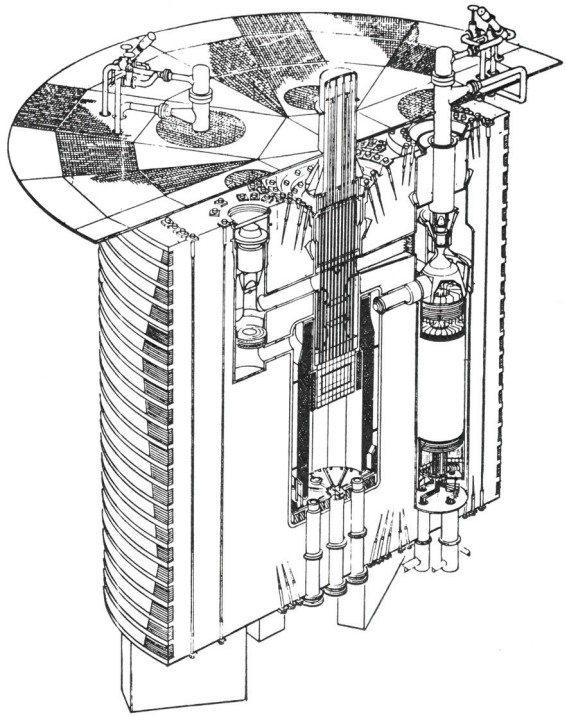

Figure 2: Primary system layout for the General Atomics GCFR Demonstration plant. The core cavity is shown empty. The overall system layout is typical for all gas-cooled reactor designs of the era. The large cavity on the right side of the core contains a boiler and a blower. The smaller cavity on the left side houses one of the active DHR systems. Figure reproduced from [4].

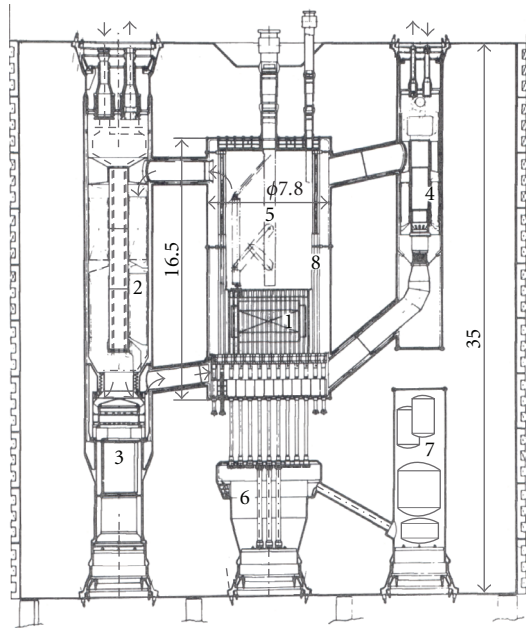

Figure 3: Vessel cross section of the PCRV for GBR-4 (1200 MWe). All dimensions in m. 1: core, 2: main steam generator, 3: main gas circulator, 4: emergency cooling loop, 5: fuel manipulator, 6: control cavity, 7: helium purification plant, 8: neutron shield.

the primary system after a Loss Of Coolant Accident (LOCA) in order to more efficiently cool the core.

3.2. US: General Atomics. In the US, General Atomics announced plans for a GCFR in 1962. GA prepared designs for a 300 MWe demonstration plant and a 1000 MWe commercial plant [3]. In 1968 the GCFR Utility Program was started to design, license, and build a 300 MWe demonstration plant [4]. In 1973 the target was set for the GCFR to start operation in 1983. The main parameters of the 300 MWe GCFR are given in Table 1, and an illustration of the plant layout is given in Figure 2 (taken from [4]). The GA design has helium coolant and UO_2 fuel in stainless steel cladding. The entire core is based on LMFBR technology with slight adjustments for the gaseous coolant. The fuel pins are roughened to enhance heat exchange. The primary system is housed in a PCRV, into which all blowers and steam generators are integrated. A last reference to the GA GCFR demonstration design was found in 1981, when the power output was increased to 350 MWe, but the safety case remained problematic [5].

3.3. Europe: The Gas Breeder Reactor Association. In Europe a number of players in the nuclear field joined forces to develop a gas-cooled fast reactor; the Gas Breeder Reactor Association. This group proposed a first design (GBR-1) in 1970, a 1000 MWe reactor featuring helium coolant, pin-type fuel, conventional outlet temperature, and a secondary steam cycle. This design was followed by GBR-2 and -3 (1971), also 1000 MWe reactors but using coated particle fuel, slightly elevated outlet temperature, and helium coolant for GBR-2; CO_2 coolant for GBR-3 [6]. The 3 designs finally evolved into the GBR-4 design, a 1200 MWe reactor with helium cooling and pin-type fuel. Table 1 lists the main design data for GBR-2, -3, and -4. Like other designs of the era, the core, blowers, and steam generators were integrated into a PCRV. A cross-section of the GBR-4 PCRV is shown in Figure 3.

For GBR-2 and GBR-3 detailed designs were prepared of the coated particles, and two designs were proposed for the fuel assemblies to hold the coated particles. The fuel assemblies for GBR-2 (helium coolant) and GBR-3 (CO_2 coolant) are illustrated in Figure 4. For GBR-2, each fuel assembly consists of 7 fuel cylinders. Each fuel cylinder consists of 2 perforated concentric annuli with coated particles packed between them. Helium flows inward to keep a compressive stress on the inner tube. The inner tube would have been made in SiC, while other parts would be stainless steel.

The GBR-3 assembly consists of a "stack of saucers". The coolant flows up through the central cylinder, then flows radially through the bed of coated particles, then flows up and out of the core. The cold parts are made of steel, and hot parts of SiC. The fuel assembly for the GBR-4 design is less ambitious, and is based on an LMFBR fuel assembly with pin fuel. An overview of the GBR-4 fuel assembly features is given in Figure 5, because it is very typical of all GCFR fuel pins designs of that time. Each fuel pin holds

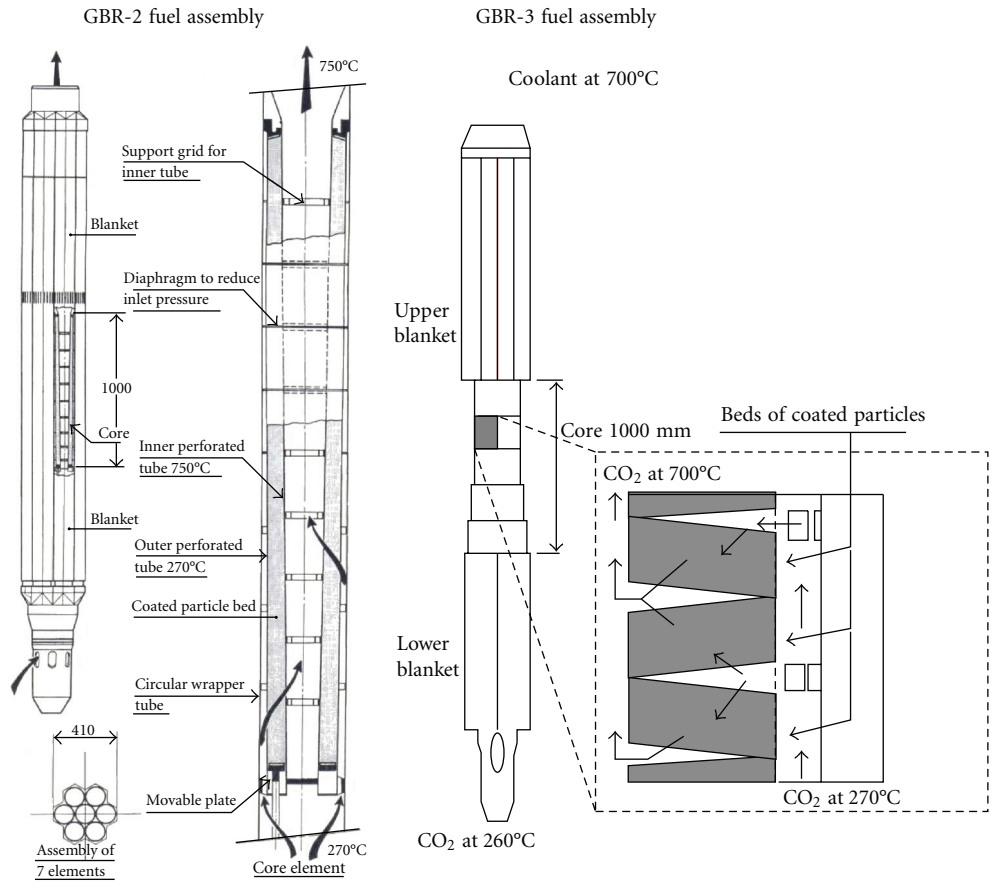

Figure 4: Fuel assemblies for GBR-2 (left) and GBR-3 (right).

a number of traditional MOx pellets. Surface roughening enhances turbulence and heat transfer. The high helium velocity requires many restraining devices to prevent the fuel pins from vibrating too violently. Spacer wires, traditionally used in fast reactors, are not strong enough. Thus grid spacers are used, which have a very intricate design to be strong enough and not introduce too much drag.

The GBR-2 design is interesting because it resurfaces in modern design proposals for GCFRs, for instance, in Japan [7]. The objective of the coated particle fuels was to increase the core outlet temperature to improve the thermodynamic efficiency of the secondary steam cycle. For both GBR-2 and -3 coated particles were only used for the driver fuel, the blankets employed traditional pin-type fuel. This solution was chosen because at the time of design reprocessing of coated particle fuel was not proven. GBR-2 and -3 required several ceramic parts, most notably the structures at the outlet side. The fabrication difficulties related to large ceramic parts led to the development of GBR-4, which is a much more conventional design. In GBR-4, the outlet temperatures are decreased, enabling the use of stainless steel components throughout the core. The plant efficiency is lower, which is offset by a larger total output of the reactor: from 1000 MWe to 1200 MWe. A last reference to the GBR-4 design was found in [8], where the safety case for large GCFR cores is discussed.

3.4. The Soviet Union: Dissociating Coolant. In the Soviet Union a GCFR programme was initiated focusing on a dissociating coolant: N_2O_4. In the core the N_2O_4 would dissociate through two endothermic chemical reactions [9]:

$$N_2O_4 \rightleftharpoons 2NO_2 \rightleftharpoons N_2 + 2O_2. \quad (3)$$

Operating temperature was comparable to those of other contemporary GCFR designs, with a somewhat higher pressure (between 16 MPa and 25 MPa). The major advantage of the dissociating coolant lies in the possibility of condensing the working fluid in the heat exchanger, thereby greatly reducing the pumping power. The system operates much like a refrigerator. Also the combined effects of evaporation and a chemical reaction absorb a large amount of heat from the core, so the mass flow of coolant can be relatively small. The N_2O_4 coolant is very corrosive. This problem was solved by the development of chromium dispersion fuel pins in the late 1970s (small inclusions of U metal or UO_2 in a matrix of chromium) and extensive research into the corrosion behavior of various steel types [10]. This last paper also mentions irradiation experiments on the chromium dispersion fuel pins in a test rig using N_2O_4. As with other GCFR programs, no references are found later than the early 1980s.

3.5. UK: ETGBR/EGCR. In the late 1970s a UK program was initiated into an "Existing Technology Gas Breeder Reactor"

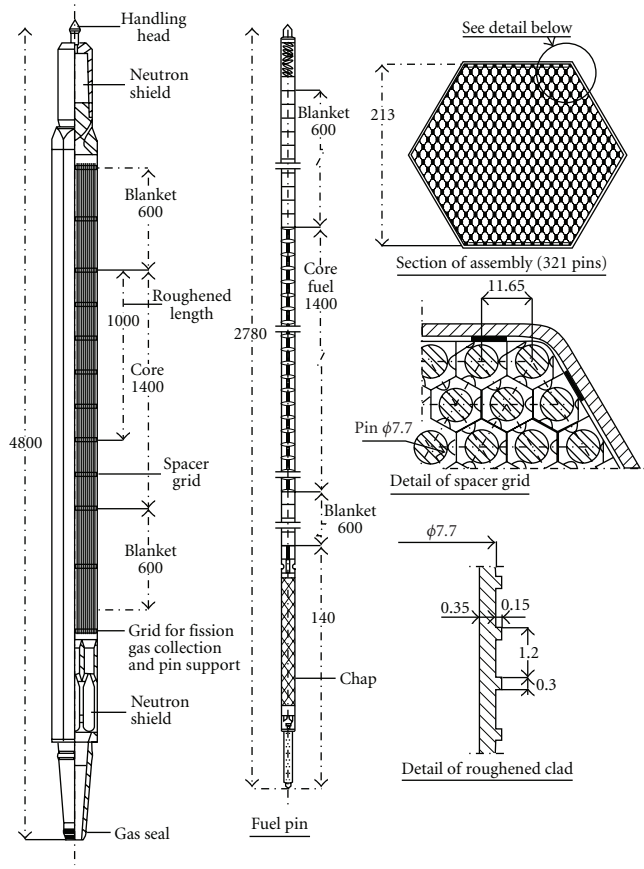

Figure 5: Overview of the GBR-4 fuel assembly. An example of roughened cladding is in the lower right figure.

(ETGBR). This design focused on joining the experience gained in the UK on sodium systems (PFR, Dounreay) and the thermal CO_2-cooled AGR reactors. The fuel assemblies used stainless steel cladding with surface roughening, while the entire system was to be housed in a concrete vessel as used for the AGRs. ETGBR used CO_2 coolant, and had a lower power density than LMFBRs, with the expected higher breeding gain to make up for the difference [11]. The ETGBR is not very different from other designs of the same era for GCFRs. However, the ETGBR idea lingered on for a long time well into the late 1990s. At that late stage, the ETGBR was rebranded as the Enhanced Gas-Cooled Reactor (EGCR). EGCR was proposed as an actinide burner, first within the European Fast Reactor (EFR) program, and later in the CAPRA/CADRA study [12]. By then the reactor featured 3600 MWth, CO_2 cooling, and nitride fuel in fuel pins.

3.6. Japan: Prismatic Fuel. In Japan a fast reactor programme was initiated in the 1960s, including sodium and gas-cooled reactor concepts. Kawasaki Heavy Industries (KHI) investigated GCFR concepts cooled with steam, CO_2, and helium [13]. The helium concept was based on LMFBR technology, but KHI opted for a very low core, to reduce the pumping power requirements. The flat core also increases breeding gain but requires a larger fissile fraction. Investigations into the GCFR concept seem to have continued without interruption in Japan, culminating in the late 1990s in a GCFR design proposal by JNC. This reactor also features a core with a low height/diameter ratio "pancake core", and uses coated particle fuel. A nitride fuel compound is chosen for the kernels. Buffer layer and sealing layers are made of TiN. Two types of fuel assemblies are proposed. One fuel assembly resembles that of GBR-2: coated particles are arranged in an annular bed, with the helium flowing radially through the bed. The other design features large prismatic blocks filled with a mixture of coated particles and a matrix material (TiN, SiC or ZrC). Coolant channels run axially through the blocks. All structural parts are made in SiC. Thermal output is 2400 MWth, with a power density of 100 MW/m^3. The coolant is helium and a direct cycle energy conversion system is envisaged [7].

4. Generation IV and a New Start for GCFR Development

The possible depletion of fossil fuel and the wish to limit CO_2 release into the atmosphere cause a new interest in nuclear energy as the only CO_2-free energy source with high capacity. There is a growing pressure from society to reduce the amount of long-lived nuclear waste material as far as possible, and to further increase the safety of nuclear power stations. These points are addressed by the Generation

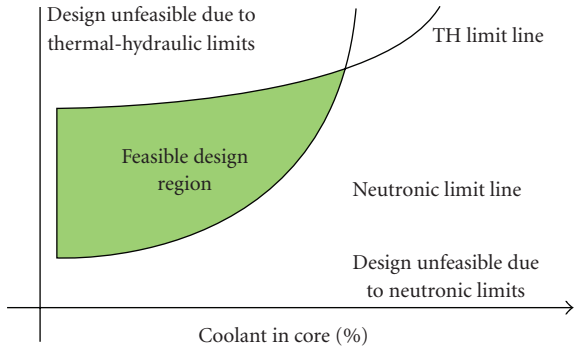

Figure 6: Schematic illustration showing a region of feasible GCFR designs bounded by neutronic and thermohydraulic (TH) limits. The x-axis gives the percentage coolant in the core.

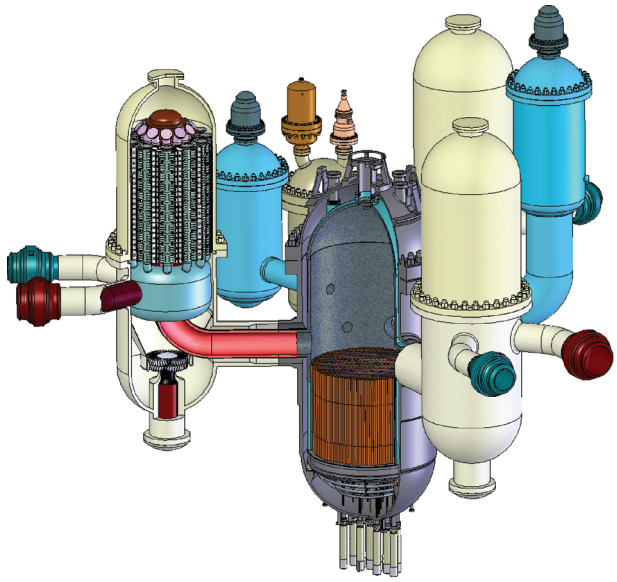

Figure 7: A cross-cut through a 2400 MWth Gen IV GCFR plant with indirect cycle operation. The large structures contain the intermediate heat exchangers. The elevated structure on the right is the decay heat exchanger. The entire system would be built into a tight-fitting secondary close containment. Image provided by [25].

IV International Forum, which is an international research initiative for the fourth generation of nuclear power plants, envisaged to enter service within the first half of the 21st century [14]. Six reactor types have been selected for further research and evaluation in the Generation IV framework, the Gas (Cooled) Fast Reactor being one of the six concepts. In the Generation IV documents, the concept is commonly referred to as "Gas Fast Reactor", abbreviated GFR, and we will follow this convention for the remainder of this paper.

The Generation IV objectives are to improve all aspects of nuclear power generation: safety and reliability, economics, sustainability, availability, and proliferation and physical protection. The six reactor types chosen all have their strong and weak points; used in a symbiotic system, the six reactor types should counterbalance their mutual weak points. There is a large surplus of reactor-grade plutonium available, and thus breeding of fissile material is no longer the primary target for the fast reactors in the short term. This enables a shift from high power density fast reactors to designs that are self-sustaining and put more emphasis on safety, especially passive decay heat removal. For completeness, the six Generation IV systems are listed here in the following.

- VHTR: Very High Temperature Reactor, graphite moderator, helium coolant, high temperature operation for direct cycle electricity production or industrial heat applications.
- SCWR: Supercritical Water Reactor (thermal, epithermal, and fast versions are under investigation).
- GFR: Gas-cooled Fast Reactor, high temperature operation using helium coolant, mainly intended for electricity production with direct or indirect cycles.
- SFR: Sodium-cooled Fast Reactor.
- LFR: Lead-cooled Fast Reactor.
- MSR: Molten Salt Reactor.

Within the Generation IV framework the GFR targets sustainability, that is, optimal use of resources while maintaining good safety and economical performance. The reference design of the Generation IV GFR features the following.

(1) Fast reactor core without fertile blankets, that is, all new fissile fuel is bred in the core. The background is that in a fertile blanket, the fissile element (e.g., Pu-239) is isotopically almost pure, which poses a proliferation concern.

(2) Breeding enough fissile material to refuel the same reactor, recycling all heavy metal, adding only fertile material; only fission products and reprocessing losses are discharged to a repository. This type of closed cycle is discussed in [15]. Scenario studies indicate that it is important to reduce the existing stockpile of minor actinides (Np, Am, and Cm) as much as possible [16, 17]. For this reason several GFR investigations focus on the potential of irradiating extra MA in the GCFR fuel [18].

(3) The fuel specific power is comparatively low, typically around 40 W/gHM. By allowing a low specific power, the volumetric power density in the core remains limited, typically between 50 MW/m^3 and 100 MW/m^3, which improves the safety characteristics. To make up for the economic penalty of low specific power, a highly efficient power conversion system with a direct coupled gas turbine in a Brayton-cycle is the reference for electricity generation [19].

(4) Initial investigation centered on a unit power is of 600 MWth (300 MWe) for a "modular" design, and a 2400 MWth (1200 MWe) design for a large-scale reactor. In practice, the 600 MWth designs proved to be very challenging for neutronics and safety, and in 2006 the decision was made to pursue the 2400 MWth design exclusively. There is no reference design for the 2400 MWth reactor; both direct and indirect cycle power conversion systems are possible, using 3 or 4 loops. At the time of writing, there is no clearly favorite design.

Table 2: Design data for several Generation IV GFRs, per July 2006. For all Direct Cycle reactors, helium is the preferred coolant. For the GFR600 Indirect Cycle variant, supercritical CO_2 (S-CO_2) is the secondary coolant. Note that the 600 MWth are currently no longer investigated. For the 2400 MWth Indirect Cycle concept, various secondary cycles and working fluids are under consideration. The JAEA GFR has blankets to breed just enough new fissile material to allow operation in a closed fuel cycle.

Concept	ETDR	GFR600	GFR600	GFR2400	GFR2400	JAEA GFR
Power [MWth]	50	600	600	2400	2400	2400
PCS	—	direct	indirect	(in)direct	direct	direct
Coolant	He	He	He/S-CO_2	He	He	He
Power density [MW/m^3]	100	103	103	100	100	90
Specific power [W/gHM]	—	45	45	—	42	36
$T_{core,in}$ [°C]	250	480	≈400	480	480	460
$T_{core,out}$ [°C]	525	850	≈625	850	850	850
Core H/D	0.86/0.86	1.95/1.95	1.95/1.95	1.55/4.44	1.34/4.77	0.9/5.9
Pressure [MPa]	7.0	7.0	7.0	7.0	7.0	7.0
Fuel type	Pins[a]	plates	plates	plates	pins	blocks
Fuel mat.	$UPuO_2$	UPuC	UPuC	UPuC	UPuC	UPuN
Struct. mat.	AIM1[b]	SiC	SiC	SiC	SiC	SiC
Refl. mat.	AIM1	Zr_3Si_2	Zr_3Si_2	Zr_3Si_2	Zr_3Si_2	SiC
Vol.% c/s/f[c]	—	55/20/25	55/20/25	40/37.6/22.4	55/23/22	25/55/20
Breeding Gain	—	−5%	−5%	−5%	0	0.03/0.11[d]

[a] Plate fuel in later stage.
[b] Austenitic Improved Material 1, a variation of 15/15Ti stainless steel (SS-316), developed especially for fast reactors (Phénix and SuperPhénix).
[c] Coolant, structural materials, fuel.
[d] Without/with blanket.

(5) Helium is chosen as the reference coolant. To obtain a high efficiency ($\eta > 50\%$) in a Brayton-cycle using helium as the working fluid, a high reactor outlet temperature is necessary (850°C), as well as elevated pressure (reference: 7 MPa). To enable operation at such high temperatures, ceramics rather than steel are used as the structural material (SiC, Zr_3Si_2, TiN). A direct-cycle operating on supercritical CO_2 can achieve a similar efficiency at lower temperature (typically 650°C) but higher pressure (25 MPa, [20, 21]). At the time of writing, only indirect cycle operation is considered seriously.

(6) The design of the core and fuel elements aims at promoting passive decay heat removal and providing adequate margins to core melt, by using refractory (high melting point) materials, and by allowing a large coolant fraction in the core. A large coolant fraction in the core increases the hydraulic diameter of the cooling channels, thereby reducing the friction pressure loss, increasing the mass flow under natural circulation. The objective is to allow decay heat extraction by passive methods during the first 24 hours following an accident. Studies into the natural convection behavior of Gen IV GFR concepts are presented for instance in [22, 23].

Outside of Gen IV, gas cooling has also been investigated for application to Accelerator Driven Systems (ADS) for actinide transmutation, but the consensus seems to be that a heavy liquid metal (Lead or Lead-Bismuth Eutectic) is preferred for ADS applications [24].

4.1. Basic Design Choices for the Gen IV GFR. The choice of zero breeding gain and the absence of blankets determine the fuel composition; there is only a narrow band of possible isotopic compositions that will result in a zero breeding gain. In the U/Pu fuel cycle, the fraction of U-238 has to be between 80% and 85%; note here that the plutonium vector has a negligible influence on the breeding gain, as the neutron capture in U-238 is the most important contribution to replace consumed fissile isotopes. The absence of blankets means that the reactor can be approximated by a simple homogeneous cylinder of a fuel/coolant mixture (neglecting the heterogeneity introduced by different fuel batches, etc.). For a homogeneous cylindrical reactor of a given volume and fuel composition, there is a *minimal* height to diameter (H/D)-ratio, below which the reactor will never become critical due to excessive neutron leakage. On the other hand, there is also an *optimal* H/D-ratio, where neutron losses by leakage are minimized. Now assume a homogeneous, cylindrical reactor of a fixed volume. If the coolant fraction is increased, the amount of fuel in the core decreases, and thus the H/D-ratio must be chosen closer to the optimal value to obtain criticality. This is illustrated in Figure 6, where the "neutronic limit" is given as a function of the coolant fraction in the core. The neutronic limit is the *minimum* value of H/D to obtain criticality with a given fraction of coolant in the core.

There is also a thermohydraulic limit on the H/D ratio of the reactor. If, for the same power density and reactor volume, the H/D ratio becomes larger (i.e., increase core height H, reduce diameter D), more power has to be transferred per coolant channel. This requires a larger coolant mass flow per coolant channel, resulting in a larger flow velocity and higher pressure drop over the core. This means that for a given fraction of coolant in the core, there is

a *maximum* value of H/D to stay below a given core pressure drop. This is illustrated in Figure 6 by the "TH limit".

A reactor can only be designed if the neutronic limit of H/D is smaller than the TH limit, as in Figure 6. Note that the neutronic limit is not necessarily smaller than the TH limit, for example, the TH limit may result in an H/D value too low to obtain criticality. In practice, choosing a low power density will enlarge the region of possibilities; lower power density means that it is easier to stay within TH-limits, and at the same time the reactor volume will be larger for the same power output, giving larger neutronic margins by reduction of leakage. Ultimately the power density has to be chosen to yield a reasonable specific power taking into account economic factors and fuel cycle considerations, such as the availability of fissile materials.

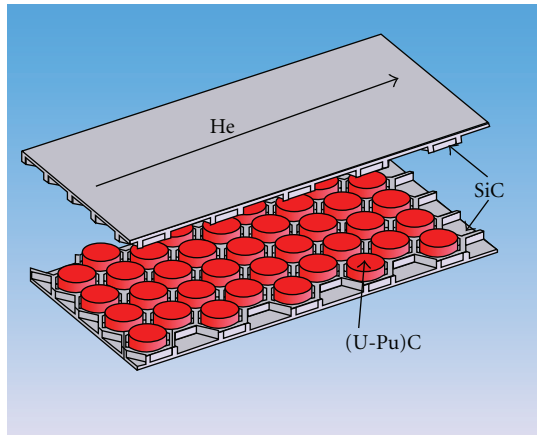

Figure 8: Fuel plate of Gen IV GCFR.

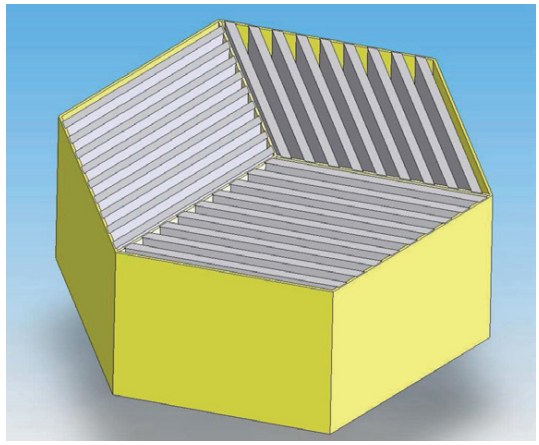

Figure 9: Fuel assembly of Gen IV GCFR.

5. Typical System Designs for Gen IV GFRs

Presently, several Gen IV GFR designs are investigated internationally. In this section, some general properties of these systems will be discussed. While direct cycle operation with a gas turbine was originally the reference design, this design proved to pose very challenging engineering problems. Therefore the indirect cycle option is presently the only seriously considered option. The reactors feature three or four power conversion loops. The wish to accommodate passive decay heat removal for a period of several hours after a depressurization translates in the need of maintaining an elevated system pressure even if the primary loop suffers a depressurization. To maintain an elevated backup pressure, the containment building can be kept sufficiently small, or a second "close containment" enveloping the primary circuit can be used. To obtain adequate flow rate by natural circulation, decay heat exchangers are located at a large elevation from the core. A proposed Gen IV GFR plant layout is illustrated in Figure 7, clearly showing the close containment ("guard vessel") and the elevated decay heat exchangers.

To improve the thermal-hydraulic performance of the GFR, a novel plate type fuel is currently under investigation. This type of fuel plate consists of a honeycomb structure, in which "pills" of fuel are embedded [26]. An illustration of a fuel plate is given in Figure 8, and a GFR fuel assembly is shown in Figure 9. The entire assembly is made from ceramic material (SiC). Diffusion of fission products is prevented by a metallic liner inside the fuel plate. Several proposed GFR fuel and structural materials are irradiated as part of the FUTURIX campaign in Phénix [27]. A large coolant faction is chosen in the core. To obtain criticality with a large fraction of coolant in the core, carbide fuels are selected because of their high density of heavy metal.

For completeness, a small overview is presented in Table 2 of some typical Gen IV GFR designs. In Europe a small-scale prototype reactor (ETDR, Experimental Technology Demonstration Reactor, recently upgraded to the ALLEGRO design) is under investigation (CEA/Euratom). It is a prototype GFR, intended to test and qualify materials and codes for Generation IV GFR designs. It will be started with a conventional core, using a pin-type MOx fuel in stainless steel cladding. The core will be gradually converted to use the ceramic fuel elements intended for Gen IV GFR. Seven proposals for large GFRs are under investigation by several research institutions within the Generation IV framework. The plate type fuel is a challenging design, and therefore pin-type fuel is maintained as a backup. The present reference Gen IV GFR design is a 2400 MWth plant with indirect cycle operation, using 3 loops, each consisting of an intermediate heat exchanger and an integrated turbogenerator.

Apart from the Generation IV GFR efforts, several designs for new Gas-cooled Fast Reactors have been published in recent years. Some of these efforts originated from Gen IV related research, or in some cases were developed "in the spirit of Gen IV". To complete the overview of recent GFR developments, they deserve to be mentioned here.

Some modern GFR proposals are based on TRISO coated particle fuel. For the specific GFR fuel cycle constraints, novel particles are proposed with advanced coating layers. It is generally accepted that the pyrolytic carbon layers in HTR TRISO particles will not withstand irradiation by fast neutrons [28]. For this reason, particles with ZrC or TiN coating layers are proposed. The TRISO particles can be

cooled directly using a fuel assembly similar to the GBR-2 design discussed earlier. Other investigators focus on fuel pebbles, either with TRISO particles inside of the pebbles (e.g., the PB-GCFR, [29]), or using a novel "hollow pebble" concept, as discussed in [30, 31]. Other proposed design feature prismatic fuel blocks with coolant channels. Some designs use blocks of coated particles embedded in a matrix (e.g., [32]), or fuel blocks entirely made of fuel material (e.g., [33]). However, all these fuel designs remain highly speculative, and especially the particle- and pebble-based designs will not fulfill the safety objective of decay heat removal by natural convection.

6. Conclusion

Gas cooling is an option for fast reactors. Several decades ago, gas cooling was seen as an option to obtain better breeding characteristics for Fast Breeder Reactors while reducing some of the problems associated with liquid sodium as a coolant. Several designs were developed in the past, but no gas-cooled fast reactors were ever constructed. In recent times gas cooling is once again pursued for fast neutron systems. In these recent designs, the design focus is on sustainability. Design tradeoffs are mainly based on safety. To enable the safety level of the GCFR concept to be high, advanced fuel concepts and advanced materials will be necessary, and are currently being investigated.

References

[1] W. F. G. van Rooijen, *Improving fuel cycle design and safety characteristics of a gas cooled fast reactor*, Ph.D. thesis, Delft University of Technology, Delft, The Netherlands, 2006, http://repository.tudelft.nl.

[2] M. Dalle Donne and C. A. Goetzmann, "Gas-cooled fast breeder reactor design, development, and safety features," in *Proceedings of the ANS Topical Meeting on Gas-Cooled Reactors: HTGR and GCFBR*, American Nuclear Society, Gatlinburg, Ten, USA, May 1974.

[3] A. E. Waltar and A. B. Reynolds, *Fast Breeder Reactors*, Pergamon Press, New York, NY, USA, 1981.

[4] R. H. Simon, J. B. Dee, and W. I. Morita, "Gas-cooled fast breeder reactor demonstration plant," in *Proceedings of the ANS Topical Meeting on Gas-Cooled Reactors: HTGR and GCFBR*, pp. 336–354, American Nuclear Society, Gatlinburg, Ten, USA, May 1974.

[5] A. Torri and D. R. Buttemer, "Gas-cooled fast reactor safety—and overview and status of the U.S. program," in *Proceedings of the Specialists Meeting on Gas-Cooled Reactor Safety and Licencing Aspects*, pp. 1–7, IAEA, Lausanne, Switzerland, September 1980, IWGGCR-1.

[6] J. Chermanne, "Past and future programmes of the GBR Association," in *Proceedings of the IAEA Study Group Meeting on Gas-Cooled Fast Reactors*, pp. 78–87, IAEA, Minsk, Belarus, July 1972, IAEA-TECDOC-154.

[7] M. Konomura, T. Saigusa, T. Mizuno, and Y. Ohkubo, "A promising gas-cooled fast reactor concept and its R&D plan," in *Proceedings of the Global 2003: Atoms for Prosperity: Updating Eisenhower's Global Vision for Nuclear Energy*, pp. 57–64, New Orleans, La, USA, November 2003.

[8] J. Chermanne and P. Burgsmüller, "Gas-cooled breeder reactor safety," in *Proceedings of the Specialists Meeting on Gas-Cooled Reactor Safety and Licencing Aspects*, pp. 39–51, IAEA, Lausanne, Switzerland, September 1980, IWGGCR-1.

[9] G. Melese and R. Katz, *Thermal and Flow Design of Helium-Cooled Reactors*, American Nuclear Society, La Grange Park, Ill, USA, 1984.

[10] V. B. Nesterenko, V. F. Zelensky, L. I. Kolykhan, et al., "Problems of creating fuel elements for fast gas-cooled reactors working on N_2O_4-dissociating coolant," in *Proceedings of the IAEA Specialists' Meeting on Gas-Cooled Reactor Fuel Development and Spent Fuel Treatment*, pp. 56–65, IAEA, Moscow, Russia, October 1983, IWGGCR-8.

[11] W. B. Kemmish, M. V. Quick, and I. L. Hirst, "The safety of CO_2 cooled breeder reactors based on existing gas cooled reactor technology," *Progress in Nuclear Energy*, vol. 10, no. 1, pp. 1–17, 1982.

[12] R. E. Sunderland, E. K. Whyman, H. M. Beaumont, and D. P. Every, "A gas-cooled dedicated minor actinide burning fast reactor: initial core design studies," in *Proceedings of the International Conference on Future Nuclear Systems (GLOBAL '99)*, American Nuclear Society, Jackson Hole, Wyo, USA, August-September 1999.

[13] H. Mochizuki, T. Izaki, K. Takitani, et al., "Design study of He gas-cooled fast breeder reactor," in *Proceedings of the IAEA Study Group Meeting on Gas-Cooled Fast Reactors*, pp. 133–164, IAEA, Minsk, Belarus, July 1972, IAEA-TECDOC-154.

[14] U.S. DOE Nuclear Energy Research Advisory Committee and The Generation IV International Forum, "A technology roadmap for Generation IV nuclear energy systems," December 2002, http://gif.inel.gov/roadmap.

[15] W. F. G. van Rooijen, J. L. Kloosterman, T. H. J. J. van der Hagen, and H. van Dam, "Definition of breeding gain for the closed fuel cycle and application to a gas-cooled fast reactor," *Nuclear Science and Engineering*, vol. 157, no. 2, pp. 185–199, 2007.

[16] J.-P. Grouiller, L. Boucher, M. Meyer, and M. Delpech, "Application with COSI code of gen IV fast reactors introduction in the French park," in *Proceedings of the International Conference on Advanced Nuclear Fuel Cycles and Systems (GLOBAL '07)*, pp. 1537–1542, American Nuclear Society, Boise, Idaho, USA, September 2007.

[17] Commissariat à l'Énergie Atomique, "Les déchets radioactifs à haute activité et à vie longue—recherches et résultats axe 1: séparation et transmutation des radionucléides à vie longue," Tech. Rep., CEA, Paris, France, December 2005.

[18] W. F. G. van Rooijen, G. J. van Gendt, D. I. van der Stok, and J. L. Kloosterman, "Multirecycling minor actinides in a gas-cooled fast reactor," in *Proceedings of the International Conference on Advanced Nuclear Fuel Cycles and Systems (GLOBAL '07)*, pp. 1205–1213, American Nuclear Society, Boise, Idaho, USA, September 2007.

[19] J. C. Garnier, N. Chauvin, P. Anzieu, et al., "Feasibility study of an advanced GFR design trends and safety options status of France & US studies," in *Proceedings of the Global 2003: Atoms for Prosperity: Updating Eisenhower's Global Vision for Nuclear Energy*, pp. 47–56, American Nuclear Society, New Orleans, La, USA, November 2003.

[20] Y. Kato, T. Nitawaki, and Y. Muto, "Medium temperature carbon dioxide gas turbine reactor," *Nuclear Engineering and Design*, vol. 230, no. 1–3, pp. 195–207, 2004.

[21] V. Dostal, P. Hejzlar, and M. J. Driscoll, "High-performance supercritical carbon dioxide cycle for next-generation nuclear

reactors," *Nuclear Technology*, vol. 154, no. 3, pp. 265–282, 2006.

[22] E. Bubelis, D. Castelliti, P. Coddington, et al., "A GFR benchmark: comparison of transient analysis codes based on the ETDR concept," *Progress in Nuclear Energy*, vol. 50, no. 1, pp. 37–51, 2008.

[23] W. F. G. van Rooijen, J. L. Kloosterman, T. H. J. J. van der Hagen, and H. van Dam, "Lithium-6-based passive reactivity control devices for a gas-cooled fast reactor," *Nuclear Technology*, vol. 159, no. 2, pp. 119–133, 2007.

[24] S. Pelloni, "Static analysis of the PDS-XADS LBE and gas-cooled concepts," *Annals of Nuclear Energy*, vol. 32, no. 1, pp. 13–28, 2005.

[25] D. Poette, "Personal communication," CEA, February 2009.

[26] P. Petkevich, K. Mikityuk, P. Coddington, and R. Chawla, "Development and benchmarking of a 2D transient thermal model for GFR plate-type fuel," *Annals of Nuclear Energy*, vol. 34, no. 9, pp. 707–718, 2007.

[27] N. Chauvin, J. Y. Malo, J. C. Gamier, et al., "GFR fuel and core pre-conceptual design studies," in *Proceedings of the International Conference on Advanced Nuclear Fuel Cycles and Systems (GLOBAL '07)*, pp. 423–433, American Nuclear Society, Boise, Idaho, USA, September 2007.

[28] D. G. Martin, "Considerations pertaining to the achievement of high burn-ups in HTR fuel," *Nuclear Engineering and Design*, vol. 213, no. 2-3, pp. 241–258, 2002.

[29] T. A. Taiwo, E. A. Hoffman, R. N. Hill, and W. S. Yang, "Evaluation of long-life transuranics breakeven and burner cores for waste minimization in a PB-GCFR fuel cycle," *Nuclear Technology*, vol. 155, no. 1, pp. 55–66, 2006.

[30] K. Ryu and H. Sekimoto, "Possibility of highly efficient uranium utilization with a pebble bed fast reactor," *Annals of Nuclear Energy*, vol. 27, no. 12, pp. 1139–1145, 2000.

[31] W. F. G. van Rooijen, J. L. Kloosterman, T. H. J. J. van der Hagen, and H. van Dam, "Fuel design and core layout for a gas-cooled fast reactor," *Nuclear Technology*, vol. 151, no. 3, pp. 221–238, 2005.

[32] N. G. Kodochigov, N. G. Kuzavkov, Y. P. Sukharev, and S. G. Usynina, "Concept of a gas cooled fast reactor," in *Proceedings of the Physics of Fuel Cycles and Advanced Nuclear Systems: Global Developments (PHYSOR '04)*, pp. 959–962, American Nuclear Society, Chicago, Ill, USA, April 2004.

[33] C. S. Handwerk, M. J. Driscoll, and P. Hejzlar, "Optimized core design of a supercritical carbon dioxide-cooled fast reactor," *Nuclear Technology*, vol. 164, no. 3, pp. 320–336, 2008.

Hindawi Publishing Corporation
Science and Technology of Nuclear Installations
Volume 2009, Article ID 282365, 9 pages
doi:10.1155/2009/282365

Research Article

Closed Fuel Cycle and Minor Actinide Multirecycling in a Gas-Cooled Fast Reactor

W. F. G. van Rooijen[1] and J. L. Kloosterman[2]

[1] *Nuclear & Radiological Engineering, Georgia Institute of Technology, 801 Ferst Dr. NW, Atlanta, GA 30332-0405, USA*
[2] *Radiation, Radionuclides and Reactors (R3) Department, Section Physics of Nuclear Reactors, Delft University of Technology, Mekelweg 15 2629 JB Delft, The Netherlands*

Correspondence should be addressed to W. F. G. van Rooijen, vanrooijen@mail.gatech.edu

Received 27 January 2009; Accepted 2 March 2009

Recommended by Guglielmo Lomonaco

The Generation IV International Forum has identified the Gas-Cooled Fast Reactor (GCFR) as one of the reactor concepts for future deployment. The GCFR targets sustainability, which is achieved by the use of a closed nuclear fuel cycle where only fission products are discharged to a repository; all Heavy Metal isotopes are to be recycled in the reactor. In this paper, an overview is presented of recent results obtained in the study of the closed fuel cycle and the influence of the addition of extra Minor Actinide (MA) isotopes from existing LWR stockpiles. In the presented work, up to 10% of the fuel was homogeneously replaced by an MA-mixture. The results are that addition of MA increases the potential of obtaining a closed fuel cycle. Reactivity coefficients generally decrease with increasing MA content. Addition of MA reduces the reactivity swing and allows very long irradiation intervals up to 10% FIMA with a small reactivity swing. Multirecycling studies show that a 600 MWth GCFR can transmute the MA from several PWRs. By a careful choice of the MA-fraction in the fuel, the reactivity of the fuel can be tuned to obtain a preset multiplication factor at end of cycle. Preliminary decay heat calculations show that the presence of MA in the fuel significantly increases the decay heat for time periods relevant to accidents (10^4–10^5 s after shutdown). The paper ends with some recommendations for future research in this promising area of the nuclear fuel cycle.

1. Introduction

In 2002 the Generation IV International Forum introduced their vision of the future of nuclear power generation, proposing six reactor concepts which could be introduced from the 2050s [1]. One of the Gen IV concepts is the Gas Cooled Fast Reactor (GCFR). This reactor concept specifically targets sustainability by a combination of resource efficiency, efficient power conversion, and waste minimization. The GCFR has been investigated in the past, but the design requirements in those days did not allow a feasible design. The most stringent problem was the requirement of a high power density in the core for efficient breeding. In the Gen IV GCFR, the breeding mission is replaced by the requirement of "self-sustainability" in a closed fuel cycle: after an irradiation campaign, fuel is allowed to cool down, and subsequently all HM isotopes are recycled from the spent nuclear fuel. An appropriate amount of fertile material is added to make a new fuel loading for the same reactor. Only fission products (and inevitable reprocessing losses) go to a repository. The reactor should thus breed just enough excess fissile material to sustain itself. This choice reduces the requirements on core power density and reopens the way for GCFR concepts.

For the present work, investigations were carried out in the scope of the European GCFR-Specific Targeted REsearch Program STREP into the potential of adding extra Minor Actinide (MA, here considered to be Np, Am, and Cm) isotopes to the standard GFR600 fuel as a way to reduce stockpiles of MA materials. Both the plutonium and the MA are assumed to be available from legacy LWR Spent Nuclear Fuel, to be retrieved in the future by advanced reprocessing methods. It is a well-established fact that a significant reduction in repository requirements can only be achieved if the amount of MA in the repository is minimized. The fuel cycle option selected in the present work is very

challenging. The homogeneous recycling of MA isotopes can cause several issues: the presence of MA isotopes in all parts of the fuel cycle poses a shielding problem; strong α-emission in the fuel causes material issues; more issues are highlighted in [2]. The present work illustrates how an ideal closed fuel cycle could work.

This paper is organized as follows: some general remarks about transmutation are given in Section 2, followed by a presentation of the GFR600 design in Section 3, and the results of single-cycle transmutations in Section 4. The paper continues with a discussion of multirecycling calculations in Section 5, followed by a discussion of decay heat calculations in Section 6. The paper closes with conclusions and recommendations for further research.

2. The Influence of Actinide Isotopes on Reactor Performance

In a closed fuel cycle, such as proposed for the Gen IV GCFR, there will inevitably be an accumulation of MA isotopes in the fuel. After an irradiation campaign, fuel is allowed to cool down, and is subsequently reprocessed, where all Heavy Metal (HM) isotopes are assumed to be refabricated into a new fuel loading. The fuel cycle target is to breed just enough fissile material during reactor operation so that the recycled fuel together with fertile material (U-238, usually) results in a new fuel with the same performance. Thus, MA isotopes with a sufficiently long half life will all be incorporated into the new fuel. By definition, MA isotopes remaining in the fuel are not very fissile, and admixing these isotopes to a nuclear fuel will generally decrease the reactivity of the fuel. As a measure of how an individual isotope influences the reactivity of the reactor, a *reactivity weight* w_i is defined, which measures how the eigenvalue of a reactor changes if the number density of a particular isotope is perturbed. In previous work [3] the following expression was derived:

$$w_i \equiv \frac{\Delta\rho}{\Delta N_i} = \frac{\langle \phi_0^+, [\lambda_0(\partial P/\partial N_i) - (\partial L/\partial N_i)]\phi_0 \rangle}{\langle \phi_0^+, P_0\phi_0 \rangle}. \quad (1)$$

In this equation, P is the production operator of neutrons, L is the loss operator, λ is the eigenvalue of the reactor, ϕ is the forward flux, and ϕ^+ is the adjoint. Equation (1) can be derived in a straightforward manner using First Order Perturbation Theory. As an example, assume for instance an infinite, homogeneous medium with one group of neutrons. The operators L_0 and P_0 are given by

$$P_0 = \nu\Sigma_f = \sum_{i=1}^{I} N_i \nu_i \sigma_{f,i},$$
$$L_0 = \Sigma_a = \sum_{i=1}^{I} N_i \sigma_{a,i}, \quad (2)$$

with the index i running over all isotopes in the system. In the 1-group formalism, ϕ_0 and ϕ_0^+ reduce to single numbers.

Table 1: Reactivity weights $\mathbf{w_i}$ for several isotopes in several types of reactors, normalized to $\mathbf{w_i}$ for Pu-239. Data sources: PWR based on EPR standard UOx fuel from [6], LMFBR based on a generic oxide fuel, sodium coolant [7], and GCFR based on GFR600 (described later in this paper).

Isotope	LWR UOx	LMFBR	GCFR
U-235	0.392	0.759	0.785
U-238	−0.007	−0.049	−0.067
Np-237	−0.507	−0.111	−0.159
Pu-238	−0.360	0.662	0.660
Pu-239	1.000	1.000	1.000
Pu-240	−3.847	0.134	0.120
Pu-241	1.485	1.418	1.484
Pu-242	−0.462	0.081	0.064
Am-241	−1.755	−0.452	−0.218
Am-243	−0.802	−0.153	−0.192
Cm-242	−0.028	0.429	0.418
Cm-243	1.787	2.374	2.481
Cm-244	−0.192	0.219	0.214
Cm-245	3.032	2.013	2.125
Cm-246	−0.020	0.150	0.145

Taking the derivatives to N_i in (2) and substituting in (1) results in

$$w_i = \frac{\phi_0^+\left(\lambda_0\nu_i\sigma_{f,i} - \sigma_{a,i}\right)\phi_0}{\phi_0^+\nu\Sigma_f\phi_0} = \frac{1}{\nu\Sigma_f}\left(\lambda_0\nu_i\sigma_{f,i} - \sigma_{a,i}\right), \quad (3)$$

which is similar to traditional definitions of reactivity weights as, for instance, found in [4]:

$$w_i = \overline{\nu_i\sigma}_{f,i} - \overline{\sigma}_{a,i}. \quad (4)$$

The differences between (3) and (4) are the presence of the factors $1/\nu\Sigma_f$ and λ_0. These factors are not problematic, because $\lambda_0 = 1$ in a critical reactor, which is usually assumed in the derivation of (4), and $1/\nu\Sigma_f$ can be removed by normalizing. Equation (1) can be evaluated by sensitivity analysis software, for example, the TSUNAMI-module in SCALE [5]. Reactivity weights calculated using (1) are given in Table 1 for a PWR with UOx fuel, an LMFBR, and a Gen IV GCFR. These weights are normalized to Pu-239.

Upon inspection of Table 1 some interesting properties are seen, for example, Pu-238 is almost as good a fuel isotope as U-235 in a fast reactor. Furthermore, some isotopes which are net absorbers in a thermal reactor (e.g., Pu-240) are in fact less detrimental to a fast reactor. For actinide (multi-) recycling, the isotopes Np-237 and Am-241 are the most important, and these are net neutron absorbers, also in fast reactors. But this is not all bad news, because these isotopes

transmute to Pu-238, which is quite a good fuel for fast reactors, or to Am-242m, which is a highly fissile isotope:

$$
\begin{aligned}
&{}^{237}\mathrm{Np} \xrightarrow[83\%]{n} {}^{238}\mathrm{Np} \xrightarrow[99\%]{\beta^-} {}^{238}\mathrm{Pu},\\
&{}^{241}\mathrm{Am} \xrightarrow[71\%]{n} {}^{242}\mathrm{Am} \xrightarrow[83\%]{\beta^-} {}^{242}\mathrm{Cm} \xrightarrow[99\%]{\alpha} {}^{238}\mathrm{Pu}, \qquad (5)\\
&{}^{241}\mathrm{Am} \xrightarrow[13\%]{n} {}^{242\mathrm{m}}\mathrm{Am}.
\end{aligned}
$$

The percentages indicate the probability of a reaction occurring in a fast neutron spectrum at a typical fast reactor flux level. Thus, addition of Np-237 and Am-241 will have a detrimental effect on the "fissileness" of fresh fuel, but upon continued irradiation their daughter products will contribute positively to the "fissileness". Thus, if a reactor is started with a MA-bearing fuel, the material remaining after an irradiation campaign may have a higher "fissileness" than that of an equivalently irradiated fuel without initial MA-isotopes in it.

3. Introduction of the GFR600 Design

The reactor investigated in the present work is GFR600, a 600 MWth Gen IV Gas Cooled Fast Reactor. GFR600 features a fast spectrum core with a high coolant fraction for safety, a carbide fuel in plate form (see Figure 1), all-ceramic components (SiC for cladding, wrapper tubes and structural components, Zr_3Si_2 as a reflector material), and high-temperature operation with an outlet temperature up to 850°C. The standard fuel is a mixture of UC and PuC (16%–18% Pu). Some basic core parameters are given in Table 2. Electrical output is 300 MWe (50% efficiency). Calculations were performed replacing up to 10% of the UC with an MA-carbide compound. The isotopic vectors of the Pu and MA mixture are given in Tables 3 and 4. The isotopic vectors represent an average compositions for Pu and MA from spent LWR fuel as they will be available in France from 2016 [8, 9]. These compositions were adopted as reference compositions for the present work. The MA is mixed homogeneously with the fuel, that is, in the fresh fuel the percentage of MA is the same everywhere; there are no special "transmutation assemblies".

Depletion calculations were performed using an in-house code package based on SCALE4.4a [10], using a homogenized 1D cylindrical reactor model. A special fast-reactor cross section library was used (175 groups, VITAMIN-J [11]), as well as an updated ORIGEN-S library for transmutation calculations [12]. A three-batch fuel zoning was used. Because the 1D model is rather simple, and because it is generally accepted that SCALE is not the best simulation package for fast reactors, a benchmark was made with our STREP partners CIRTEN, who used the 3D code MONTEBURNS [13] in which the fuel plates were simulated individually. The results of this comparison show satisfactory agreement between the 1D and 3D calculations as far as mass-flows of materials were concerned. Because of the short calculation time compared to the MONTEBURNS calculations, it was chosen to use the 1D model for the present calculations. Details of the benchmark calculations are reported in [14].

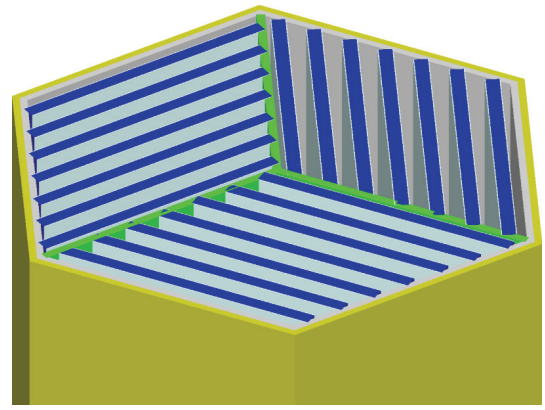

Figure 1: GFR600 fuel assembly. Each assembly contains 21 fuel plates and a central restraining device. All components are made of SiC.

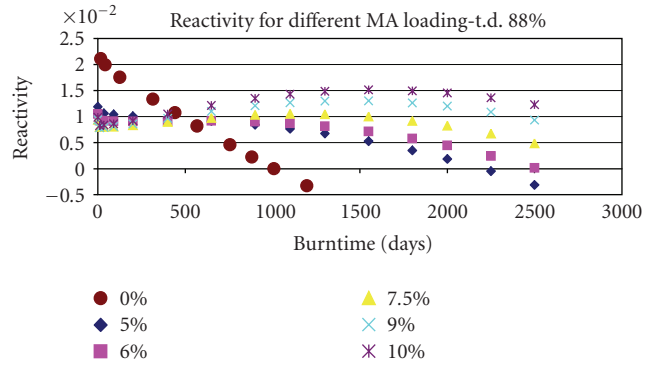

Figure 2: The reactivity for different MA loadings. The reactivity swing decreases for increased MA loading. For an MA loading above 6%, the reactivity increases during the irradiation.

4. Results for Single-Cycle Irradiations

The first calculations were done on one irradiation cycle. The MA fraction was allowed to vary between 0% and 10%, while the porosity of the fuel was reduced from 15% to 12% to offset the lower reactivity of the MA fuel. The effect on k_{eff} is illustrated in Figure 2. The reference fuel (0% MA) is designed to allow an irradiation interval of 1300 days, resulting in a burnup of some 5% FIMA. With extra MA, the initial k_{eff} of the fuel is lower, but the reactivity swing is lower, becoming positive if the MA loading is larger than 6%, resulting in the potential of much longer irradiation intervals. The effect of transmutation of absorbing isotopes to fissile isotopes in the MA mixture as described earlier is evident. An irradiation interval of 2500 days was chosen as the reference for MA-containing fuel,

Table 2: Core parameters for GFR-600 design.

Reactor core parameters			
Unit power	600 MWth	Height	1.95 m
Average power density	103 MW/m^3	Diameter	1.95 m
He average pressure	70 bar	Ratio fuel/struct/cool	35%/10%/55%
Fuel element type	Plate	Refl. material	Zr_3Si_2
Subassembly design, fuel composition			
Plates per S/A	21	Vol.% SiC	30%
Fuel plates per rhom.	7	Vol.% fuel	70%
Fuel S/A in core	112	Pu content	16%
Specific power	40 W/gHM	UPuC density	13.6 g/cm^3
Core volume	5.8 m^3	SiC density	3.16 g/cm^3
Fuel mass	16 tons	Fuel porosity	15%–12%
Temperatures [°C]			
$T_{\text{core in}}$	480	Max fuel temperature	<1200
$T_{\text{core out}}$	850	Max clad temperature	1000
Fuel temperature	990	Coolant temperature	665
Clad temperature	665	Reflector temperature	565

Table 3: Isotopic vector of the plutonium, corresponding to the average plutonium expected to be available in France from 2016 [8].

Pu-238	2.70%
Pu-239	56.00%
Pu-240	25.90%
Pu-241	7.40%
Pu-242	7.30%
Am-241	0.70%

Table 4: Isotopic vector of the Minor Actinide mixture. This mixture represents an average composition expected to be available from 2016 in France [8].

Np-237	16.86%
Am-241	60.64%
Am-242m	0.32%
Am-243	15.69%
Cm-242	0.02%
Cm-243	0.07%
Cm-244	5.14%
Cm-245	1.25%
Cm-246	0.10%

resulting in a final burnup of around 9.9% FIMA and a total electricity production of 18 TWhe. In a 5% MA fuel, 260 kg of MA is destroyed for a core inventory of 800 kg MA (−14.4 kg/TWh); in a 10% MA fuel 650 kg is destroyed for a core inventory of 1600 kg MA (−36.1 kg/TWhe). For comparison, in [2] some canonical numbers are given for the production of MA in PWRs per TWhe: +3.2 kg/TWhe for a PWR using UOx fuel, and +22.5 kg/TWhe for a PWR using MOx fuel. Thus, one GFR600 could support several PWRs if UOx fuel is used, and GFR600 can help in MA-management during the switch from a PWR-based to a fast-reactor-based fuel cycle. Furthermore, all MA loaded into the GFR600 will not go to a repository.

In Figure 3 the effect on the value of β_{eff} is illustrated (calculated with the VAREX-code [15]). As expected, β_{eff} decreases with increasing MA content. Two reasons for this effect can be found. One is the fact that the delayed neutron fraction in general decreases with increasing proton number, thus fissions in MA isotopes release less delayed neutrons. The second reason is neutron capture (mainly due to Am-241). Neutron capture generally increases with decreasing neutron energy, and since delayed neutrons are born at a lower energy than fission neutrons, they are preferentially removed. Both these effects result in a lower effective delayed neutron fraction. In Figure 4 is illustrated the reactivity expressed in dollars during the irradiation cycle. It is seen that the reactivity swing is within a narrow bandwidth of about 3$ for 5% and 10% MA in the fuel. This is advantageous from a control point of view.

In Figure 5 is shown the fuel temperature coefficient (FTC) for the various fuel compositions, calculated as

$$\text{FTC} = \frac{k(T_0 + \Delta T) - k(T_0)}{k(T_0)} \frac{1}{\Delta T}. \tag{6}$$

The FTC is badly affected by the increase of the MA content, going from about −1 pcm/K for the standard fuel to about −0.35 pcm/K for the 10% MA fuel. A fully satisfactory explanation for this effect has not yet been found, and more refined methods will be needed in this area. The void coefficient was calculated between fully pressurized (7 MPa) and at atmospheric pressure. The result is given in Table 5. The void coefficient generally increases with increasing MA content. This can be explained as follows: the helium is neutronically almost inert, so its presence or absence should not influence the reactivity of the reactor. But the helium does introduce a little bit of moderation, thus upon voiding the spectrum will become harder, leading to higher neutron production

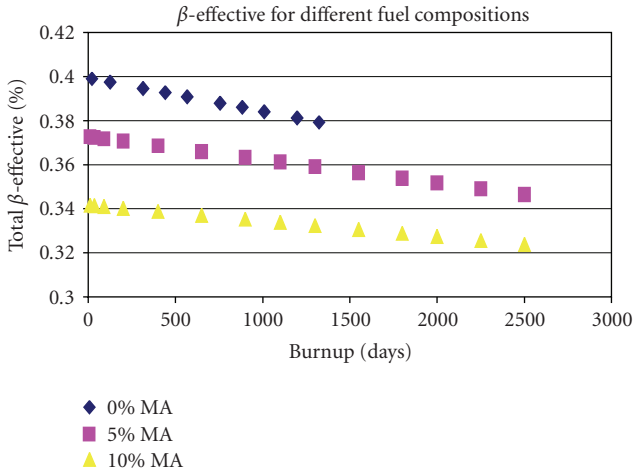

Figure 3: The effective delayed neutron fraction decreases by 15% when the MA-fraction increases from 0% to 10%.

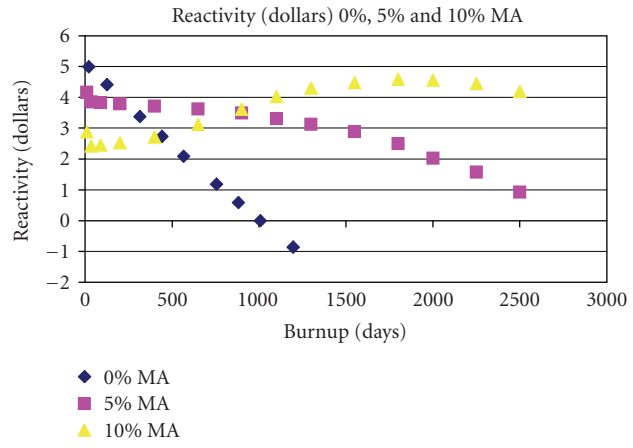

Figure 4: The reactivity for different MA loadings expressed in dollars. Note that a very long irradiation interval can be achieved with a very low reactivity swing.

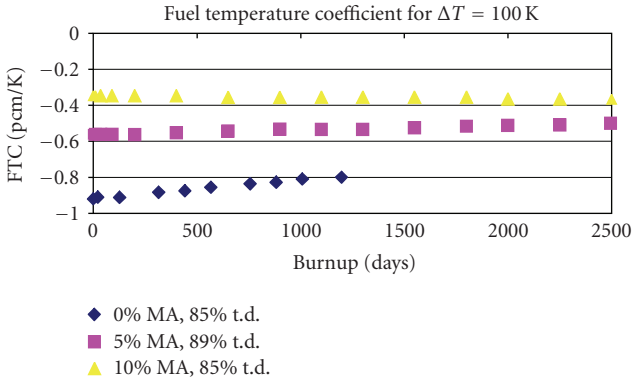

Figure 5: The fuel temperature coefficient as a function of MA-fraction in the fuel.

Table 5: Void coefficient as a function of MA-loading in the core, in dollars between fully pressurized and atmospheric pressure.

MA%	VC [$]
0%	+4.23
5%	+5.29
10%	+6.41

per fission (η increases with energy). Furthermore, many of the MA isotopes are threshold fissioners, and thus harder spectrum will increase the fission rate in the reactor. At the same time, the reduction of scattering increases the leakage, but since the reactor is laid out in a minimum leakage configuration ($H/D = 1$), this effect is not very strong. Thus the increase of the void coefficient with increasing MA content is reasonable (but still undesirable).

Concluding, the addition of MA to the fuel will allow a burnup with a low reactivity swing, but at the expense of a worsening of the safety parameters, that is, addition of MA reduces the effective delayed neutron fraction and fuel temperature coefficient, while increasing the void coefficient. Despite the fact that GFR600 is small, it can destroy the MA from several PWRs using UOx fuel. With an MA destruction of 14.4 kg/TWhe, one GFR600 can support approximately 4 PWRs using UOx fuel (MA production +3.2 kg/TWhe). For a PWR using MOx fuel (MA production +22.5 kg/TWhe), one or two of GFR600 would be needed, depending on the MA fraction in the GFR fuel.

5. Results for Multirecyling Irradiations

GFR600 is envisaged to run in a closed fuel cycle. As a result, no two successive fresh fuel compositions will be the same due to the accumulation of MA isotopes in the fuel. In the ideal case, addition of fertile material to the reprocessed fuel should suffice to make a new fuel load. During the cooling period prior to reprocessing the reactivity of the fuel changes, for example, reactivity is lost by the decay of Pu-241 to Am-241. Three refueling scenarios were investigated. In each case, the cooling period is six years, and all HM material is used to make new fuel (reprocessing losses were assumed negligible).

(i) Refueling with Depleted Uranium (DU) only.

(ii) Refueling with a constant fraction of MA in the fresh fuel (MA).

(iii) Refueling with a constant reactivity weight of the fresh fuel (CW).

The reactivity weight of the fuel is defined as

$$w(t) = \sum_{i=1}^{I} w_i N_i(t), \tag{7}$$

where N_i is the number density of isotope i, and w_i is the corresponding reactivity weight according to (1). It is expected that the CW strategy most closely approximates

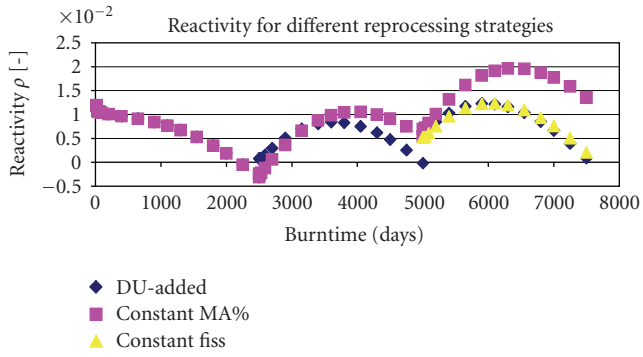

Figure 6: For 3 subsequent fuel irradiations in a closed fuel cycle, the k_{eff} as a function of time. The "Constant fiss." curve corresponds to the constant reactivity weight refueling strategy.

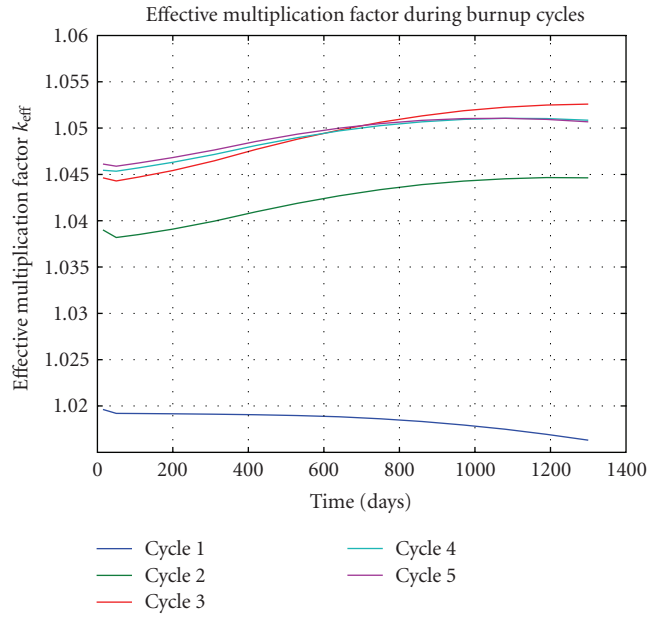

Figure 7: Succesive irradiation campaigns, changing the MA-fraction added in reprocessing to achieve $k_{\text{eff,final}} = 1.05$, starting from a 0% MA fuel. From the third cycle, the objective is met.

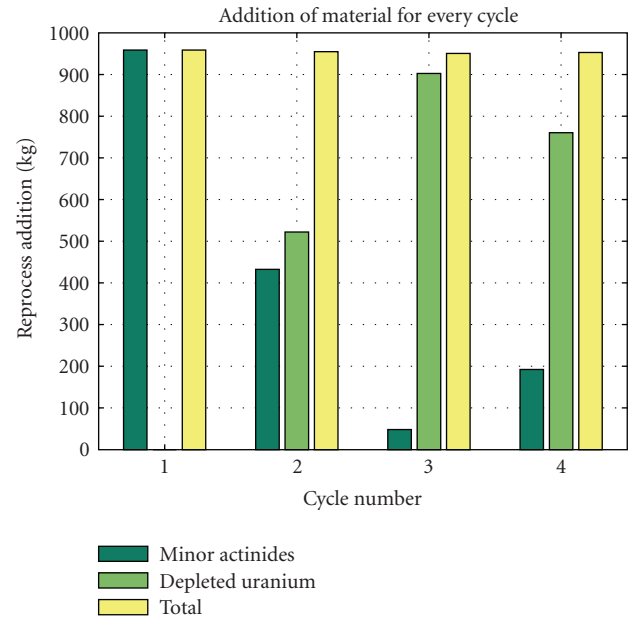

Figure 8: Amounts of MA and DU added to the fuel after each cycle, in order to make $k_{\text{eff,final}} = 1.05$. In the first reprocessing, purely MA is added to increase the end-of-cycle k_{eff} in the next irradiation campaign. In subsequent campaigns, a mix of MA and DU is used.

a truly closed fuel cycle, because each new fuel loading is similar to a previous one as far as the fuel reactivity is concerned. Three refuelings are simulated, spanning a total of some 40 years of reactor operation (7 years of irradiation, 6 years of cooling and a year of reprocessing and refabrication). One typical result is reported in Figure 6, for a 5% MA loading in the fuel (more information is available in [14]). It is seen that keeping the MA content in the fuel constant increases the reactivity of the fuel over successive cycles due to transmutation of fertile to fissile isotopes. Refueling with DU only is also possible, because sufficient extra fissile material is being bred from the MA mixture. The CW case is similar to the DU case.

One of the typical results is that the reactivity swing follows a "parabola-like" curve for most fuels with a sufficient amount of MA. The CW refueling was shown to not always be possible, for example, if too much fissile material is bred during irradiation, the reactivity weight of the new fuel will be higher even if only DU is added. An investigation was done into the possibility of tuning the MA-fraction added during reprocessing to obtain a target value of k_{eff} at the end of the cycle and have a low reactivity swing. Several permutations of this strategy were calculated, and a typical result is given in Figure 7, where the k_{eff} is shown for successive irradiations (in these investigations, the standard irradiation time of 1300 days is used, but the MA is allowed to vary between cycles). In this case, the target was set at $k_{\text{eff,final}} = 1.05$. The first cycle uses the standard 0% MA fuel. In Figure 8 is given the amounts of MA added after each cycle. Thus, after the first cycle the target k_{eff} is not achieved, and only MA is added to the fuel to increase the end-of-cycle k_{eff} of the new fuel. The second cycle ends with a higher k_{eff}, so afterwards a mix of DU and MA is added. In the third cycle, the target k_{eff} is obtained, and subsequently maintained by carefully choosing the correct amount of DU and MA to be added after each cycle.

Overall, addition of MA has positive effects on the possibility of obtaining a closed fuel cycle: fuel made from reprocessed material will have a higher reactivity with MA present in the fuel, and it is possible to tune the fraction of MA in the fuel for desired fuel performance. It is acknowledged that addition of MA is not a truly closed fuel cycle, but the amount of MA required is small, only a few percent of the total fuel mass. It is difficult to assign a support ratio to the multirecycling calculations, because there is no clear picture of the transition scenario when GFR600 will be introduced.

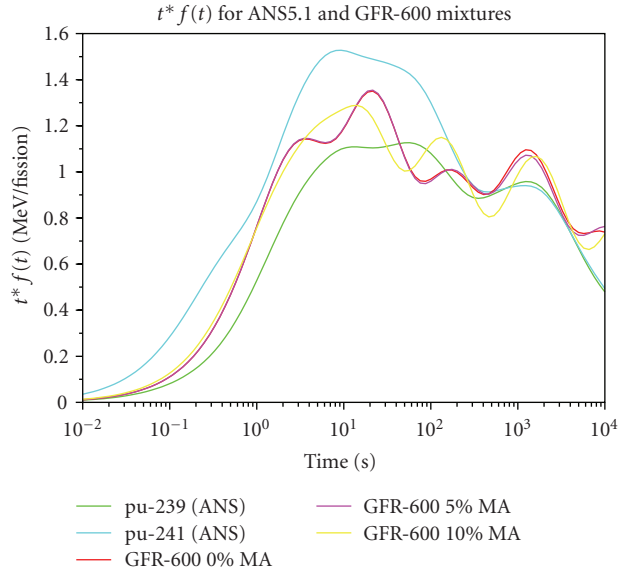

Figure 9: Plot of $t \cdot f(t)$ for the two plutonium isotopes in the ANS5.1 standard and for the 3 GFR-600 mixtures.

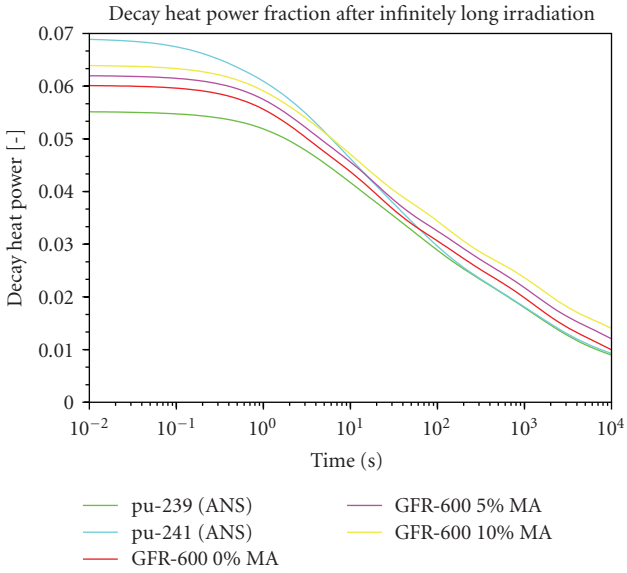

Figure 10: Decay power after an infinitely long irradiation period for the two plutonium isotopes present in the ANS5.1 standard and for the 3 GFR-600 mixtures (cf. (11)).

6. Decay Heat Calculations

One of the prime safety targets of the GFR600 design is to allow Decay Heat Removal (DHR) by natural convection under pressurized conditions. An accurate determination of the decay heat emanating from the fuel with various amounts of MA loading is thus important. For light water reactors, the amount of decay heat is commonly calculated based on a decay heat standard (such as the ANSI/ANS-5.1 standard [16] or the DIN standard [17]). These standards only take into account decay heat due to fission products. In reactors with high MA loading, the decay heat of the MA needs to be taken into account as well. The presence of MA in the core will increase the decay heat for long time scales. The applicability of the decay heat standards to GFR600 is limited. For these reasons, limited investigations were done of the decay heat in GFR600 with various MA loadings.

The decay power is commonly described as the time dependent power following one fission in isotope j as

$$f(t) = \sum_{k=1}^{K} \gamma_{jk} \exp\left(-\mu_{jk} t\right) \tag{8}$$

in units of MeV $\cdot$ s^{-1} per fission. This formulation assumes that all fission products can be grouped into K fission product groups (usually between 23 and 33). Each group has a decay constant μ_{jk}, and a contribution γ_{jk} to the total decay power. The function $f(t)$ is an impulse response and can be extended to an arbitrary fission rate history $\psi(t)$ by convolution to find the decay heat at time t_0:

$$P_d(t_0) = \int_0^{t_0} \psi(t-\tau) f(\tau) d\tau. \tag{9}$$

To calculate the decay heat after shutdown, (9) should be solved with knowledge of $\psi(t-\tau)$. This method is commonly used in thermal-hydraulic codes. The "worst case" decay heat from a single isotope can be calculated as follows. Assume a unit fission rate present over a time interval I, and evaluate the decay heat power at time t after shutdown of the fission source. Then, (9) can be rewritten for nuclide j as

$$\begin{aligned} P_d(t) &= \int_t^{t+I} \sum_{k=1}^{K} \gamma_{jk} \exp\left(-\mu_{jk} t\right) dt \\ &= \left[\sum_{k=1}^{K} \frac{-\gamma_{jk}}{\mu_{jk}} \exp(-\mu_{jk} t) \right]_t^{t+I} \\ &= \sum_{k=1}^{K} \frac{\gamma_{jk}}{\mu_{jk}} \exp\left(-\mu_{jk} t\right) \left[1 - \exp\left(-\mu_{jk} I\right)\right]. \end{aligned} \tag{10}$$

If the irradiation interval I is infinitely long, the second term on the RHS equals one and the time dependent decay heat after shutdown is found as:

$$P_d(t) = \sum_{k=1}^{K} \frac{\gamma_{jk}}{\mu_{jk}} \exp\left(-\mu_{jk} t\right). \tag{11}$$

For three fuel compositions, that is, 0%, 5% and 10% MA, the decay heat for GFR-600 was calculated using ORIGEN-S [18] with special fast reactor data libraries based on JEF and EAF data [12]. ORIGEN-S calculates the decay heat power density in the fuel elements. The result is normalized to the total reactor power, giving a curve of decay heat power as a percentage of nominal reactor power after shutdown. The parameters for the model were estimated by fitting the following equation to the curves:

$$P_d(t) = \sum_{k=1}^{11} \alpha_k \exp(-\lambda_k t). \tag{12}$$

The parameters found from the fit can be readily converted to the form of (11) by introducing new parameters $\alpha_k^{'}$ such that $\alpha_k^{'}/\lambda_k = \alpha_k$. The parameter sets are subsequently converted to units of MeV per fission using the total removable fission power, which is a number calculated by ORIGEN-S and available in the ORIGEN-S output. In Figures 9 and 10 illustrations are given of $tf(t)$ and $P_d(t)$ (as a percentage of the total removable energy per fission), for GFR600 with 0%, 5%, and 10% MA loading. For comparison, the decay heat due to thermal fission in Pu-239 and Pu-241 as calculated using the ANS standard, is also illustrated. From these results, one can make the following observations.

(i) As a generality, the decay heat in GFR600 is in line with what is to be expected from a system where Pu-239 and Pu-241 are the main fissioning isotopes, for example, the initial amount of decay heat is between Pu-239 and Pu-241.

(ii) Given that the ORIGEN-S results for GFR600 are in line with the ANS5.1 standard for short cooling times in Figure 9 increases confidence in the results (see [19] for a discussion of decay heat calculations in ORIGEN-S for short cooling times).

(iii) For long cooling times, the GFR600 decay heat is much larger than the ANS predictions. This is where one sees the effect of the decay heat due to nonfission products, such as α-decay of MA isotopes, which is not taken into account in the ANS standard.

(iv) The GFR600 decay heat is significantly higher than the ANS predicted values, especially for long cooling times. For short cooling times, the amount of decay heat is as predicted by the ANS standard for the main fissioning isotopes in GFR600 fuel. As a result, a "conservative" estimation based on "ANS+10%", which is sometimes proposed, may be overly pessimistic for short cooling times and not pessimistic enough for long cooling times.

7. Conclusions and Recommendations

In this paper a general overview is given of a typical fuel cycle for a Gen IV Gas Cooled Fast Reactor, using a closed fuel cycle. This reactor concept focuses on sustainability, by efficient resource utilization and minimizing waste. The Gen IV GCFR is designed with a strong focus on (passive) safety. Results were reported on the effects of admixing extra Minor Actinide isotopes to the fuel of GFR600, a 600 MWth GCFR. The results of these investigations are that addition of MA to the fuel will reduce the reactivity swing and increase the irradiation interval, due to the transmutation of fertile MA isotopes into fissile isotopes. A high burnup may be achieved (about 10% FIMA) with a relatively low reactivity swing over the cycle (about 4\$). A low reactivity swing is generally desirable from a safety and control point of view. Addition of MA will lower the reactivity of the fresh fuel, but subsequent transmutation of MA isotopes can in fact increase the reactivity of the new fuel made from recycled materials. Thus the presence of MA increases the range of possibilities for a closed fuel cycle. It was shown that MA addition can be used to tune the k_{eff} over the irradiation cycle. Thus, for the fuel cycle the addition of MA to the fuel is beneficial. But there are disadvantages: the delayed neutron fraction is smaller, the fuel temperature coefficient is smaller, and the void coefficient, measured in \$, is higher. Only a more detailed thermal-hydraulic investigation of the primary and secondary circuits can clarify if the safety parameters are still acceptable. Initial calculations of decay heat from the MA-bearing fuel indicate that for short cooling times the decay heat is in line with existing decay heat standards, but for long cooling times (10^4 s) the decay heat is significantly larger.

Recommendations for further research include the following: in the presented work, the production of helium gas in the fuel due to α-decay of the MA was not taken into account. However, the pressure caused by the helium could become a limiting factor for the fuel design. The plate fuel design adopted in this study is still speculative, and several improvements have already been identified [20]. The reported decrease of the Fuel Temperature Coefficient requires a fundamental explanation. A lack of cross section and resonance data for the MA isotopes may be the cause, but only a detailed investigation can shed more light. The radioactivity, and related to that the feasibility of reprocessing, needs to be ascertained for the MA-bearing fuel compounds. Open questions in this area concern the availability of MA separation technology, the neutron emission from the fuel after multiple irradiation cycles, the feasibility and safety of carbide fuel reprocessing, and the metallurgical and ceramics implications of 10% MA addition.

Acknowledgments

The authors would like to acknowledge the support of the European Commission through the GCFR STREP program, carried out under Contract no. 012773 (FI6O) within the EURATOM 6th Framework Program from March 1, 2005 to February 28, 2009. The main part of the work reported here was carried out when W. van Rooijen was employed by Delft University of Technology in The Netherlands. The authors acknowledge the work of their students G. J. van Gendt and D. I. van der Stok.

References

[1] U.S. DOE Nuclear Energy Research Advisory Committee and the Generation IV International Forum, "A technology roadmap for Generation IV nuclear energy systems," December 2002, http://gif.inel.gov/roadmap/.

[2] Commissariat à l'Énergie Atomique, "Les déchets radioactifs à haute activité et à vie longue—recherches et résultats axe 1: séparation et transmutation des radionucléides à vie longue," December 2005.

[3] W. F. G. van Rooijen, J. L. Kloosterman, T. H. J. J. van der Hagen, and H. van Dam, "Definition of breeding gain for the closed fuel cycle and application to a gas-cooled fast reactor,"

Nuclear Science and Engineering, vol. 157, no. 2, pp. 185–199, 2007.

[4] M. Salvatores, "Fast reactor calculations," in *Handbook of Nuclear Reactor Calculations*, vol. 3, pp. 263–363, CRC Press, Boca Raton, Fla, USA, 1986.

[5] SCALE, *A Modular Code System for Performing Standardized Computer Analyses for Licensing Evaluations, Vols I–III*, Oak Ridge National Laboratory, Oak Ridge, Tenn, USA, ORNL/TM-2005/39, Version 5.1, Available from Radiation Safety Information Computational Center at Oak Ridge National Laboratory as CCC-732, 2006.

[6] G. Sengler, F. Forêt, G. Schlosser, R. Lisdat, and S. Stelletta, "EPR core design," *Nuclear Engineering and Design*, vol. 187, no. 1, pp. 79–119, 1999.

[7] J. Rouault, A. Judd, J. C. Lefèvre, and G. Mühling, "CAPRA preliminary feasibility studies, synthesis and conclusions," Tech. Rep., CEA, Cedex, France, 1994.

[8] J. C. Bosq, "Personal communication," CEA Cadarache, March 2005.

[9] K. D. Weaver, T. C. Totemeier, D. E. Clark, et al., "Gen IV nuclear energy systems, gas-cooled fast reactor (GFR). FY-04 annual report," Tech. Rep. INEEL/EXT-04-02361, Idaho National Engineering and Environmental Laboratory, Idaho Falls, Idaho, USA, September 2004.

[10] SCALE, *A Modular Code System for Performing Standardized Computer Analyses for Licensing Evaluation*, Oak Ridge National Laboratory, Oak Ridge, Tenn, USA, NUREG/CR-0200, version 4.4a, 2000.

[11] R. E. MacFarlane and D. W. Muir, "The NJOY nuclear data processing system," Tech. Rep. Version 91 LA-12740-M, Los Alamos National Laboratory, Los Alamos, NM, USA, October 1994.

[12] J. E. Hoogenboom and J. L. Kloosterman, "Generation and validation of ORIGEN-S libraries for depletion and transmutation calculations based on JEF2.2 and EAF3 basic data," *Nuclear Engineering and Design*, vol. 170, no. 1–3, pp. 107–118, 1997.

[13] D. L. Poston and H. R. Trellue, "User's manual, version 2.0 for MONTEBURNS version 1.0," Tech. Rep. LA-UR-99-4999, Los Alamos National Laboratory, Los Alamos, NM, USA, 1999.

[14] W. F. G. van Rooijen, J. L. Kloosterman, G. van Gendt, et al., "Actinide transmutation in GFR (option 1): final report, 2007," Tech. Rep. GCFR-STREP D31, European Commission Sixth Framework Program, Work Package 1.1 Task 4, 2008.

[15] J. L. Kloosterman and J. C. Kuijper, "VAREX, a code for variational analysis of reactivity effects: description and examples," in *Proceedings of the ANS International Topical Meeting on Advances in Reactor Physics (PHYSOR '00)*, ANS, Seoul, Korea, October 2000.

[16] ANSI, "Decay heat power in light water reactors," Tech. Rep. ANS-5.1-1994. W2004, ANSI/ANS, La Grange Park, Ill, USA, 2004.

[17] DIN, "Berechnung der Nachzerfallsleistung der Kernbrennstoffe von Leichtwasserreaktoren; Nichtrezyklierte Kernbrennstoffe," Tech. Rep. DIN 25463-1, Deutsches Institut für Normung e. V., Berlin, Germany, May 1990.

[18] I. C. Gauld, O. W. Hermann, and R. M. Westfall, *ORIGEN-S: SCALE System Module to Calculate Fuel Depletion, Actinide Transmutation, Fission Product Buildup and Decay, and Associated Radiation Source Termes*, Oak Ridge National Laboratory, Oak Ridge, Tenn, USA, 2005.

[19] I. Gauld, "Validation of ORIGEN-S decay heat predictions for LOCA analysis," in *Proceedings of the ANS International Topical Meeting on Advances in Reactor Physics (PHYSOR '06)*, pp. 1–10, ANS, Vancouver, Canada, September 2006.

[20] N. Chauvin, J.-Y. Malo, J.-C. Garnier, et al., "GFR fuel and core pre-conceptual design studies," in *Proceedings of the International Conference on Advanced Nuclear Fuel Cycles and Systems (GLOBAL '07)*, pp. 423–433, ANS, Boise, Idaho, USA, September 2007.

Hindawi Publishing Corporation
Science and Technology of Nuclear Installations
Volume 2009, Article ID 573481, 8 pages
doi:10.1155/2009/573481

Research Article

GCFR Coupled Neutronic and Thermal-Fluid-Dynamics Analyses for a Core Containing Minor Actinides

Diego Castelliti,[1,2] Eleonora Bomboni,[1] Nicola Cerullo,[1,3] Guglielmo Lomonaco,[1] and Carlo Parisi[4]

[1] *Dipartimento di Ingegneria Meccanica, Nucleare e della Produzione (DIMNP), Università di Pisa (UNIPI), CIRTEN, Largo Lucio Lazzarino n. 1, 56126 Pisa, Italy*
[2] *Studiecentrum voor Kernenergie, Centre d'Etude de l'énergie Nucléaire (SCK CEN), Belgium*
[3] *Dipartimento di Ingegneria della Produzione, Termoenergetica e Modelli Matematici (DIPTEM), Università di Genova (UNIGE), Via all'Opera Pia n. 15/a, 16145 Genova, Italy*
[4] *Gruppo di Ricerca Nucleare San Piero a Grado (GRNSPG), Università di Pisa (UNIPI), Largo Lucio Lazzarino n. 1, 56126 Pisa, Italy*

Correspondence should be addressed to Nicola Cerullo, cerullo@docenti.ing.unipi.it

Received 27 January 2009; Accepted 2 March 2009

Recommended by Jan Leen Kloosterman

Problems about future energy availability, climate changes, and air quality seem to play an important role in energy production. While current reactor generations provide a guaranteed and economical energy production, new nuclear power plant generation would increase the ways and purposes in which nuclear energy can be used. To explore these new technological applications, several governments, industries, and research communities decided to contribute to the next reactor generation, called "Generation IV." Among the six Gen-IV reactor designs, the Gas Cooled Fast Reactor (GCFR) uses a direct-cycle helium turbine for electricity generation and for a CO_2-free thermochemical production of hydrogen. Additionally, the use of a fast spectrum allows actinides transmutation, minimizing the production of long-lived radioactive waste in an integrated fuel cycle. This paper presents an analysis of GCFR fuel cycle optimization and of a thermal-hydraulic of a GCFR-prototype under steady-state and transient conditions. The fuel cycle optimization was performed to assess the capability of the GCFR to transmute MAs, while the thermal-hydraulic analysis was performed to investigate the reactor and the safety systems behavior during a LOFA. Preliminary results show that limited quantities of MA are not affecting significantly the thermal-fluid-dynamics behavior of a GCFR core.

1. Introduction: The Generation IV Project

Generation IV proposals have been specifically advanced in order to meet the new challenges for nuclear energy production, increasing also the ways and purposes in which nuclear energy can be used. Six new reactor designs have been proposed, all of them aiming to satisfy requirements of reliability, sustainability, economics, and resistance to proliferation that characterize the Gen IV [1].

Among the six Gen IV reactor projects, there are two with a thermal neutronic spectrum (High, Temperature Gas Reactor (HTGR), Supercritical Water Reactor (SCWR)), three with a fast spectrum (Gas-Cooled Fast Reactor (GCFR), Sodium Fast Reactor (SFR), Lead Fast Reactor (LFR)), and one with epithermal spectrum (Molten Salt Reactor (MSR)).

An important Gen IV target is Minor Actinides (MAs) transmutation. This paper presents an analysis of the GCFR fuel cycle with MAs and a thermal-hydraulic analysis of a GCFR-prototype, charged with such composed fuel, under steady-state and transient conditions. The fuel cycle has been designed in order to asses the capability of the GCFR to transmute MAs, while the thermal-hydraulic investigation was performed in order to investigate the reactor and the safety system behaviors during one of the Design Basis Accidents (DBAs), the Loss-of-Flow Accident (LOFA). Sensitivity analyses are also presented for assessing the effects

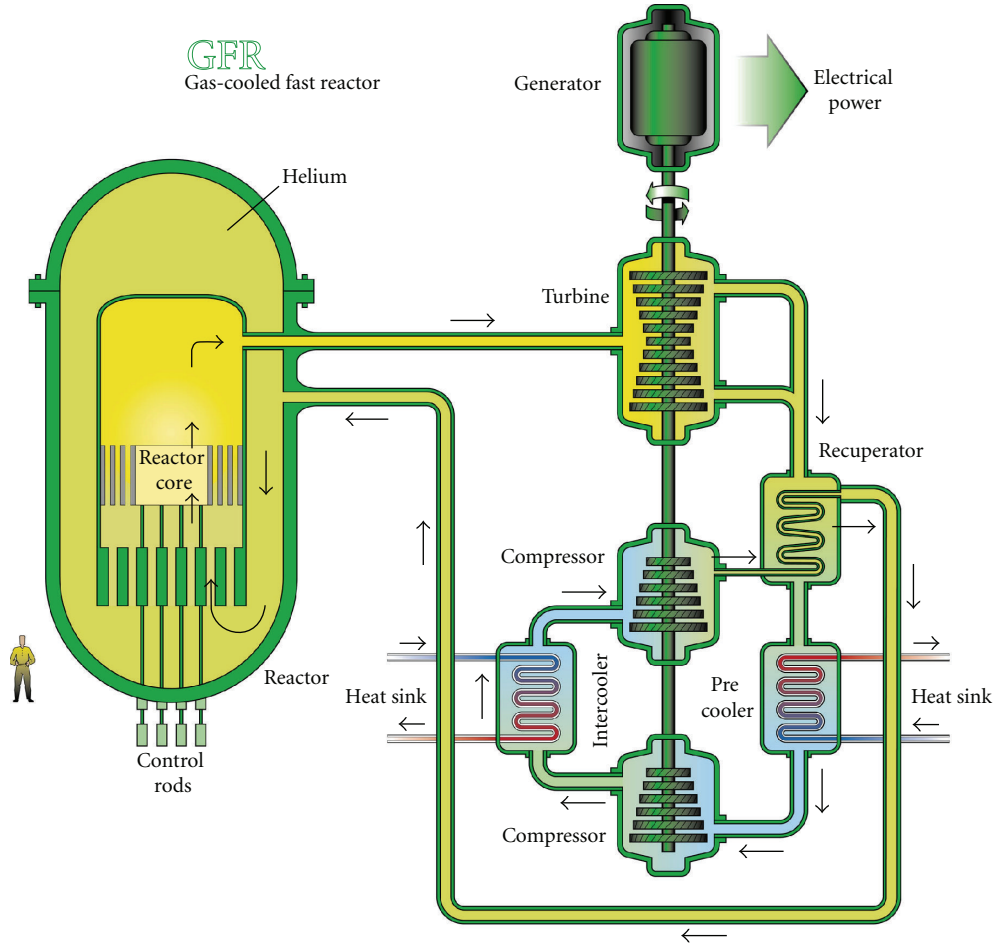

Figure 1: GCFR scheme [3].

of the presence of different MAs concentration on the fuel performance.

2. The Gas-Cooled Fast Reactor

Generation IV reactor projects are finalized to answer to new challenges that nuclear energy must face in this new century. Those mandatory projects have to meet Gen IV criteria [1], namely:

(1) sustainability;

(2) economics;

(3) proliferation-resistance;

(4) reliability.

Criteria (1), (2), and (3) include, as important target, the MAs transmutation.

The capability of removing the heat produced in the core (both in nominal and accidental conditions) is a key point (particularly for this reactor) of criterion (4); this work (in conjunction with what already published in [2]) gives a positive (even if still partial) answer to this request.

The GCFR proposed in the frame of Gen IV initiative (Figure 1) uses a direct-cycle helium turbine for electricity generation. This reactor can be employed both for electricity generation and in CO_2-free thermochemical production of hydrogen. Besides, the use of a fast spectrum allows the transmutation of the actinides, minimizing the long-lived radioactive waste production in an integrated fuel cycle (one of main targets of Gen IV).

Furthermore, the GCFR fast spectrum makes the use of available fissile and fertile materials (including depleted uranium) possible in a more efficient way compared to the thermal reactors. GCFR has better safety features than liquid metals reactor, and it can be quite flexible in Pu management [3].

The GCFR has a high power density, about 100 KW/l, similar to a PWR, but in this case the power has to be removed by a noncondensable gas (helium) instead of water.

The proposed GCFR initial design shares several components with HTGR technology, and it uses a direct Brayton cycle (without any Intermediate Heat Exchanger, or IHX). This allows to combine a high thermal efficiency (thanks to the high coolant temperatures) with a high MAs transmutation and fertilization rate (thanks to the fast neutron spectrum). The high coolant output temperatures make the reactor suitable for industrial applications, too.

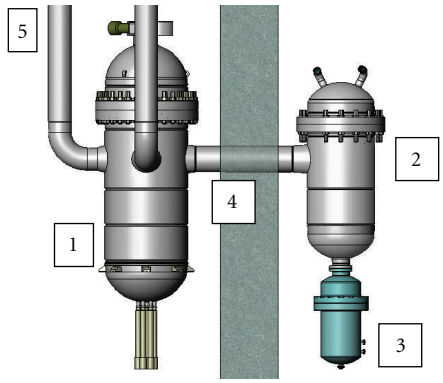

Figure 2: : ETDR plant overview [12].

However, the direct Brayton cycle design is considered very challenging; so a "more conventional" version with a He, N_2, or CO_2 secondary loop could be preferred [4]. The inevitable performance loss is accepted, in order to achieve better plant safety features. The ETDR experimental facility moves in this direction (see Section 3).

Preliminary analysis results confirmed that it is possible to have a self-breeding core without any fertile blanket (i.e., Breeding Gain slightly greater than zero in order to meet nonproliferation constraints) from a starting fuel based on Pu and depleted U. More details on proposed technical solutions for GCFR can be found in [3, 5–11].

3. ETDR: Core and Plant Characteristics

Actual realization of a commercial GCFR is scheduled not before the year 2040. An experimental and demonstration facility is scheduled for the year 2020, with the purpose to test the technical solutions proposed for the GCFR concept. The name of this demonstration facility is Experimental and Testing Demonstration Reactor (ETDR). The ETDR will represent a milestone on the way approaching the final GCFR configuration, thanks to the numerous technical solutions that will be tested despite a quite different power size. While the GCFR is projected to have a nominal thermal power of 2400 (or 3000) MW_{th} (600 MW_{th} in the modular version), ETDR nominal power will be limited at 50 MW_{th}, with no electricity production and a secondary water-cooled loop. It will be the first gas cooled, fast neutron spectrumnuclear plant ever built.

ETDR plant scheme is illustrated in Figure 2.

In Figures 1, 2 and 3 we can recognize.

(1) core and vessel;

(2) main heat exchanger;

(3) main blower;

(4) main cross duct;

(5) decay heat removal loop;

(6) decay heat removal blower (supposed inactive in the LOFA transient);

(7) tertiary air cooling system (not modeled).

A more detailed ETDR plant description can be found in [10].

Decay Heat Removal (DHR) system is composed by three loops ($3 \times 100\%$ redundancy) connected to vessel and should have the same design that will be installed on the commercial 600 MW_{th} GCFR. One of those three loops has no blowers and it relies on natural circulation (NC) only (full passive system), while the second loop is equipped with a blower that is supposed to work only for 24 hours after the DHR valve is opened (few seconds later incidental event) and before NC takes place. Finally, the third DHR loop is totally based on active safety systems (blower). The NC loop is particularly efficient in transient events where there is not a fast depressurization of primary circuit (structural integrity preserved), while active devices are especially suitable for fast depressurization events (LOCA) (Blower in second loop is meant to work with a system residual pressure of about $7 \div 10$ bars (SBLOCA), while blower in third loop can work with He at nearly 1 bar (LBLOCA), requiring a higher pumping power.)

As previously said, DHR system is connected to the reactor pressure vessel (RPV). Hot leg is connected to the upper plenum, while helium from cold leg flows into downcomer. Therefore the core is cooled by bottom-to-top coolant flow. During normal operation, reactor power is removed via a counter-current U-tubes helium-water HX. The secondary side is then cooled by forced air circulation.

Concerning the DHR HXs, the primary to secondary heat removal is achieved by the use of counter-current straight vertical tubes helium-water HX. NC is established thanks to difference of 15 m between the primary and secondary side thermal barycenters.

DHR secondary circuit, containing water pressurized at 10 bars, is exchanging the removed power from the primary side with the final heat sink, a water pool at atmospheric pressure. The height difference between secondary-side thermal barycenters is about 4 m.

4. ETDR: Core Fuelled with Minor Actinides

Several studies and calculations have been performed on thermal-hydraulics of ETDR systems, both in steady-state and transients conditions, but most of these analyses have not considered any neutronic feedback in the core.

We tried to obtain some results by analyzing a core charged with a small quantity of MA. (In the present design it is not possible to exceed 10% of MAs content because of reactor control problems.) In fact, one of most important features of this system is the capability to burn MAs, greatly reducing wastes and producing energy by fast fissions as well.

In order to make some preliminary evaluations of the dynamic effects on a GCFR core due to MAs presence in the fuel, we performed some point neutron kinetics-(NK-)TH calculations on the ETDR design. For comparison purposes, we chose to analyze Steady State and a LOFA transient because there are validated data already available for these cases [2]. Neutronic data (Doppler coefficient, void coefficient, etc.) implemented in our calculations are taken

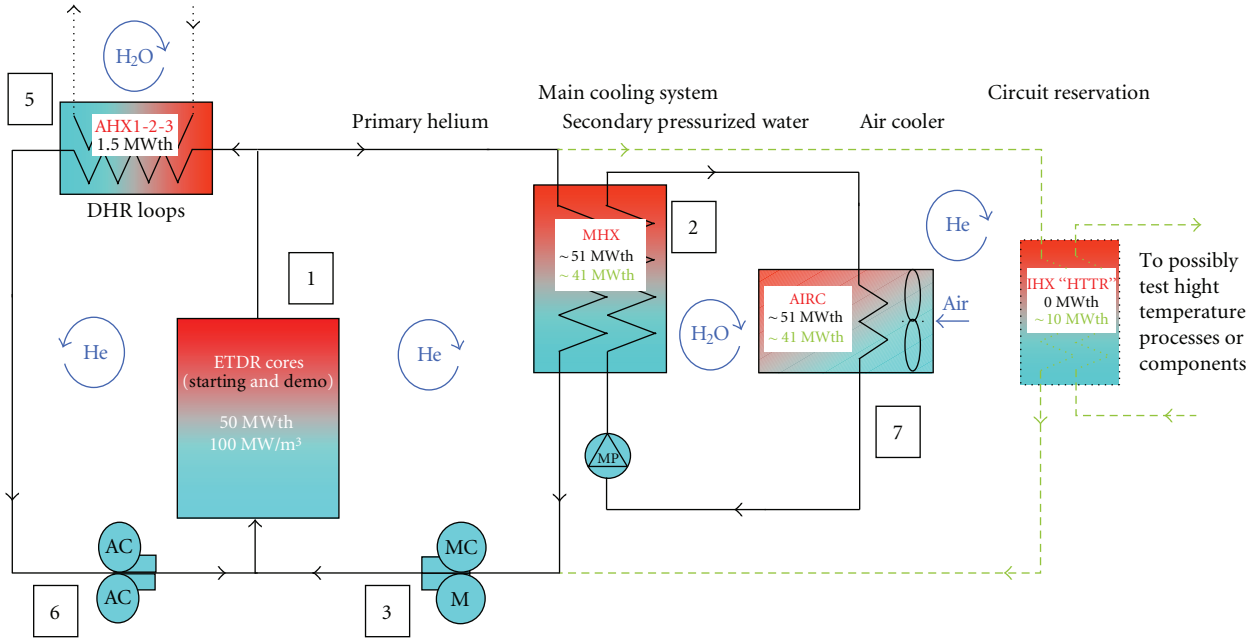

Figure 3: ETDR flux diagram [12].

from the MCNP calculations performed for the GCFR core (600 MH_{th}) see [3, 5–11]. As already anticipated, to perform a complete ETDR LOFA analysis [2], a point NK analysis is necessary, taking into account the variations of reactivity coefficients (e.g., Doppler and void coefficients) due to the fuel isotopic changes.

Calculations were performed with and without the presence of MAs in the fuel. The code used for the point NK-TH calculations was the RELAP5-3D [13] .

We performed, at first, MCNP5 [14] calculations, assessing Doppler and void coefficients, delayed neutron fractions, and prompt neutron average life, in order to run a point NK-TH calculation. We considered, at first, isotope mass fractions shown in Table 1 (first column, LWR discharge). This composition appears to be quite performing, according to criticality, as previously shown in [15].

In conclusion, we assumed, from MCNP calculations.

(i) Delayed neutron fraction $\beta = 332$ pcm.

(ii) Prompt neutron average life = 0.364 μs.

(iii) Reactivity insertion from 1200 K to 500 K =+98 pcm.

(iv) Reactivity insertion from full depressurization (7.0 MPa → 0.1 MPa) = +68 pcm.

Then, these data were used as input for the point NK model.

5. RELAP-3D Model Used

For the thermal-hydraulic calculations, a RELAP-3D model has been built, based on the start-up core design [16]. The model is illustrated in Figure 4.

The RELAP5-3D nodalization of the ETDR reactor can be divided in the following blocks:

(i) vessel and core (components from 100 to 240);

(ii) main cross duct (component 250, 450, 480);

(iii) main heat exchanger (primary side and secondary side components from 290 to 400 and from 700 to 760);

(iv) blower (component 350);

(v) decay heat removal system (components from 800 to 880 and from 900 to 999).

It is important to note that secondary system has been modeled as boundary condition.

6. Point-NK TH Steady State Calculations with and without MA

Three calculations have been performed:

(1) "imposed power" calculation (performed with no NK data. The 50 MW reactor power is provided with no neutronic feedbacks; so power is constant, and system does not "feel" any changes in reactivity due to neutronic feedback);

(2) reference core composition with NK feedbacks added;

(3) reference core with MA and NK feedbacks added (different fuel composition; see Section 4).

A comparison between those calculations is shown in Table 2.

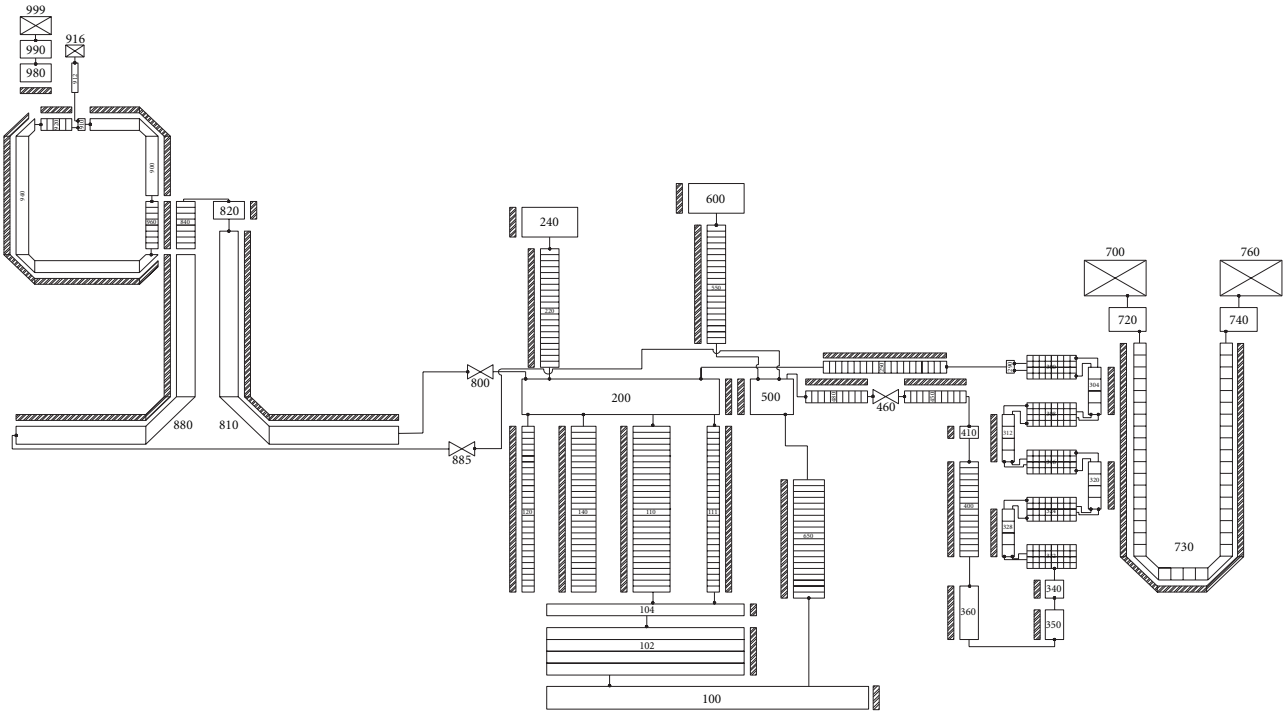

Figure 4: RELAP5-3D ETDR nodalization [10].

Table 1: Core isotopic compositions considered [15]

Isotope	Mass fraction LWR discharge (%)	Mass fraction 5% MAs (%)
U^{235}	0.2	0.571
U^{238}	79.811	80.991
Np^{237}	0.92	0.87
Pu^{238}	0.46	0.446
Pu^{239}	9.804	9.251
Pu^{240}	4.302	4.278
Pu^{241}	2.281	1.222
Pu^{242}	1.241	1.206
AM^{241}	0.56	—
AM^{242m}	—	0.017
AM^{243}	0.32	0.81
Cm^{242}	—	0.001
Cm^{243}	—	0.002
Cm^{244}	0.1	0.265
Cm^{245}	—	0.065
Cm^{246}	—	0.005

As it can be seen above, the differences between all the relevant TH parameters are negligible, even with different fuel vectors (→ different neutronic feedbacks, different reactivity insertions).

It is interesting to notice that adding the MA into the fuel is not affecting the safety relevant parameters (e.g., cladding and fuel temperatures). Therefore reactor safety-related steady state TH parameters are roughly independent in the range of considered fuel compositions.

7. Point-NK TH LOFA Calculations

In the previous paragraph we showed that the introduction of small quantities of MAs in the fuel will have substantially no effect on the steady state calculations. No particular differences were also found comparing two scram curves, one with standard imposed decay heat [10] and the other one considering the effects of the small fractions of MAs. The difference of relative power (relative error) is never going beyond 1.4% [10].

We present now, in the following figures, LOFA transient analyses performed with the MAs concentration illustrated in Table 1, compared with results from the standard imposed scram curve.

LOFA analyses were performed using the run-down blower curve provided by CEA [2].

The sequence of events leading to the LOFA transient is hereafter illustrated (the steady state condition is achieved after about 50 seconds. Transient sequence is started at second 378 of run (as suggested by benchmark data [16])):

(1) time 0 second: main blower loss of power;

(2) time 0.75 second: reactor scram (relative blower speed going below 90%);

(3) time 173.66 second: closure of main loop valves and opening of DHR loop valves.

Table 2: Point Neutron Kinetics (NK) core parameters (with and without MA)

Parameters	Imposed power	Reference core (point NK values)	Reference core + MA (point NK values)
Reactor power	50 MW	50.02 MW	50.02 MW
Total system flow rate	32.10 Kg/s	32.13 Kg/s	32.11 Kg/s
Flow rate in hot channel	0.581 Kg/s	0.581 Kg/s	0.581 Kg/s
Flow rate in average channel	0.595 Kg/s	0.595 Kg/s	0.595 Kg/s
Reactor pressure at top of vessel	6.92 MPa	6.924 MPa	6.92 MPa
Reactor mass of coolant without DHR	389.75 Kg	389.75 Kg	389.75 Kg
Reactor mass of coolant with DHR	473.54 Kg	473.54 Kg	473.54 Kg
Core inlet temperature	263.9	263.1	262.8
Core average exit temperature	563.7	564.5	564.6
Coolant temp rise in the core	299.8	300.5	299.3
Exit coolant temp in hot channel	615.6	616.5	616.6
Exit coolant temp in avg. Channel	562.7	563.5	563.6
Max clad temp in hot channel	687.6	693.5	691.7
Max clad temp in avg. channel	621.2	626.5	624.9
Max fuel temp in hot channel	1069.5	1073.9	1070.4
Max fuel temp in avg. channel	946.0	949.9	946.8
Main blower speed	523.6 rad/s	523.6 rad/s	523.6 rad/s
Main blower rated head	8007.8 m^2/s^2	8321 m^2/s^2	8319 m^2/s^2
Main blower rated torque	2009.1 $Pa \cdot m^3$	2024.2 $Pa \cdot m^3$	2024.5 $Pa \cdot m^3$
MHX heat transfer area	157.3 m^2	157.3 m^2	157.3 m^2

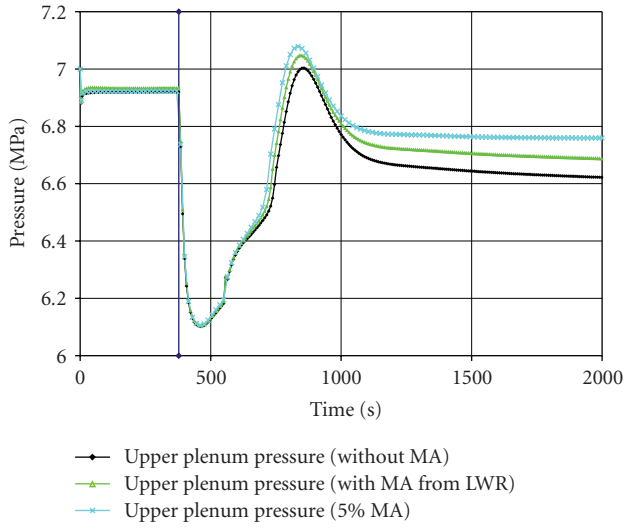

Figure 5: Pressure at the top of the vessel.

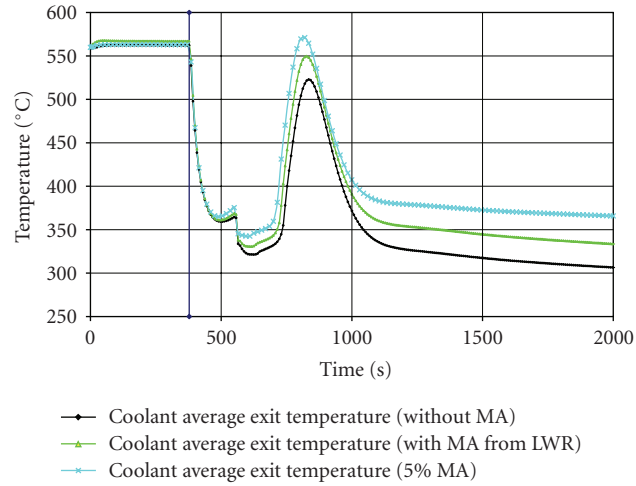

Figure 6: Core average exit temperature.

It should be noted that we perform the MAs analyses referring to a concentration deriving from a typical LWR discharge (see Table 1) and to an imposed concentration of 5% of MAs in the fuel composition.

Some differences are expected because of the different isotopic composition of compared fuels, leading to different decay head profiles: in detail, higher pressures and temperatures are expected from the presence of higher quantity of MAs in the fuel, especially in the third transient phase (long term cooling), because of the higher activity in the fuel.

In the next figures, the LOFA transient evolution is shown. After the scram event, pressure and temperatures in the primary system start to drop, due to the stopped power generation in fuel. Before the closure of main circuit valves and opening of DHR valves, we can notice (~100 seconds after scram) pressures and temperatures to start rising again, because of mass flow becoming too low.

After 173 seconds after scram, blower relative rotational velocity falls below 10%, allowing the main valves to close and the DHR circuit to be opened, thus starting the insetting of Natural Circulation (NC).

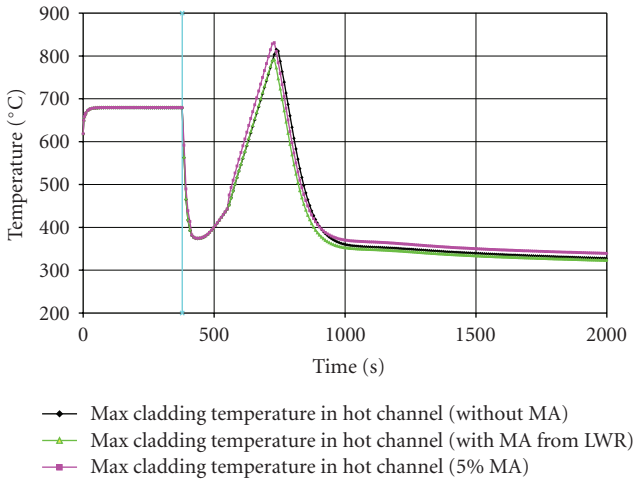

Figure 7: Maximum fuel temperature in hot channel.

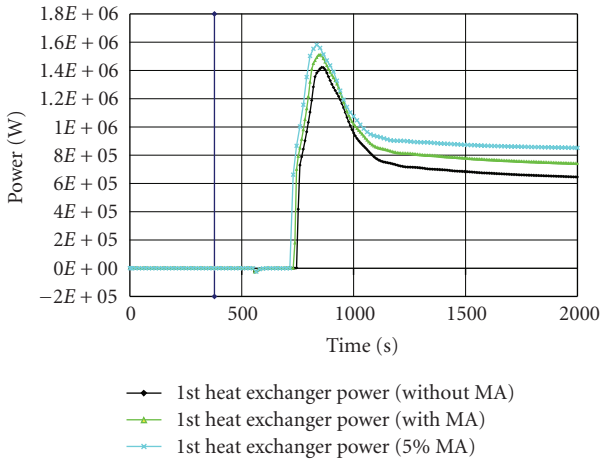

Figure 8: Exchanged power in 1st DHR HX.

Helium in DHR tubes starts flowing downwards because of lower temperature and higher pressure than core, refraining the NC to incur and causing the raise of pressure and temperature (see Figures 4, 5 and 6).

Eventually, after ~470 seconds from start of transient, conditions are met for the NC to incur, starting the long term cooling phase.

In Figure 5, the behavior of pressure at top of the RPV for different types of fuels is shown. The increasing pressure in the RPV is due to greater decay heat of MA isotopes.

Also the rising of core average exit temperature (Figure 6) is the consequence of the same cause.

The curve in Figure 7 shows that the most important parameter of the thermal-fluid-dynamics core design (maximum clading temperature in hot channel) is basically the same for all the analyzed situations.

Figures 8 and 9 show the power exchanged in both DHR HXs (primary-secondary side helium-water HX and secondary-final heat sink water-water HX), showing the convergence of the exchanged power.

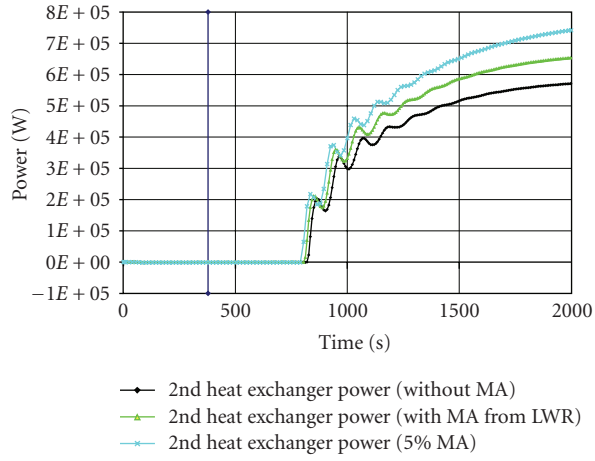

Figure 9: Exchanged power in 2nd DHR HX.

8. Conclusions

From the calculations we can note that there are no relevant differences in both steady state and transient behavior between cases with and without MAs inside the fresh fuel.

The transient analyses showed that a limited insertion of MAs (~5%) does not significantly affect transient behavior of a GCFR system. Small differences are noticed after about 400 seconds from the LOFA starting point, when NC occurs. In addition very small pressure differences were identified (0.04 MPa), and they are mostly due to a higher residual pressure in the system and to higher coolant, cladding, and fuel temperatures (about 20 higher than the reference case).

DHR system performed well under all analyzed cases. Generally speaking the capability of removing the relevant amount of heat produced in the core (both in nominal and LOFA conditions) is demonstrated even in presence of (relatively) limited amount of MAs.

In conclusion, we can state that the influence of adding limited quantities of MAs is negligible considering the proposed GCFR design.

The MA quantity that can be added is currently limited by safety and control problems related to lower β values for MA. Therefore further investigations about this topic could clarify the capabilities of GCFR system in increasing the MA input quantities. In that case the (foreseen) introduction of greater quantities of MA into the fuel for maximizing transmutation should be supported by a larger set of neutronic and thermal-hydraulic analyses.

Acknowledgments

The work presented in this paper has been partially funded by the European Union Sixth Framework Program under contracts GCFR and PuMA. The authors would like to thank Professor P. Coddington of PSI, Dr. C. Mitchell of AMEC-NNC, Professor J. L. Kloosterman of TUD, and Dr. J. Kuijper of NRG for their support and collaboration. The authors also thank Professor G. Forasassi of DIMNP for useful discussions and Professor F. D'Auria of GRNSPG for his precious suggestions and help in using RELAP5-3D code.

References

[1] Generation IV Official, http://www.gen-4.org/index.html.

[2] E. Bubelis, D. Castelliti, P. Coddington, et al., "A GFR benchmark comparison of transient analysis codes based on the ETDR concept," in *Proceedings of the International Congress on Advances in Nuclear Power Plants (ICAPP '07)*, vol. 3, pp. 1916–1925, Nice, France, May 2007.

[3] C. Poette, B. Mathieu, J. C. Garnier, A. Conti, and J. P. Gaillard, "Preliminary design of an advanced gas cooled fast reactor—cores, fuel forms and primary system concepts," in *Proceedings of the International Congress on Advances in Nuclear Power Plants (ICAPP '03)*, Córdoba, Spain, May 2003.

[4] J. Y. Malo, N. Alpy, F. Bertrand, et al., "Gas cooled fast reactor 2400 MWth, end of the preliminary viability phase," in *Proceedings of the International Congress on Advances in Nuclear Power Plants (ICAPP '08)*, Anaheim, Calif, USA, June 2008.

[5] J. C. Bosq, A. Conti, G. Rimpault, J. C. Garnier, and J. Rouault, "Status of GFR design work at CEA: core physics studies (600–2400 MWth)," in *Seminario GFR/ETDR*, CEA-Cadarache, France, Novembre 2004.

[6] A. Conti and J. C. Bosq, "600 MWth GFR cores containing plates CERCER—characteristics," CEA-Cadarache, France, December 2004.

[7] J. C. Garnier and J. Rouault, "The Gen IV GFR program," in *Seminario GFR/ETDR*, CEA-Cadarache, France, Novembre 2004.

[8] P. Dumaz, P. Allègre, C. Bassi, J. C. Garnier, and J. Y. Malo, "DHR studies and design integration for the GFR," in *Seminario GFR/ETDR*, CEA-Cadarache, France, Novembre 2004.

[9] A. Conti and A. Ravenet, "GCFR fuel element and sub-assembly concepts," in *Seminario GFR/ETDR*, CEA-Cadarache, France, Novembre 2004.

[10] D. Castelliti, *Il reattore GCFR (a gas a spettro veloce). Gli aspetti termofluidodinamici ed il suo contributo al bruciamento delle scorie nucleari*, M.S. thesis, Università di Pisa, Pisa, Italy, 2007, http://etd.adm.unipi.it/theses/available/etd-05112007-113534.

[11] J. P. Gaillard, G. Mignot, and A. Conti, "Thermal-hydraulic design of a gas cooled fast reactor," in *Proceedings of the International Congress on Advances in Nuclear Power Plants (ICAPP '03)*, Córdoba, Spain, May 2003.

[12] G. Lomonaco, *Analisi termofluidodinamica dei reattori nucleari innovativi refrigerati a gas*, Ph. D. thesis, Università di Pisa, Pisa, Italy, 2007, http://www.tesionline.it/default/tesi.asp?idt=17893.

[13] Idaho National Engineering and Environmental Laboratory, RELAP5-3D Code Development Team, "RELAP5-3D© Code Manual. Volume I: Code Structure, System Models, and Solution Methods," INEEL-EXT-98-00834, Rev. 2.4, June 2005.

[14] J. F. Briefmeister, "MCNP—A General Monte Carlo N-Particle Transport Code, Version 5," Tech. Rep. LA-CP-03-0245, Los Alamos National Laboratory, Los Alamos, NM, USA, 2003.

[15] N. Cerullo, G. Lomonaco, and E. Bomboni, "CIRTEN Contribution to WP1.1 Task 4," GCFR EU Project, Pisa, Italy, November 2006, http://www.gcfr.org/.

[16] C. Poette, C. Bassi, J. Y. Malo, and F. Morin, "GCFR FP6 ETDR benchmark exercise design data," CEA draft technical appendix, rev. 7, Novembre 2005, http://www.gcfr.org/.

Hindawi Publishing Corporation
Science and Technology of Nuclear Installations
Volume 2009, Article ID 797461, 13 pages
doi:10.1155/2009/797461

Research Article

Decay Heat Removal in GEN IV Gas-Cooled Fast Reactors

Lap-Yan Cheng[1] and Thomas Y. C. Wei[2]

[1] *Brookhaven National Laboratory, Energy Sciences and Technology Department, P.O. Box 5000, Upton, NY 11973-5000, USA*
[2] *Argonne National Laboratory, Nuclear Engineering Division, 9700 S. Cass Avenue, Argonne, IL 60439, USA*

Correspondence should be addressed to Lap-Yan Cheng, cheng@bnl.gov

Received 30 January 2009; Accepted 3 June 2009

Recommended by Colin Mitchell

The safety goal of the current designs of advanced high-temperature thermal gas-cooled reactors (HTRs) is that no core meltdown would occur in a depressurization event with a combination of concurrent safety system failures. This study focused on the analysis of passive decay heat removal (DHR) in a GEN IV direct-cycle gas-cooled fast reactor (GFR) which is based on the technology developments of the HTRs. Given the different criteria and design characteristics of the GFR, an approach different from that taken for the HTRs for passive DHR would have to be explored. Different design options based on maintaining core flow were evaluated by performing transient analysis of a depressurization accident using the system code RELAP5-3D. The study also reviewed the conceptual design of autonomous systems for shutdown decay heat removal and recommends that future work in this area should be focused on the potential for Brayton cycle DHRs.

1. Introduction

With the advent of the U.S. led GEN IV initiative to develop an entirely new generation of nuclear reactor plants, there is now the opportunity to revisit the design of the gas-cooled fast reactor (GFRs) and enhance the safety case. It was recognized even during the 1960s when gas-cooled fast reactors (GCFRs) [1] were being considered and advocated as an alternative to the mainstream world-wide program development of the liquid metal fast breeder reactor (LMFBRs) that gas coolant be it helium or carbon dioxide, had in the low-pressure range poor heat transfer properties and low thermal mass inertia compared to liquid metal coolant, in particular sodium. This early realization led to the focus on extensive research programs and development of reliable active decay heat removal systems.

The design of decay heat removal (DHR) systems and the question of whether or not passive heat removal mechanisms can play a useful role are in a large part determined by the definition of the design basis. Most accident sequences can be accommodated by the provision of reliable/highly reliable system design of which active decay heat removal systems are the key to long-term recovery and stable cooldown. Depressurization initiators with loss of off-site power and a loss of a shut-down train (single failure criteria) have all been accommodated in the design basis of the earlier GCFRs.

For the early design work on active DHR systems, forty years ago the general residual heat removal (RHR) system criteria were that; two independent, diverse, and functionally redundant decay heat removal systems were to be provided to ensure that a loss of coolable core geometry resulting from decay heat removal failure should not have a frequency greater than 10^{-6} per reactor year [2]. The GA design for the 300 MW(e) gas-cooled fast reactor (GCFRs) demonstration plant had two separate RHR systems which provided the reliability required for forced-convection shutdown core cooling in the GCFR. The normal operational RHR was provided by the three main loop cooling systems (MLCS) with their associated steam-driven helium circulators and steam generators. A diverse backup safety RHR capability was provided by a core auxiliary cooling system (CACS), which consisted of three independent auxiliary loops with electric-motor-driven helium circulators and pressurized water heat exchangers. Heat rejection for the MLCS was accomplished through the normal power conversion system components or by direct steam relief to the atmosphere for a limited time. For the initial shutdown heat removal phase of main loop cooling, reactor decay heat provides the heat source

for generating circulator drive steam and makeup feedwater supplied by individual shutdown feedwater pumps. The initial phase lasted for about 30 minutes following shutdown. Following this, long-term decay heat removal was initiated, with oil-fired auxiliary boilers providing circulator drive steam and the steam generators serving as heat dumps. Heat rejection for the CACS was accomplished through individual pressurized water loops with heat rejection to the atmosphere by air-cooled heat exchangers.

To define what constituted an adequate RHR system for the GCFR, a target probability of 10^{-6} per reactor year was adopted for loss of coolable core geometry. For this design analysis, it was further assumed that the major portion of this target could be allocated to the loss of RHR systems, implying that loss of coolable core geometry due to failure of the reactor shutdown systems or to gross structural failures can be reduced to a small fraction of the overall target. This assumption was supported by earlier analyses. A further suballocation of the overall target into a failure rate target of 10^{-2} per year for the MLRHR (main loop RHR) system and a target of 10^{-4}/demand of the CACS failure rate was utilized. The early design work indicated that the CACS system could be expected to meet its target but that the MLRHR system required improvements. These targets implied that only once in 100 years of reactor operation would there be a demand for the CACS to perform the RHR function and that intersystem dependencies were systematically eliminated. Since the MLRHR function was supported by the main loop heat removal train, the power supply system, and a number of auxiliary and support systems, a further suballocation of the 10^{-2} per year target for each required system was necessary and resulted in an allocation of 10^{-3} per year for the failure rate of the MLRHR train.

One of the principal improvements considered was the addition of a backup system to the MLRHR system called the shutdown cooling system (SCS), which shared the main circulator shaft and impeller and the steam generator with the MLRHR system. The SCS shared the steam generators and the main circulator with the MLCS, except that the circulator was driven by a pony motor with a safety-grade power supply. Heat rejection in the SCS was accomplished through three air water coolers, which rejected heat to the atmosphere. The water was recirculated to the steam generator through three separate shutdown feedwater pumps.

The reference system of SCS and CACS was limited by power supply reliability. This was evidenced by the substantial reduction in the statistically independent RHR failure probability by a factor of 30 for pressurized RHR and by a factor of 500 for depressurized RHR with repressurization. For a revised design with separate emergency power supplies of the SCS and the CACS, the dominance of RHR failure by electric power supplies was removed to the extent that the running reliability during long downtime events was now controlling. These long downtime events are identical with the events which require depressurization and therefore, the revised design was controlled by the RHR reliability for depressurized events. Substantial gains in RHR reliability were indicated due to natural circulation for pressurized RHR and for depressurized RHR with repressurization.

Within the space of the last ten years, the thermal gas-cooled reactors have redefined the safety envelopes. Both the HTGR and the PBMR [3] have claimed walk-away safety. With the failure of reactivity scram systems, failure of active heat removal systems including the decay heat removal systems, total loss of electric power both off-site and emergency, and for depressurization events the position is that no core meltdown would occur. Given this background, it would appear appropriate for the GEN IV GFR to have such a safety goal too. From the view point of decay heat removal accidents this would mean that protected depressurization initiators with total loss of electric power would not result in core meltdown. In other words, a station blackout combined with a depressurization would not lead to a severe accident. This is a major challenge and it should be understood that this postulated beyond-design basis accident is a very low probability event in residual risk space. Passive safety mechanisms would need to be utilized.

The GFR being one of the six reactor concepts selected in the framework of the Generation IV Initiative (GEN IV), has been undergoing active international design development in the past few years. In particular several design concepts have been studied to address the issue of decay heat removal in a loss of coolant accident (LOCA). The reference French CEA DHR concept [4] consists of a dedicated DHR system that removes decay heat by forced convection (battery powered blower) in the short term and natural convection in the long-term. In order to provide the back pressure to sustain natural circulation through the reactor core and the DHR system, a guard containment has been designed to enclose the whole primary system and maintain a pressure of 10 bar. Other design considerations, such as the need to provide an isolation valve in the cold leg of the cross-duct to avoid core bypass when the DHR system is activated and the injection of nitrogen into the guard containment to provide back pressure are discussed in [5, 6]. Performance of the dedicated DHR system in a LOCA has been analyzed using system codes TRACE and CATHARE for a GFR with plate-type fuel [7]. Other means of providing decay heat removal have been reported previously and they include: use of power conversion loops instead of dedicated DHR systems [8], injection of gas into the reactor vessel [9], and standalone Brayton cycle turbomachinery [10]. This paper discusses a parallel design study conducted in the US to address decay heat removal in a direct cycle GFR with a pin core design.

2. Passive Conduction/Radiation

Table 1 summarizes the potential passive decay heat removal mechanisms. The DOE supported GFR GEN IV project, [11], and I-NERI project [12] have produced results for a small modular GFR (600 MWt), and a large reactor (2400 MWt) with a pin core design. Based on the sum total of these lessons learned, a number of conclusions can be drawn for each of the potential mechanisms identified in Table 1.

The major design parameter for conducting/radiating core decay heat passively to the ultimate heat sink is core fuel power density. However, current fuel cycle economic

Table 1: Passive decay heat removal mechanisms.

1. Heat Transfer
radiation/conduction cooldown to
vessel boundary
core internal heat sinks (cooled or uncooled)
primary system heat sinks (cooled or uncooled)
natural convection heat transport to
vessel boundary
core internal heat sinks (cooled or uncooled)
2. Inertia
increasing fuel form thermal inertia
increasing flow coastdown times

factors for a uranium startup core would set a minimum power density range on the order of 70–100 W/cc. This is still a major reduction from the historical GCFR parameter of a 250 W/cc range. To summarize, fuel power density is definitely a very important parameter in the feasibility of proposed passive decay heat removal mechanisms. Reducing fuel power density would aid the safety case. However, economics and in particular fuel cycle economics sets the lower limits on the power density. The range of 70–100 W/cc should probably be the range. With core fuel power density of 70–100 W/cc, the thermal gas reactor "conduction cooldown" mode of passive heat transfer of core generated heat through conduction and/or radiation inter- and intrafuel elements to the vessel boundary is not possible for the GFR. This is regardless of fuel form, block/plate, pin or pebble. With the limited conductivity of the potential core fuel and structural materials, even 1 to 2% decay heat would lead to core disruption conditions. With the high temperature requirements of the GEN IV GFR (~850°C coolant outlet) and the fuel flux/fluence conditions, the set of potential materials is small. However, even if graphite with its neutron-spectrum-softening disadvantage, utilized in the thermal gas reactor cores, was used, success would not be attained. The crux of the matter is the low (~5 W/cc) power density of the thermal gas reactor. Lowering the density of the fuel by adding diluents, could lower the power density and still retain the high specific power requirements. This would also be attractive from the view point of adding thermal inertia. However a fast reactor core requires significantly higher fuel densities/loading to maintain criticality over a high burnup fuel cycle (~30% volume fraction of 10 gm/cc ceramic fuel with 20% fissile). Moreover the thermal properties of potential diluents are in the same range of the fuel. Adding diluents is not a potential solution for the GFR given the state of current core material development work. Adding thermal inertia to absorb decay power in sensible heat until ~0.1% decay power is reached, is not feasible.

Unless substantially higher conductivity core materials can be developed, passive removal of decay heat (>1% nominal power) through pure conduction cooldown alone to the vessel boundary will not be feasible for economic operations of the GFR. Moreover, the heat rates by radiation from the core outer boundary to the vessel walls are much smaller than for HTGRs because of an order of magnitude smaller GFR core volume dictated by the higher power density. This is not a thermal gas-cooled reactor where as discussed previously, a power density of 5 W/cc is economically acceptable. This points out that conduction alone is not the sole difficulty in transporting core decay heat to the wall boundary through the fuel elements. For fuel forms such as the pin, as opposed to monolithic blocks, radiation heat transfer is a major component of the fuel element-to-fuel element heat transfer. To compare the relative effectiveness of conductivity relative to radiation in transferring heat from fuel element to fuel element to the vessel wall boundary, reference should be made to [13]. The results show that the resistance to radiation heat transfer is by far the largest hurdle at the core power density of interest.

3. Natural Convection

In facilitating natural convection decay heat removal for the GFR, a passive system based on an in-vessel emergency heat exchanger was first studied, followed by a more detailed study that instituted a hybrid passive system for decay heat removal. The hybrid system consists of two ex-vessel components, a battery-powered blower and an emergency heat exchanger that operates on natural circulation cooling. The blower is designed to work during the early phase of the depressurization accident while natural circulation cooling will provide for the long-term cooling needs of the reactor system.

3.1. Pure Passive. A self-sustaining method for decay heat removal has been investigated and it is based on an in-vessel emergency heat exchanger, which will remove heat from the primary system and transfer it to the outside environment. The emergency heat exchanger will establish natural circulation flow through the reactor core thus removing decay heat in a passive manner. A check valve inline with the in-vessel emergency heat exchanger will open upon loss of forced flow providing a flow path from the upper plenum to the downcomer of the reactor vessel, thus completing the natural circulation loop. In order for natural circulation cooling to function efficiently the primary system and the containment might need to be pressurized to ensure a sufficiently high coolant density. This will be accomplished by having a guard containment structure around the primary system.

Figure 1 is a node diagram showing the RELAP5 model of the reactor system (600 MWt) that is used to investigate the passive cooling in a depressurization accident. A guard containment that surrounds the whole system is modeled as a volume that provides the back pressure to the reactor system via the assumed break that is in the cold duct of the reactor vessel. Figure 2 is a node diagram of the emergency heat exchanger system. It consists of an in-vessel heat exchanger of HEATRIC design, a secondary loop of compressed CO_2, and an external water heat exchanger that dissipates the energy to a heat sink.

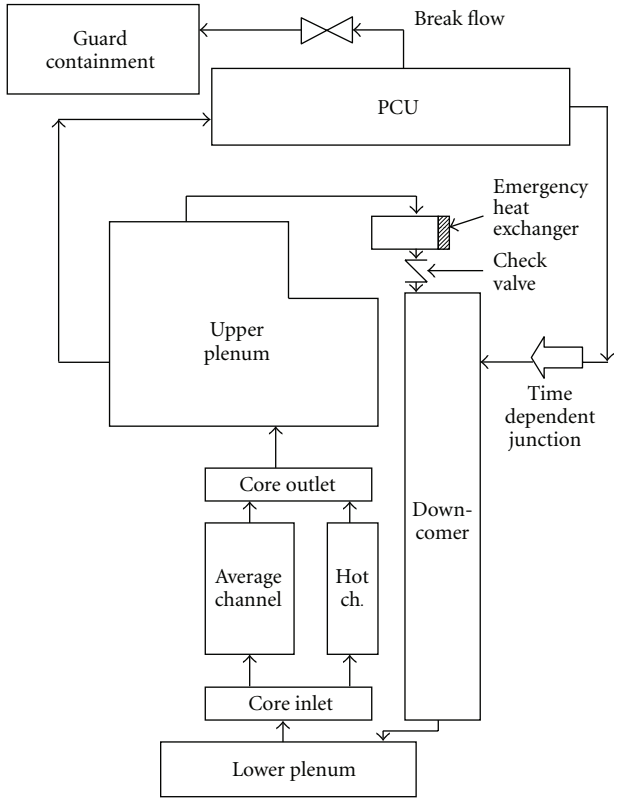

Figure 1: RELAP5 model of the GFR system.

In this preliminary study the power conversion unit (PCU) is approximated by a series of pipe components only and no turbomachinery or heat exchanger is modeled. One end of the PCU volume is connected to the reactor outlet in the upper plenum region (the hot duct). The other end of the PCU is connected to the reactor inlet in the downcomer region (the cold duct) via a time-dependent junction. The time-dependent junction is used to simulate the coasting down of forced flow through the reactor as a result of the PCU tripping on a depressurization accident. In addition a junction between the PCU and the downcomer will open when flow stops in the time-dependent junction, simulating the flow path between the reactor and the PCU.

The depressurization accident is initiated by opening a trip valve on the cold duct of the PCU volume. The assumed break area is 0.000645 m^2 (1 in^2). The break flow goes to a pipe component representing the guard containment. The main objective of the preliminary study is to assess the back pressure requirement for a successful decay heat removal via a passive system. The figure of merit for success is to maintain the maximum fuel temperature below 1600°C. A relatively large guard containment volume (18720 m^3) was used in the analyses to moderate the rise in the guard containment pressure as a result of leakage from the pipe break. This way the back pressure could be easily changed by varying the initial pressure parametrically.

A success case is achieved when the guard containment pressure is initially set to 2.0 MPa. In this transient the pressures in the reactor and the guard containment converge to about 2.5 MPa (see Figure 3). The emergency heat exchanger is able to match the decay power (see Figure 4) and the fuel temperature (see Figure 5) is well below the 1600°C limit. A similar analysis is done for an initial guard containment pressure of 1.0 MPa. In this case the maximum fuel temperature (see Figure 6) exceeds the 1600°C limit at about 3000 seconds after the initiation of the break.

3.2. Hybrid Active/Passive. The purely passive decay heat analysis suggests that passive heat removal is possible if the system back pressure is high enough to sustain sufficient natural circulation flow through the core and the emergency heat exchanger. The amount of the required natural circulation flow is dependent on the heat load, that is, the decay heat. If some other mechanism(s) can maintain core cooling in the early phase of a shutdown transient then the requirement can be relaxed for natural circulation cooling (passive cooling) in the later phase of the transient. A hybrid active/passive combination approach to the decay heat removal is evaluated for the advanced 2400 MWt GEN-IV gas-cooled fast reactor. The hybrid system is an emergency cooling system (ECS) (external to the reactor) consisting of battery-powered blower and natural circulation heat exchanger designed to remove decay heat both actively and passively. For the first 24-hours after shutdown when natural circulation alone may not be sufficient to cool the core, the ECS will operate in the active mode with the blower running. The ECS heat exchangers are sized to enable a self-sustaining method for long-term heat removal (after 24-hours) by natural circulation cooling when the blower is off. Since the natural circulation mass flow rate through the ECS primary circuit and the corresponding heat removal rate both increase with system pressure, a guard containment structure surrounding the primary system is designed to support an elevated back pressure condition in a depressurization accident.

A series of transient analyses using the system code RELAP5-3D (version 2.4.1.1a) has been performed to confirm the efficacy of the proposed hybrid active/passive emergency cooling system. The accident sequence of interest is a station blackout simultaneous with a small break (10 sq. inch/0.0645 m^2) in the reactor vessel. The analyses cover the three phases of decay heat removal in a depressurization accident: (1) forced flow cooling by the power conversion unit (PCU) coast down, (2) active forced flow cooling by a battery powered blower, and (3) passive cooling by natural circulation. The RELAP5 model [14] includes the helium-cooled reactor, the ECS (primary and secondary side), the PCU with all the rotating machinery (turbine and compressors) and the heat transfer components (recuperator, precooler and intercooler), and the guard containment that surrounds the reactor and the PCU.

In the latest pin core design [15], the 2400 MWt GFR reference core consists of 427 hexagonal fuel subassemblies, surrounded radially by 174 reflector subassemblies and 318

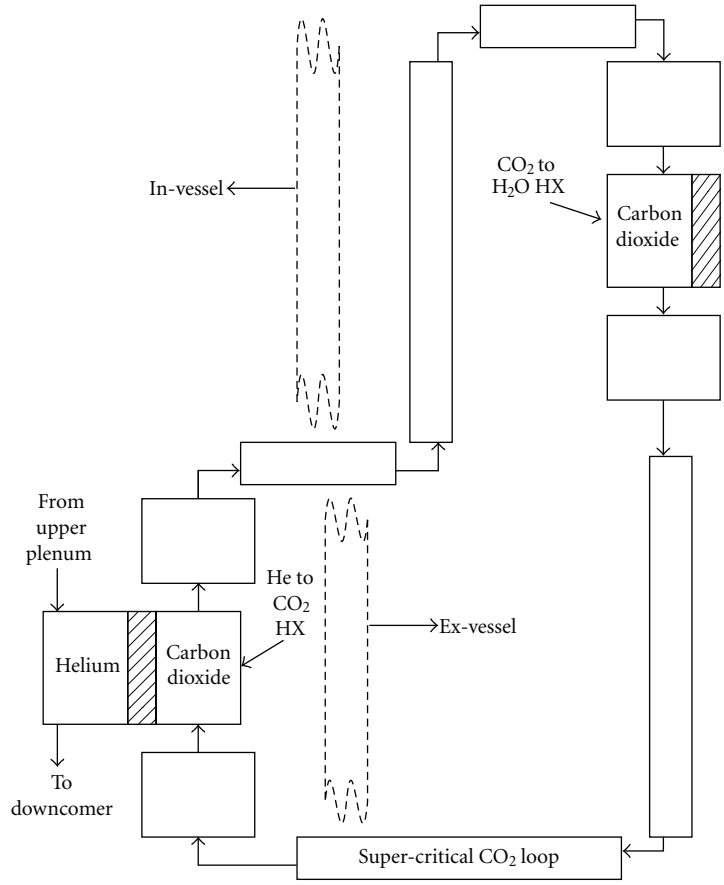

Figure 2: RELAP5 model of emergency heat exchanger system.

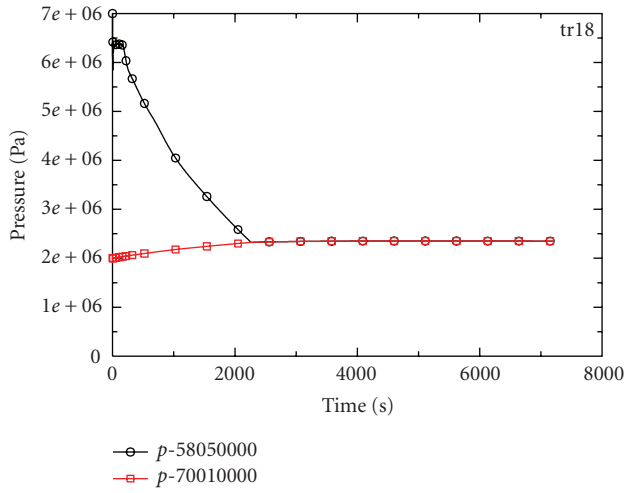

Figure 3: Pressures in the upper plenum and the guard containment.

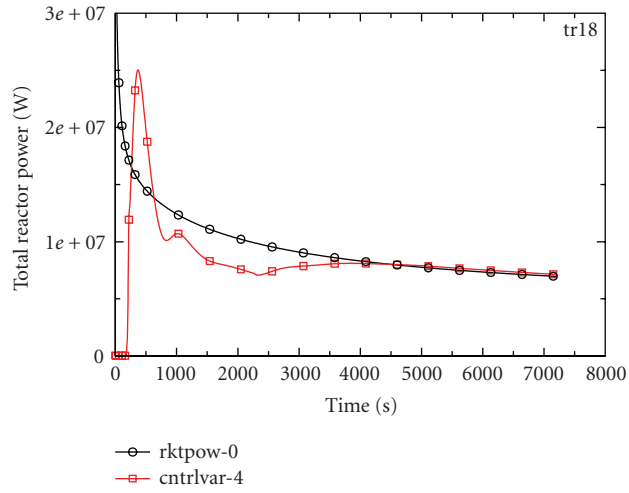

Figure 4: Reactor power and power removed by in-vessel emergency heat exchanger.

shield subassemblies. There are two types of fuel subassemblies, regular and control. Each regular subassembly has 271 fuel pins housed in a hexagonal can. Each control subassembly has 234 fuel pins with either a central control rod or a central shutdown rod. Each fuel pin in the subassembly has three axial regions, a top and bottom axial reflector section at each end and an active mid core section (1.34 m) consisting of fissile material (uranium carbide (UC) annular pellets). The cladding material for the fuel pin is silicon carbide (SiC). In the RELAP5 model, fuel subassemblies in

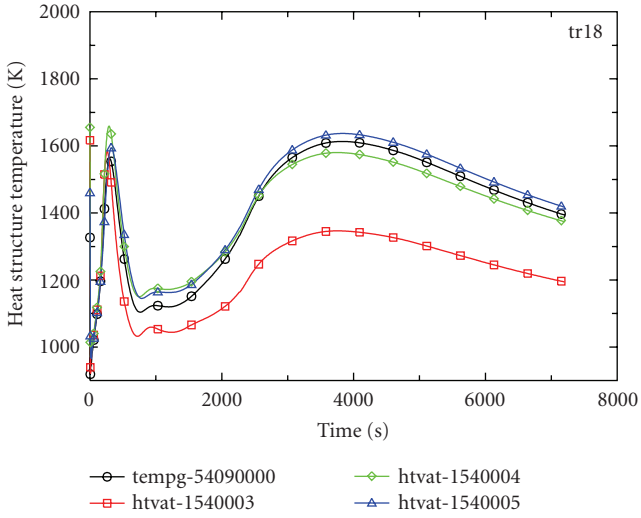

Figure 5: Temperatures in the core hot channel, gas and fuel.

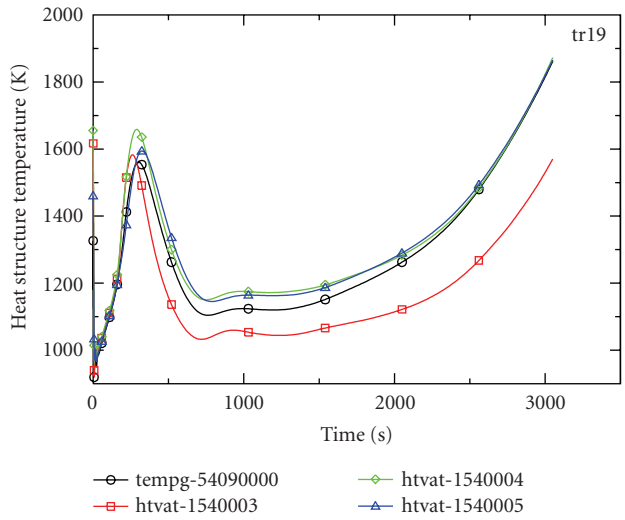

Figure 6: Temperatures in the core hot channel, gas and fuel (1 MPa case).

the core are grouped into three radial zones by power, which are hot assembly, hot zone, and average zone. Each radial zone with its own heat structure and hydraulic channel is further divided into ten axial zones (nodes) with mid-core symmetry and a cosine axial power shape. The fraction of total power generated in the three radial zones is shown in Table 2.

The GFR is designed for a system pressure of 7.0 MPa and a core Δp of 5.2×10^4 Pa. Primary coolant flow (helium) is 1249 kg/s and the core inlet and outlet temperatures are 480°C and 850°C respectively. Other core parameters are summarized in Table 3.

The RELAP5 representations of the primary system and the power conversion unit (PCU) by hydraulic volumes are shown in Figure 7. The thermal cycle utilized in the GFR plant is a recuperative gas turbine cycle with intermediate cooling. Rotating components of the PCU (turbomachines),

Table 2: Power distribution in core radial zones.

	Hot assembly	Hot zone	Average zone
Regular assembly	6	48	303
Control assembly	0	7	54
Power fraction (%)	1.7	14.1	84.2
Relative radial Power shape	1.31	1.21	0.967

Table 3: Core parameters.

Flat-to-flat of hexagonal duct (outside), mm	215
Duct wall thickness, mm	3.7
Interassembly gap, mm	7
Number of pins per core subassembly	271
Number of rings (excluding center one)	9
Number of spacers	3
Hydraulic diameter, mm	12.2
Pin pitch (average), mm	12.6
Total pin length, m	3.34
Fuel pellet diameter, ID/OD mm (annular)	3.02/7.37
Fuel clad thickness, mm	1.0
Fuel pin diameter, mm	9.57

Table 4: Case definitions.

Case	Definition
17	Constant spacer loss coefficients (not Reynolds number dependent). Trip valve isolates PCU at $t = 9010$s.
26	Similar to Case 17 but has the spacer loss coefficient becoming Reynolds number dependent after $t = 13000$s.
32	Similar to Case 17 but with Reynolds number dependent spacer loss implemented at $t = 1000$s. Constant guard containment pressure of 800 kPa is initiated at $t = 1250$s.

namely, the generator, turbine, low- and high-pressure compressors, are all on one shaft. A bypass valve that connects the high- and low-pressure side of the PCU is used for the over-speed protection of the turbine.

The emergency cooling system (ECS) is sized to handle 2% decay heat removal by natural convection in a $4 \times 50\%$ configuration, that is, four separate loops of 1% power capacity. In the RELAP5 model the emergency heat removal system is represented by a single loop with a $2 \times 50\%$ capacity and one heat exchanger, which is sized to handle 2% of full power. A battery powered blower downstream of the heat exchanger is sized to provide sufficient forced flow cooling

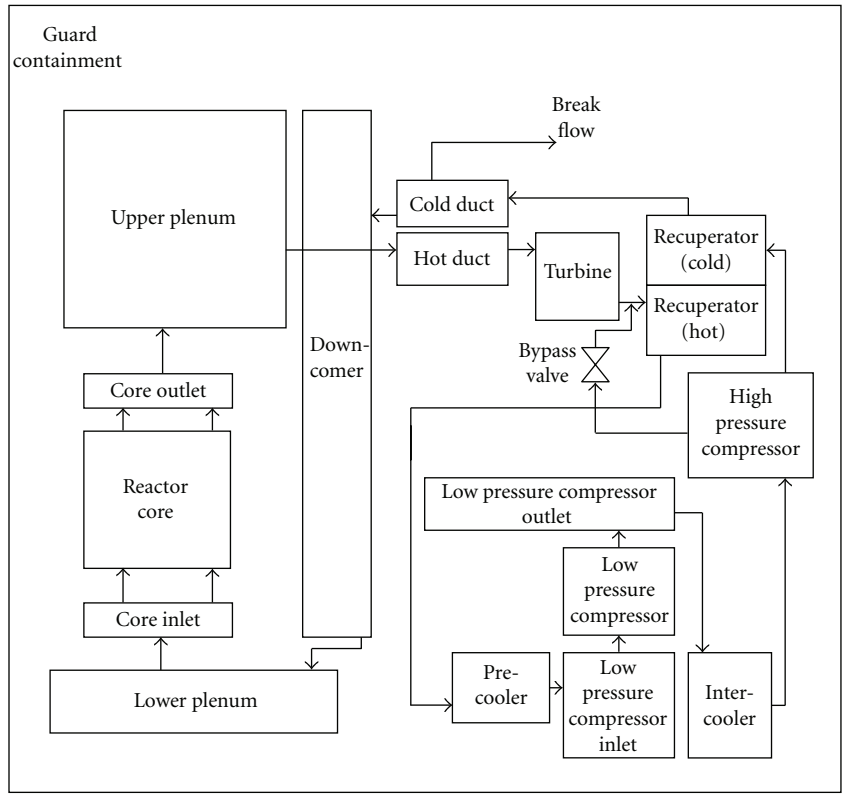

Figure 7: Reactor vessel and power conversion unit volume arrangement.

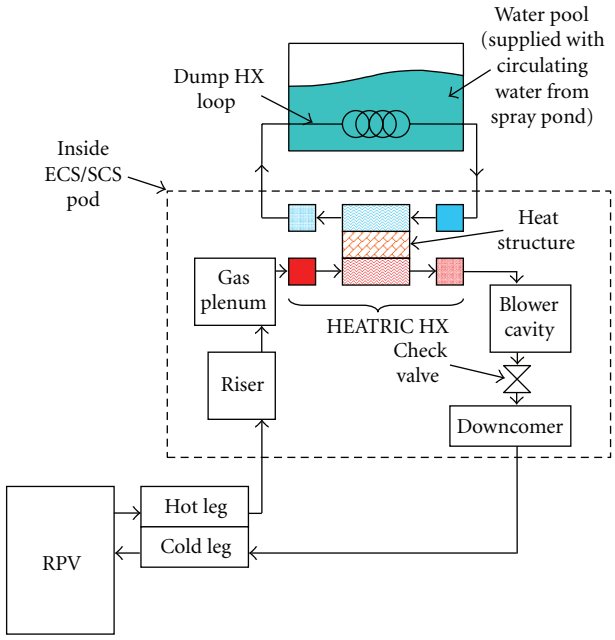

Figure 8: Schematic of emergency cooling system.

during the first 24 hour after a reactor shutdown. Details of the volume representation of the ECS are shown in Figure 8.

The evaluation of the hybrid decay heat removal scheme is by way of analyzing a depressurization accident initiated by a break in the reactor pressure boundary (assumed at the high point of the reactor vessel) followed by a scram on low system pressure. Three transient calculations, defined in Table 4, have been performed to assess different aspects of modeling assumptions.

Helium flow through the core becomes laminar when natural circulation is established subsequent to turning off the battery powered blower. Case 26 is designed to examine the impact of increased form losses of grid spacers in laminar flow [14].

One of the ways to increase the natural circulation flow is by increasing the back pressure of the guard containment. This is realized in Case 32 by connecting a constant pressure time-dependent volume to the guard containment. The time-dependent volume, simulating a gas accumulator, maintains the back pressure at 800 kPa (8 bars) by injecting helium gas at 20°C when necessary. All three transient cases (no. 17, 26 and 32) assume a guard containment free volume of 2025 m^3.

The success criteria for the transients are:

(1) maximum fuel temperature less than 1600°C (1873 K).

(2) maximum core outlet temperature (helium) less than 850°C (1123 K).

Both Cases 26 and 32 are restart cases. So they share the same result as for Case 17 up to the point of the restart, t = 13000s for Case 26 and t = 1000s for Case 32. The

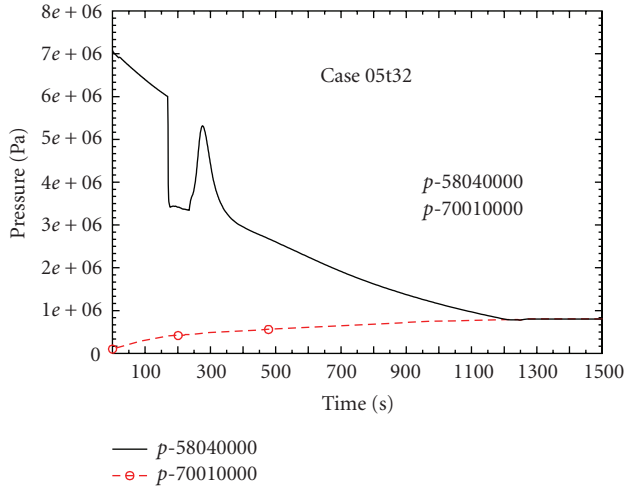

FIGURE 9: Reactor (solid) and guard containment (dash) pressure.

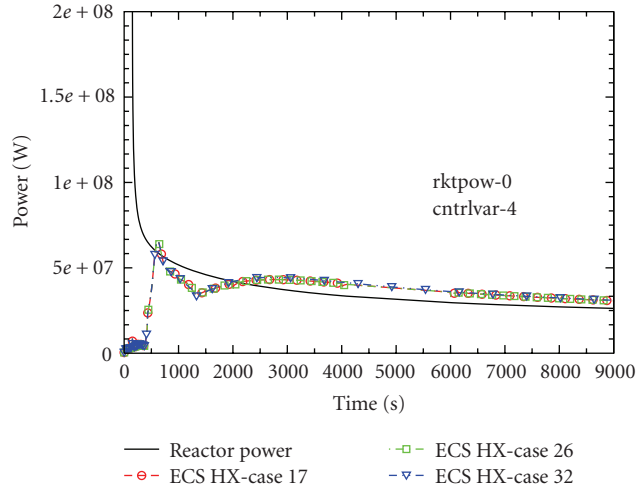

FIGURE 10: Reactor power and heat removal rate of ECS ($t < 9000$s).

timeline for one of the cases (Case 32) is shown in Table 5 to illustrate the progression of the accident.

During the early phase of the transient, core flow is first driven by the power conversion system, followed by a battery powered blower. Preliminary results of the analysis indicate that the core is adequately cooled when the blower is running. It is then not necessary to simulate every second of the first 24-hours while the blower is in operation. A fast forward in time in simulation is done by linearly decreasing the reactor power from 26.2407 MW at $t = 9000$s to 13.9748 MW at $t = 15000$s. The later power level is equivalent to the decay power 24-hours after a shutdown. At 15000s the blower is turned off and the reactor power is maintained constant at the 24 hour decay power level for the rest of the calculation.

Preliminary results also indicate that with the blower off, the high-pressure point of the system is in the downcomer of the reactor. There are two flow paths from the downcomer, one leads to the core and the other goes to the PCU via the cold duct. With the blower off RELAP5 predicts about half of the natural circulation flow bypassing the core and instead flows through the PCU in the reverse direction (normal flow is from the hot duct to the cold duct). The PCU bypass flow is prevented by simulating a check valve, "activated" at $t = 9050$s, that isolates the PCU from the downcomer.

Since the early phase of the transient is common for all three cases, results from Case 32 are used to illustrate the pressure responses of the reactor and the guard containment to a depressurization accident initiated by a 0.0645 m^2 (10 sq. inch) break at time zero. It takes about 170s for the system pressure, as shown in Figure 9, to reach the scram setpoint of 6 MPa. The sudden drop in reactor pressure after scram is due to the opening of the turbine bypass valve in the PCU to control overspeeding of the rotating components. As a way to restore full turbine output, the bypass valve is reclosed at $t =\sim 220$s and the reactor pressure responded positively. The pressures in the reactor and the guard containment slowly become equalized and the pressure equalization point occurs at a pressure of ~800 kPa

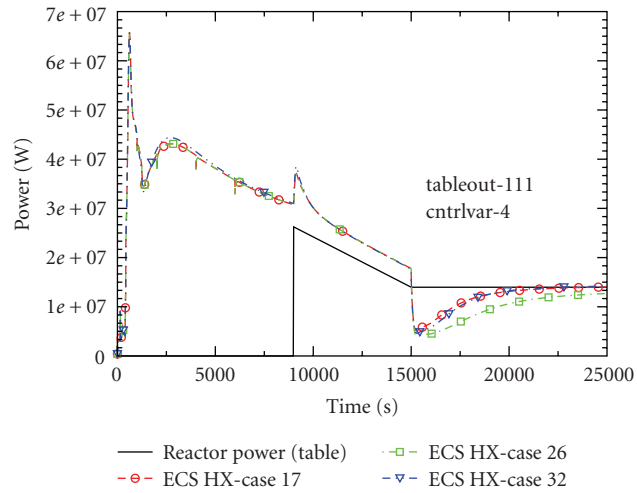

FIGURE 11: Reactor power and heat removal rate of ECS.

and at $t =\sim 1250$s. In Case 32 an accumulator is assumed to inject helium into the guard containment after $t = 1250$s to maintain a constant back pressure of 800 kPa for the reactor system.

Plotted in Figures 10 and 11 is the rate of heat transfer into the heat exchanger in the emergency cooling system. The reactor power also is shown in the figures for comparison. Except for a period before $t = 2000$s the ECS heat exchanger is able to remove all the decay power while the blower is running (before $t = 15000$s). For the two cases #17 and 32 the energy removed by the ECS heat exchanger under natural circulation (for $t > 15000$s) is seen to approach the decay power toward the end of the simulation. The increase in heat removal rate at $t \sim 9000$s is due to the closure of the core bypass flow path through the PCU thus directing all flow through the ECS heat exchanger.

Figure 12 shows the peak fuel temperature as a function of time for the three transient cases. Before the reactor scrams at $t = 169$s there is a reduction in core flow due to system depressurization. This is accompanied by a corresponding

Table 5: Timing of significant events for case 32.

0s	10 sq. in break initiated.
169.3s	Reactor tripped on low-pressure. Generator tripped off line and turbine bypass is opened.
234.92s	Turbine bypass reclosed when PCU flow dropped below 20% of rated value.
382.92s	Compressors replaced by dummy volumes when PCU flow again dropped below 20% of rated value.
420s	Blower turned on with a flow velocity of 3.5 m/s.
1250s	Helium accumulator connected to guard containment to maintain pressure at 800 kPa. Accumulator is modeled by a time-dependent volume of constant pressure (800 kPa) and constant temperature (303.15 K)
9000s	Case restarted by defining reactor power as a function of time in the form of a table. Reactor power decayed linearly from 26.2589 MW at $t = 9000$ seconds to 13.9748 MW at $t = 15000$ seconds. The later power level is equivalent to the decay power 24-hours after a shutdown.
9050s	Trip valve located at the junction between the PCU outlet and the reactor downcomer was closed. This was used to simulate the action of a check valve that would have prevented flow from entering the PCU via the reactor downcomer.
15000s	Blower speed reduced to zero in 5 seconds. Reactor power was maintained constant at the 24-hour decay heat level.
25000s	Case ended.

increase in fuel temperature as shown in Figure 12. There is a rapid drop in fuel temperature after the reactor scram but the temperature starts to increase again after the compressors of the PCU have stopped running. The rate of temperature increase is abated slightly when the blower is turned on at $t = 420$s. By about $t = 2000$s the energy removal power of the ECS heat exchanger exceeds the decay power (see Figure 10) and the fuel temperature starts to turn around in a downward trend. The peak fuel temperature is seen to be lower in Case 32 than the other two cases between $t = 2000$s and 15000s. This is due to the higher blower flow in Case 32 as a result of higher helium density from the higher system pressure.

The accelerated drop in the peak fuel temperature at $t = 9010$s is an artifact of the accident scenario that calls for the isolation of the PCU from the downcomer of the reactor. With this action the helium flow can no longer bypass through the PCU and the full blower flow is now directed to the core. The linear rate of decrease of the peak fuel temperature between $t = 10000$s and 15000s is a reflection of the imposed linear decay in reactor power. At a state of reduced power and reduced pressure, the natural circulation flow is much lower than the blower flow and the effect is evident in the rapid increase in the peak fuel temperature after the mode of heat transfer has changed from forced to natural convection at $t = 15000$s.For Cases 17 and 32 the leveling off of the peak fuel temperature toward the end of the calculation is indicative of natural circulation cooling matching the energy output of the reactor.

The general trend of the core outlet temperature, as shown in Figure 13 resembles that of the peak fuel temperature in Figure 12. The similarity between the responses of these two temperatures is not surprising because the location of the peak fuel temperature is generally near the core outlet. For cases 17 and 32, the core outlet temperature reaches a quasi-steady value of ~1000 K while the temperature of Case 26 exceeds the success criterion of 1123 K.

The above results shows that Case 17 is a success case meeting both success criteria on fuel temperature and core outlet temperature at the end of the calculation at $t = 25000$s. Case 26 with the realistic spacer losses (Reynolds number dependent) results in reduced natural circulation (as compared to Case 17) and the core outlet temperature exceeding the success criterion. At the end of the calculation at $t = 25000$s the maximum fuel temperature has reached about 1400 K and is still increasing. For Case 32 where a constant back pressure of 800 kPa is maintained in the guard containment both the maximum fuel temperature and core outlet temperature have reached a quasi-steady state value by the end of the calculation and are within the success criteria. Case 32 demonstrates that it is possible to rely on natural circulation flow alone to remove decay power 24-hours after shutdown.

4. Autonomous Active Systems

Figure 14 shows a schematic diagram for a direct-cycle plant with an autonomous shutdown decay heat removal system (inside the dotted perimeter) in parallel with the main power conversion unit. If the main power conversion unit (on the left side of the figure) were not present and all of the primary flow went to the autonomous system, the plant layout would essentially be that of a reactor plant with a small simplified PCU also running on Brayton cycle. There is a precooler heat exchanger between the turbine and the compressor part of this small PCU, or heat engine, and the heat exchanger rejects heat to the water side of the RHR system. It could produce electric power, via a generator/motor if desired. The autonomous system is designed to run off the core decay heat except when perhaps the decay power is extremely low. The electricity generated by this system could be separate from the main (site) power grid and is therefore available even when the plant becomes disconnected from the main power grid.

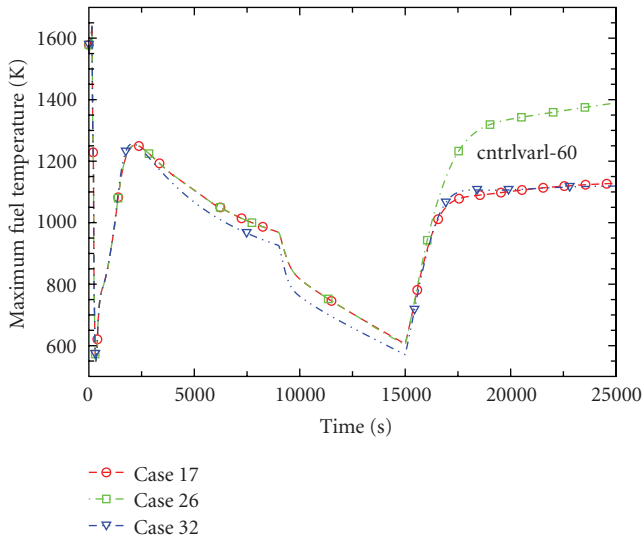

Figure 12: Peak fuel temperature core-wide.

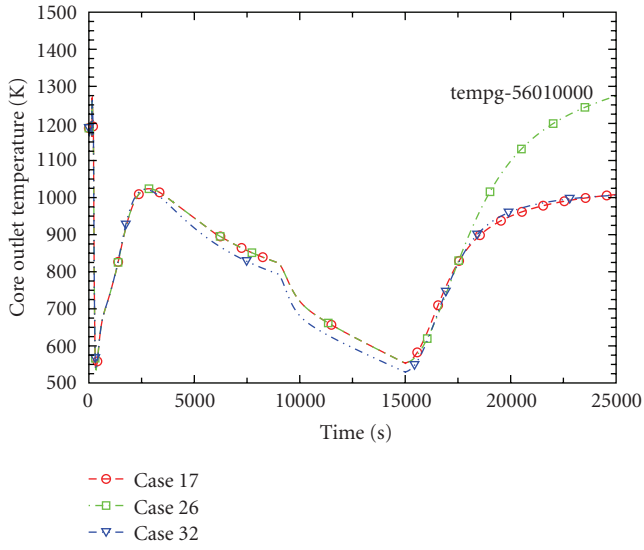

Figure 13: Core outlet temperature.

When there is a loss of site power, the core power converted by the autonomous system continues to provide the motive power for the compressor, shown in Figure 14, that drives flow through the core and the heat exchanger. If the autonomous system is not running all the time then there is a start-up device, which could be a compressed gas accumulator in the circuit to the turbine and the compressor. This would actuate in the event that there is an interruption in power supplied to the plant systems and also for situations when the core power gets too low to keep the main PCU running. In the latter case, the autonomous system would enable the flow to keep circulating longer and the plant to continue removing decay heat longer. The core decay heat provides the motive power to keep the core cooled and the flow removes the decay heat.

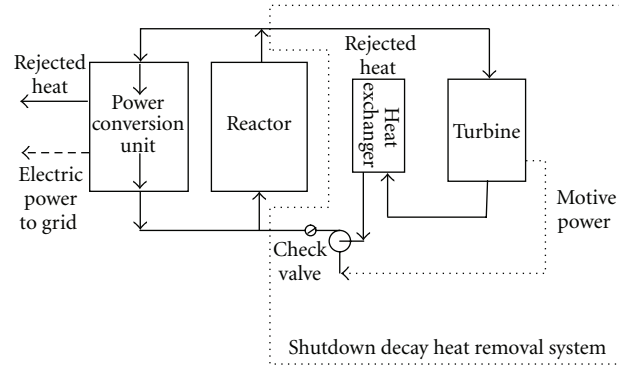

Figure 14: Direct-cycle layout with an autonomous shutdown decay heat removal system.

In the event the autonomous system fails during normal operation it may be necessary to shut the plant down. During normal operation of the reactor plant, the compressors in the power conversion unit keep the pressure at the reactor inlet higher than that at the outlet and thereby drive the flow though the reactor core. If the compressor in the autonomous system was not running, then the pressure differential across the reactor core would cause most of the main primary flow to bypass the reactor core and go backward through the primary side of the heat exchanger that is connected to the auxiliary heat engine. Therefore, a check valve, shown in Figure 14, is needed to prevent backward flow if the compressor for the autonomous system is not be running.

The autonomous system could be running all of the time, including normal operation of the reactor plant, so that it would always be available and does not need to be started during an emergency. Therefore, the system would be removing heat all of the time and would impact plant efficiency unless it also generated electricity. Also, the system would have to be designed to insure that it ran properly at both full system pressure and at depressurized conditions, which in some plant designs could be as low as one atmosphere. The autonomous system potentially could be usable for normal decay heat removal while the plant is shutdown and during fuel handling.

During a depressurization accident there would probably be only outflow through the break from the pressurized primary circuit to the reactor containment and no concurrent ingress of cold containment gases. After the depressurization, however, it may be possible for cold gases to enter through the break. This represents a potential problem. If cooled gases from the containment entered the primary system through the break and prevented hot coolant from the reactor core from reaching the turbine that is powering to the autonomous system, the auxiliary heat engine would stop running. This could be the result of a large break in or near the reactor vessel outlet plenum, for example. Therefore, it may be highly desirable to place the system inside the primary vessel so that there is no external primary piping between the vessel and the system, for example, the heat exchangers that are added to the primary circuit could be

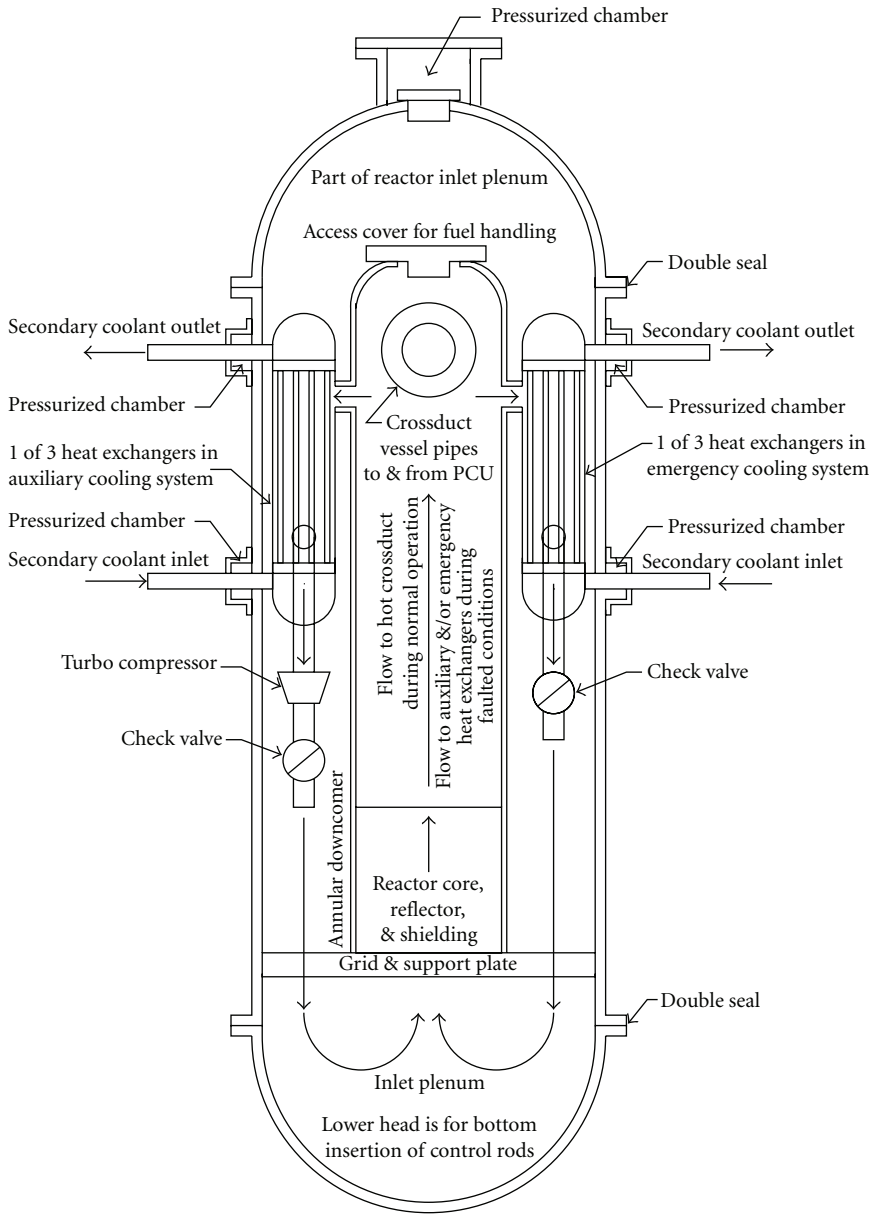

Figure 15: Reactor vessel layout for natural convection or autonomous system in direct-cycle plant.

placed inside the primary vessel, as shown in Figure 15 for a direct-cycle plant.

An important issue is the potential for check valve failures. If during normal full reactor power operation, the check valves failed to prevent backflow through the primary side of the auxiliary engine heat exchanger, a significant part of the primary flow could bypass the reactor core. Autonomous systems have moving parts and therefore cannot be considered to be passive systems. They may be classified as "semipassive", as opposed to "active", because they do not necessarily need to be started up in an emergency, as one would need to do with a backup diesel-powered electric generator.

5. Summary and Conclusions

With the advent of the U.S. led GEN IV initiative to develop an entirely new generation of nuclear reactor plants, there is now the opportunity to revisit the design of the gas-cooled fast reactor (GFRs) and enhance the passive safety case. The GFR safety approach for the passive removal of decay heat in a protected depressurization accident with total loss of electric power needs to be different from that taken for the HTRs. The HTR conduction cooldown to the vessel wall boundary mode for economically attractive core designs is not feasible in the case of the GFR because the high power densities require decay heat fluxes well beyond those achievable by the heat conduction and radiation heat transfer

mode. A set of alternative design options has been evaluated for potential passive safety mechanisms characteristics of the GFR. For the pin design core, two approaches to decay heat removal, autonomous systems and natural convection have been identified. For direct-cycle plants both concepts require that one or more additional primary flow loops be added to the plant. These loops have heat exchangers that either power the autonomous systems or merely dump decay heat. These extra loops require check valves to help prevent reverse flow that could cause a significant portion of the main coolant flow to bypass the reactor core. An issue that is common to the use of either autonomous or natural convective systems is a break in the primary system boundary that would allow cold containment gas to enter the reactor vessel between the reactor outlet plenum and the inlet to the decay heat removal system. This could be detrimental for an autonomous system, since it is powered by the heated coolant from the reactor core. This would also be detrimental for a natural convection system, since it would diminish the buoyancy that drives the primary flow around the natural convective circuit. In order to avoid this problem, or minimize its likelihood of occurrence, it was suggested that the heat exchangers that are added to the primary circuit to be placed inside the primary vessel, as shown in Figure 15 for a direct-cycle plant. To bolster the safety case for natural convection, the primary vessel will be enclosed within a guard containment (secondary containment) to maintain the coolant pressure at some significant level. Since autonomous systems add complex machinery to the plant, they cannot be considered to be passive, but may be considered to be semipassive. Natural convective systems do not work at atmospheric conditions and therefore require some form of pressurized confinement, but if this pressurized confinement is provided, the system can be passive. Natural convective systems are less complex than autonomous ones, but providing a confinement/guard containment with sufficient pressure capability could be a challenge.

The decay power immediately after scram from full power is close to 7% of full power. Since natural convective decay heat removal systems typically can remove no more than only about 1 or 2% of decay power, the excess decay energy must be temporarily stored in the reactor until the decay power has declined sufficiently. A RELAP5 transient model was used to assess natural convection in a direct-cycle plant in which the natural convection heat exchanger was assumed to be 10 m about the reactor fueled region. The results showed that for helium coolant the guard containment pressure would have to be about 13 bar if the primary system temperature were not to exceed about 850°C. The accident analyzed was the protected major depressurization accident with total loss of electric power. The results obtained with the model show that there is significant margin from the assumed fuel disruption criteria when the guard containment postevent pressure is 20 bar. The current consensus reached on the natural convention approach to the depressurized decay heat accidents is a combination of both active and passive means. A guard containment surrounding the primary system is utilized which is designed for 0.7 to 1.0 MPa back-up pressure. This back-up pressure plus whatever natural convection is available at this pressure level will be utilized to reduce significantly the blower power of the active decay heat removal system (DHR) sized to remove 2-3% decay power. The objective is to be able to use power supplies such as batteries without the need for startup. This back-up pressure level should then be sufficient to support natural convection removal of the decay heat after ~24-hours. The power requirement would be also be decreasing during this period as the after-heat further decays. Furthermore, additional work should be pursued to extend the primary system coast-down upon trip of the main power conversion units (PCUs) which are Brayton cycle turbo-compressors. With the use of the Brayton cycle turbo-compressors there is the potential for using the core decay heat to provide the driving power for the turbo-machinery flow thus maintaining core cooling by the primary coolant flow. As a complementary autonomous concept, turbo-compressor sets could be used in place of electrically-driven blowers in the DHR system. The target is to remove the need for electric power in these accident situations.

In conclusion, a design for a pin-type core that employs a natural convective heat removal system has been selected and the modeling capability to analyze it has been assembled and a system evaluation has been performed. It is recommended that follow-on GEN-IV project work is performed to consider the implications of an autonomous system for this core design and safety approach for the primary vessel design, the balance-of-plant layout and the containment considerations.

Acknowledgments

This manuscript has been authored by employees of Brookhaven Science Associates, LLC under Contract no. DE-AC02-98CH10886 with the U.S. Department of Energy. The publisher by accepting the manuscript for publication acknowledges that the United States Government retains a nonexclusive, paid-up, irrevocable, world-wide license to publish or reproduce the published form of this manuscript, or allow others to do so, for United States Government purposes. The ANL work was supported by the U.S. Department of Energy under Contract numbers W-31-109-Eng-38 and DE-AC02-98CH10886. This material is based upon work supported by the U.S. Department of Energy under the I-NERI and GEN IV programs.

References

[1] G. Melese, *Thermal and Flow Design of Helium-Cooled Reactors*, chapter 10, ANS, Lagrange Park, 1986.

[2] D. R. Buttemer and A. Torri, "Safety features of the gas-cooled fast breeder reactor," *Nuclear Engineering and Design*, vol. 40, no. 1, pp. 43–54, 1977.

[3] J. H. Gittus, "ESKOM pebble bed modular reactor," *Nuclear Energy*, vol. 38, no. 4, pp. 215–221, 1999.

[4] P. Dumaz, P. Allègre, C. Bassi, et al., "Gas-cooled fast reactors—status of CEA preliminary design studies," *Nuclear*

Engineering and Design, vol. 237, no. 15–17, pp. 1618–1627, 2007.

[5] J. Y. Malo, et al., "Gas cooled fast reactor 2400 MWth, end of the preliminary viability phase," in *Proceedings of the International Conference on Advances in Nuclear Power Plants (ICAPP '08)*, Anaheim, Calif, USA, June 2008.

[6] F. Bertrand, et al., "Preliminary safety analysis of the 2400 MWth gas-cooled fast reactor," in *Proceedings of the International Conference on Advances in Nuclear Power Plants (ICAPP '08)*, Anaheim, Calif, USA, June 2008.

[7] A. Epiney, et al., "Comparative transient analysis of the 2400 MWth GFR with the TRACE and CATHARE codes," in *Proceedings of the International Conference on the Physics of Reactors "Nuclear Power: A Sustainable Resource" (PHYSOR '08)*, Interlaken, Switzerland, September 2008.

[8] P. Dumaz, "Decay heat removal system design and calculations of the gas cooled fast reactor (GFR)," in *Proceedings of the International Conference on Advances in Nuclear Power Plants (ICAPP '08)*, Anaheim, Calif, USA, June 2008.

[9] A. Epiney, K. Mikityuk, and R. Chawla, "Heavy gas injection in the generation IV gas-cooled fast reactor to improve decay heat removal under depressurized conditions," in *Proceedings of the 13th International Topical Meeting on Nuclear Reactor Thermal Hydraulics (NURETH '09)*, Kanazawa City, Japan, September-October 2009.

[10] A. Epiney, et al., "Preliminary design of a Brayton cycle as a standalone decay heat removal system for the gas-cooled fast reactor," in *Proceedings of the International Topical Meeting on Nuclear Reactor Thermal Hydraulics (NURETH '09)*, Kanazawa City, Japan, September-October 2009.

[11] J. Rouault and T. Y. C. Wei, "Development of GEN-IV advanced gas-cooled reactors with hardened/fast neutron spectrum," in *Proceedings of the Transactions of the American Nuclear Society and Embedded Topical Meetings*, vol. 88, p. 191, San Diego, Calif, USA, June 2003.

[12] J. C. Garnier, N. Chauvin, P. Anzieu, et al., "Feasibility study of an advanced GFR, design trends and safety options, status of France and U.S. studies," in *Atoms for Prosperity: Updating Eisenhower's Global Vision for Nuclear Energy (GLOBAL '03)*, New Orleans, La, USA, November 2003.

[13] T. Y. C. Wei, P. Hejzlar, E. E. Feldman, and W. C. Williams, "A semi-passive approach to GFR depressurized decay heat removal accidents," in *Proceedings of the International Conference on Advances in Nuclear Power Plants (ICAPP '05)*, vol. 1, pp. 28–37, Seoul, Korea, May 2005.

[14] L. Y. Cheng, H. Ludewig, and J. Jo, "Emergency decay heat removal in a GEN-IV gas-cooled fast reactor," in *Proceedings of the International Conference on Nuclear Engineering (ICONE '06)*, July 2006.

[15] M. T. Farmer, et al., "generation IV nuclear energy system initiative pin core subassembly design," Tech. Rep. ANL-GenIV-070, Argonne National Laboratory, 2006.

Hindawi Publishing Corporation
Science and Technology of Nuclear Installations
Volume 2009, Article ID 291453, 10 pages
doi:10.1155/2009/291453

Research Article

The Influence of the Packing Factor on the Fuel Temperature Hot Spots in a Particle-Bed GCFR

G. Lomonaco,[1,2,3] W. Grassi,[2] and N. Cerullo[1,3]

[1] *DIMNP, University of Pisa, CIRTEN, Largo L. Lazzarino No. 2, 56126 Pisa, Italy*
[2] *Department of Energetics, University of Pisa, Largo L. Lazzarino No. 1, 56126 Pisa, Italy*
[3] *DIPTEM, University of Genova, Via all'Opera Pia No. 15/a, I-16145 Genova, Italy*

Correspondence should be addressed to G. Lomonaco, g.lomonaco@ing.unipi.it

Received 17 April 2009; Revised 14 July 2009; Accepted 24 October 2009

Recommended by Colin Mitchell

In the recent past the so-called GCFR has been again a subject of study by the international scientific community. This type of reactors, although still in a preliminary stage of development, is a very interesting perspective because combines the positive characteristics common to all the fast reactors with those of the reactors cooled by helium. Up to now, almost all the analyses on the GCFR thermodynamic aspects have been performed starting from a "global" point of view: generally the core has been modelled as a porous medium and only the global parameters have been taken into account. The local effects have been included in *adhoc* corrective peak factors. The analyses carried out in the present research will be devoted to the characterization of the local effects, on a microscopic scale. In order to have reliable "global" nuclear and thermal-fluid-dynamic data, the performed analyses will be based on simulations previously performed using the RELAP5-3D code, assuming as input parameters the ETDR core ones. For each considered case, the variation ranges of the evaluated parameters have been estimated on the basis of the "best" and the "worst" cases. To summarize the obtained results, even in transient conditions, the variations of the considered input parameters are less significant for the local output values if compared to those due to the assumed packing factor. As a consequence, in a more general core calculation, the obtained local temperature (and velocity) values will have to be corrected by a proper factor that would have to take into account the results of this research.

1. Introduction

Thermal-Fluid-Dynamics (TFD) is fundamental for the analysis of the Nuclear Power Plants (NPPs). A nuclear reactor is (virtually) capable to produce all the wanted power provided that it is possible to remove it from the core. This characteristic, already known since the first studies on nuclear energy, is sometimes indicated as the "First Reactor Theorem" [1]. Therefore a complete analysis of the reactor energy balance is always mandatory [2].

Among the six Gen IV reactor projects, there are two with a thermal neutronic flux (High-Temperature Gas Reactor or HTGR, Supercritical Water Reactor or SCWR), three with a fast flux (Gas-Cooled Fast Reactor or GCFR, Sodium Fast Reactor or SFR, Lead Fast Reactor or LFR), and one with epithermal flux (Molten Salt Reactor or MSR).

Generation IV reactor projects have to answer to new challenges that nuclear energy must face in this new century. The selected systems have to meet Gen IV criteria [3], namely:

(1) Sustainability,

(2) economics,

(3) proliferation-resistance

(4) safety and reliability.

The capability of removing the heat produced in the core (both in nominal and accidental conditions) is a key point of criterion 4, particularly for GCFR. In fact this reactor has a high power density (up to 100 MW/m^3) similar to an LWR, but in this case the power has to be removed by a noncondensable gas (helium) instead of water.

Up to now, almost all the analyses on the GCFR thermodynamic aspects have been performed starting from a "global" point of view: generally the core has been modelled

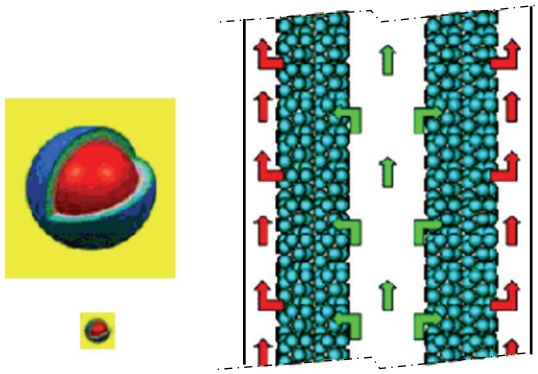

Figure 1: Particle-bed GCFR fuel element [9].

as a porous medium and only the global parameters have been taken into account. The local effects have been included in *adhoc* corrective peak factors.

On the contrary, the analyses carried out in the present research will be devoted to the characterization of the local effects, on a microscopic scale (by using the FLUENT CFD code [4]). The first step will be to setup a proper "microcell" that is used to evaluate the effects induced by the variation of some parameters (packing factors, mean temperature level, etc.) on the local parameters (temperature, coolant velocity, etc.). Then some parametric analyses will be performed in order to find which are the most significant one with reference to the temperature distribution and velocity field inside the microcell. The final purpose is to supply further data in order to develop a more realistic and accurate way to derive the already mentioned corrective peak factors.

In order to have reliable "global" nuclear and TFD data on a GCFR core, the performed analyses will be based on simulation previously performed [5] using RELAP5-3D code [6], assuming input parameters from the ETDR core [5] (Please note that the Experimental Test Demonstration Reactor (ETDR) is now known as ALLEGRO) . For each considered case, the variation range of the evaluated parameters has been estimated on the basis of the "best" and the "worst" cases.

2. Preliminary Considerations on the GCFR Energy Balance

The gas-cooled nuclear reactors are usually characterized by a (relatively) low power density. On the contrary in the GCFR power density ranges from 25 to 100 MW/m^3. It is clear that the more demanding heat transfer conditions makes accurate TFD calculations necessary. As an example, the hot spots characterization issue could be relevant already at the nominal operating conditions.

On the basis of a wide bibliographical research, it can be stated that some studies exist on the gas-cooled nuclear reactors TFD (e.g., [7, 8]) and on the particle-bed configuration. However all of them are substantially different from this paper, where the following has been taken into account:

(i) very small particle dimensions (diameter < 1 mm),

(ii) internal heat production,

(iii) high power density.

Particularly studies on the following were found [2]:

(i) particle-bed configurations without internal heat production,

(ii) CFD applied to gas-cooled nuclear reactors but almost all of them are referred to block type cores and not to pebble (or particle) bed cores (so, among the other features, the stochastical particle arrangement is missing),

(iii) CFD-Neutronic coupled studies on pebble (or particle) bed gas-cooled nuclear reactors; however the bed is not modelled in detail, mainly due to the great number of elements and it is usually simulated by the porous medium approximation: as a consequence, it is not possible to calculate the maximum local temperature and the real temperature gradient inside the fuel elements.

3. TFD Simulations

The considered GCFR core was made of annular fuel elements (FEs) containing beds of coated particles (CPs), stochastically packed. Particularly the considered FE is shown in Figure 1. The CPs are double-sized in order to limit the pressure drops inside the core. As a first simplification, in this study the elementary cells taken into account are made only by the smaller CPs (diameter ~1 mm). The CPs are TRISO-like but the ratio of kernel to external layer dimensions is quite large with respect to "classical" TRISO (i.e., typical CPs for HTR). The coolant (helium) flows through the CPs.

So, it is necessary to use a model, specifically designed for these conditions.

As a first step, by search of the available scientific literature, suitable physical models were selected. Particularly the models able to evaluate the helium pressure drops through the core and the heat transfer between CPs and coolant were researched.

Regarding the pressure drops through cylindrical beds (some modifications would be needed for taking into account also radial flow through an annular bed), it has been found that they can be evaluated (at least in the porous medium approximation) by Kugeler and Schulten model [7]. The latter model has been designed in order to describe the pressure drops in a reactor similar (at least from this point of view) to the considered GCFR. Particularly the pressure drops Δp could be evaluated by using the following formula:

$$\Delta p = \psi \frac{1-\varepsilon}{\varepsilon^3} \frac{H}{d} \frac{1}{2\rho} \left(\frac{\dot{m}}{A}\right)^2, \tag{1}$$

where

$$\psi = \frac{320}{(\mathrm{Re}/(1-\varepsilon))} + \frac{6}{(\mathrm{Re}/(1-\varepsilon))^{0.1}}, \tag{2}$$

ε = packing factor.

Alternatively other models could be used, as the formula by Ergun [10]:

$$F = \left(\frac{\Delta P}{\Delta z}\right) = 150\frac{(1-\varepsilon)^2}{\varepsilon^3}\frac{\mu v}{D_p^2} + 1.75\frac{(1-\varepsilon)}{\varepsilon^3}\frac{\rho|v|v}{D_p}. \quad (3)$$

Looking at the heat transfer, there have been considered some models.

Among the others are Kugeler's [7] and Shirai's [11] formulae:

$$\mathrm{Nu}_p = 1.27\frac{\mathrm{Pr}^{0.33}}{\varepsilon^{1.18}}\mathrm{Re}_p^{0.36} + 0.033\frac{\mathrm{Pr}^{0.5}}{\varepsilon^{1.07}}\mathrm{Re}_p^{0.86}, \quad (4)$$

$$\mathrm{Nu}_p = \frac{2.0}{\varepsilon} + \frac{0.75}{\varepsilon}\mathrm{Pr}^{1/3}\left(\mathrm{Re}_p\right)^{1/2}. \quad (5)$$

4. Models

All the models shown in the previous paragraphs have been designed considering the whole core as a continuum (usually modelled by porous medium approximation). Therefore they are useful to evaluate the core's global behaviour, both in terms of pressure drops and temperature distribution. However those models cannot deal with the local (microscale) phenomena, like the hot spots. While in the thermal HTRs these phenomena are not so relevant, they could assume a key role in the fast GCFR, where the power density is much higher.

The considered problem (1-phase coolant flow in complex geometry with the aim to obtain very accurate data) suggests that CFD codes should be used. So, the problem was simulated using FLUENT code [4].

In order to define preliminary fluid-dynamic conditions (laminar or turbulent regime) of the problem, it was necessary to estimate the Re value for the considered cases. It is important to highlight that this is a different formulation of Re by that required by (1)—(5). Starting from already published data (see as an example [5] or [12]), it was chosen the formula for Re in pebble-bed proposed in [12]:

$$\mathrm{Re} = \frac{G_e' D_e'}{\mu}, \quad (6)$$

where

$$G_e' = \frac{\dot{m}'}{A_{\mathrm{flows}}'} = \frac{\dot{m}'}{(\pi(D_e'/4))},$$

$$D_e' = \frac{4(V' - V_s')}{A_s'}, \quad (7)$$

$$\dot{m}' = (\dot{m}_t)\left(\frac{A_{\mathrm{core}}'}{A_{\mathrm{core}}}\right),$$

where V' is the total core volume, V_s' is the CPs volume, A_s' is the CPs surface, $\dot{m}_t$ is the coolant flow, A_{core}' is the CPs cross section, A_{core} is the whole core cross section.

As a result, for all the considered cases (adopting the above mentioned formula) Re well above 10000 have been obtained, so they are characterized by a fully turbulent regime.

5. Methods

5.1. Minimum Cell Dimensions. In order to model the turbulence correctly, the three "classical" approaches have been considered:

(i) Direct Numerical Simulation (DNS),

(ii) Reynolds Averaged Navier Stokes (RANS) equations [13],

(iii) Large Eddy Simulation (LES) [12, 14].

For the calculations a segregated numerical method has been chosen and the turbulence has been treated by an RANS approach, using an RNG k-ε, model. This latter, in comparison with the simple k-ε model could be extended also to the laminar region near the wall without adopting the so-called wall functions [15]. RNG k-ε model is based on a well-known mathematical theory as described in [16].

As a first step, in order to define the minimum cell dimensions for a meaningful model, the influence of the number of CPs number in the considered area has been investigated: particularly many different cell sizes (ranging from 4 to 32 CPs) have been considered. Due to the limited geometrical dimensions, as an approximation, a constant and uniform heat production inside the CPs has been imposed equivalent for the whole core to 40 MW/m^3 [9] (this relatively "low" value was assumed taking into account that the maximum power density for a particle-bed GCFR is limited if compared to a GCFR with a different fuel form, as indicated also in [13, 17]). The previous assumption could be plainly justified if we look at the (considered) CP dimensions (diameter ~1 mm): those dimensions are so limited that a single CP cannot significantly modify the incident fast neutron flux; as a consequence the reaction rates remain substantially unchanged.

For boundary conditions, the He inlet velocity has been set at 30 m/s (opposite to gravity direction) while the coolant outlet pressure has been set at 69 bar [9]. In addition symmetry (cyclic) boundary conditions along x and y directions. have been imposed(This hypothesis was based on the assumption to consider the cell well inside the core and not near the physical boundaries.) .

As a result we have obtained that no significant differences have been found for a CP numbers inside the cell ranging from 8 to 32. So the minimum basic cell is composed by 8 CPs.

5.2. Packing Factor Influence. As a second parameter to be investigated, the packing factor (PF) has been considered. So, in order to identify the influence of this parameter, two basic cells (with the highest and the lowest packing factors) have been considered. The first one (Simple Cubic, SC with a PF = 0.52) is reported in Figure 2, while the second (Face-Centred Cubic, FCC with a PF = 0.74) in Figure 3. For comparison, the experimental average PF in a typical PBMR core is ~0.61 [18].

For this comparison the boundary conditions have been assumed, as anticipated, on the basis of simulations previously performed[5] using RELAP5-3D code[6], assuming

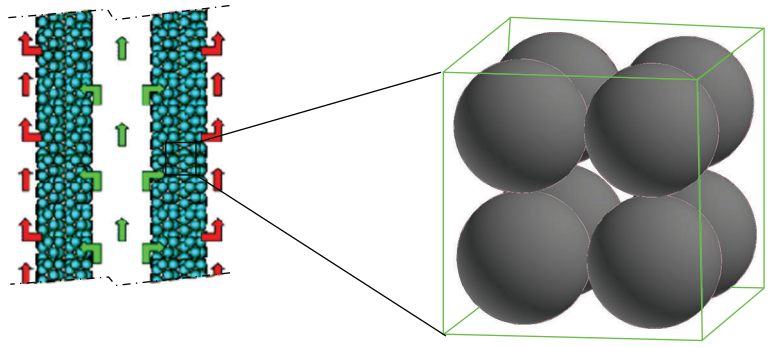

Figure 2: Basic GCFR core cell (Simple Cubic, SC).

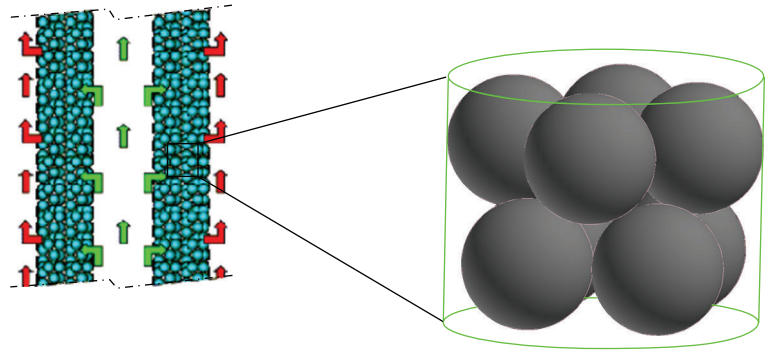

Figure 3: Basic GCFR core cell (Face-Centred Cubic, FCC).

the input parameters from the ETDR core[5]. Particularly some relevant points have been selected from the results obtained for the steady state and the transient RELAP calculations, distinguishing between the average and the hot channels.

So, some of the global values supplied by the RELAP simulations (i.e., the pressure level, the average temperature at the inlet of the cell) have been assumed as input parameters for the FLUENT local calculations while the others have been evaluated starting from the same global values. For example, looking at Figure 5, in order to evaluate the mean outlet temperature for a cell located at the point "new2" z-level (z^{new2}), a linear temperature trend between the points "new2" ($T = T^{\text{RELAP\_new2}}$) and "new3" ($T = T^{\text{RELAP\_new3}}$) has been assumed; then, for the cell located in "new2", the outlet temperature (i.e., the T value at $z = z_{\text{out}}^{\text{cell\_new2}}$) has been calculated with the following formula:

$$T_{\text{out}}^{\text{cell\_new2}} = T^{\text{RELAP\_new2}} + \left(T^{\text{RELAP\_new3}} - T^{\text{RELAP\_new2}}\right) \cdot \frac{z_{\text{out}}^{\text{cell\_new2}} - z^{\text{new2}}}{z^{\text{new3}} - z^{\text{new2}}}. \quad (8)$$

For each point two different FLUENT simulations (one for SC and the other for FCC cells) have been performed.

6. Calculations

As already anticipated, all the CFD calculations were performed using as boundary conditions the results obtained by previous RELAP5-3D simulations on the ETDR plant [5, 19], both for Steady State and Transient conditions. So, in the following subparagraphs, all the general temperature trends reported in the figures were obtained in those RELAP simulations [5, 19] and were used as basis for the CFD simulations.

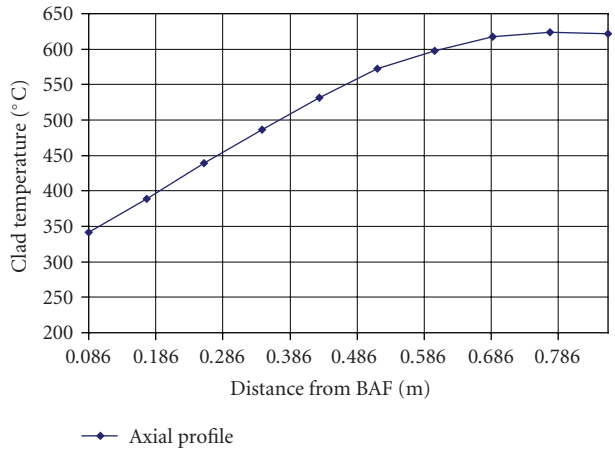

Figure 4: Temperature axial profile—Steady State—Average Channel.

6.1. Steady State—Average Channel. The temperature axial trend in the average channel for the steady state condition is reported in Figure 4.

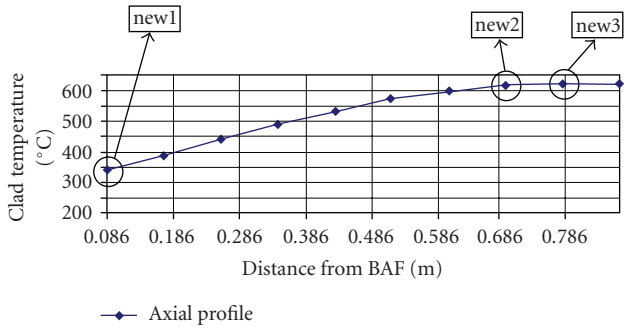

Figure 5: Temperature axial profile (Steady State—Average Channel) with the points selected for the CFD simulations identified.

In Figure 5 the same profile is reported with the points selected for the CFD simulations evidenced by a circle and identified by an abbreviation.

The main results obtained for the "new1" point are reported in the following Figures 6, 7, 8 and 9.

In order to evaluate (at least qualitatively) the velocity field and the amount of stagnation points (where the velocity magnitude is zero or just above zero), some velocity magnitude bar charts are reported in Figures 8 and 9. Please note that the normalization was automatically performed by the code.

The results obtained for "new2" and "new3" points show that temperature profiles and velocity fields are quite similar from a qualitative point of view.

6.2. Steady State—Hot Channel. The temperature axial trend in the hot channel for the steady-state condition is reported in Figure 10.

In Figure 11 the same profile is reported with the points selected for the CFD simulations evidenced by a circle and identified by an abbreviation.

The obtained results for the "hot1," "hot2," and "hot3" points show that temperature profiles and velocity fields are quite similar to those shown in Figures 6, 7, 8 and 9 (at least from a qualitative point of view).

6.3. Transient (LOFA)—Average Channel. In order to extend the range of potential cases to be studied by FLUENT code, there has been simulated [5, 19] (by RELAP5-3D) also a transient, namely, a Loss Of Flow Accident (LOFA). This particular transient was chosen for two reasons.

(i) We had all the needed data to perform this calculation [20].

(ii) It is a quite serious transient for the considered plant.

The temperature axial trends in the average channel for the transient condition are reported in Figure 12.

In Figure 13 the same profiles are reported with the points selected for the CFD simulations evidenced by a circle and identified by an abbreviation.

Again the results obtained for all the selected points show temperature profiles and velocity fields quite similar, at least from a qualitative point of view. So, in order to avoid to show too many similar figures, it will be shown in the next Figures 14, 15, 16 and 17 some results related only to "trs1" case.

Again, in order to evaluate (at least qualitatively) the velocity field and the amount of stagnation points (where the velocity magnitude is zero or just above zero), some velocity magnitude bar charts are reported in Figures 16 and 17. Please note that the normalization was automatically performed by the code.

6.4. Transient (LOFA)—Hot Channel. The last considered case is the hot channel for the LOFA transient. The related temperature axial trends are reported in Figure 18.

In Figure 19 the same profiles are reported with the points selected for the CFD simulations evidenced by a circle and identified by an abbreviation.

Once again the results obtained for all the selected points shows temperature profiles and velocity fields that are quite similar, (at least from a qualitative point of view) to those already shown.

7. Discussion

From the obtained results there appears the great influence of the PF on the local parameters. Even if we look at the variations of other "macroscopic" parameters (average helium temperature in the cell, mean coolant temperature difference between inlet and outlet, etc.) in reasonable conditions (i.e., as determined by RELAP simulations), it appears that the PF remains the key factor. To underline this consideration it is useful to have a look to Tables 1 and 2, where for each considered point, the following has been reported:

(i) maximum temperature difference between two points inside the cell ($\Delta T^{\max}$),

(ii) absolute value of the mean coolant temperature difference between inlet and outlet ($|\Delta T_{\text{out-in}}|$),

(iii) average helium inlet temperature (T_{in}).

Looking at the tables it could be noted that, even for the wide variations of the considered "global" parameters, $\Delta T^{\max}$ ranges for the SC cell between 9.46°C and 10.92°C while for the FCC cell it ranges between 14.78°C and 15.34°C.

From the obtained results it can be also noted the presence of some stagnation points, where the velocity magnitude is zero or just above zero. As evidenced in some figures (look as an example at Figures 8 and 9), due to the geometrical configuration, the number of stagnation points is higher for FCC cell than for SC one.

To summarize, even in transient conditions, the variations of the considered parameters (average helium temperature in the cell, mean coolant temperature difference between inlet and outlet, pressure drops, etc.) are less significant for the local parameters when compared with those due to the assumed PF. As a consequence, in a more general core calculation (usually modelled by a porous medium), the obtained temperature (and velocity) values will have to be

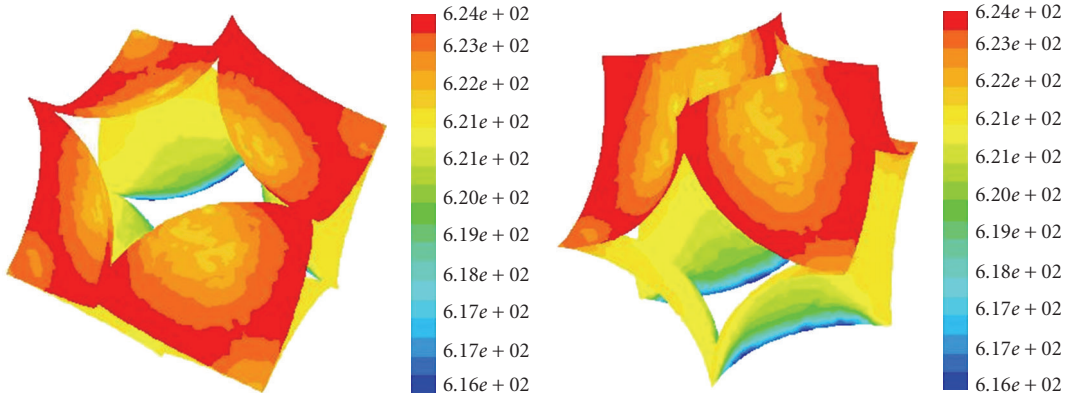

Figure 6: Two views of the wall temperature distribution (in Kelvin degrees) for SC cell "new1" (Steady State—Average Channel).

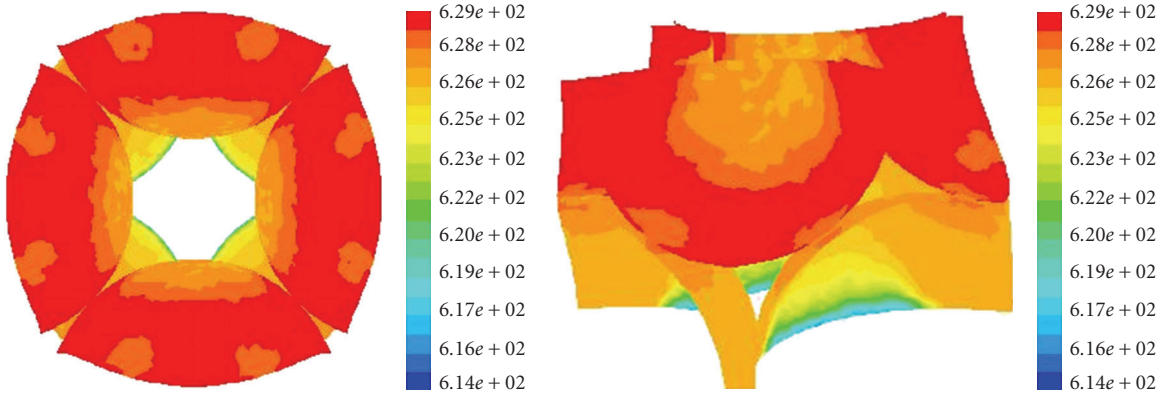

Figure 7: Two views of the wall temperature distribution (in Kelvin degrees) for FCC cell "new1" (Steady State—Average Channel).

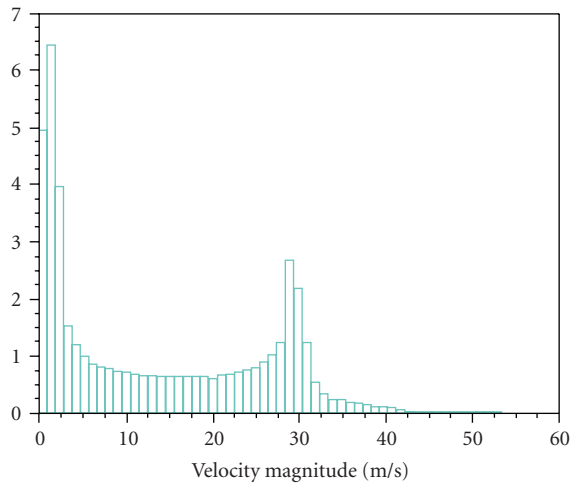

Figure 8: Bar chart showing (normalized) number of points versus velocity for SC cell "new1" (Steady State—Average Channel).

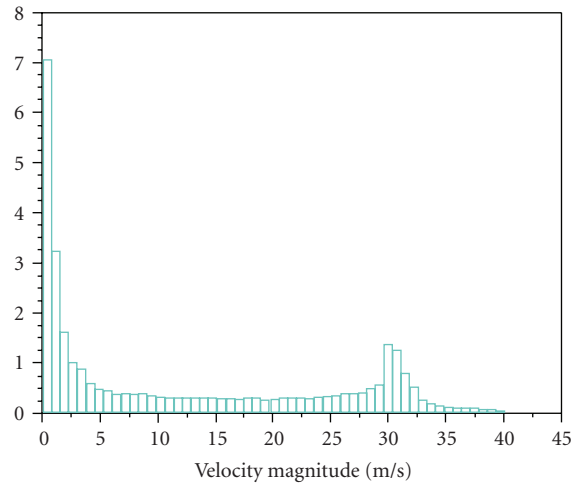

Figure 9: Bar chart showing (normalized) number of points versus velocity for FCC cell "new1" (Steady State—Average Channel).

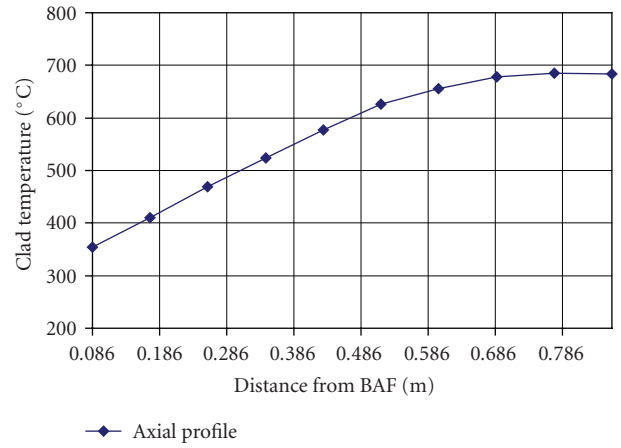

Figure 10: Temperature axial profile—Steady State—Hot Channel.

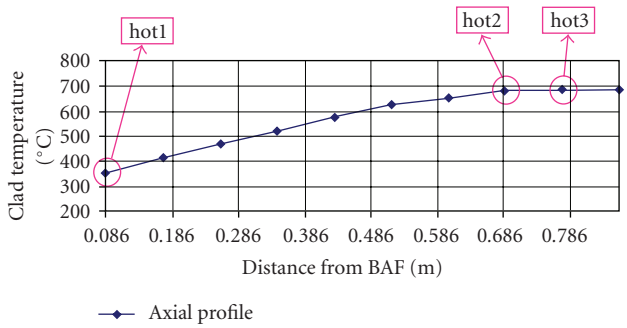

Figure 11: Temperature axial profile (Steady State—Hot Channel) with the points selected for the CFD simulations identified.

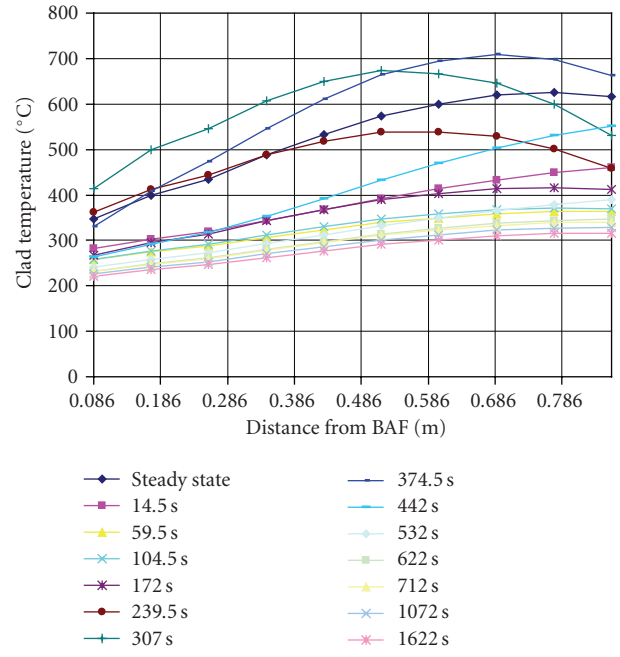

Figure 12: Temperature axial profile—LOFA—Average Channel.

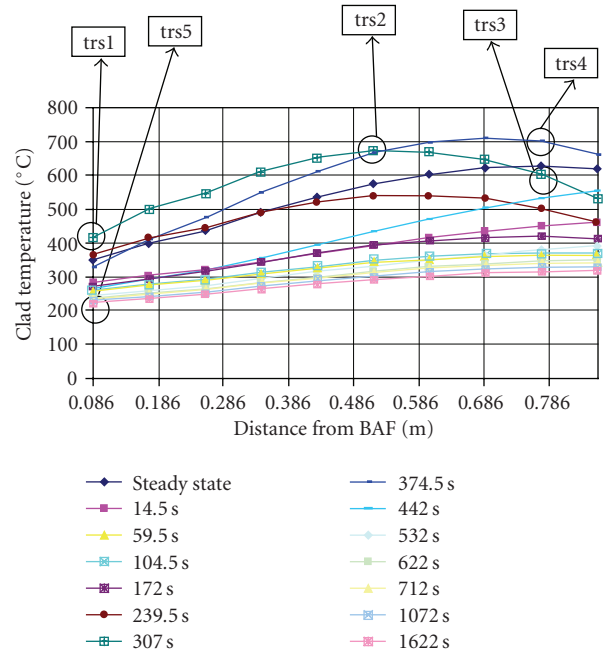

Figure 13: Temperature axial profile (LOFA—Average Channel) with the points selected for the CFD simulations identified.

Table 1: Parameters for SC cell.

	ΔT^{max} [°C]	$\lvert\Delta T_{out\text{-}in}\rvert$ [°C]	T_{in} [°C]
trs5	9.51	0.328	221.376
new1	9.5	1.1	341.155
hot1	9.5	1.29	354.606
trs1	9.5	1.97	414.342
trh1	9.71	0.384	503.457
trs3	10.92	1.622	600.272
new2	9.88	0.13	617.766
new3	9.5	1.63	623.314
trs2	9.56	0.16	673.815
hot2	9.46	0.16	678.606
hot3	9.51	0.04	685.416
trs4	10.3	0.833	698.148
trh5	10.15	1.47	724.635
trh3	9.76	0.417	807.809

corrected by a factor that takes into account in the results of this research. In fact it is important to highlight that the results have been obtained for a cell with height $h \leq 2$ mm, while a real core will have a total height >2000 mm. Although the corrective peak factors could not be calculated in a simple additive way, the global values (and relative differences) will be obviously much higher than those calculated here.

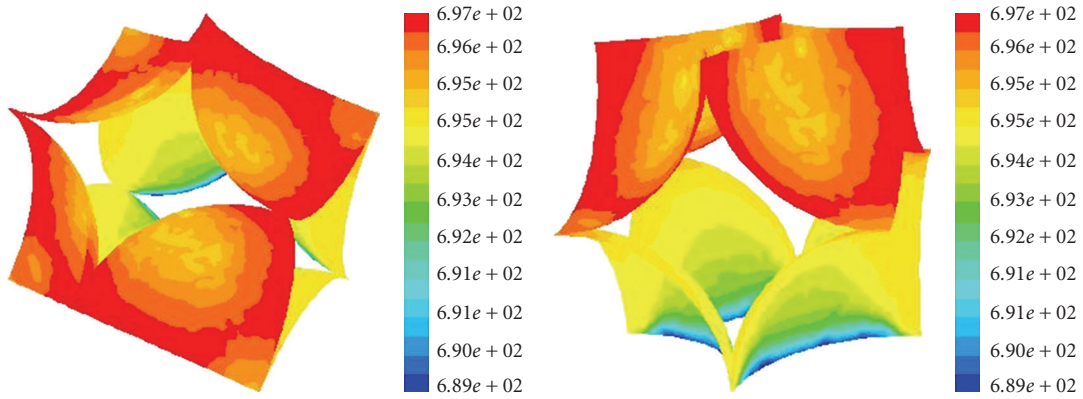

Figure 14: Two views of the wall temperature distribution (in Kelvin degrees) for SC cell "trs1" (LOFA—Average Channel).

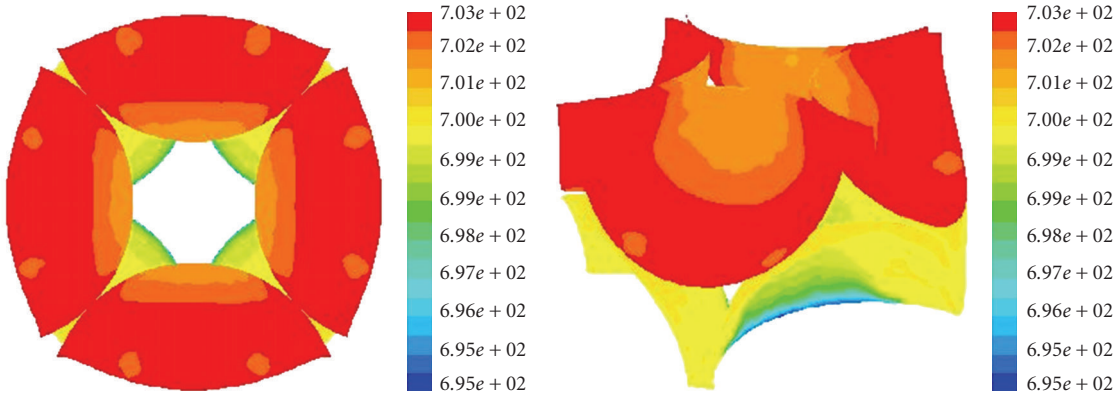

Figure 15: Two views of the wall temperature distribution (in Kelvin degrees) for FCC cell "trs1" (LOFA—Average Channel).

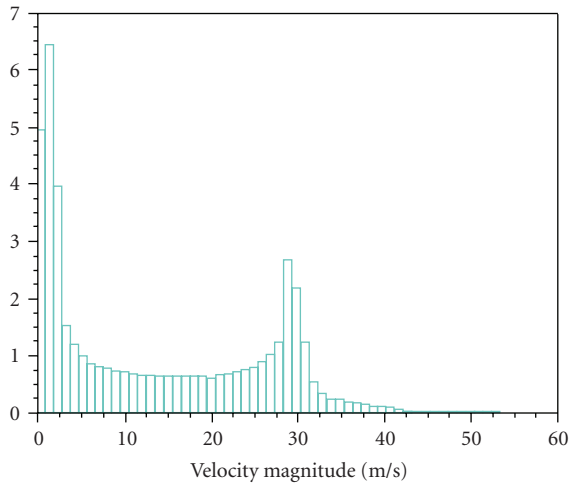

Figure 16: Bar chart showing (normalized) number of points versus velocity for SC cell "trs1" (LOFA—Average Channel).

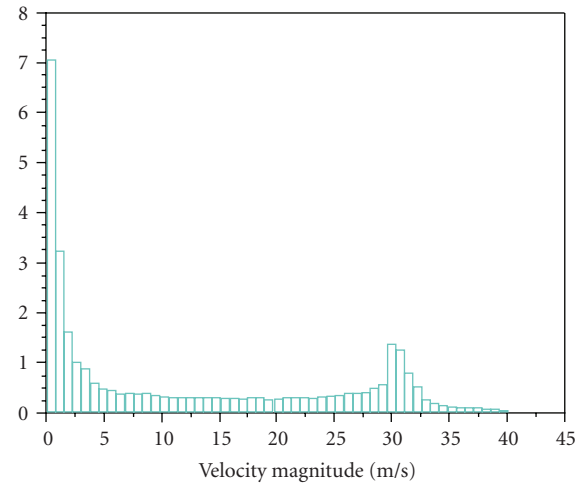

Figure 17: Bar chart showing (normalized) number of points versus velocity for FCC cell "trs1" (LOFA—Average Channel).

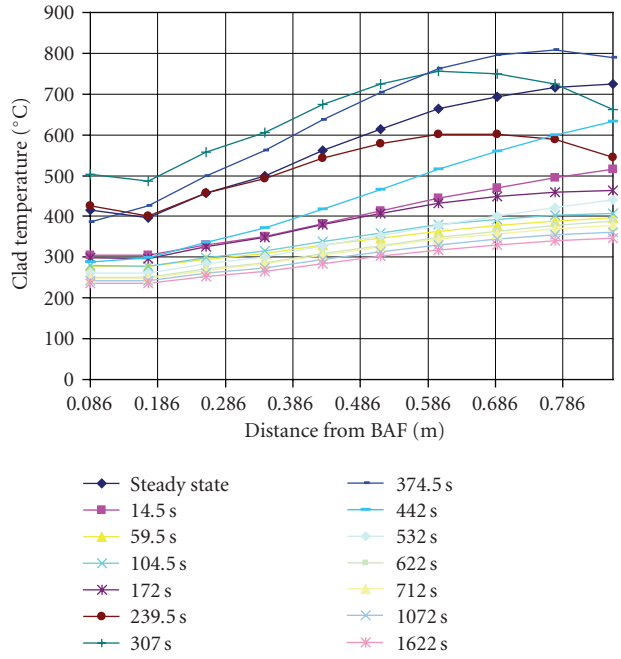

Figure 18: Temperature axial profile—LOFA—Hot Channel.

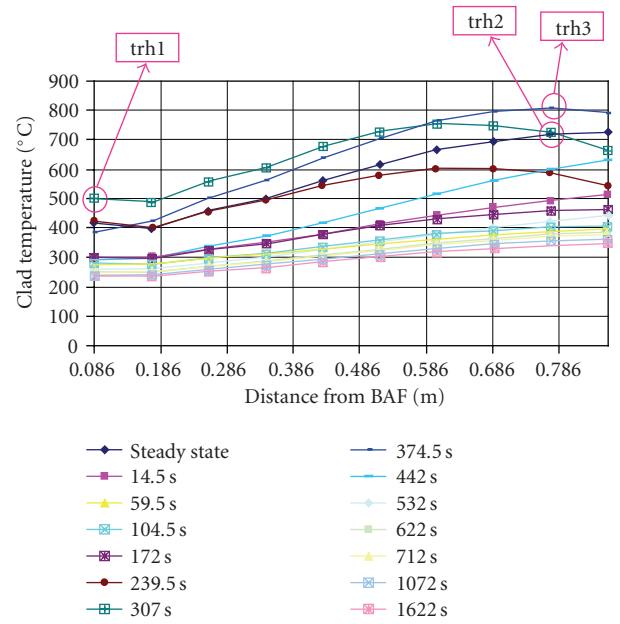

Figure 19: Temperature axial profile (LOFA—Hot Channel) with the points selected for the CFD simulations identified.

8. Conclusions

The issue related to the cooling by helium of a high power density GCFR core is complex and, up to now, not extensively studied. Also for this reason this research seems to be quite original and innovative, although the obtained results will have to be further validated by code-to-experiment comparisons, too.

Table 2: Parameters for FCC cell.

	ΔT^{max} [°C]	$\lvert\Delta T_{out\text{-}in}\rvert$ [°C]	T_{in} [°C]
trs5	14.8	0.28	221.376
new1	14.79	0.94	341.155
hot1	14.79	1.1	354.606
trs1	14.79	1.7	414.342
trh1	14.95	0.33	503.457
trs3	15.34	0.71	600.272
new2	14.79	0.11	617.766
new3	14.81	0.03	623.314
trs2	14.78	0.16	673.815
hot2	15.24	0.14	678.606
hot3	14.8	0.03	685.416
trs4	15.21	0.833	698.148
trh5	15.15	1.47	724.635
trh3	14.96	0.36	807.809

From a deep analysis of the analyzed problem, the influence of the PF on the local temperatures distributions and velocity fields looks quite evident. Particularly looking at the obtained results it could be noted that, even for wide variations of the considered "global" parameters, ΔT^{max} ranges for SC cell between 9.46°C and 10.92°C while for FCC cell it ranges between 14.78°C and 15.34°C. So, even in transient condition, the variations of the considered parameters (average helium temperature in the cell, mean coolant temperature difference between inlet and outlet, pressure drops, etc.) are less significant for the local parameters when compared with those due to the assumed PF.

In a real case the CP distribution will be stochastical. Therefore it will be necessary, during the design stage, to assume (in a conservative way) the higher hot spot values, at least until it will be possible to have a reliable way to shrink the PF variation range. At least at the moment, in a more general core calculation (usually modelled by a porous medium), the obtained temperature (and velocity) values will have to be corrected by a factor that would have to take into account the results of the present research.

Finally, as another possible future development, it is important to highlight that, in order to have a reliable and accurate TFD evaluation of an innovative gas-cooled reactors, it will be mandatory to quantify adequately the neutronic source term. So it will be important to perform coupled iterative neutronic-TFD calculations, where the power generation will be the output for the neutronics and a boundary condition for TFD, while, the temperature distribution will be the output for TFD and a boundary condition for the neutronics. That could be made either by multi-physics coupled codes or by coupling separate neutronic and TFD codes which are run in parallel.

Acknowledgments

The work presented in this paper was partly funded by the European Union Sixth Framework Program, under contracts GCFR, PuMA and RAPHAEL. First of all the authors like

to thank Engineer Castelliti of SCK•CEN, Dr. Kuijper and Dr. van Heek both of NRG, Professor Kloosterman of TUD, Dr. von Lensa of FZJ and Dr. Mitchell and Dr. Stainsby both of AMEC-NNC for their support. Finally they want to thank Professor Forasassi of DIMNP for his very appreciated collaboration and Dr. Bufalino of SORIT for his precious suggestions and help.

References

[1] N. Cerullo, G. Guglielmini, A. F. Massardo, and M. Paganini, "Il reattore modulare a gas ad alta temperatura con turbina a gas in ciclo diretto: un impianto nucleare intrinsecamente sicuro ad alta efficienza," *La Termotecnica*, vol. 48, no. 11, 1994.

[2] N. Cerullo, W. Grassi, and G. Lomonaco, "Analisi termofluidodinamica della configurazione a letto di particelle per un reattore nucleare veloce refrigerato a gas," in *Congresso Nazionale UIT sulla Trasmissione del Calore (UIT '05)*, Parma, Italy, June 2005.

[3] The Generation IV International Forum, http://www.gen-4.org/index.html.

[4] http://www.ansys.com/products/fluid-dynamics/fluent/.

[5] G. Lomonaco, *Analisi termofluidodinamica dei reattori nucleari innovativi refrigerati a gas*, Ph.D. thesis, University of Pisa, Pisa, Italy, May 2007, Ph.D. Thesis in Thermal and Electric Energetics, supervisors: Prof. N. Cerullo, Prof. W. Grassi, http://www.tesionline.it/default/tesi.asp?idt=17893.

[6] The RELAP5-3D© Code Development Team, "*RELAP5-3D© Code Manual*" INEEL-EXT-98-00834, rev. 2.3, April 2005.

[7] M. van Staden, C. van Rensburg, and L. le Grange, "Thermo-hydraulic modeling of heat removal for the PBMR helium gas cooled reactor using CFD," in *Proceedings of International Congress on Advances in Nuclear Power Plants (ICAPP '03)*, Cordoba, Spain, May 2003.

[8] O. Cioni, M. Machand, G. Geffraye, and F. Ducros, "Thermal hydraulic 3D calculations on the core of a high temperature gas cooled reactor," in *Proceedings of the 2nd International Topical Meeting on High Temperature Reactors (HTR '04)*, pp. 1–16, Beijing, China, September 2004.

[9] A. Conti and A. Ravenet, "GCFR fuel element and sub-assembly concepts," in *GFR/ETDR Seminar*, CEA-Cadarache, Grenoble Cedex, France, Novembre 2004.

[10] K. Kugeler and R. Schulten, *Hochtemperatur-Reaktortechnik*, Springer, Berlin, Germany, 1989.

[11] S. Ergun, "Fluid flow through packed columns," *Chemical Engineering Progress*, vol. 48, no. 2, pp. 89–94, 1952.

[12] G. Yesilyurt and Y. A. Hassan, "LES simulation in pebble bed modular reactor core through randomly distributed fuel elements," in *Proceedings of the International Conference on Global Environment and Advanced Nuclear Power Plants (GENES4/ANP '03)*, Kyoto, Japan, September 2003.

[13] H. Ohshima and T. Nagata, "Numerical study on thermal hydraulics in coated-particle-type fuel assembly of helium gas cooled fast reactor," in *Proceedings of the 12th International Conference on Nuclear Engineering (ICONE-12)*, Washington, DC, USA, April 2004.

[14] G. Yesilyurt and Y. A. Hassan, "Large eddy simulation for high temperature gas reactors," in *Proceedings of International Congress on Advances in Nuclear Power Plants (ICAPP '03)*, Cordoba, Spain, May 2003.

[15] G. Comini, G. Croce, and E. Nobile, *Fondamenti di Termofluidodinamica Computazionale*, SGE, Padova, Italy, 2004.

[16] V. Yakhot and S. A. Orszag, "Renormalization group analysis of turbulence—I: basic theory," *Journal of Scientific Computing*, vol. 1, no. 1, pp. 3–51, 1986.

[17] T. A. Taiwo, T. Y. C. Wei, E. E. Feldman, et al., "Particle-bed gas-cooled fast reactor (PB-GCFR) design. Project final technical report (September 2001–August 2003)," Tech. Rep. NERI 01-022, Argonne National Lab., Argonne, Ill, USA, September 2003.

[18] International Atomic Energy Agency, "Thorium fuel utilization: options and trends," IAEA-TECDOC-1319, November 2002.

[19] D. Castelliti, E. Bomboni, N. Cerullo, G. Lomonaco, and C. Parisi, "GCFR coupled neutronic and thermal-fluid-dynamics analyses for a core containing minor actinides," *Science and Technology of Nuclear Installations*, vol. 2009, Article ID 573481, 8 pages, 2009.

[20] E. Bubelis, D. Castelliti, P. Coddington, et al., "A GFR benchmark comparison of transient analysis codes based on the ETDR concept," in *Proceedings of International Congress on Advances in Nuclear Power Plants (ICAPP '07)*, Nice Acropolis, France, May 2007.

Hindawi Publishing Corporation
Science and Technology of Nuclear Installations
Volume 2009, Article ID 238624, 7 pages
doi:10.1155/2009/238624

Project Report

Gas Cooled Fast Reactor Research and Development in the European Union

Richard Stainsby,[1] Karen Peers,[1] Colin Mitchell,[1] Christian Poette,[2] Konstantin Mikityuk,[3] and Joe Somers[4]

[1] *AMEC, Booths Park, Chelford Road, Knutsford, Cheshire WA16 8QZ, UK*
[2] *Commissariat à l'Energie Atomique, CEA Cadarache, 13108 Saint Paul Les Durance, France*
[3] *Paul Scherrer Institut, Villigen PSI, Villigen 5232, Switzerland*
[4] *Joint Research Centre, Institute for Transuranic Elements (ITU), P.O. Box 2340, Karlsruhe 76125, Germany*

Correspondence should be addressed to Richard Stainsby, richard.stainsby@amec.com

Received 7 April 2009; Accepted 14 October 2009

Recommended by Guglielmo Lomonaco

Gas-cooled fast reactor (GFR) research is directed towards fulfilling the ambitious goals of Generation IV (Gen IV), that is, to develop a safe, sustainable, reliable, proliferation-resistant and economic nuclear energy system. The research is directed towards developing the GFR as an economic electricity generator, with good safety and sustainability characteristics. Fast reactors maximise the usefulness of uranium resources by breeding plutonium and can contribute to minimising both the quantity and radiotoxicity nuclear waste by actinide transmutation in a closed fuel cycle. Transmutation is particularly effective in the GFR core owing to its inherently hard neutron spectrum. Further, GFR is suitable for hydrogen production and process heat applications through its high core outlet temperature. As such GFR can inherit the non-electricity applications that will be developed for thermal high temperature reactors in a sustainable manner. The Euratom organisation provides a route by which researchers in all European states, and other non-European affiliates, can contribute to the Gen IV GFR system. This paper summarises the achievements of Euratom's research into the GFR system, starting with the 5th Framework programme (FP5) GCFR project in 2000, through FP6 (2005 to 2009) and looking ahead to the proposed activities within the 7th Framework Programme (FP7).

1. Introduction

The European Commission (EC) Gas Cooled Fast Reactor GCFR project was initiated in 2000 under the 5th Framework Programme ([1–3]) and followed in March 2005, by a 4-year project within the 6th Framework Programme [4]. Between the two projects, there was a significant change in emphasis from an evolutionary development, which could be realised on a relatively short timescale, to an ambitious innovative development that could achieve the full potential of the system. This change in emphasis coincided with the Generation IV International Forum (GIF) initiative, which was launched in 2000 and selected GFR as one of the promising systems for development.

The FP6 project recognised that the European experience in gas cooled reactor technology was unparalleled with more than a thousand years of gas thermal reactor operating experience together with the construction of four large sodium-cooled fast reactors and a number of in-depth design studies for gas cooled fast rectors. This experience was dispersed within the member countries and research centres, and the FP6 GCFR STREP was an opportunity to ensure that the value of this experience was realised, further developed, and retained in the next generation of scientists and engineers.

The FP5 GCFR project ([1–3]) was in three parts; the first part reviewed the relevant gas cooled reactor experience to re-establish the extent of the knowledge base and to provide assurance that the lessons had been learnt from previous studies. This formed one of the work packages with two others devoted to safety of gas cooled fast reactors and integration in the nuclear fuel

cycle. The FP5 project concluded that the evolutionary concepts were sound and that experience from the thermal reactor operation provided further support for the system and sodium-cooled fast reactor operation provided added confirmation for the fuel, core, and fuel reprocessing. A safety approach was proposed as part of the FP5 project for future GCFRs, which was developed further within FP6, and some critical transients were analysed. The fuel cycle study demonstrated the flexibility of the GFR to adapt to the prevailing needs of the fuel cycle ranging from the traditional breeder role to an incinerator of plutonium and minor actinides.

The renewed interest in GFRs from the 1990s (albeit with a modest level of support) continued the evolutionary development path pursued by the European Gas Breeder Reactor Association and General Atomics during the 1970s. The important change that took place between FP5 and FP6 was the removal of the time constraint that limited the extent of innovation that was possible (see, e.g., [5] for a GFR based on existing technology). Hence the requirement of the 1970s, to be able to introduce a prototype GFR within 2 years, without the intermediate step of an experimental reactor, was transformed to the current situation, where commercial series construction may not be required until the middle of the 21st century. This opens the opportunity to realise the full potential of GFR through innovative design and development.

The FP6 GCFR STREP was fully integrated into the Generation IV development programme for GFR and shared its ambitious goals. Together with a direct contribution from the European Commission's Joint Research Centre (JRC) towards development of the fuel and core materials, it formed Euratom's contribution to the Generation IV International Forum (GIF). The GCFR STREP was jointly funded by the European Commission and more than 10 participating companies, R&D organizations, and universities, with a total budget of €3.6 M over four years.

During the FP6 project, the European Commission established the "Sustainable Nuclear Energy Technology Platform (SNE-TP)" [6]. This platform sets out a vision for the development of nuclear fission systems within Europe with the aim of increasing sustainability through better use of natural resources, minimisation of waste, and by the replacement of less- (or non-) sustainable technologies. The aims of the SNE-TP are largely aligned with those of Generation IV, but stated from a European perspective. Understandably, fast reactors feature strongly within the strategic research agenda (SRA) [7] of the SNE-TP, as does the development of the nonelectricity applications, such as hydrogen production, using high temperature reactors. The SNE-TP identifies sodium-cooled fast reactors as the best near-term technology that will allow commercial fast reactors to be deployed on the shortest timescale. The alternatives of GFR and the lead-cooled fast reactor (LFR) are considered as being promising candidate technologies for improving the performance of fast reactors in the longer term with the potential of inheriting the non-electricity applications from the high temperature thermal reactors.

The research programme for GFR within the 7th Framework is being drafted at the time of writing this paper. Again, the European project will serve as Euratom's contribution to the GIF, but now this also has to be aligned with vision and the strategic research agenda of the SNE-TP, in which GFR must earn its place as a viable longer term fast reactor technology. Whilst the FP6 project was wide ranging in keeping with spirit of the Gen IV exploratory and preconceptual phases, the FP7 project is more narrowly focused and must demonstrate the viability of GFR for deployment as commercial system.

2. Realising the Full Potential of GFR

The GFR is one of six reactor concepts selected within the GIF [8], three of which are dedicated fast reactors that are attractive because of their potential to meet the Gen IV sustainability goal by both dramatically improving the utilisation of fissile material and by substantially reducing the quantity and radiotoxicity of radioactive waste. Particular merits of GFR are the hard neutron spectrum and the synergy it has with the Very High Temperature Reactor (VHTR), which is also one of the six selected Gen IV concepts. The latter is important for the GFR development strategy, in order to take full advantage of the VHTR development. The two reactor concepts have a common coolant (helium) and both aim for high core outlet temperatures to maximise the thermal efficiency for electricity generation and enhance prospects for hydrogen generation and, as such, share much materials and components technology.

In addition to sustainability, there are important Gen IV goals for Proliferation Resistance, Economics and Safety. The Gen IV goals and their influence on the GFR concept are identified in the GFR System Research Plan [9] and are summarised as follows.

(i) *Sustainability.* This is the key objective for the GFR system. This means full utilisation of uranium resources and calls for the recycling of actinides in a closed cycle. Furthermore, the minimisation of waste and its radiotoxicity requires recycling of both plutonium and the minor actinides together in an integral homogeneous recycling of all actinides present in used fuel. The removal and recycling of certain long-lived fission products (LLFPs) will also be considered.

(ii) *Nonproliferation.* The necessity to avoid, as far as possible, separated materials in the fuel cycle potentially implies minimising the use of fertile blankets. The objective of high burn-up together with actinides recycling results in spent fuel characteristics (isotopic composition) that are unattractive for handling. High burn-ups are the final objective (10–15 at % or more). Minimisation of fuel transport would help proliferation concerns and could be realisable, if very compact facilities can be designed, with onsite fuel treatment.

(iii) *Economics.* A high outlet temperature (850°C or more) is selected for high thermal efficiency, with the

use of gas turbine or combined (gas turbine + steam turbine) power conversion cycle and the potential for hydrogen production via the thermo-chemical splitting of water. Gen IV objectives for construction time and costs are also considered.

(iv) *Safety.* The design objective is for no offsite radioactivity release and it requires effectiveness, simplicity, robustness, and reliability of systems and physical barriers. The main development challenges, therefore, are refractory fuels with good fission product retention capability at high temperature (1600°C, or above), the selection of robust structural materials, and the design of effective and highly reliable decay heat removal systems.

With regard to the above goals, two design parameters, temperature and power density, have particular importance. High temperatures are particularly challenging and require innovative fuel and encapsulation concepts. As these are key to the system reaching its full potential, this largely sets the developmental timescale. The power density has a wide-ranging influence, affecting economics (minimisation of fuel inventory, of fuel cycle cost, compactness of the primary vessel), sustainability (reactors with low enough plutonium inventories to allow sufficient flexibility in the fuel cycle for long-term deployment), and safety (in particular decay heat removal in the case of a depressurisation event). Economics and sustainability require higher power densities and safety suggests lower values. The tentative range, approaching 100 MWth/m^3, lies well above gas-cooled thermal reactor values of about 5 MWth/m^3, but still significantly less than sodium-cooled fast reactor power density of about 400 MWth/m^3.

Whilst a phased development path may be drawn from the thermal to the fast-spectrum gas-cooled systems, significant innovation is required to address the technology gaps in order to achieve the ambitious GFR goals. The main technical challenges which are specific to the GFR that must be addressed in demonstrating the viability of the reactor, core and safety systems, and the fuel and fuel cycle processes are:

(i) fuel forms for high temperature operation and tolerance of fault conditions,

(ii) core design, achieving a core that is self-sustaining in fissile material but without the use of heterogeneous fertile "breeder" blankets,

(iii) safety, including decay heat removal systems that address the significantly higher power density (in the range of 100 MWth/m^3) and the reduction of the thermal inertia provided by the moderator in thermal reactor designs, or the liquid metal coolant in other fast reactor systems,

(iv) fuel cycle technology, including simple and compact spent-fuel treatment and refabrication for recycling,

(v) development of core materials with superior resistance to fast-neutron fluence under very-high-temperature conditions with good fission product retention capabilities.

The developmental challenges related to the power conversion system are shared and generally less onerous than those of the VHTR. Alternative conversion cycles are possible and an indirect cycle based on an indirect supercritical CO_2 offers the possibility of a less-challenging moderate-temperature option whilst retaining high thermal efficiency. This option removes the possibility of hydrogen production via thermo-chemical splitting, but still allows its economic production using electrolysis. The latter cycle introduces specific R&D challenges for the power conversion systems that are not shared with the VHTR.

3. Euratom GFR Projects

Two parallel tracks of work have been pursued throughout the FP6 project. These were to develop the concept for a medium-sized to large commercial GFR and to develop the design of a small demonstration plant which has subsequently become known as ALLEGRO. Parallel activities existed in both tracks, concentrating on system design, system safety studies, and methods development. In addition there was a cross-cutting fuels work package aimed at developing fuel concepts for both systems.

3.1. ALLEGRO: A GFR Demonstrator. An experimental reactor is an essential step to establish confidence in the innovative GFR technology. This is in marked contrast to the earlier GCFRs of the 1970s which were based on existing technology to justify the short cut to a prototype/demonstration plant at large size. The proposed experimental reactor, named ALLEGRO, would be the first ever gas cooled fast reactor to be constructed. It will be a small experimental reactor with a power of around 80 MWth. The objectives of ALLEGRO are to demonstrate the viability and to qualify specific GFR technologies such as the fuel, the fuel elements, and specific safety systems, in particular, the decay heat removal function, together with demonstrating that these features can be integrated successfully into a representative system. ALLEGRO will be an essential step in the decisions to be made by 2019 for the launching of a prototype GFR system. As such, it intervenes in the fuel development programme between the small-scale irradiation of materials and fuel samples in material test reactors (MTRs), and available fast reactors, and the full-scale demonstration phase in the prototype GFR.

An important element of the strategy is to take advantage of the synergies with VHTR development. The helium coolant and concepts for energy conversion using a gas turbine are common to both systems, so materials and component research carried out for VHTR are largely relevant to GFR. The implications are that ALLEGRO addresses only the development that is specific to GFR, and having a low power output, it does not require a power conversion system. The main elements of the ALLEGRO system are shown in Figure 1.

ALLEGRO is intended to have three distinct phases of operation based on three different core configurations: a starting core, a starting core in which some of the fuel elements are replaced by modified GFR ceramic fuel

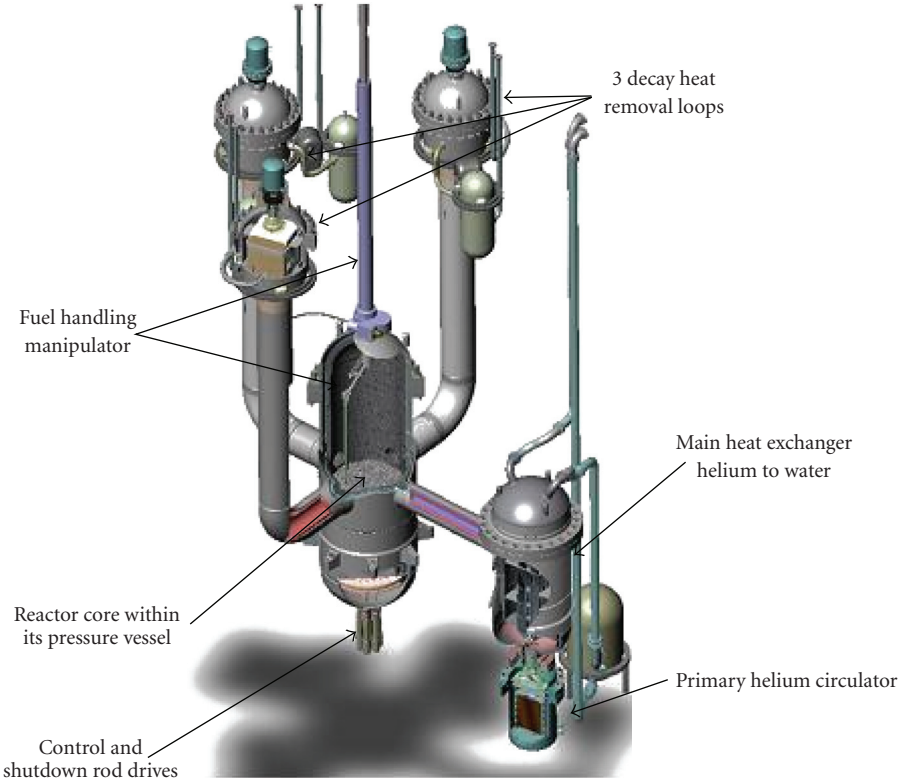

Figure 1: Proposed layout of ALLEGRO, the GFR demonstrator.

elements, and finally a GFR-style all-ceramic demonstration core. The starting core is a fairly conventional fast reactor core based on metallic hexagonal subassemblies containing metal-clad fuel pins which contain mixed-oxide ceramic fuel pellets. Having metal-clad fuel, the outlet temperature of the starting core will be limited to 550°C. The demonstration elements, that will be irradiated within a limited number of positions within the starting core, will contain high-temperature ceramic fuel plates or pins contained within an internally insulated metallic hex-tube, however. The final demonstration elements will be representative of the GFR core and will feature ceramic hex-tubes, such that the core outlet temperature will be increased to 850°C.

The FP6 Euratom contribution to ALLEGRO has been on specific design and safety studies. In-depth studies have been performed in the following areas:

(i) reactor primary system arrangement,

(ii) physics of the starting core,

(iii) fuel subassembly design,

(iv) absorber assembly design,

(v) control and instrumentation,

(vi) reflector and shielding design,

(vii) integration of the design and safety studies,

(viii) risk minimisation measures,

(ix) accident transient analysis.

With regard to the last point, a major programme of benchmarking of transient analysis codes was carried out by cross-comparing the simulations for reference scenarios obtained by different users and different computer codes, ahead of the application of the analysis of real plant transients [10]. This work will be extended in the 7th Framework Programme by comparing the results of these codes against specifically commissioned experimental studies. The current status of the ALLEGRO design can be found in [11].

3.2. GFR Development. At the start of the exploratory phase, a matrix was prepared for the Gen IV GFR studies to facilitate sharing the work between the members. This matrix identified seven combinations of design options. These option studies lead to a preselection of a reference concept and alternatives. The GFR options were as follows:

(1) 600 MWth reference case: high volumetric power ($\sim$100MW/m^3), challenging dispersed fuel (high ratio fuel/matrix), and high temperature direct cycle,

(2) 600 MWth step to reference case: high volumetric power ($\sim$100MW/m^3), challenging dispersed fuel (high ratio fuel/matrix), He at lower temperature as primary coolant, and SC CO_2 as secondary coolant,

(3) 2400 MWth dispersed fuel case: high volumetric power ($\sim$100MW/m^3), more accessible cercer fuel (50/50), and high temperature direct cycle,

(4) 2400 MWth pin case: high volumetric power, SiC clad fuel, and high temperature direct cycle,

(5) 2400 MWth, or more, particle fuel case: moderate volumetric power, particle fuel, and high temperature direct cycle,

(6) 2400 MWth, or more, pin case: moderate volumetric power, SiC clad oxide fuel, and high temperature direct cycle,

(7) generic 2400 MWth indirect cycle (He, SC CO_2) case.

Cases 1 to 5 were with dense fuel (carbide or nitride) and actinide compound. The option grid allowed comparison between concepts as follows:

(i) Case 1 ⇔ Case 2: direct versus indirect cycle comparison at 600 MWth,

(ii) Case 1 ⇔ Case 3: 600 MWth versus 2400 MWth comparison,

(iii) Cases 3, 4, 5, and 6: fuel options and design effect,

(iv) Cases 3 and 4 ⇔ Case 7: direct versus indirect cycle comparison at 2400 MWth.

When the seven cases were shared between the international partners, the European Union took responsibility for the comparison between Cases 1 and 2. These had a common core design with 600 MWth unit power, high volumetric power (~100 MW/m^3), and the challenging dispersed fuel (high ratio fuel/matrix). A low-pressure loss core was also a design objective to enhance the prospect of natural circulation under loss of flow conditions and to reduce blower power consumption under depressurisation faults. The Euratom FP6 project was therefore able to compare the impact of the direct /indirect power conversion cycle on a common basis.

The first priority for the project was to establish an overall reference definition for the 600 MWth GFR direct cycle design. The preliminary system layout is shown in Figure 2. This shows the reference arrangement with a vertical power conversion system (on the right in the figure) with control rod drive mechanisms (CRDMs) above the core and upward flow of the coolant, although alternatives, such as CRDMs below the core, were also considered. This reference serves as the basis for the design and safety studies, which will eventually be fed back into the GFR reference design.

Studies of the impact of minor actinides recycling on the self-sustaining core were carried out, both from the point of view of core neutronic design and the impact of including minor actinides on the safety characteristics of the core. A design concept was established based on the 600 MWth reference that was used as the basis for these actinide transmutation safety studies.

The main objective of the work was to compare the performance of the direct and indirect cycle options. The reference design for the direct cycle was based on the assumption that the helium Brayton cycle developed for the GT-MHR high temperature reactor concept [12] was suitable, provided that a reactor outlet temperature of 850°C could be achieved. The arrangement of the reactor and PCS vessels was taken to be the same as for GT-MHR, that is,

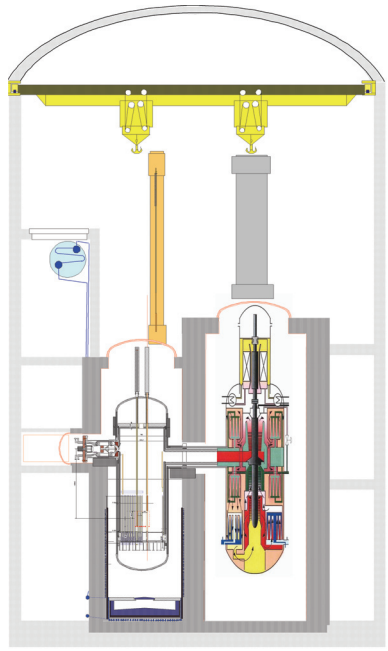

Figure 2: Proposed layout for a 600 MWth GFR with direct cycle.

the "side-by-side" arrangement based on the use of a vertical axis turbomachine, as shown in Figure 2. The indirect cycle was based on a supercritical CO_2 gas turbine cycle which required a lower core outlet temperature of 680°C. To some extent the choice of direct or indirect cycle was superseded by the shift of emphasis, instigated by the GIF, towards the 2400 MWth plant. Using four 600 MWth power conversion units was considered impractical because of the poor economics of scale resulting from a four-fold increase in the number of moving parts. Similarly, extrapolation of helium turbine and magnetic bearing technology up to the 2400 MWth was considered to be too large and to carry too much technological risk. About the same time, in some HTR programmes, combined cycles were indicating much less risk and more favourable economics. In such a cycle, a small helium (or helium-nitrogen) gas turbine makes best use of the high-temperature heat source, whilst the bulk of the power is generated by a large steam turbine that makes use of the waste heat from the gas turbine. This is an established technology in gas-fired plant, and requires a small extrapolation to be matched with a nuclear heat source. The layout of the containment building for the reference concept for a 2400 MWth GFR with an indirect cycle is shown in Figure 3.

3.3. Fuel Concepts Development. The greatest challenge facing the GFR is the development of robust high temperature refractory fuels and core structural materials, capable of withstanding the in-core thermal, mechanical, and radiation environment. Safety (and economic) considerations demand a low-core pressure drop, which favours high coolant volume fractions. The zero breeding gain demand restricts the level of plutonium enrichment leading to a demand for high fissile material volume fractions.

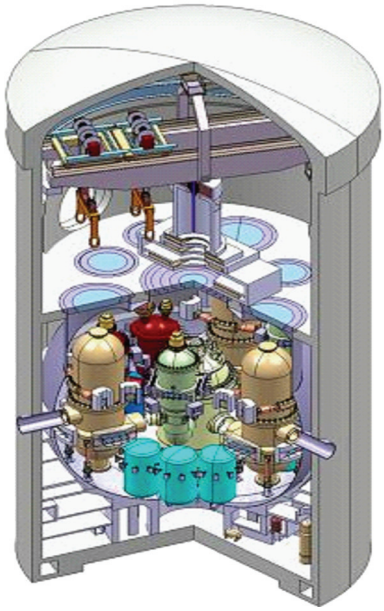

Figure 3: Layout of the 2400 MWth GFR in its containment building.

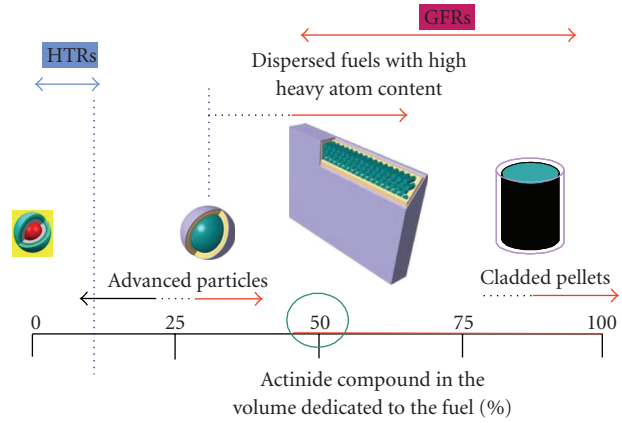

Figure 4: Candidate fuel concepts for GFR.

The concepts now considered are based on incremental innovation of the traditional pellet/pin concept and in the longer term deployment of more radically innovative concepts such as the ceramic coated fuel elements embedded in a ceramic or metallic matrix (CERCER or CERMET); see Figure 4. Candidate compositions for the fissile compound include carbides, nitrides, as well as the oxides. Materials for the encapsulation include ODS steel and SiC for pin formats and ceramic matrices (e.g. SiC, ZrC, TiN) for dispersion fuels in a plate format. Initial selection of the fuel and its cladding will be guided by irradiation tests to be carried out in materials test reactors, such as the High Flux Reactor at Petten, or in available sodium-cooled fast reactors. The final selection and confirmation of the fuel and its encapsulation will require feedback from irradiation in ALLEGRO and because of the high degree of innovation, parallel development paths are required. Whilst there is most experience with oxide fuel, which will be used for the ALLEGRO starting core with conventional stainless steel cladding, the Gen IV goals drive towards the higher density carbide and nitride fuels and high temperature clad. The nitride and carbide are preferred to the oxide as they enable a higher content of actinide per unit volume and permit lower operating temperatures, on account of their superior thermal conductivity.

A review was carried out which covered the irradiation experience in a number of former programmes in which pellet/rod, particle rod, and particle plate geometries were deployed. Fabrication technology to produce new fuel types has been studied and developed. Promising processes have been identified within the review, some of which have been assessed and compared, with further work required in the 7th Framework Programme. A strategy for the development of selected processes will be produced. Finally, the planning and design of irradiation tests of promising fuel and cladding material candidates will be undertaken in the 7th Framework Programme.

3.4. Dissemination of Project Information. The knowledge generated in the Euratom GFR projects contributes to the long-term development programme, which will span a number of Framework Programmes and is planned for successful completion over 3 decades. The access to knowledge generated within the project is made available to all the participants of any given project. It is intended that the knowledge generated contributes to the collaboration on Gen IV GFR and in return the knowledge generated by the Gen IV GFR partners will be available to participants with the Euratom projects.

It is important to raise public awareness and improve the public's perception generally of the nuclear industry. The project maintains a communication action plan to facilitate this. As well as contributing papers to journals and international conferences, Euratom projects provide material and contribute to the initiatives that are taken by the European Commission in the preparation of public information announcements and in engaging wider international involvement of non-European nations.

3.5. Education and Training. The objective of the training activities within Euratom's GFR projects is to contribute, in this particularly innovative field, to the transfer of knowledge from experienced scientists to the young engineers and researchers.

It is essential to have a project with a vision and long-term goal to attract newly qualified scientists and engineers. This is the first requirement, and the gas cooled reactor projects of which the Euratom GFR projects are important contributions, as well as giving access to the larger Gen IV GFR project. It is also important to have a project of sufficient size to be able to deploy a balanced multidisciplinary team combining experienced engineers and scientists together with those who are being trained.

There is a significant knowledge base on gas cooled and fast reactor technologies within Europe, which is essential to pass on to the next generation. An important way to do

this effectively is by application to a project with challenging R&D goals that require the knowledge base and can continue to further develop the knowledge. Euratom recognises that much of this experience rests in "old" hands and appreciates the need to promote young engineers and scientists who will progressively assume responsibility so that they have leading roles taking the project into the future framework programmes.

During the course of the 7th Framework Programme, training courses for young scientists and engineers will be organised, related to the GFR activities, some of which will be in conjunction with the sister sodium-cooled fast reactor and high temperature gas reactor projects.

4. Conclusions

Euratom has sponsored research programmes into the development of the gas cooled fast reactor system within the 5th and 6th Framework Programmes and has called for a follow-on project in FP7. The FP6 and FP7 projects provide Euratom's input into the GFR system in the Generation IV International Forum. These projects have been prepared by many European companies, research institutions and are fully integrated in the Gen IV GFR programme which is now dependant upon the task sharing between partners, including the Euratom contribution, to achieve the milestones up to the end of the viability phase in 2012.

In detail, the FP6 project has covered

(i) 600 MWth and 2400 MWth plant options,

(ii) ALLEGRO core and system design,

(iii) GFR and ALLEGRO safety analyses, including the analysis of selected transients,

(iv) qualification and benchmarking of the transient analyses codes through a series of benchmark exercises,

(v) a review of candidate fuels and core materials, including their fabrication and irradiation;

(vi) education and communication to foster understanding of the growing needs for nuclear power in general, and for the technology of the GCFR in particular, are a specific goals of the project.

An important outcome from the exploratory studies is the identification of the R&D needs and the specification of the programme by which they will be achieved, leading to construction of ALLEGRO and its missions in the GFR R&D programme. This programme will form the basis for the on-going Euratom 7th Framework Programme contribution from 2009 onwards.

Acknowledgments

The authors wish to thank all of the partners of the Euratom FP6 GCFR STREP (AMEC, AREVA, CEA, Nexia Solutions, Empresarios Agrupados, EC Joint Research Centres ITU and IE, NRG, PSI, TU Delft, CIRTEN, and latterly, Imperial College London) and express their appreciation of support by the European Commission. The GCFR STREP was carried out under Contract Number 012773 (FI6O) within the EURATOM 6th Framework Programme.

References

[1] C. Mitchell, N. N. C. Limited, B. Hall, et al., "Gas cooled fast reactor concept review studies (GCFR)," in *Proceedings of the Conference on EU Research in Reactor Safety (FISA '01)*, Luxembourg, UK, November 2001.

[2] C. Mitchell, et al., "Gas cooled fast reactor concept review studies (GCFR)," in *Proceedings of the International Congress on Advances in Nuclear Power Plant (ICAPP '03)*, Córdoba, Spain, May 2003, paper no. 3167.

[3] C. Mitchell, "Final technical report, gas cooled fast reactor (GCFR) EC 5th framework programme," Final Report NNC/C6395/TR/0012, October 2002, http://www.cordis.lu/fp5-euratom/src/lib_finalreports.htm.

[4] C. Mitchell, M. McDermott, and K. Peers, "Gas cooled fast reactor GCFR," in *Proceedings of the Conference on EU Research and Training in Reactor Systems (FISA '06)*, European Commission, Luxembourg, UK, March 2006.

[5] M. Nakano, et al., "Conceptual design for the enhanced gas cooled reactor (EGCR)," in *Proceedings of the Global*, Paris, France, September 2001.

[6] "SNE-TP vision report," EUR22842, European Commission, 2008, http://www.snetp.eu.

[7] "SNE-TP strategic research agenda," Final Draft, European Commission, February 2009, http://www.snetp.eu.

[8] "A Technology Roadmap for Generation-IV Nuclear Energy Systems," USDOE GIF-002-00, December 2002.

[9] "System research plan for the Gas-cooled fast reactor R&D program," U.S. DOE Nuclear Energy Research Advisory Committee and the Generation IV International Forum, 2005.

[10] E. Bubelis, D. Castelliti, P. Coddington, et al., "A GFR benchmark comparison of transient analysis codes based on the ETDR concept," in *Proceedings of the International Congress on Advances in Nuclear Power Plants (ICAPP '07)*, vol. 3, pp. 1916–1925, Nice Acropolis, France, May 2007.

[11] C. Poette, V. Brun-Magaud, F. Morin, et al., "ETDR, the European Union's experimental gas-cooled fast reactor project," in *Proceedings of the International Conference on the Physics of Reactors (PHYSOR '08)*, Interlaken, Switzerland, September 2008.

[12] IAEA, "Current status and future development of modular high temperature gas cooled reactor technology," Tech. Rep. IAEA-TECDOC-1198, IAEA, Vienna, Austria, February 2001.